Improvement of the mechanical model for mode 1 T-stub plastic strength

Auteur : Neutelers, Arnaud
Promoteur(s) : Jaspart, Jean-Pierre; Demonceau, Jean-Francois
Faculté : Faculté des Sciences appliquées
Diplôme : Master en ingénieur civil des constructions, à finalité spécialisée en "civil engineering"
Année académique : 2022-2023
URI/URL : http://hdl.handle.net/2268.2/17864

University of Liège

Faculty of Applied Sciences

Improvement of the mechanical model for mode 1 T-stub plastic strength

Master thesis carried out to obtain the master's degree of Civil Engineer

by Neutelers Arnaud

Promotor : Jaspart J.-P.
Co-promotor : Demonceau J.-F.

Jury : Corman A.
Mihaylov B.
Weynand K.

2^{nd} Master degree in Civil Engineering

Academic year 2022-2023

Acknowledgments

First and foremost, I would like to dedicate a special acknowledgment to my exceptional supervisor, Adrien Corman, whose kindness, devotion, and unwavering support have made an indelible impact on my thesis. I would like to express my deepest appreciation and heartfelt thanks to him. His extraordinary mentorship and genuine care have made this academic journey not only enriching but also a truly transformative experience.

Then, I extend my deepest appreciation to my professors Jean-Pierre Jaspart and Jean-François Demonceau, for their expert guidance, and invaluable insights. Their wealth of knowledge, patience, and constructive feedback have played a pivotal role in shaping this research. I am truly grateful for their continuous support and mentorship.

I would like to extend my sincere gratitude to the members of my thesis committee, Boyan Mihaylov and Klaus Weynand for their valuable time, feedback, and suggestions. Their expertise and diverse perspectives have greatly enhanced the quality of this research. I am grateful for their constructive criticism and thoughtful input, which have pushed me to strive for excellence.

I would also like to express my appreciation to my friends and especially François Delsemme, Héloïse Delsemme and Renaud Manguette for their camaraderie, intellectual discussions, and collaborative spirit. Their friendship and encouragement have created a positive and inspiring atmosphere, making this work enjoyable and fulfilling.

Lastly, I extend my deepest gratitude to my family for their unconditional love, understanding, and constant encouragement. Their unconditional support, both emotionally and morally, has been the driving force behind my success. I am grateful for their belief in my abilities.

Summary

Title : Improvement of the mechanical model for mode 1 T-stub plastic strength

In structural robustness studies, column loss events are considered. Such situations require the structure to be calculated in its deformed configuration. Joints response therefore plays a crucial role in such an analysis. However, nowadays , the component method for characterising joints has been developed essentially for the elastic domain. Researches are currently being carried out on components to extend this method up to joint failure. The component studied in this thesis is the T-stub.

First, the state-of-the-art is reviewed. A detailed presentation of this component is given. The same applies to various characterisation models. These range from the current standards, which is conservative and easy to apply, to the most recent and complex research models.

Next, a multitude of test campaigns were searched in the literature. From these, the most relevant specimens were selected for the study of **short unstiffened back-to-back T-stubs with one bolt row and made from mild steel welded plates**. The previously presented characterisation models are applied to these tests. As a result, an inadequate assessment of plastic strength is observed. This observation will be investigated in the remainder of this thesis.

Numerical modelling of the Timisoara test campaign was carried out. This enabled the modeling procedure to be validated.

In addition, a parametric study was carried out on three dimensionless parameters. These investigated the ratios of plates thickness to plates length, plates thickness to bolts diameter and the position of prying forces. From this study, it was observed that membrane effects are, indeed, negligible at yielding. Nevertheless, it was shown that the position of the plastic hinges is poorly evaluated. The same applies to the stress distribution under the bolt head. It has also been shown that the position of prying forces is safely overestimated. Finally, it has been observed that the range of application of the short T-stub theory is reduced in comparison with what the theory predicts. Indeed, non-rectilinear failure mechanisms were obtained.

Finally, analytical developments and formulations are proposed. Empirical formulae are proposed for the position of the hinges. Then, the work of the bolt head is re-evaluated by integrating the actual position of the hinges and a more realistic triangular stress distribution. For the non-rectilinear mechanism, an effective length is proposed. MV interaction is also introduced in the model to prove its influence. Last but not least, the EuroCode T-stubs classification criterion is invalidated and another one based on stiffness is proposed.

In conclusion, number of perspectives are suggested for further researches and improvements of the model proposed here. These include the establishment of a more accurate formula for the position of the hinges, and a more rigorous evaluation of the hybrid mechanism and the prying forces position. Once this has been done, a variation in the length of the T-stub can be considered.

Résumé

Titre : Amélioration du modèle mécanique de la résistance plastique des profilés en T périssant sous mode 1

Dans le cas d'études de robustesse des structures, des évènements de perte de colonne sont envisagés. De telles situations nécessitent de calculer la structure dans sa configuration déformée. La réponse des assemblages joue par conséquent un rôle crucial dans une telle analyse. Cependant, la méthode des composantes permettant la caractérisation des assemblages, est à ce jour essentiellement développée pour le domaine élastique. Des recherches sur les composantes sont actuellement menées pour étendre cette méthode jusqu'à la ruine de l'assemblage. La composante faisant l'objet de cette thèse est le profilé en T.

Dans un premier temps, un état de l'art est dressé. Une présentation détaillée de ladite composante est proposée. Il en va de même pour divers modèles de caractérisation. Ces derniers vont de la norme actuelle, sécuritaire et simple d'application, aux modèles de recherche les plus récents et les plus complexes.

Ensuite, une multitude de campagnes d'essais ont été cherchées dans la littérature. Parmi ces dernières ont été sélectionné les spécimens significatif pour l'étude des **profilés en T flexible courts non-raidis à une rangée de boulon et réalisés avec une nuance d'acier standard et des plats soudés**. A ces tests seront appliqués les modèles de caractérisation précédemment présentés. Ainsi, une insuffisance quant à l'évaluation de l'effort plastique est constatée. Cette observation est investiguée dans la suite de cette thèse.

Ainsi, une modélisation numérique de la campagne de Timisoara est réalisée. Ceci permettant de valider la procédure de modélisation numérique mise en place.

En outre, une étude paramétrique est réalisée sur trois paramètres adimensionnels. Ces derniers investiguent les rapports épaisseur sur longueur de la semelle, épaisseur des plats sur le diamètre du boulon et la position des efforts de levier. De cette étude, il a été observé que les efforts membranaires sont, en effet, négligeable à la plastification. Néanmoins, il a été prouvé que la position des rotules plastiques est mal évaluée. Il en va de même pour la distribution des contraintes sous la tête du boulon. Il a également été démontré que la position des efforts de levier est surestimée de façon sécuritaire. Enfin, il a été observé que le domaine d'application de la théorie des profilés en T courts est réduit en comparaison de ce que prévois la théorie. En effet, des mécanismes de ruines non rectilignes ont été obtenu.

Finalement, des développements et formulations analytiques sont proposées. Des formules empiriques sont développées pour la position des rotules. Ensuite, le travail de la tête du boulon est ré-évalué en y intégrant ce dernier point et une distribution de contrainte triangulaire plus réaliste. En ce qui concerne le mécanisme non rectiligne, une longueur effective est proposée. L'interaction MV est également introduite dans le modèle pour en démontrer son influence. Enfin, le critère de classification des profilés en T de l'EuroCode est remis en cause au profit d'un critère basé sur la rigidité.

Pour conclure, des perspectives de recherches et d'améliorations du modèle ici proposé sont suggérées. Celles-ci consistent en l'établissement d'une formule moins sécuritaire pour la position des rotules et en une évaluation plus rigoureuse du mécanisme hybride et du positionnement des efforts de levier. Une fois ceci fait, une variation de la longueur du profilé en T peut être envisagée.

Nomenclature

α	A material parameter in Pavlovic triaxiality criterion
β	A material parameter in Pavlovic triaxiality criterion
ΔE	The internal energy of deformation of the plastic mechanism
ΔW	The virtual external work of the plastic mechanism
Δ	A displacement
δ_p	The plastic displacement of a T-stub
Δ_u	The T-stub ultimate displacement
Δ_y	The T-stub displacement at yielding
δ_{H1}	The distance between the weld toe and the first plastic hinge
δ_{H2}	The distance between the bolt axis and the second plastic hinge
ν	The Poisson coefficient
ϕ	The relative rotation of a joint
Ψ	The ratio of the plate bending stiffness to the bolt axial stiffness
ρ	The MV interaction coefficient
ρ_{H1}	The MV interaction coefficient applied at the first hinge at the weld toe
ρ_{H2}	The MV interaction coefficient applied at the curved part of the second hinge at the bolt axis
σ	A stress
σ_{eng}	The engineering stress
σ_{mises}	The equivalent stress of Von Mises
$\sigma_{pl,true,damaged}$	The equivalent plastic stress at damage initiation
$\sigma_{pl,true}$	The plastic part of the true stress
σ_{true}	The true stress
σ_{xx}	The normal stress in the x direction
σ_{yy}	The normal stress in the y direction
σ_{zz}	The normal stress in the z direction
θ	The stress triaxiality or the unitary rotation of the plastic mechanism
θ_p	The plastic rotation of a plastic hinge
θ_{p1}	The plastic rotation of the plastic hinge at the weld toe
θ_{p2}	The plastic rotation of the plastic hinge at the bolt axis
ε	A strain

ε_f The strain at failure for steel

ε_h The strain at the end of the plastic plateau

ε_m The true strain associated to the true ultimate stress

ε_u The ultimate strain of steel

ε_y The yielding strain of steel

$\varepsilon_{el,eng}$ The elastic part of the engineering strain

ε_{eng} The engineering strain

$\varepsilon_{f,b}$ The strain at failure for a bolt

$\varepsilon_{pl,eng}$ The plastic part of the engineering strain

$\varepsilon_{pl,true,damaged}$ The equivalent plastic strain at damage initiation

$\varepsilon_{pl,true}$ The plastic part of the true strain

ε_{true} The true strain

$\varepsilon_{u,b}$ The ultimate strain of a bolt

$\varepsilon_{y,b}$ The yielding strain of a bolt

ζ A parameter introduced to simplify the bolt head work equations

A The true stress at the onset of necking

A_s The area of the threaded shaft of a bolt

a_w The weld thickness

A_{bolt} The area of the bolt cross section

B The width of the T-stub or the bolt load

b A constant in the linear part of Ling damage formulation

B^* The equivalent load of the triangular stress distribution under the bolt head

B_1 The equivalent load of the non working part of the decomposed triangular stress distribution under the bolt head

B_2 The equivalent load of the rectangular working part of the decomposed triangular stress distribution under the bolt head

B_3 The equivalent load of the triangular working part of the decomposed triangular stress distribution under the bolt head

$B_{t,Rd}$ The plastic strength of one bolt

C The distance between the weld toe and the bolt axis

c The distance between the interior bolts of a row

D The variable damage

d_b The bolt diameter

d_h The diameter of the bolt hole

d_w The washer diameter

D_{cr} The critical damage

d_{head} The diameter of the bolt head

E The Young modulus

e The distance between the bolt axis and the flange edge in the width direction

e_1 The distance between the bolt axis and the edge of the flange in the length direction

E_h The hardening modulus

E_u The ultimate modulus

e_w The distance between the bolt axis and the equivalent bolt load point of application in the Jaspart model

F An applied load

F_u The ultimate force

f_u The ultimate stress of steel

F_y The plastic force

f_y The yielding stress of steel

f_y^{MV} The yielding stress penalized with MV interaction

F_{EC} The plastic strength of the mode 1 computed according to the EuroCode model

$f_{f,b}$ The failure stress of a bolt

F_{hybrid} The yield strength computed with the hybrid yield line patter

F_{MV} The yield strength computed with the hybrid pattern and the MV interaction

$F_{Neutelers}$ The plastic strength of the mode 1 computed according to the Neutelers model

$F_{pl,Abaqus}$ The plastic strength obtained with ABAQUS©

F_{pl} The plastic strength

$F_{T,1,Rd}$ The plastic strength of mode 1

$F_{T,2,Rd}$ The plastic strength of mode 2

$F_{T,3,Rd}$ The plastic strength of mode 3

$F_{T,Rd}$ The plastic strength of the T-stub

$f_{u,b}$ The ultimate stress of a bolt

$f_{y,b}$ The yielding stress of a bolt

$f_{y,nominal}$ The nominal yielding stress of steel

G A parameter introduced to simplify the bolt head work equations

h_f The projection of the weld thickness

I_{plate} The plate bending inertia

K A coefficient in the exponential part of Ling damage formulation

$K_{1stub,init}$ The initial stiffness of one T-stub

$K_{2stubs,init}$ The initial stiffness of two back-to-back T-stubs

K_{bolt} The stiffness of a bolt row

$K_{column,flange}$ The stiffness of a column flange T-stub

$k_{eff,tot}$ The effective stiffness of a joint

$K_{end-plate}$ The stiffness of an end-plate T-stub

K_{plate} The stiffness of a plate

k_{rel} The stiffness ratio of the bolt to the plate

$k_{stub,st}$ The hardening stiffness of a T-stub

k_{stub} The stiffness of a T-stub

$k_{stub}, init$ The initial stiffness of a T-stub

L The length of the T-stub

L_b The bolt length

L_{char} The characteristic length of the mesh

$L_{eff,1}$ The effective length of mode 1

$L_{eff,2}$ The effective length of mode 2

$L_{eff,c,w}$ The effective length of Warnant circular yield line pattern

$L_{eff,c}$ The effective length of the circular yield line patter

$L_{eff,nc,w}$ The effective length of Warnant non circular yield line pattern

$L_{eff,nc1}$ The effective length of Zoetemeijer yield line pattern

$L_{eff,nc2}$ The effective length of the short yield line pattern

L_{H1} The length of the first hinge at the weld toe

L_{H2} The length of the second hinge at the bolt axis

L_{hybrid} The length of the hybrid yield line pattern

L_{short} The length of the short yield line pattern

m The distance between the bolt axis and the point located at 80% of the projection of the weld thickness

M_j The bending moment transmitted by a joint

M_u The ultimate bending moment

$M_{pl,1,Rd}$ The plastic bending moment of mode 1

$M_{pl,2,Rd}$ The plastic bending moment of mode 2

$M_{pl,H1}$ The plastic bending moment of the first hinge at the weld toe

$M_{pl,H2}$ The plastic bending moment of the second hinge at the bolt axis

$M_{pl,mean}$ The average plastic bending moment transmitted by a hinge in a plastic mechanism

m_{pl} The plastic bending moment by unit of length

m_{pl}^{MV} The plastic bending moment by unit of length penalized with MV interaction

N The true strain at the onset of necking

n The distance between the bolt axis and the prying forces location

n_{mode1} The distance between the bolt axis and the prying forces location for mode 1

p The distance between two bolts of the same row

p_1 The distance between two bolts rows

p_{eq} The equivalent stress

Q The prying forces

q The mean stress

$S_{j,init}$ The rotational stiffness of a joint

T The support thickness

t_f The flange thickness

t_w The web thickness

$u_{pl,eq,displ}$ The equivalent plastic displacement

$v_{ed,H1}$ The shear load applied by units of length at the first hinge at the weld toe

$v_{ed,H2}$ The shear load applied by units of length at the curved part of the second hinge at the bolt axis

v_{ed} The shear load applied by units of length

v_{Rd} The shear resistance by units of length

W A weighted coefficient between the linear and exponential part of Ling damage formulation

X^* The distance between the bolt hole axis and the point of application of B^*

X_1 The distance between the bolt hole axis and the point of application of B_1

X_2 The distance between the bolt hole axis and the point of application of B_2

X_3 The distance between the bolt hole axis and the point of application of B_3

Table of contents

Chapter 1

Introduction

In past years, some dramatics events such as Ronan Point or the World Trade Center have showed the lack of robustness in buildings. In response, structures are now designed to not collapse even under accidental loadings consisting in fire, earthquake, terrorist attack,...

The common feature of all those examples is that they could lead to the loss of a bearing element. In that case, the structure should be able to sustain large deformations and attain a new state of equilibrium (see FIGURE (1.1)). From this perspective, catenary effect cannot be disregarded and by further extend, the rotation capacity of the joints. To do so, the widely accepted component method developed by the Pr. Jaspart is used to assess both the resistance and deformation of the joint. However, this method was mainly proposed for the elastic response of the joint and needs further investigations to accurately model the plastic response up to failure. Some components, as the shear web panel, have already been studied while some as the T-stub are still under investigations.

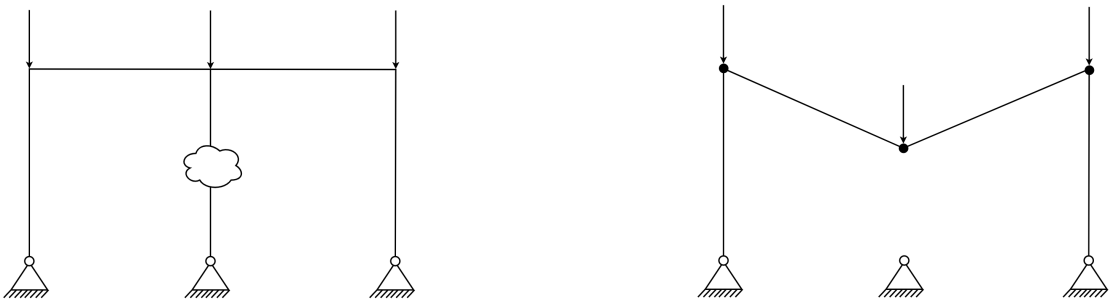

(a) Initial configuration (b) New achieved equilibrium

FIGURE 1.1 – Lost of a column event

The current thesis is an additional contribution to the T-stub studies previously performed at the University of Liège by Warnant A. [**1**] and Leruth B. [**2**]. Some lacks of the current design standards have been pointed out in those works. In consequence, a rigorous state-of-the-art gathering several characterisation models from the simplest to the most complex is realised. Those models are applied to specimens issued from experimental test campaigns. Thus, some inconsistencies can be observed and are deeply investigated.

Then, those specimens are modeled in the non linear finite element software ABAQUS©. The purpose of this is to develop and validate a procedure of modelling that can be extended to a parametric analysis. Thus, all the assumptions of the current models can rigorously checked and validated or not.

Finally, analytical developments are carried on to solve the identified problems. The main goal of this thesis is to contribute in the accurate assessment of the T-stub response and improve the predictions made by the current characterisation models.

Chapter 2

State-of-the-art

In this chapter, a brief summary of the knowledge on the current topic is proposed. This one first presents the component method, a model that characterises both resistance and stiffness of joints. Then, an emphasis is made on the T-stub component, its typology, failure modes and so on. Afterwards, both standards and research models of characterisation are developed by order of growing complexity. Finally, conclusions are drawn on those models and the assumptions they rely on.

2.1 The component method

Historically, for sake of simplicity, joints were assumed to be perfectly hinged or moment resisting. In reality, their behaviour is much more complex and can be classified by mean of three criteria represented on Figure (2.1).

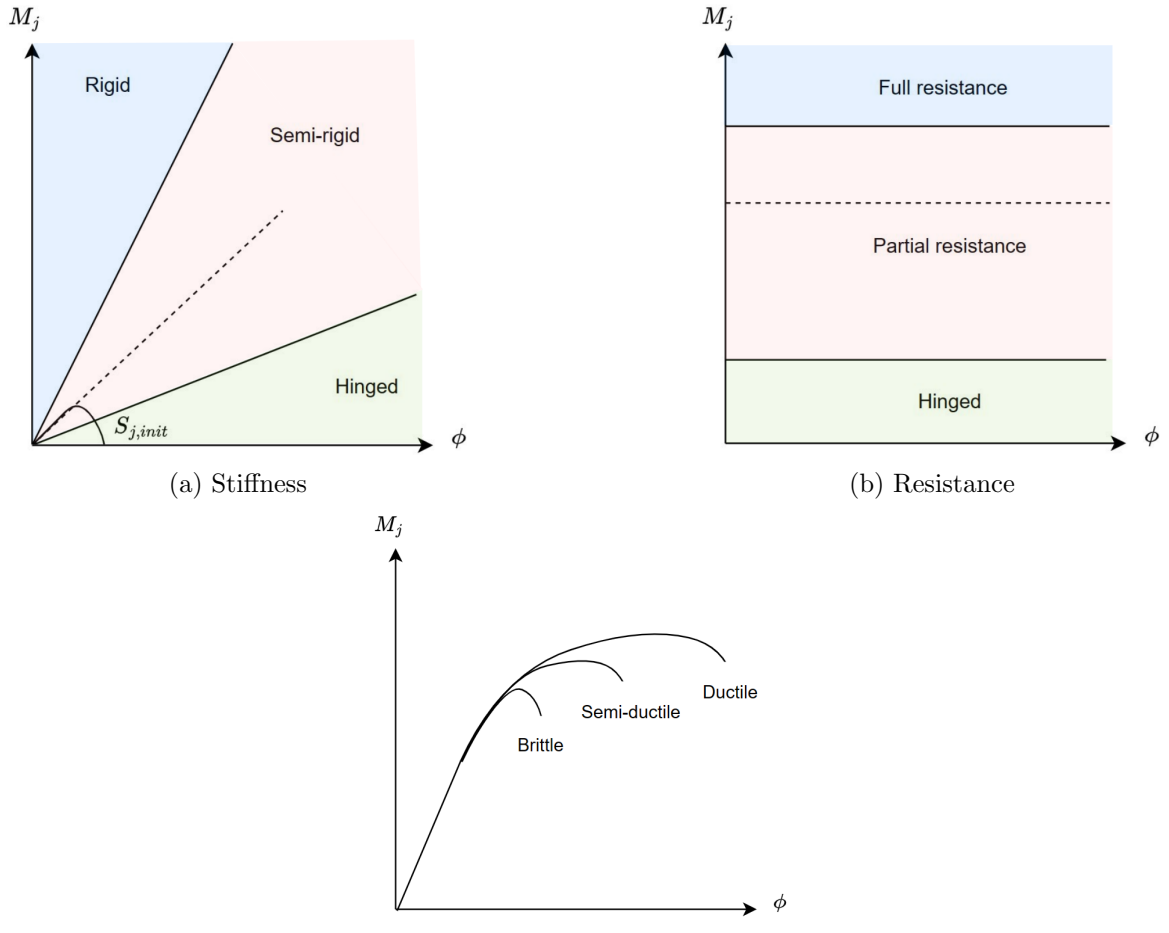

(a) Stiffness

(b) Resistance

(c) Ductility

Figure 2.1 – Joint classification adapted from [**1**]

— A **rotational stiffness** $S_{j,init}$ which boundary are strictly defined in [**3**] and stated how the joint should be modelled.

— A **relative rotation** ϕ characterising the ductility or brittleness of the joint.

— A **transmitted bending moment** M_j.

The principle of the component method is to consider that a joint is an assembly of many pieces called **components** which contribute to the joint response. The first step of this method is to **identify the active components**. As example, the case of a beam-to-column joint is developed and illustrated on FIGURE (2.2). The bending moment applied to this joint can be seen as two axial loads applied at both flanges of the beam (the distance between them acts as the lever arm). Thus, the upper flange is submitted to tension while the other is compressed. Once those loads reach the joint, a tension zone and a compression zone can respectively be identified.

Concerning the tension zone, the load flows from the flange to the **End-Plate in Bending** (EPB). Notice that for the second bolt row only, the **Beam Web in Tension** (BWT) acts like a stiffener and should be taken into account in the model. Then, the load in transmitted to the **Column Flange in Bending** (CFB) by the intermediate of the **Bolts in Tension** (BT). Finally, the load is in the column and must flows up to the left flange of the column. To do so, the **Column Web in Tension** (CWT) component is activated as well for the **Column Web panel in shear** (CWS) due to the induced shear zone.

Regarding the compression zone, the load is simply transmitted by contact from the **Beam Flange and Web in Compression** (BFWC) to the **Column Web in Compression** (CWC). Thus, the applied bending moment applied to the joint is transmitted to the column by all the active components.

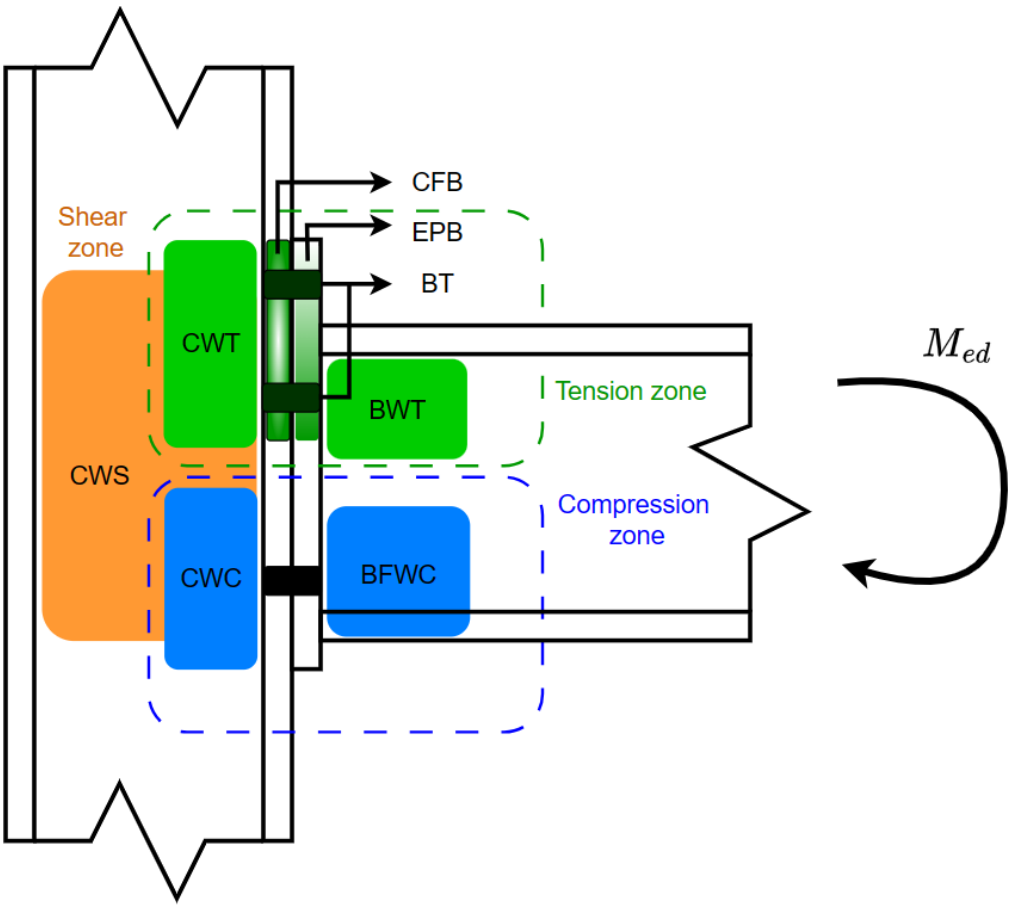

FIGURE 2.2 – Identification of the active components of a beam-to-column joint [**3**]

The second step of the method is to **characterise each components**. This is rigorously done in the European standards [**3**] and not developed in this thesis for sake of concisely. The results of this important step are that all the previously identified components can be modelled either as an equivalent tension spring or a dash-pot. This operation can be seen on FIGURE (2.4). Notice that some components are highlighted, they can be modelled by an equivalent unstiffened T-stub which is the topic of this thesis. Stiffened T-stubs can also be modelled by taking the Beam Web Tension component into account.

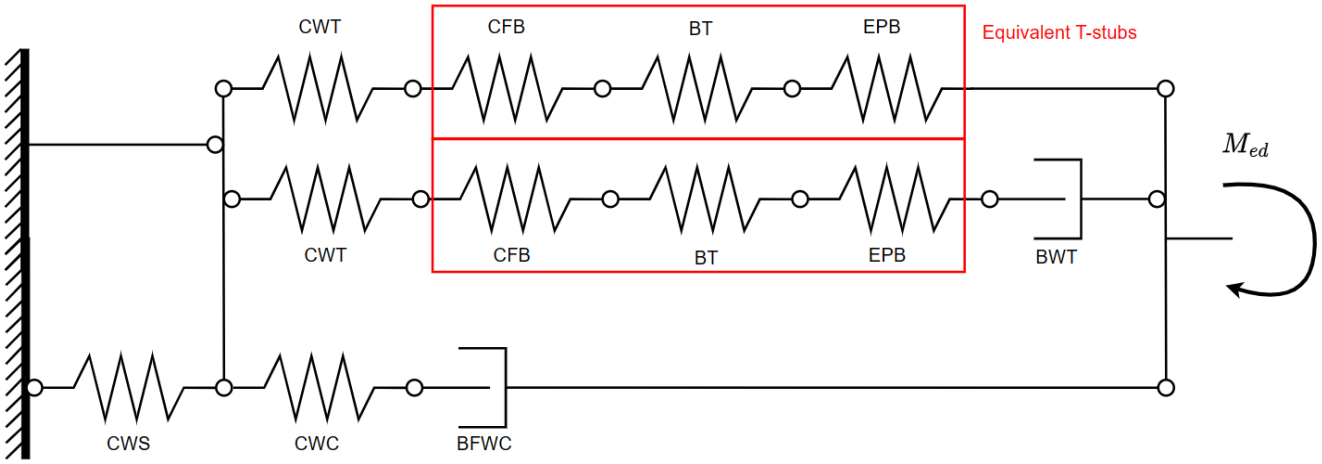

FIGURE 2.3 – Spring model of a beam-to-column joint [**3**]

The third and last step of the component method is the **assembly**. Once all the components are characterised, they can be assembled according to the **static theorem** to assess the joint response. This theorem states that **the stress distribution assumed is conservative if the equilibrium is achieved while respecting the material constitutive laws both in term of strength and displacement**. In the assembly process, it intervenes in the simplification of the many springs into an effective one as represented on FIGURE (2.4). The same philosophy lies to the force distribution applied on the model.

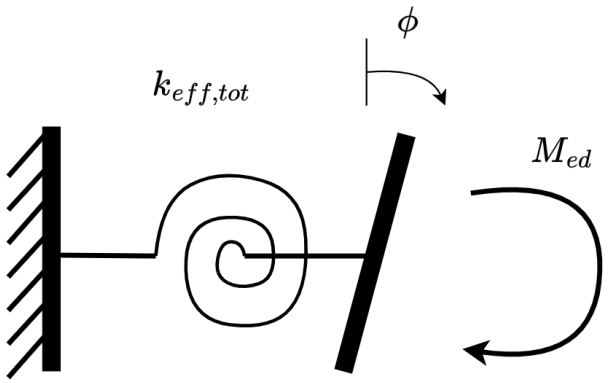

FIGURE 2.4 – Equivalent torsional spring model of a beam-to-column joint [**3**]

At this point, the joint response is fully characterised. It can be introduced into a structural or a robustness analysis as an equivalent torsional spring. Thus, the deformation due to the joint ductility can taken into account into the analysis and may highlight the catenary effect. However, an important reserve of ductility is required to activate such a contribution. As previously explained, T-stubs are still not fully characterised up to failure and may possess that reserve of ductility.

2.2 The T-stub component

According to the method presented in the previous SECTION, both the column flange and the bended end plate connected with fastened bolts can be modelled as equivalent T-stubs. This profile is uniformly loaded by its web. Its thickness corresponds to the physical dimensions of the represented elements while its length is theoretically idealised as an effective length which provides the T-stub a resistance similar to the real components.

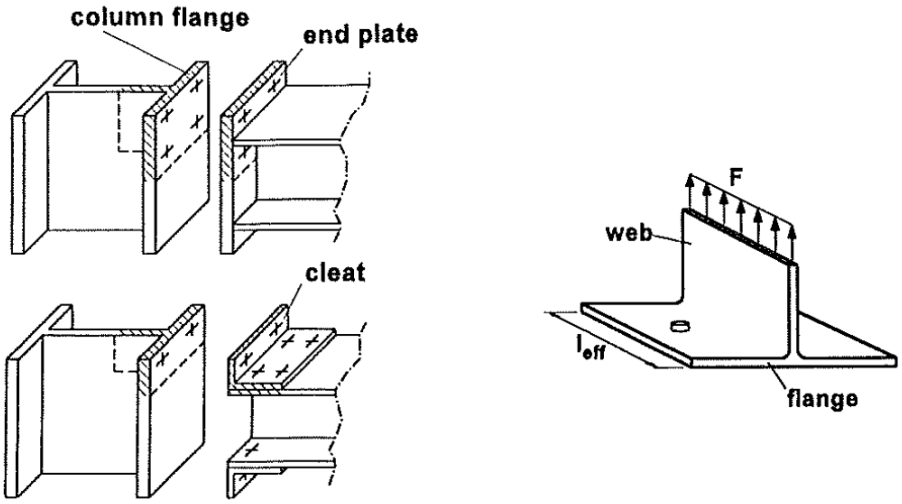

FIGURE 2.5 – T-stub idealization [**4**]

The response of the idealised T-stub under loading mainly depends of its geometrical and material properties. However, three main behaviours at failure can be shown :

- In case of thick plates in comparison of the bolts, the failure is expected to be located in the bolts in tension either with nut stripping or thread necking. This failure mode is called **mode 3** and shows a very brittle behaviour. This collapse mode is illustrated on FIGURE (2.6c) and can be characterised as follows :

$$F_{T,3,Rd} = \sum B_{t,Rd} = \sum 0.9 f_{u,b} A_s. \tag{2.1}$$

- If the bolts do not fail prior the plate yielding, a plastic hinge is formed at the weld toe and a partial mechanism takes place. Prying forces appear at the edges of the T-stub and overload the bolts. In case of thin plates, the bolts are not expected to fail and a second plastic hinge is formed in the bolt hole axis which leads to a complete plastic mechanism (see FIGURE (2.6a)). This type of failure is related as **mode 1** .

$$F_{T,1,Rd} = \frac{4M_{pl,1,Rd}}{m} = \frac{4m_{pl}L_{eff,1}}{m}. \tag{2.2}$$

- An additional contribution improving the strength of mode 1 is proposed by Jaspart J.-P. in his thesis [**4**]. It consists in considering the bolt head virtual work when computing the yield mechanism by Johanssen's method [**6**]. For any additional proof or demonstration of formula (2.2) and (2.3), please, refer to APPENDIX (B).

$$F_{T,1,Rd} = \frac{(32n - 2d_w)M_{pl,1,Rd}}{8mn - d_w(m+n)} \tag{2.3}$$

- In the other case, the bolts fail due to the prying overloading and the failure is stated as **mode 2**. This configuration can be found on FIGURE (2.6b).

$$F_{T,2,Rd} = \frac{2M_{pl,2,Rd} + n\sum B_{t,Rd}}{m+n}. \tag{2.4}$$

Finally, the collapse mode that occurs first is the one with the minimum resistance.

$$F_{T,Rd} = \min(F_{T,1,Rd}\,;\, F_{T,2,Rd}\,;\, F_{T,3,Rd}). \tag{2.5}$$

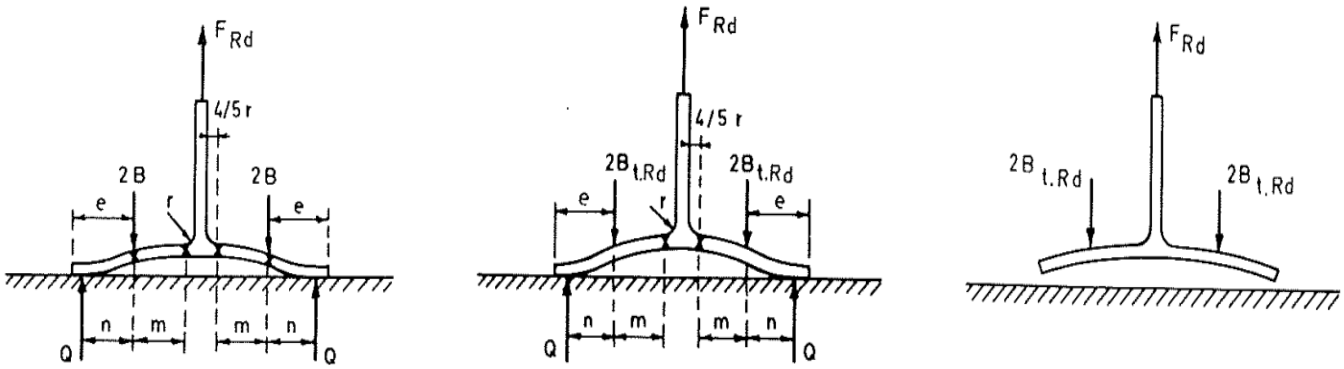

(a) mode 1 (b) mode 2 (c) mode 3

FIGURE 2.6 – T-stub failure modes [**4**]

A T-stub is qualified as **short** or **idealised** when $L_{eff,i} = L$. As a consequence, its yield mechanism is two straight lines at the weld toe and the bolts holes (see FIGURE (2.7b)). This is fundamental for this thesis since it focuses on **unstiffened back-to-back short T-stubs with one bolt row and made of mild steel welded plates**. More importantly, this definition is vividly discussed later on in SECTION (6).

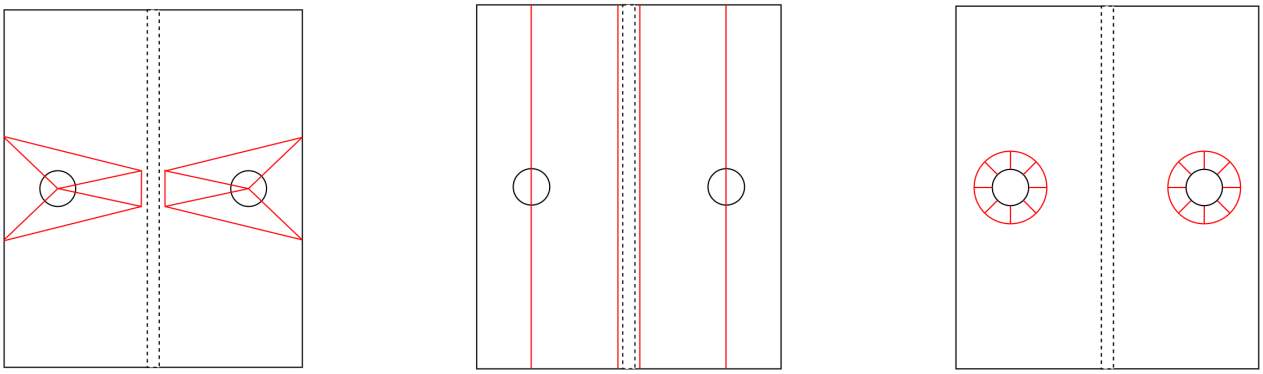

(a) $L_{eff,nc1}$ (b) $L_{eff,nc2}$ (c) $L_{eff,c}$

FIGURE 2.7 – Effective lengths

As stated previously, the T-stub effective length allows to model longer non-idealised T-stubs with a more complex plastic mechanism into an idealised T-stub as previously described. Notice that all the mechanisms presented hereafter show one bolt row since a focus is made on this configuration especially. This problematic was first studied by Zoetmeijer P. in [**5**]. From this study are issued the commonly acknowledged yielding mechanisms and their associated effective lengths. Those patterns are represented on FIGURE (2.7).

$$L_{eff,nc1} = 4m + 1.25n \tag{2.6}$$

$$L_{eff,nc2} = L \tag{2.7}$$

$$L_{eff,c} = 2\pi m \tag{2.8}$$

In addition to that, some researchers also proposed their own effective lengths although they are not in the standard designs. This is the case of the two patterns on FIGURE (2.8) developed by Warnant A. in [**1**].

$$L_{eff,nc,w} = \frac{Lm}{2(m+n)} + m\left(0.0876\left(\frac{n}{m}\right)^3 - 0.6816\left(\frac{n}{m}\right)^2 + 3.1143\frac{n}{m} + 0.9786\right) \tag{2.9}$$

$$L_{eff,c,w} = L - m + \frac{\pi m}{2} \tag{2.10}$$

(a) $L_{eff,nc,w}$ (b) $L_{eff,c,w}$

FIGURE 2.8 – Warnant's effective lengths [**1**]

According to Johansen plates theory [**6**], the first mechanism to appear is the one which minimises the energy, i.e. the one with the shortest effective length. In consequence, the following equations can be deduced. Notice that due to its definition, the 2nd failure mode is not able to present a circular yielding pattern at collapse.

$$L_{eff,1} = \min(L_{eff,nc1}, L_{eff,nc2}, L_{eff,c}L_{eff,nc,w}, L_{eff,c,w}) \tag{2.11}$$

$$L_{eff,2} = \min(L_{eff,nc1}, L_{eff,nc2}, L_{eff,nc,w}) \tag{2.12}$$

2.3 Existing models of characterisation for T-stub

In this section, some models issued from both the standard designs and the literature are presented. Their purposes is to characterise the failure modes described in SECTION (2.2). Similarly, according to the component method philosophy, they also predict the component initial and hardening stiffness to assess as accurately as possible the displacement of the T-stub. The following models are developed in a growing complexity order : the EuroCode model, the Jaspart model, the Piluso model, the Zhao model and the Francavilla model.

2.3.1 EuroCode model (2005)

The first model proposed is the one found in the European design codes [**3**]. In this reference, the T-stub is modelled as a bended beam as illustrated hereafter on FIGURE (2.9).

Through equilibria and energy balances, the component resistance can be expressed by EQUATIONS (2.1) to (2.5). Notice that the standards do not acknowledge all the research effective length models. Thus, only EQUATIONS (2.6) to (2.8) should be used in the current characterisation model.

In addition to that, the EuroCode relies on some assumptions mostly to achieve user-friendly and clause formulation of the problem. They consist in neglecting all the geometrical non linearities, the 3D effect, the MV interaction and the flexion in the bolts. Indeed, as explained, the T-stub is computed as a beam in its initial configuration. Thus, the 1D model does not take into account any geometrical non linearities. The model also assumes that the loads applied to the bolts are perfectly to their axes, neglecting by consequence the flexion.

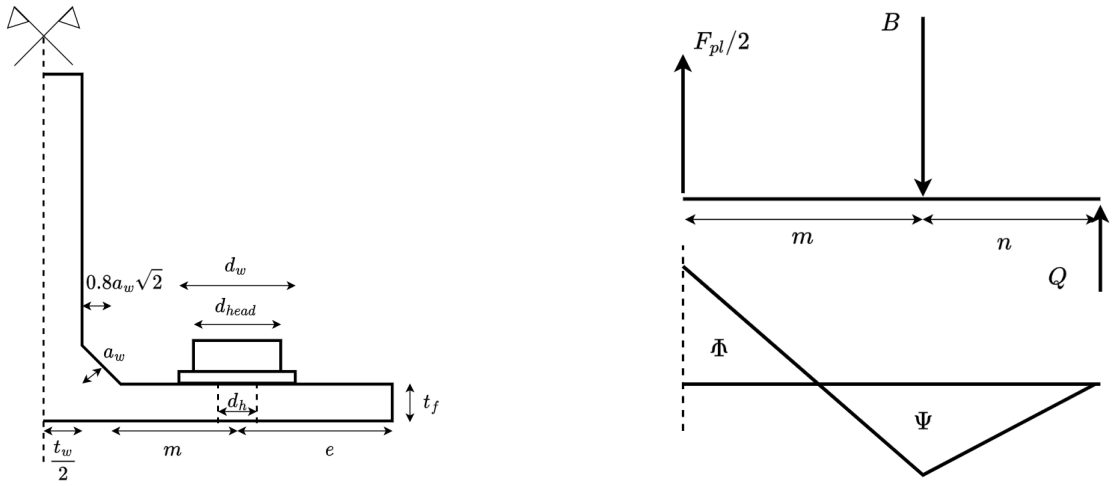

(a) Geometry (b) Beam model

FIGURE 2.9 – EuroCode model

Concerning the constitutive laws, the bolts are assumed to remain in the elastic domain up to failure while the plates have an elastic-perfectly plastic behaviour as represented on FIGURE (2.10). Also notice that the constitutive laws are expressed here in terms of engineering stress-strain.

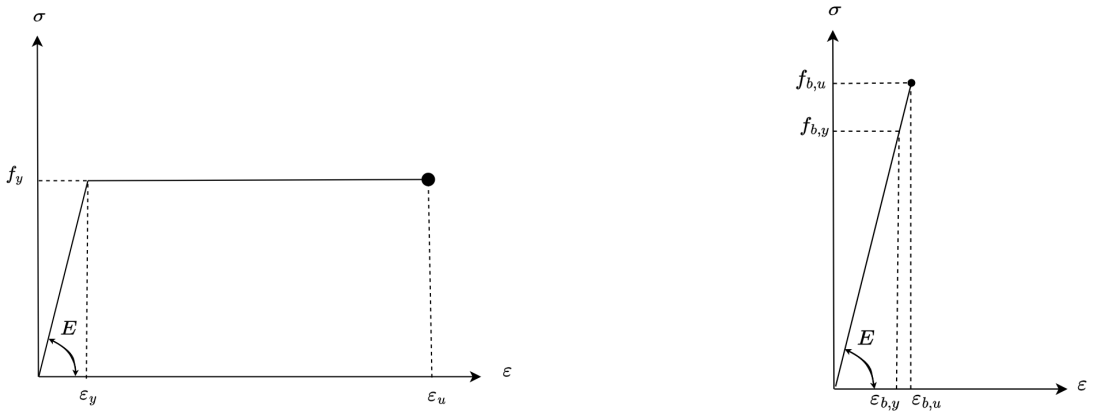

(a) Plate's constitutive law (b) Bolt's constitutive law

FIGURE 2.10 – Material laws used in EuroCode models

Following the component method's philosophy, the active components of the T-stub are the plates in bending and the bolts in tension. It can be represented as on FIGURE (2.11) and the stiffness can be expressed through the following assembly.

$$K_{2stubs,init} = \frac{1}{\frac{2}{K_{plate}} + \frac{1}{K_{bolt}}} \tag{2.13}$$

Notice that the stiffness of equation (2.13) stands for two back-to-back T-stubs. Therefore, to evaluate the stiffness of one T-stub, it is appropriate to divide that expression by 2. This manipulation will be implicitly suggested by using the notation $K_{1stub,init}$.

$$K_{plate} = \frac{0.9 L_{eff} t_f^3}{m^3} E \tag{2.14}$$

$$K_{bolt} = \frac{1.6 A_s}{L_b} E \tag{2.15}$$

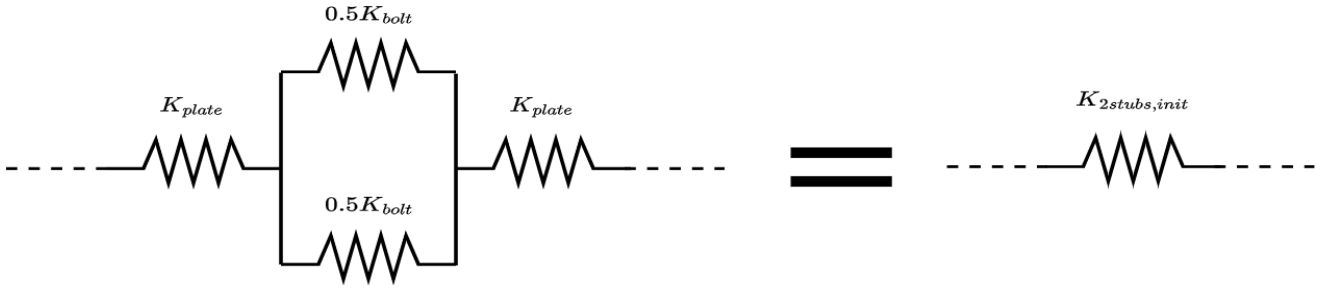

FIGURE 2.11 – Spring model of the T-stub according to EuroCode

Finally, knowing both resistance and stiffness of the component, the force-displacement response of the component can be built with a bilinear or trilinear curve. Those two methods are illustrated on FIGURE (2.12). Concerning the trilinear curve, an intermediate stiffness is used to model the transition between the elastic and the plastic response of the T-stub by taking one third of the initial stiffness. Notice that the EuroCode does not provide any information on the ultimate strength and deformation of the component due to its assumptions on the constitutive laws. In addition to that, this model constitutes the reference which the research models introduced afterwards are compared to.

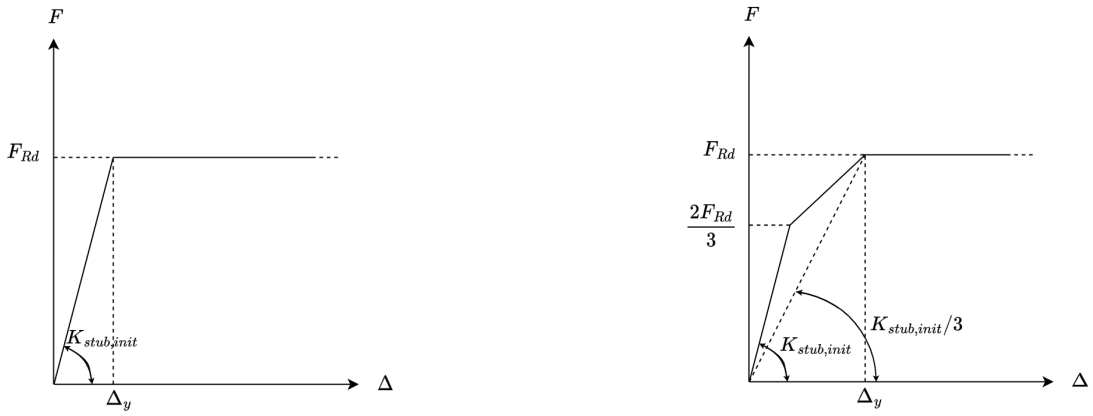

(a) Bilinear curve (b) Trilinear curve

FIGURE 2.12 – Force-displacement curves of Eurocode model

2.3.2 Jaspart model (1997)

The first research model introduced is the Jaspart model presented in his thesis [**4**]. In fact most of this work was included in the EuroCode previously described. By consequence, the assumptions on which the model relies on are identical. As a reminder, it means that all the geometrical non linearities, the 3D effects and the MV interaction are disregarded. However, the purpose of the current model is to assess the real joint response up to failure. To do so, hardening was initially introduced in the plates constitutive law. This contribution can be seen on the bilinear engineering stress-strain curve illustrated on FIGURE (2.13). Concerning the bolts, since they do not show a ductile behaviour and do not allow plastic redistribution in section, it was decided to idealise their constitutive law by an elastic line up to failure.

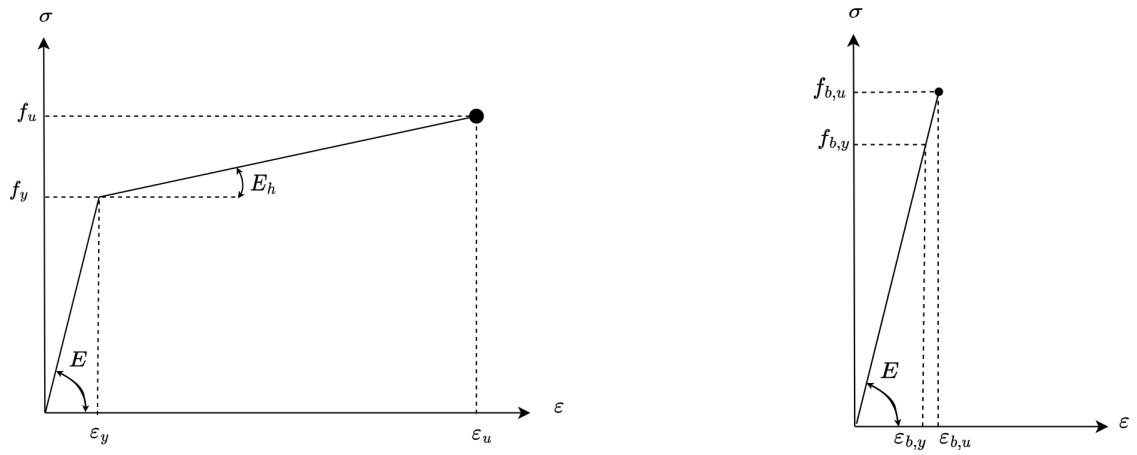

(a) Plate's constitutive law (b) Bolt's constitutive law

FIGURE 2.13 – Material laws used in Jaspart model

A major discovery found in this thesis [**4**] was to take into account the contribution of the bolt head work. Indeed, in the first models, the bolt force was assumed punctual as represented on FIGURE (2.14a). In this configuration, the bolt force does not undergo any displacement when computing the virtual work of the plastic mechanism. This configuration derives in EQUATION (2.2). In contrast, by assuming a uniformly distributed load as depicted on FIGURE (2.14b), half of the bolt head undergoes a displacement and contributes to the virtual work. This configuration gives EQUATION (2.3) and was introduced as such in the standards from [**4**].

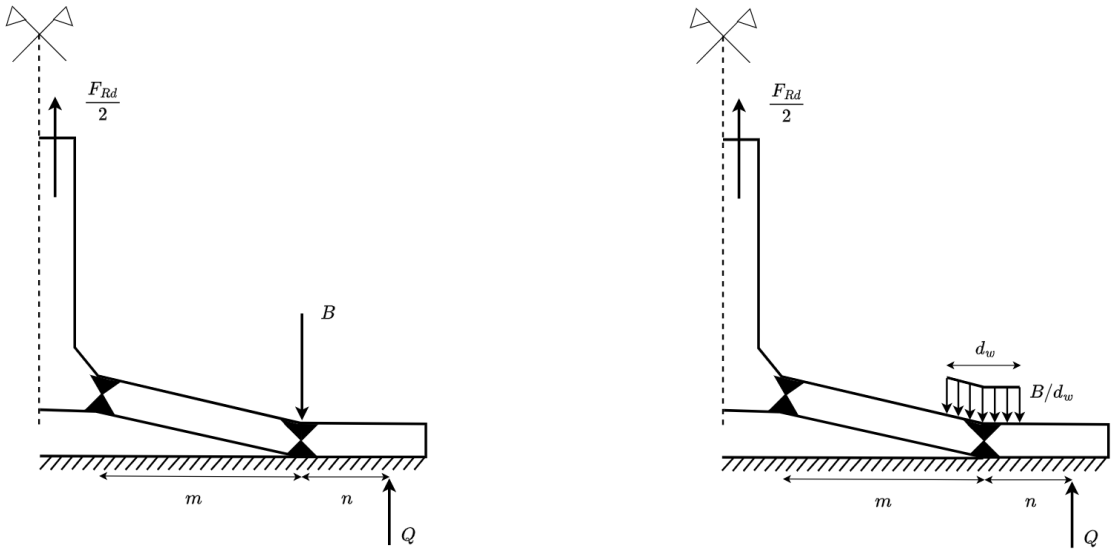

(a) Punctual bolt force (b) Uniformly distributed bolt force

FIGURE 2.14 – Modelisation of the bolt force adapdted from [**4**]

Then, the initial stiffness of the component lies in the elastic response of the bended plates and the bolts in tension. However, the latter contributes to both T-stubs responses in a back-to-back configuration. In consequence, the compatibility of displacement has to be ensured. Owing this, the stiffness of one T-stub can be found as represented on FIGURE (2.15). Notice that the bolts can be pre-loaded or not in this model. However, for sake of simplicity and inclusion in the standards, this contribution was disregarded. In addition to that, it was decided to consider the T-stub as an assembly of components itself. As consequence, the stiffness coefficient is simplified into EQUATIONS (2.13) to (2.15). Remind that those expressions stand for the **initial** response of the T-stub. To take into account both plasticity and hardening in the plates, the **hardening modulus** E_h should be used instead of the Young modulus E. If the former term is unknown, Jaspart proved in [**4**] that $E/50$ is a good approximation of E_h.

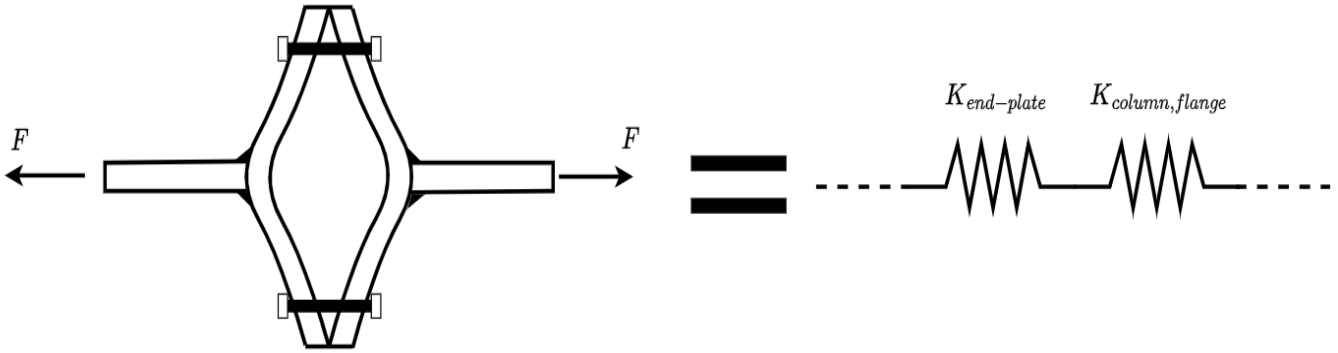

FIGURE 2.15 – Spring model of the T-stub according to Jaspart [**4**]

Finally, the force-displacement curve of the T-stub can be built. The principle applied is similar in all points with the EuroCode model. The major difference that is highlighted by FIGURE (2.16) is the post-yielding behaviour of the response in opposition to the plastic plateau shown by the previous model. Notice that the **plastic strength** is defined as **the intersection of the vertical axis with the prolongation of the plastic response of the component**. To allow a proper comparison, this definition is kept later on in this thesis.

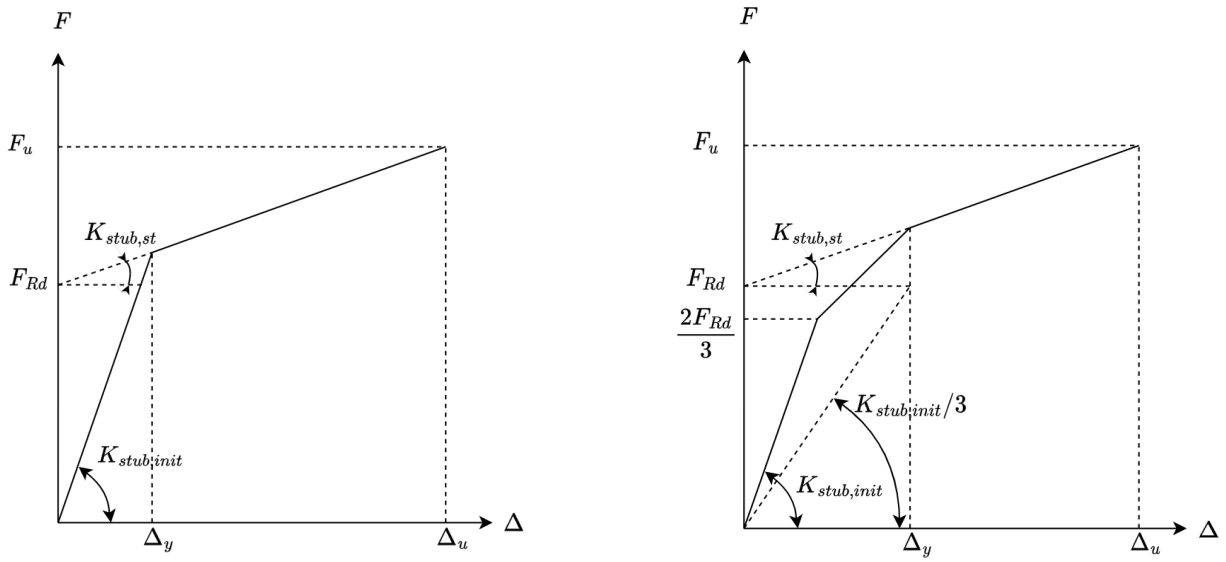

(a) Bilinear curve (b) Trilinear curve

FIGURE 2.16 – Force-displacement curves of Jaspart model

2.3.3 Piluso model (2001)

The second research model considered is the Piluso model. It was first introduced in [**7**] and then validated in [**8**]. The main goal of this model is to improve the characterisation of the post yielding behaviour. In consequence, the plate constitutive law is complexified. Indeed, the one used by the model is a quad-linear **true stress - true strain** model. This is illustrated on FIGURE (2.17). The transition between true properties and engineering ones can be done by using the two following EQUATIONS :

$$\varepsilon_{true} = \ln(1 + \varepsilon_{eng}) \tag{2.16}$$

$$\sigma_{true} = \sigma_{eng}(1 + \varepsilon_{eng}) \tag{2.17}$$

Concerning the other assumptions, they all remain unchanged and any additional improvement is done. The geometrical non linearities, the 3D effects and the MV interaction are still disregarded.

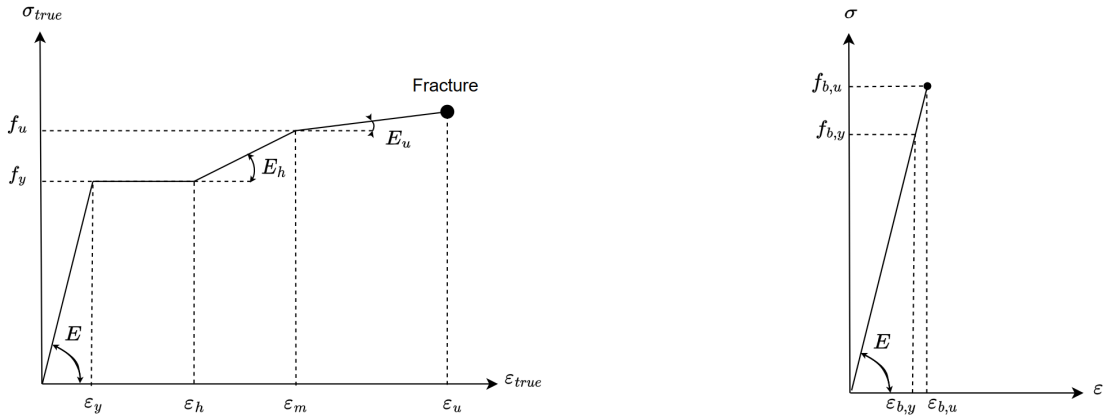

(a) Plate's constitutive law (b) Bolt's constitutive law

FIGURE 2.17 – Material laws used in Piluso model [**7**]

As previously said, the virtual work principle is applied to assess the T-stub resistance. However, a drawback of this method is that it is unable to assess the displacement. To counter this, both Jaspart and the EuroCode used the notions of initial and hardening stiffness. Piluso, in its model, proposes another approach of the problem. By the means of the more complex plate material law, a curvature χ can be found for a fixed applied bending moment. Then, this curvature can be integrated over the thickness of the plate to evaluate the rotation of the section. It results that the rotation of the plastic hinges is known and so the plastic displacement. This principle can be seen on FIGURE (2.18) :

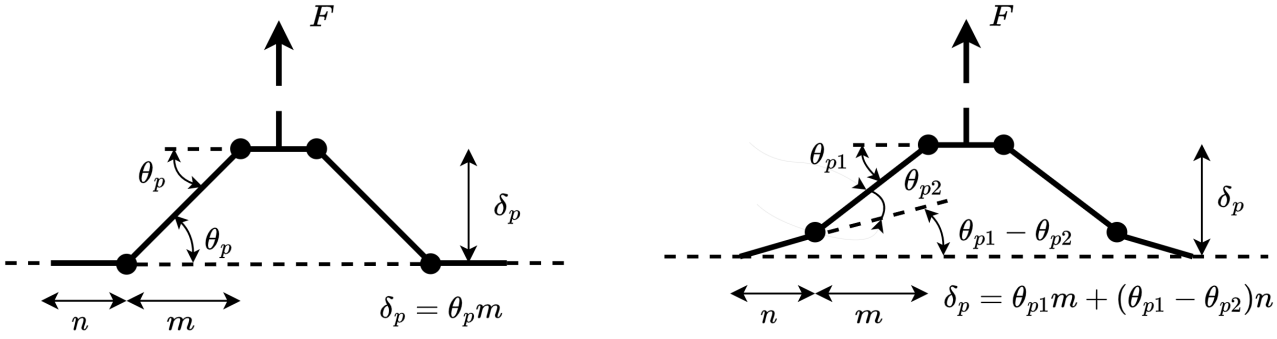

(a) Mode 1 (b) Mode 2

FIGURE 2.18 – Failure mode according to Piluso [**7**]

Finally, the total displacement is simply the sum of both elastic and plastic contributions. Notice that **the compatibility of displacements between the bolts and the plate is not taken into account**. Concerning the strength, it consists in using EQUATIONS (2.1) to (2.4) with the bending moment corresponding to the curvature used when assessing the rotations.

The force-displacement response of this model is represented on FIGURE (2.19). It is a quad-linear curve which points are assessed using the characteristics values of the plate constitutive law. Notice that this can be refined by computing additional points with others $M - \chi$ couples.

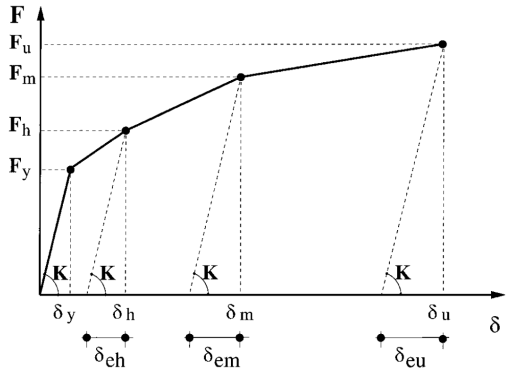

FIGURE 2.19 – Force-displacement curve of Piluso model [**7**]

2.3.4 Zhao model (2023)

In [**9**], both Jaspart and Piluso models were tested on various configurations of T-stubs. From this study was concluded that the former was too conservative while the latter overestimates the ultimate displacement. Moreover, it was highlighted that **the bolts can fail even in mode 1** (see FIGURE (2.6a)). So two sub-classifications were proposed. The collapse is called **mode 1-BR** if the rupture is located in the bolts otherwise, it is due to cracking in the flange and the failure is characterised as **mode 1-FF**. This difference can be seen in FIGURE (2.22).

In reaction to that, Zhao proposed his own model which consists in an improvement of the Piluso model. Indeed, the displacement is assessed in such a way that the compatibility of displacements between the flange and the bolts is ensured. In addition to that, a more complex engineering stress-strain law taking into account both plasticity and necking of the bolts is considered. For the plates, the same true stress-true strain law is used as for the Piluso model. Those two constitutive laws are illustrated on FIGURE (2.20). Concerning the others assumptions, while MV interaction and 3D effects are still disregarded, the geometrical non lineraties are estimated.

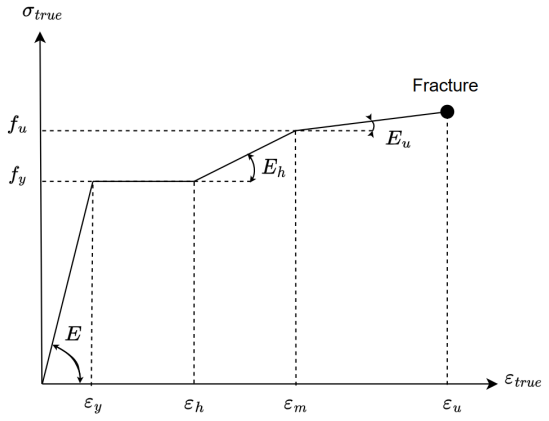

(a) Plate's constitutive law

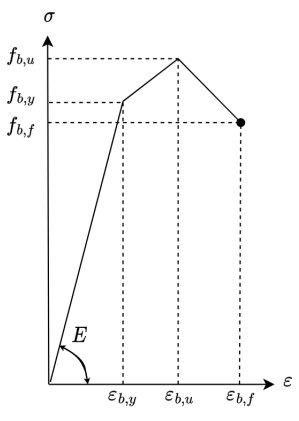

(b) Bolt's constitutive law

FIGURE 2.20 – Material laws used in Zhao model

In this model, the T-stub is considered as an assembly of the bolts and plates. From this perspective, the displacement is evaluated as the sum of the bolts elongation Δ_2 and the plate plastic mechanism deformation Δ_1. This model can be seen on FIGURE (2.21) and is more in accordance with the component method philosophy. This totally contrasts with the Piluso model where all the displacement was due to the plastic hinges and disregarding the compatibility with the bolts elongation.

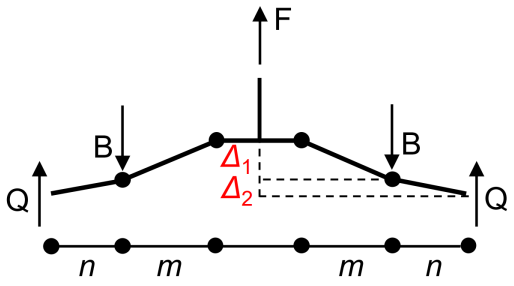

FIGURE 2.21 – Zhao model [**10**]

The first displacement can be studied with a procedure similar to the Piluso model. Knowing the bending moment applied to the section, a curvature can be found. Then, through integration over the thickness, the rotation of the plastic hinge at the weld toe can be computed. Finally, the plate force-displacement response can be built. Notice that no modification is done to the resistance. So, those terms can be computed with EQUATIONS (2.1) to (2.4). The second displacement can easily be obtained by multiplying the bolt law by the net cross section since the bolts are assumed to work in tension only.

Once the T-stub components responses assessed, they can be assembled. For a fixed strength, a displacement can be determined for both the plate and the bolts. By adding those two terms, the T-stub displacement is computed for the associated force. The failure occurs when the minimum of the ultimate bolt bearing capacity and the ultimate bending strength of the plate is attained. Notice that through this assembly, the two sub-classifications for mode 1 can be differentiated as illustrated on FIGURE (2.22) hereafter.

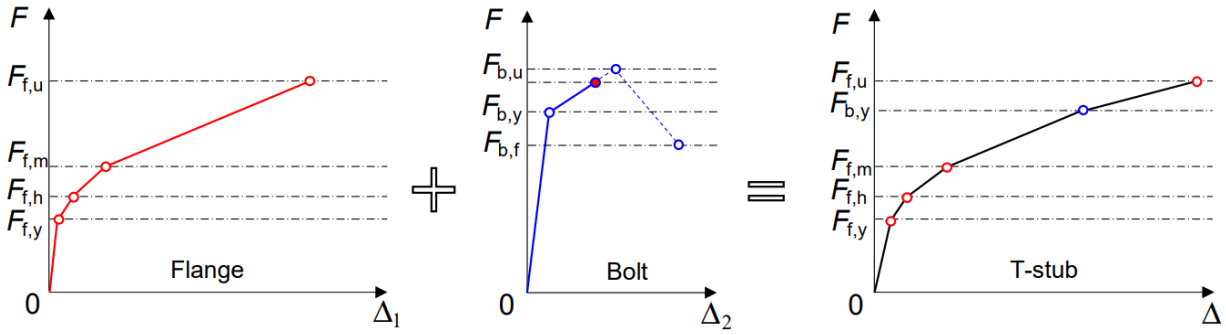

(a) Flange failure

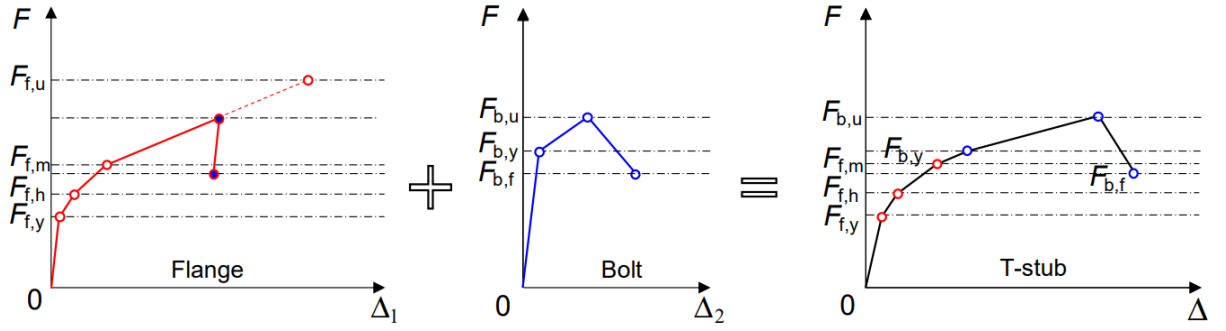

(b) Bolt failure

FIGURE 2.22 – Force-displacement curves of Zhao model [**10**]

2.3.5 Francavilla model (2021)

In the previous SECTION, the model presented was already complex but could be improved to increase the accuracy of the results. The Francavilla model goes a step further by proposing an **iterative procedure** to evaluate the force-displacement response of T-stubs on **rigid foundations** [**11**]. Before detailing this procedure, the assumptions which the model relies on must be noted. Some are identical to the previous model such as neglecting the MV interaction, the flexion in the bolts and 3D effects. A new feature is that the prying forces are no longer assumed fixed and may translate during the loading. Concerning the constitutive laws, the same true stress-true strain law as the two previous models is used for the plate. The bolts, on the other hand, are assumed to have an elastic-perfectly plastic behaviour expressed in terms of engineering stress-strain. Those laws are illustrated on FIGURE (2.23).

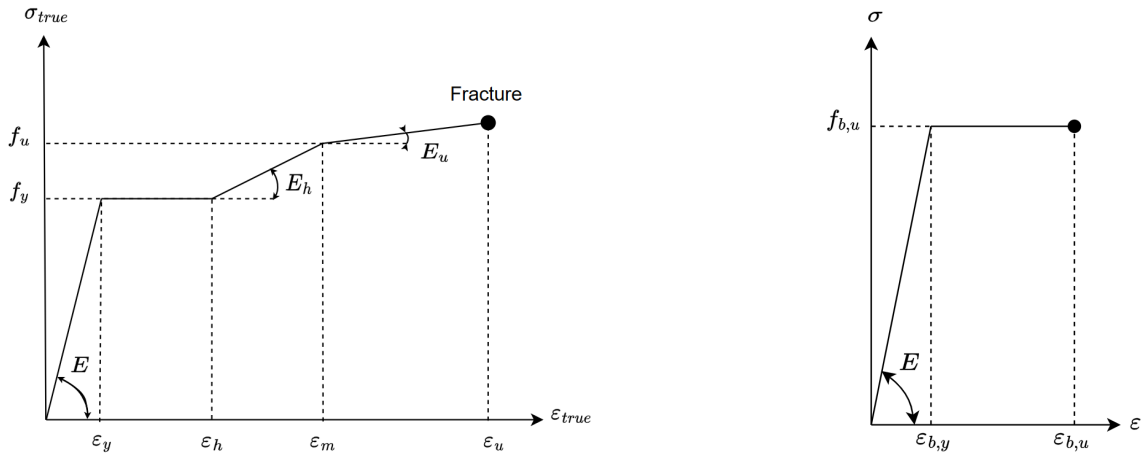

(a) Plate's constitutive law (b) Bolt's constitutive law

FIGURE 2.23 – Material laws used in Francavilla model [**11**]

In this model the bolt is idealised as a couple of translational springs as depicted on FIGURE (2.24). The vertical one models the bolt in tension while the other represents a complex interaction between the hole in bearing, the shear in the bolt and the friction forces.

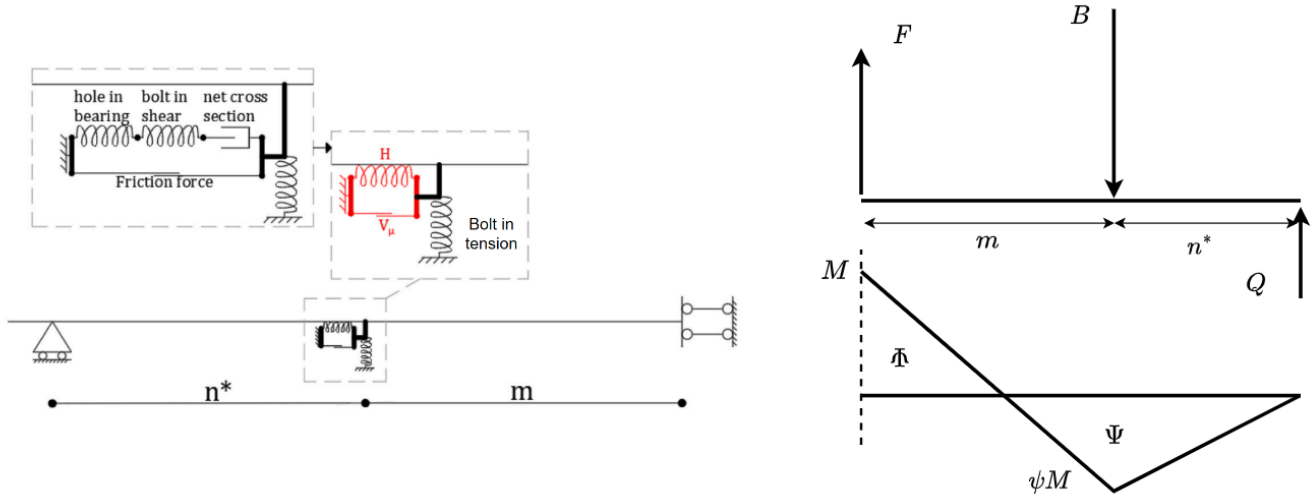

FIGURE 2.24 – Francvilla model [**11**]

The algorithm to be applied is represented on FIGURE (2.25). At the first Step, the bending moment at the weld toe has to be chosen in a range between 0 and the ultimate bending capacity of the plate. Then the location of the prying forces must be assumed between the flange and washer edges (Step 2). Next, the bending moment diagram is built by guessing the flexion located at the bolt location. Afterwards, the

rotations of the plastic hinges can be computed by integrating the curvature of the section over its depth as Piluso and Zhao previously did. This operation is the fourth Step. Knowing this, the forces applied on the T-stub can be assessed and the real flexion at the bolt location can be evaluated (Step 5). This means that, as the sixth Step, the assumptions made in Step 3 can be checked. If it is not the case, return to Step 3, otherwise, the displacement compatibility in the contact zone can be performed (Step 7). Similarly, if this condition is not met, then return to Step 2 by assessing again the prying forces location. In the other case, the penultimate Step can be performed by computing both flange and bolt displacements. In the last Step, each collapse mode should be checked. The outcomes of this step are either that the failure is achieved, either a point of the force-displacement curve was found. In the latter case, the procedure has to be restart from beginning to compute the next points until collapse is attained.

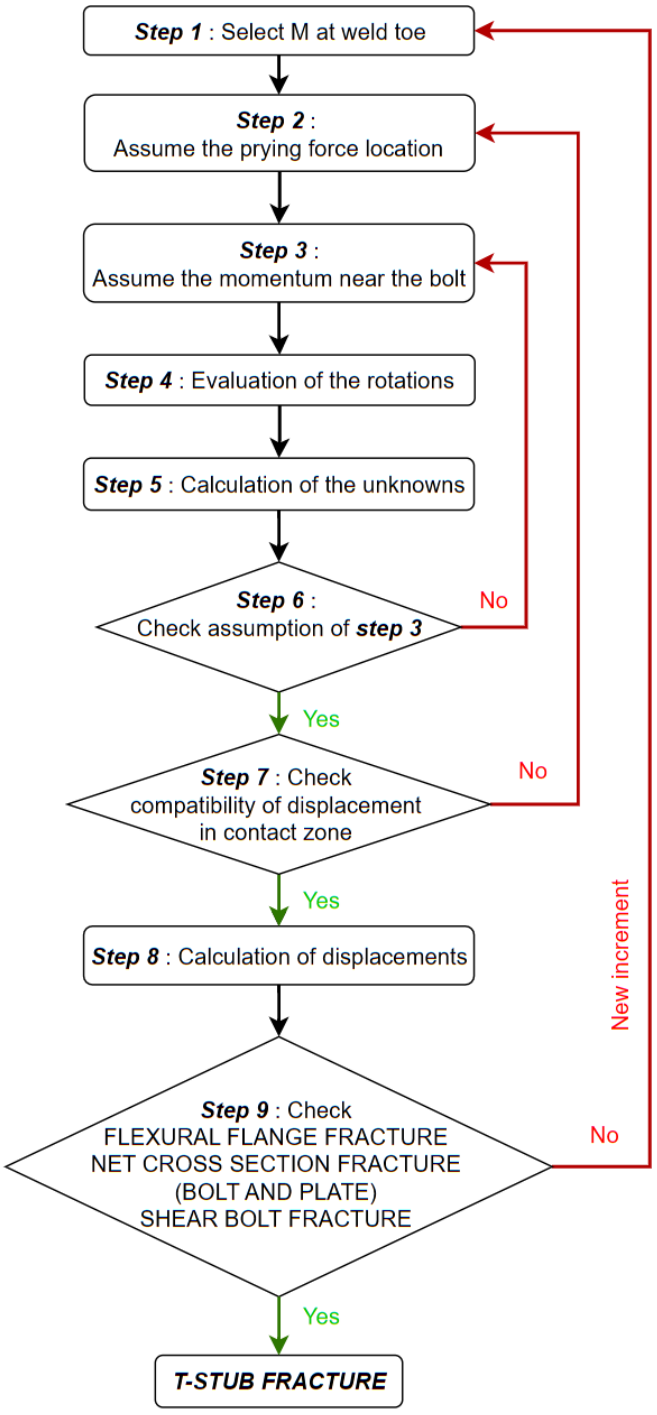

FIGURE 2.25 – Iterative procedure of Francvilla model adapted from [**11**]

2.4 Conclusions

In this Section was presented in depth the T-stub from its place in the component method, to the various methods to characterise its behaviour. Considering the number of models presented, a summary of the required inputs for the plate and the bolts is proposed in Tables (2.1) and (2.2) respectively.

Authors	Model	Elastic domain	Plastic domain	Necking domain	Engineering VS True
EuroCode	bi and tri-linear	E, f_y	/	/	Engineering
Jaspart	bi and tri-linear	E, f_y	E_h, f_u	/	Engineering
Piluso	quad-linear	E, f_y	ε_h, E_h, f_u	E_u, ε_f	True
Zhao	quad-linear	E, f_y	ε_h, E_h, f_u	E_u, ε_f	True
Francavilla	quad-linear	E, f_y	ε_h, E_h, f_u	E_u, ε_f	True

Table 2.1 – Plate constitutive law required inputs

Authors	Model	Elastic domain	Plastic domain	Necking domain	Engineering VS True
EuroCode	linear	$E, f_{b,y}$	/	/	Engineering
Jaspart	linear	$E, f_{b,u}$	/	/	Engineering
Piluso	linear	$E, f_{b,u}$	/	/	Engineering
Zhao	tri-linear	$E, f_{b,y}$	$\varepsilon_{b,u}, f_{b,u}$	$f_{b,f}, \varepsilon_{b,u}$	Engineering
Francavilla	bi-linear	$E, f_{b,u}$	$\varepsilon_{b,u}$	/	Engineering

Table 2.2 – Bolts constitutive law required inputs

Regarding the assumptions, all models neglect the MV interaction, 3D effects and the flexion in the bolts. The geometrical non linearities were approximated in Zhao model and properly evaluated in the Francavilla model otherwise, they were disregarded. Some unique particularities linked to a specific model can be listed :

— The compatibility of displacements is not ensured in the Piluso model. This leads to an overestimation of the ultimate displacement.

— The Francavilla model verifies some local failure near the bolts. The cost of this operation is that a closed formulation cannot be found.

— The Zhao model differentiates the mode 1 failing due to bolt rupture and the one collapsing due to cracking in the flange.

— EuroCode is the only model to not consider hardening and thus, is unable to estimate both ultimate strength and displacement.

— Bolt preloading can be taken into account only in the Jaspart model.

In addition to that, it must be noticed that both effective length and strength are evaluated with formulae common to all models. A consequence of this is that the plastic strength of the T-stub is identical independently of the model used. At failure the observed differences are only due to the considered material properties.

Chapter 3

Experimental study

The next step in this thesis is to confront all the models from Chapter (2) to practice. Thus, a multitude of tests campaigns available through literature were gathered to build a database. Then, all the campaigns relevant for the study of **short back-to-back T-stubs with one bolt row and made of mild steel welded plates** are selected. An in depth comparison between the experimental data and the results given by the models is performed. Finally, conclusions are drawn from the analysis of this comparison.

3.1 Existing experimental campaigns

3.1.1 Timisoara

This test campaign take place in the **CODEC** project [**12**], [**13**]. This robustness project studies a multistory structure under accidental actions from conception to collapse. From this perspective, the joint response was studied up to failure and the question of the T-stub response naturally emerged. To answer this question, a test campaign was performed. The geometry of the tested T-stubs is illustrated on Figure (3.1) and can be found in Table (3.1).

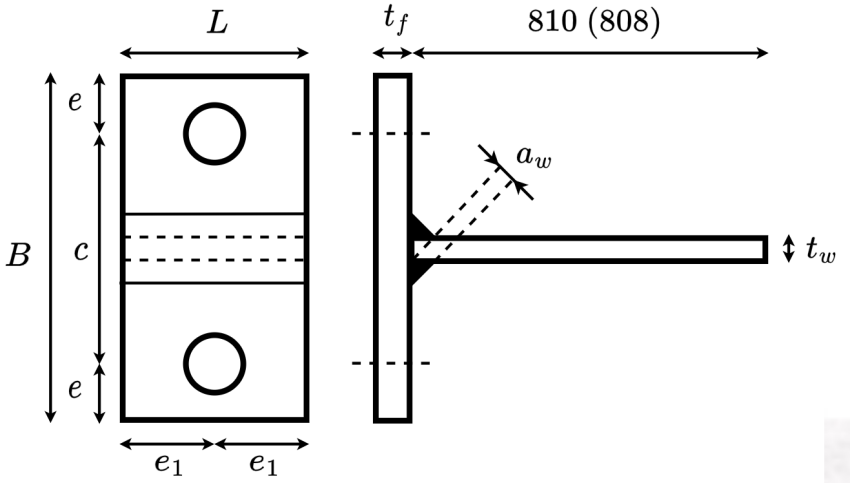

Figure 3.1 – Geometry of Timisoara configuration adapted from [12]

The designation of the specimens should read $T - t_f - d_b - c$. From this denomination, the main parameters studied are highlighted. All the T-stubs can be defined as **short** according to the EuroCode definition given in Section (2.2). The loading is applied by an imposed displacement which is measured at the web edge. In consequence, both web deformation and stiffness should be taken into account when assessing the displacement and the T-stub initial stiffness respectively. However, it was proved in [**12**] that this contribution can be neglected due to the high axial rigidity of the web in respect to the bending stiffness of the flanges. Notice that the unusual dimension of the web can be attributed to an inappropriate test setup.

Test	t_w [mm]	t_f [mm]	B [mm]	e [mm]	c [mm]	L [mm]	e_1 [mm]	a_w [mm]
T-10-16-100	10	9.6	160	30	100	90	45	7
T-10-16-120	10	9.7	180	30	120	90	45	7
T-10-16-140	10	9.7	200	30	140	90	45	7
T-12-16-100	10	11.8	160	30	100	90	45	7
T-12-16-120	10	11.8	180	30	120	90	45	7
T-12-16-140	10	11.8	200	30	140	90	45	7
T-15-16-100	10	15	160	30	100	90	45	7
T-15-16-120	10	15	180	30	120	90	45	7
T-15-16-140	10	15	200	30	140	90	45	7
T-18-16-120	10	18	180	30	120	90	45	7
T-18-16-140	10	18	200	30	140	90	45	7

TABLE 3.1 – Timisoara geometrical properties [**12**] and [**13**]

Concerning the material properties, the steel grade used for the flange is S235 while S355 is used for both welds and web. In addition to that, tests on coupons were performed which give the true properties of the steel noted in TABLE (3.2). The same goes for the M16 10.9 bolts. However, no coupon test is available for this type of element. Notice that the bolts are snug tightened and no control of the preloading was performed.

Element		f_y [Mpa]	f_u [Mpa]
Web	10 [mm]	390	569
Plate	10 [mm]	310	408
	12 [mm]	305	445
	15 [mm]	275	395
	18 [mm]	420	583
Bolt	M16 10.9	968	1080

TABLE 3.2 – Timisoara material properties [**12**] and [**13**]

3.1.2 Stuttgart

This test campaign takes place in an European project about High Strength Steel in Seismic Resistant Building Frames (**HSS-SRBF**). More specifically, the purpose of this campaign was to characterise the effects of the weld type and the use of High Strength Steel (= HSS) in T-stubs. In response to this problematic, four series of tests were proposed. They are illustrated on FIGURE (3.2) and consist in unstiffened T-stubs with normal bolts (serie 100), stiffened T-stubs (serie 200), "BOX SECTION" T-stubs (serie 300) and unstiffened T-stubs with long bolts (serie 400).

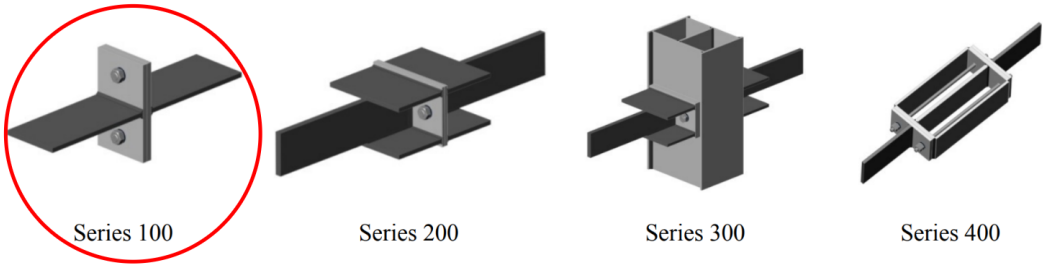

FIGURE 3.2 – Test series of Stuttgart campaign [**14**]

In this thesis, only the series 100 is presented in TABLE (3.3) and FIGURE (3.3). Each T-stubs from this series can be defined as **short** according to EuroCode. The main parameters studied are the flanges thickness, the steel grade and the weld type as expected from the project guidelines.

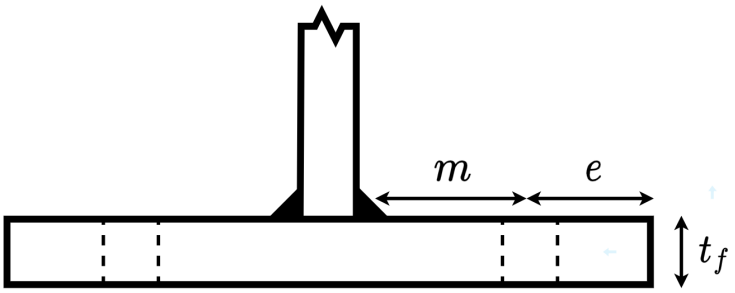

FIGURE 3.3 – Geometry of Stuttgart configuration adapted from [**14**]

Test	steel grade	t_f $[mm]$	m $[mm]$	e $[mm]$	L $[mm]$	weld type
TST-101	S460	18	85	60	100	fillet
TST-102	S460	18	85	60	100	full penetration
TST-103	S460	25	70	60	100	fillet
TST-104	S460	25	70	60	100	full penetration
TST-105	S690	15	80	70	100	fillet
TST-106	S690	15	80	70	100	full penetration
TST-107	S690	20	70	60	100	fillet
TST-108	S690	20	70	60	100	full penetration

TABLE 3.3 – Stuttgart geometrical properties [**14**]

The setup used for the campaign is depicted on FIGURE (3.4). From this FIGURE, it can be seen that six transducers were used. Two pairs were located at the flange edges in the bolt axis. Their purpose is to measure the elongation of the bolt. The last pair is positioned at the web axis at the bottom of the flange. In consequence, the evaluated displacement corresponds to the deformation of the plates.

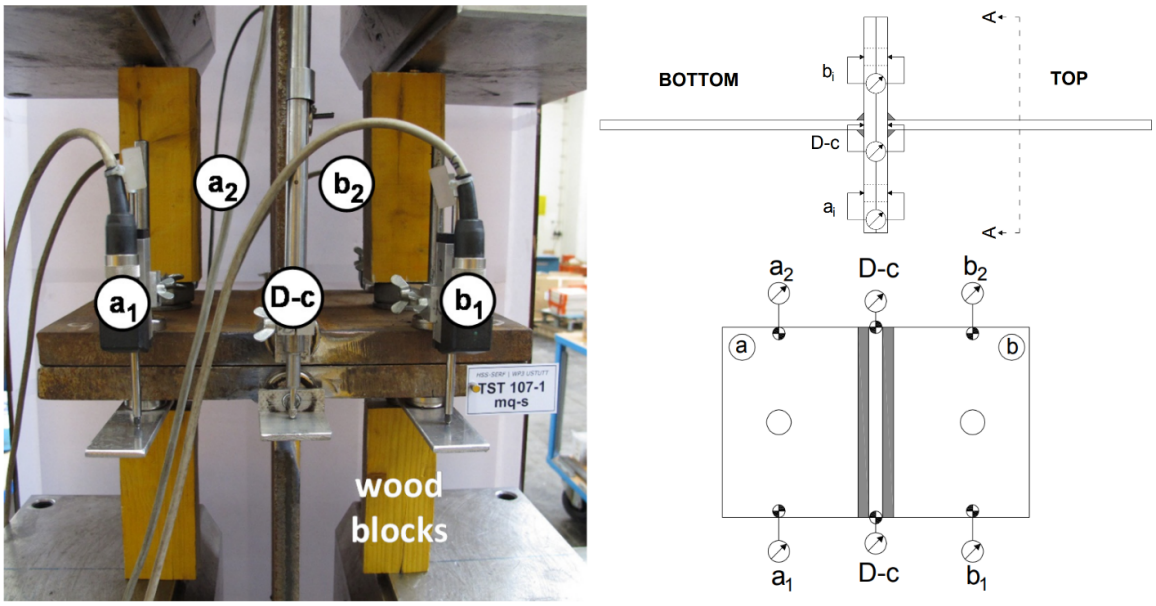

FIGURE 3.4 – Stuttgart test setup [**14**]

Finally, both plates and bolts were tested and their properties are summarised in TABLE (3.4). Moreover, for the plates, the stress-strain curves obtained from the coupon tests are available. Unfortunately, those curves are not provided for the bolts. Notice that a preloading of 70% of the bolt ultimate bearing capacity was applied on each test.

Element		f_y [Mpa]	f_u [Mpa]
S460	18 [mm]	490	633
plate	25 [mm]	469	608
S690	15 [mm]	796	823
plate	20 [mm]	801	834
Bolt	M24 x 60	/	1085
	M24 x 65	/	1,122
	M24 x 75	/	1,099
	M24 x 80	/	1,120
	M24 x 85	/	1,120

TABLE 3.4 – Stuttgart material properties [**14**]

3.1.3 Trento

Once again, the current test campaign takes place in a European project [**15**] whose purpose is to assess the robustness of a structure due to the joint ductility (**RFCS**). In this perspective, tests were performed on entire joints and some of its components. In this paper, only the tests relative to unstiffened T-stubs under axial load are presented. However, notice that some T-stubs were stiffened while some were tested under a combination of axial and shear loads.

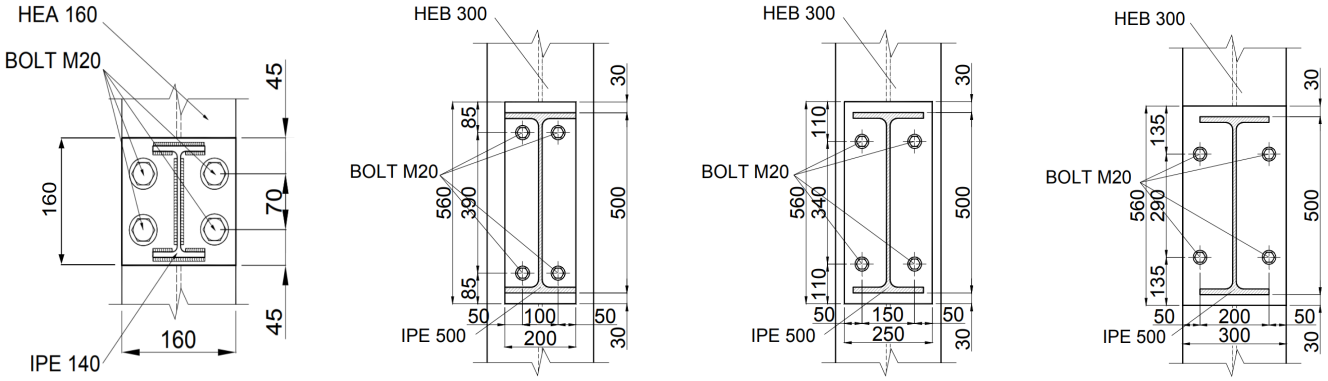

(a) CS series (b) SJBC1 series (c) SJBC2 series (d) SJBC3 series

FIGURE 3.5 – Trento test configurations [**15**]

The specimen T-stubs are issued from beam-to-column joints illustrated hereabove on FIGURE (3.5). To study the ductility of their response, some variants of those configurations were proposed. The two main parameters investigated are the length and the flange thickness. An illustration of the geometry considered can be found on FIGURE (3.6) and detailled in TABLE (3.5).

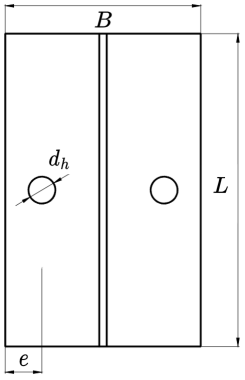

FIGURE 3.6 – Geometry of Trento configuration adapted from [**15**]

Test	B [mm]	L [mm]	e [mm]	d_h [mm]	t_f [mm]	t_w [mm]	a_w [mm]
CS-1BA	160	80	30	22	8	5	3
CS-1BB	160	256	30	22	8	5	3
CS-1BC	160	256	30	22	8	5	3
CS-1CA	160	80	30	22	9	6	10.61
CS-1CB	160	256	30	22	9	6	10.61
CS-1CC	160	256	30	22	9	6	10.61
SJBC1-5CA	300	170	100	21	19	11	19.09
SJBC1-5BAA	200	254	50	21	8	10.2	4
SJBC1-5BAB	200	254	50	21	12	10.2	4
SJBC1-5BAC	200	254	50	21	16	10.2	4
SJBC2-5CB	300	285	75	21	19	11	19.09
SJBC2-5BB	250	353	50	21	12	10.2	4
SJBC3-5CC	300	354	50	21	19	11	19.09
SJBC3-5BC	300	443	20	21	12	10.2	4

TABLE 3.5 – Trento geometrical properties [**15**]

The setup used to perform the test is shown on FIGURE (3.7) hereafter. From this illustration, four pairs of transducers can be identified. On the bolts axis are positioned three pairs. The first one is located near the bolts itself to measure their elongation. On the other hand, the two remaining pairs can be found at the flange edges. The purpose of this disposition is to evaluate the displacement at various points of the flange. Indeed, non-idealised failure mechanism are expected to appear. By consequence, the displacement near the bolts and at the flange edges are not identical. The last pair of transducers is positioned in the web plane at the bottom of the flange. Proceeding this way, only the displacement related to the plate bending deformation is measured. Notice that on the same FIGURE, it can be seen that the support was stiffened and thus, can be considered as a rigid foundation.

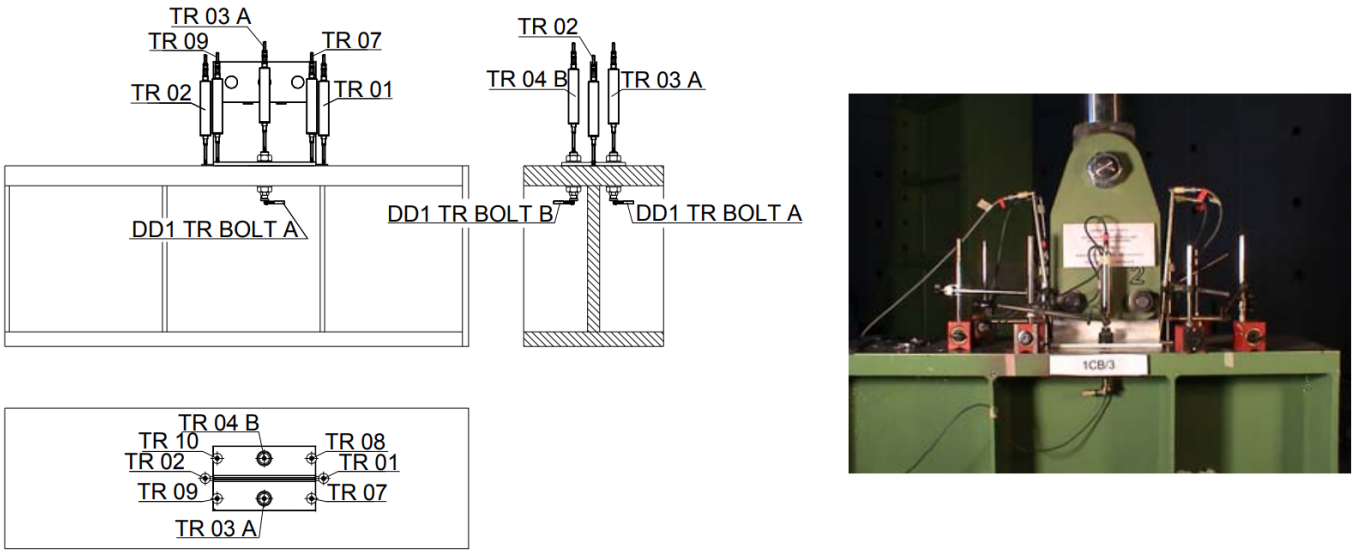

FIGURE 3.7 – Trento test setup [**15**]

As for the other campaigns, tensile tests were performed on coupon tests and the bolts. The latter properties are detailed in TABLE (3.6) herebelow. In addition to that, the stress-strain curves can be found in [**15**]. The same stands for the plates. For the CS series, the bolts used are M20 8.8 grade and may be either snug tightened, either have a 228.8 [kN] preload. The same principles apply to the SJBC series but with M20 10.9 grade and a preload of 280.1 [kN].

Test	f_y [MPa]	f_u [MPa]	E [MPa]
CS-1BA	412.5	550.9	213,324
CS-1BB	412.5	550.9	213,324
CS-1BC	412.5	550.9	213,324
CS-1CA	392.2	523.2	194,600
CS-1CB	392.2	523.2	194,600
CS-1CC	392.2	523.2	194,600
SJBC1-5CA	396.1	536.6	198,400
SJBC1-5BAA	569.3	663.4	198,800
SJBC1-5BAB	378.5	537	208,800
SJBC1-5BAC	515.9	584.4	209,100
SJBC2-5CB	396.1	536.6	198,400
SJBC2-5BB	378.5	537	208,800
SJBC3-5CC	396.1	536.6	198,400
SJBC3-5BC	378.5	537	208,800

TABLE 3.6 – Trento material properties [**15**]

3.1.4 Tongji

As explained in [**9**], the current campaign was designed to investigate various yield lines patterns and failure modes for back-to-back T-stubs either stiffened or not. The conclusions drawn by the authors are presented in SECTION (2.3.4). Notice that, for sake of concisely, only the unstiffened series are detailed hereafter.

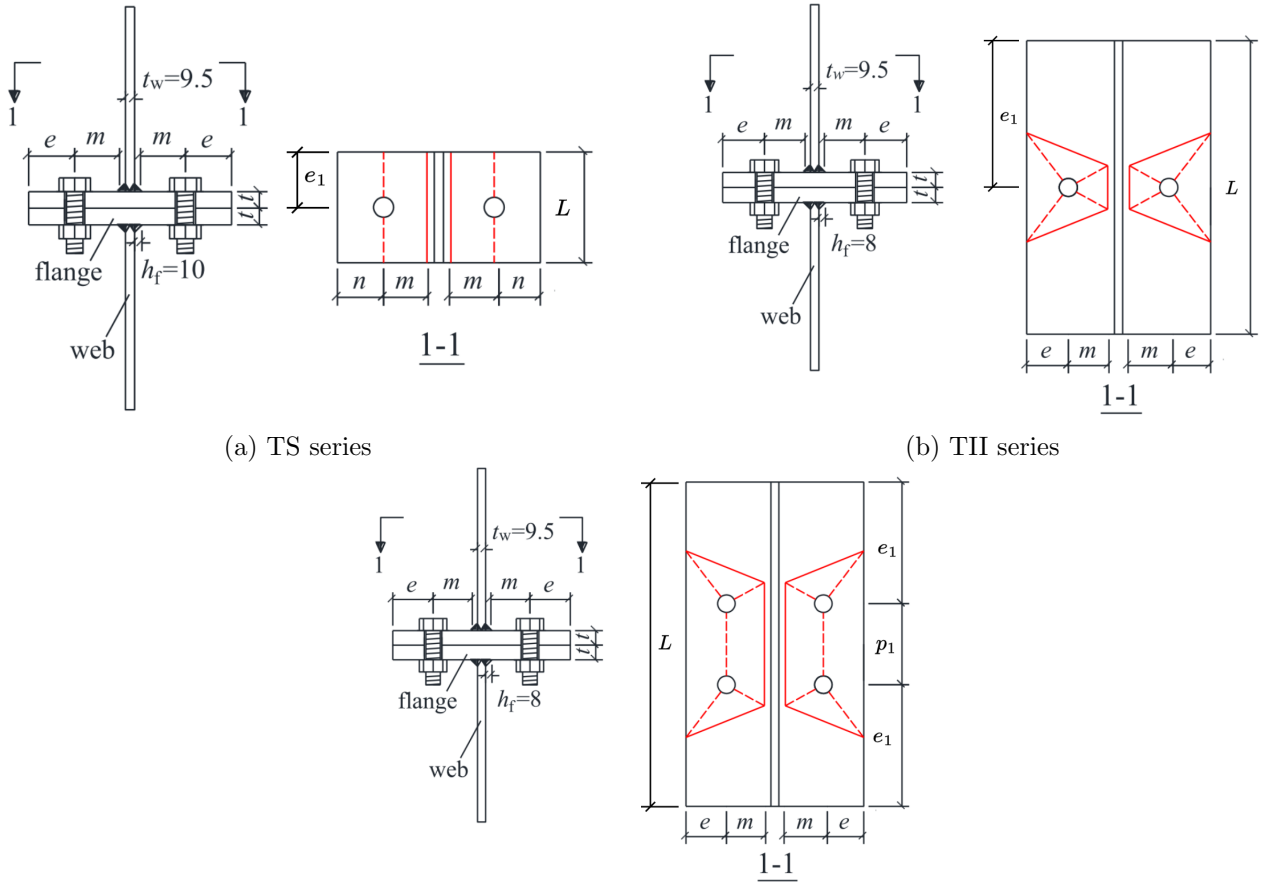

(a) TS series

(b) TII series

(c) TEG series

FIGURE 3.8 – Geometry of Tongji configuration adapted from [**9**]

On FIGURE (3.8) can be seen the TS, TII and TEG series. The first acronym stands for T-stub Standard because the specimens of this series can be considered as **short** according to the EuroCode. The other series can be characterised as non-idealised T-stubs. They represent a T-stub Inner bolt-row considered Individually (TII) and a T-stub End bolt-row in a Group (TEG). The studied parameters internal to each series are the steel grade and the bolt diameter. The specimens are named in the following way : $Series - t_f\ steel\ grade - d_b$. The full geometry is detailed in TABLE (3.7).

Test	m [mm]	h_f [mm]	e [mm]	p_1 [mm]	e_1 [mm]	L [mm]	t_f [mm]	t_w [mm]	Steel grade	Bolt
TS-17.5a-18	47.2	10	50	/	60	120	17.5	9.5	Q235	M18
TS-11.5a-18	47.2	10	50	/	60	120	11.5	9.5	Q235	M18
TS-11.5b-18	47.2	10	50	/	60	120	11.5	9.5	Q345	M18
TS-11.5b-20	47.2	10	50	/	60	120	11.5	9.5	Q345	M20
TII-9.5a-18	48.8	8	50	/	200	400	9.5	9.5	Q235	M18
TII-9.5b-18	48.8	8	50	/	200	400	9.5	9.5	Q345	M18
TII-9.5b-16	48.8	8	50	/	200	400	9.5	9.5	Q345	M16
TEG-9.5a-18	48.8	8	50	120	140	400	9.5	9.5	Q235	M18
TEG-9.5b-18	48.8	8	50	120	140	400	9.5	9.5	Q345	M18
TEG-9.5b-16	48.8	8	50	120	140	400	9.5	9.5	Q345	M15

TABLE 3.7 – Tongji geometrical properties [**9**]

The setup used for this campaign can be found in FIGURE (3.9). To measure the displacement of the T-stubs, two pairs of transducers are used. They are located in the web axis at the flanges edges to measure both flanges displacement. By consequence, the web stiffness can be disregarded when computing the T-stub force-displacement response.

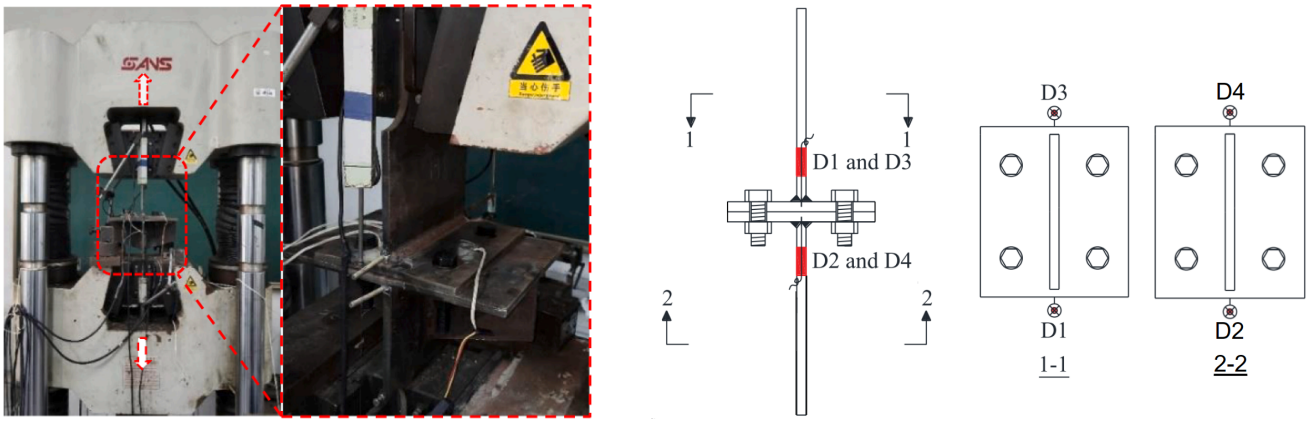

(a) Test setup (b) Transducers location

FIGURE 3.9 – Tongji test setup [**9**]

All the elements used in this campaign were tested. Their **engineering** properties can be consulted in TABLE (3.8). Notice that the true properties up to failure can be found in [**10**]. Unfortunately, no stress-strain curve can be found in both references. Concerning the bolts, a preloading is applied in each specimen. For the M16 8.8, the preload is 89 [kN] while this value is 100 and 143 [kN] for the M18 and M20 respectively.

Element		f_y [Mpa]	f_u [Mpa]	ε_u [%]	ε_f [%]
Q235	9.5 [mm]	266	417	26.4	33.6
	11.5 [mm]	274	430	27.1	35.5
	17.5 [mm]	261	453	26.4	31.6
Q345	9.5 [mm]	325	495	26.0	33.3
	11.5 [mm]	338	499	25.6	33.0
Bolt	M16	634	814	4.70	11.5
	M18	656	820	10.0	18.5
	M20	663	836	11.2	19.3

TABLE 3.8 – Tongji material properties [**9**]

3.1.5 Wuhan

In [**16**], the lacks of knowledge for T-stubs made of High-Strength Steel was highlighted. In response to that, a campaign was designed to assess the accuracy of the current models in such case. Three series depicted on the FIGURE (3.10) herebelow are proposed.

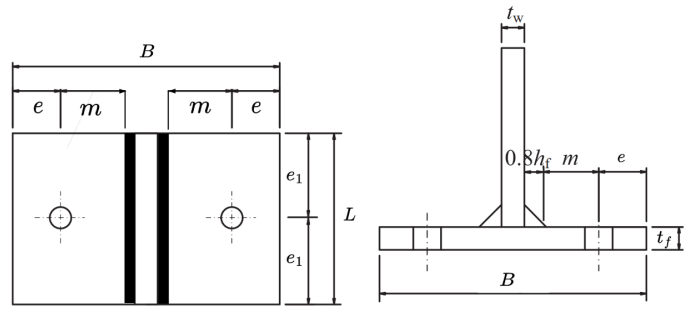

(a) TS series

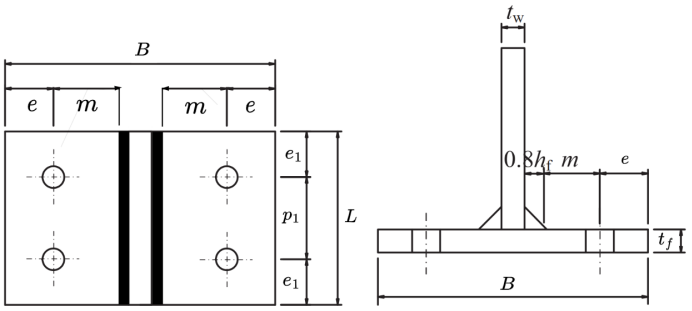

(b) TD series

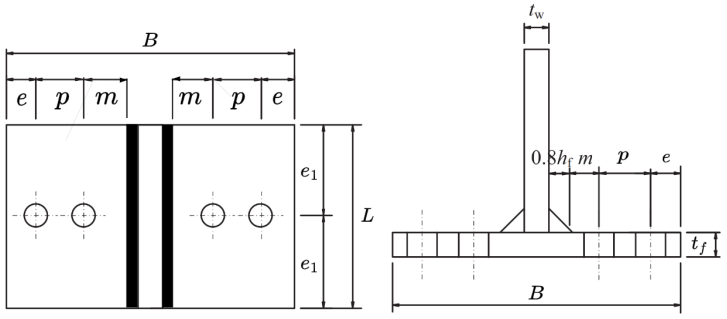

(c) TF series

FIGURE 3.10 – Geometry of Wuhan configuration adapted from [**16**]

Since the purpose of the campaign was to investigate as widely as possible the thematic of the HSS, no parameter is especially studied. This tendency can be observed in TABLE (3.10) detailing the geometry of each specimen.

Test	Steel grade	Bolt	d_b [mm]	p [mm]	e [mm]	m [mm]	p_1 [mm]	L [mm]	B [mm]	$t_f = t_w$ [mm]	h_f [mm]	Preload [kN]
T-S1	EN 1.4301	A4-70	16	/	50	50.2	/	120	222	11.85	6	59.1
T-S2	EN 1.4301	A4-80	12	/	35	65.2	/	120	222	11.85	6	27.5
T-S3	EN 1.4462	A4-80	16	/	50	50.2	/	90	222	12.58	6	58.3
T-S4	EN 1.4462	A4-80	12	/	50	53.0	/	120	222	7.72	5	21.3
T-S5	EN 1.4462	A4-80	16	/	50	53.0	/	90	222	7.72	5	59.1
T-S6	EN 1.4301	A4-80	12	/	50	53.0	/	120	222	7.85	5	30.6
T-S7	EN 1.4462	A4-80	16	/	50	53.0	/	120	222	7.72	5	56.9
T-S8	EN 1.4301	A4-70	16	/	50	50.2	/	90	222	11.85	6	56.2
T-S9	EN 1.4301	A4-80	12	/	35	65.2	/	120	222	11.85	6	1.3
T-D1	EN 1.4301	A4-70	16	/	50	50.2	70	150	222	11.85	6	44.3
T-D2	EN 1.4301	A4-80	12	/	35	65.2	70	150	222	11.85	6	29.1
T-D3	EN 1.4462	A4-70	16	/	35	68.0	70	150	222	7.72	5	53.1
T-D4	EN 1.4462	A4-70	16	/	35	65.2	70	150	222	12.58	6	48.0
T-D5	EN 1.4462	A4-70	16	/	50	50.2	70	150	222	12.58	6	45.2
T-D6	EN 1.4301	A4-80	16	/	35	65.2	70	150	222	11.85	6	45.8
T-D7	EN 1.4301	A4-80	12	/	35	65.2	54	110	222	11.85	6	29.4
T-D8	EN 1.4301	A4-80	12	/	35	65.2	70	150	222	11.85	6	1.8
T-F1	EN 1.4301	A4-70	12	50	30	73.0	/	120	322	7.85	5	23.7
T-F2	EN 1.4301	A4-70	16	50	30	70.2	/	90	322	11.85	6	36.8
T-F3	EN 1.4301	A4-80	12	40	70	40.2	/	90	322	11.85	6	23.5
T-F4	EN 1.4462	A4-80	16	50	30	70.2	/	120	322	12.58	6	39.6
T-F5	EN 1.4462	A4-80	12	50	30	73.0	/	90	322	7.72	5	29.3
T-F6	EN 1.4301	A4-70	12	50	30	70.2	/	120	322	11.85	6	23.9
T-F7	EN 1.4301	A4-80	16	50	30	70.2	/	120	322	11.85	6	34.7
T-F8	EN 1.4301	A4-70	12	50	30	70.2	/	90	322	11.85	6	25.8
T-F9	EN 1.4462	A4-80	12	50	30	73.0	/	120	322	7.72	5	27.9
T-F10	EN 1.4301	A4-80	12	40	70	40.2	/	90	322	11.85	6	1.5

TABLE 3.9 – Wuhan geometrical properties [**16**]

FIGURE (3.11) shows the setup used for experimentation. For each test, Strain Gauges (= SG) were placed where plastic hinges were expected to form. In other words, the gauges were placed at the weld toe and on the bolts axes. By proceeding this way, the rotation of the plastic hinges were measured. In addition to that, a pair of transducers was positioned at the web free end where the tension load is applied. In consequence, the deformation induced by the web deformability is taken into account in the measured displacement. Notice that due to its high stiffness in respect to the T-stub flange, the support can be considered rigid.

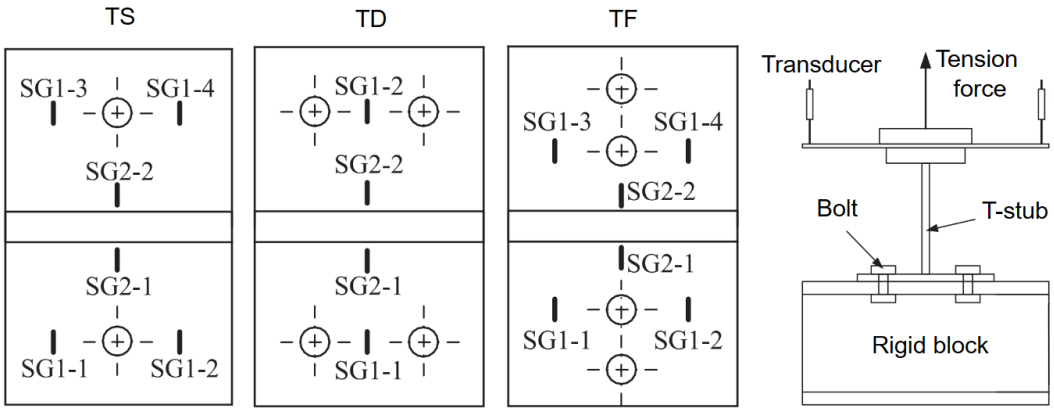

FIGURE 3.11 – Wuhan test setup [**16**]

Finally, coupon tests were performed for both plates and bolts. The properties determined may be consulted in TABLE (3.10). The stress-strain curves related to those tests are available in the reference [**16**].

Element	t_f or d_b [mm]	ν [-]	E [Mpa]	f_y [Mpa]	f_u [Mpa]	ε_u [%]	ε_f [%]
EN 1.4301	7.85	0.257	180,700	291.7	706.0	/	62.9
EN 1.4301	11.85	0.258	182,800	280.4	719.6	/	57.7
EN 1.4462	7.72	0.207	188,700	551.4	738.4	19.3	33.0
EN 1.4462	12.58	0.226	184,000	464.6	705.3	23.3	37.4
A4-70	12	/	175,400	522.6	758.1	8.5	36.5
A4-70	16	/	173,000	484.6	732.7	26.0	44.9
A4-80	12	/	184,500	553.9	794.0	5.9	29.7
A4-80	16	/	175,300	524.4	765.4	9.8	33.4

TABLE 3.10 – Wuhan material properties [**16**]

3.1.6 London

The last campaign to be presented is proposed by Faralli in [**17**]. In her paper, Faralli emphasizes the need to investigate geometrical second order effects. Remind that the same conclusion was drawn in SECTION (2.4). To study those effects, a test campaign was designed. A representation of the specimens geometry can be found on FIGURE (3.12) hereafter.

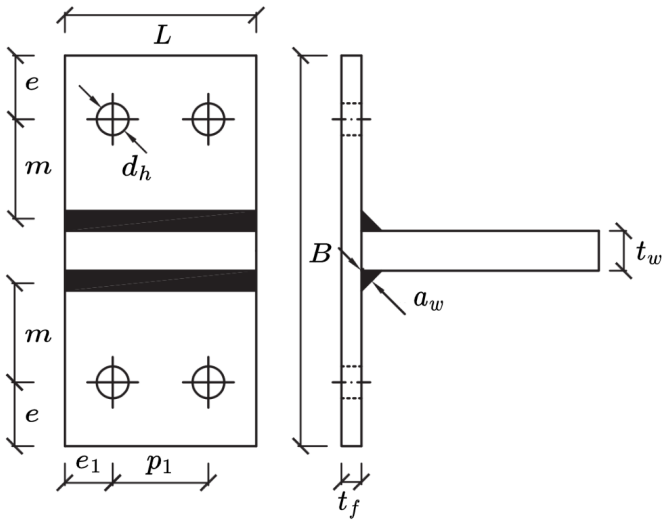

FIGURE 3.12 – Geometry of London configuration adapted from [**17**]

In addition to that, TABLE (3.11) contains the values of the previously illustrated configuration. Notice that the support thickness is denoted as T. As suggested by their denomination, the mains studied parameters are the flange thickness, the bolt diameter and a dimensionless ratio assessing the T-stub relative stiffness between the plate and the bolt ($\mathrm{M}d_b - m/d_b - t_f$). The steel grade used is S275 while the bolts are 10.9. As expected, those elements were tested to evaluate their real properties. The stress-strain curves of both plates and bolts can be consulted in [**17**]. Notice that due to its relatively high stiffness with respect to the plates in bending, the support can be assumed rigid. In consequence, shear tests were also performed on the bolts. No information is provided if the bolts are snug tightened or preloaded.

Specimen	t_f [mm]	t_w [mm]	a_w [mm]	e [mm]	m [mm]	e_1 [mm]	B [mm]	L [mm]	p_1 [mm]	d_h [mm]	T [mm]
M16-3-10	10.1	19.6	7.1	31.9	47.2	23.4	196	96	48	17.8	25
M16-5-10	10.15	19.7	7.1	31.8	77.7	24.2	260	96	48	18.3	25
M16-5-15	15.2	19.8	7.1	31.5	77.1	23.6	260	96	48	17.7	25
M18-3-10	10.2	19.6	7.1	36.1	51.6	26.8	216	108	54	20.1	25
M18-5-10	10.2	19.7	7.1	34.3	90.3	26.7	288	108	54	19.5	25
M18-4-15	15.2	19.9	7.1	36.5	67.1	25.6	252	108	54	19.7	25
M18-5-15	15.3	19.7	7.1	37.1	87.6	25.3	288	108	54	19.5	25
M20-3-10	9.9	20.4	10	39.2	60.2	30	242.4	120	60	22	25
M20-5-10	9.9	20.5	10	39.5	92.6	26.6	322.4	120	60	22	25
M20-4-15	15.2	20.5	10	39.4	77.5	30.2	282.4	120	60	21.8	25
M20-5-15	15.3	20.7	10	40.2	98.4	31.2	322.4	120	60	22.9	25
M20-4-20	19.75	20.5	10	39.3	75.2	29.7	282.4	120	60	21.9	30
M20-5-20	19.7	20.4	10	39.9	96.4	28.8	322.4	120	60	22	30

TABLE 3.11 – London geometrical properties [**17**]

Finally, the test setup is illustrated on FIGURE (3.13). This FIGURE shows that no transducer or strain gauge was used to measure the displacement. In current campaign, the method consists in using the machine displacement imposed at the web free end. By consequence, when computing the displacement with models of SECTION (2.3), the web stiffness should be taken into account. For some tests, a full-field strain mapping was applied on the lateral face of the specimen. With this method, the displacement of each point of the mapping can be accurately captured during the test. By consequence, the rotation of the plastic hinges can be measured as well.

(a) Test setup (b) Full-field strain mapping

FIGURE 3.13 – London test setup [**17**]

3.2 Selected experimental campaigns

In the previous SECTION, various test campaigns found in the literature were presented. However, they are not all relevant when studying **short unstiffened back-to-back T-stubs with one bolt row and made of mild steel welded plates**. Thus, a sort should be performed. Considering the criterion that the foundation should not be rigid, half of the campaigns should be disregarded. Remains only campaigns from Timisoara, Tongji and Stuttgart. However, the last one cannot be used either since the T-stubs are made of High-Strength Steel. In addition to that, in Tongji campaign, three series were presented. The first one consists in short T-stubs while the other two are long. In conclusion, the tests that met all the selected criteria are issued from Timisoara test campaign and from the TS series of Tongji. Those fifteen tests are highlighted in their respective TABLES.

An application of the models presented in SECTION (2.3) on those tests is proposed hereafter. Notice that, since it was essentially developed for T-stubs on rigid foundation, the Francavilla model is not implemented. In addition to that, Piluso model is not considered when the collapse is a mode 2. Indeed, the current thesis focuses mainly on mode 1. Considering that another implementation is required for Piluso second mode and that the results are expected to be unsafe [**9**], it was decided to neglect this model for this type of failure.

3.2.1 Timisoara test campaign

a) T-10-16-100

The first test to be investigated is the T-10-16-100. The results can be consulted on the following FIGURE (3.14) and TABLE (3.12). The most noticeable observation that can be done from this test is that the predicted resistance is far underestimated both at failure and yielding. On the other hand, it can be seen that the initial stiffness is correctly estimated in general. Piluso model is the only one that underestimates this value. The results found for the ultimate displacement are also quite unexpected. Indeed, in [**9**], Jaspart model was concluded to be "too conservative" and the opposite for the Piluso model. However, the exact opposite can be observed on the FIGURE. To ensure the reader the accuracy of the proposed results, a worked example of each model for this specimen is developed in APPENDIX (A).

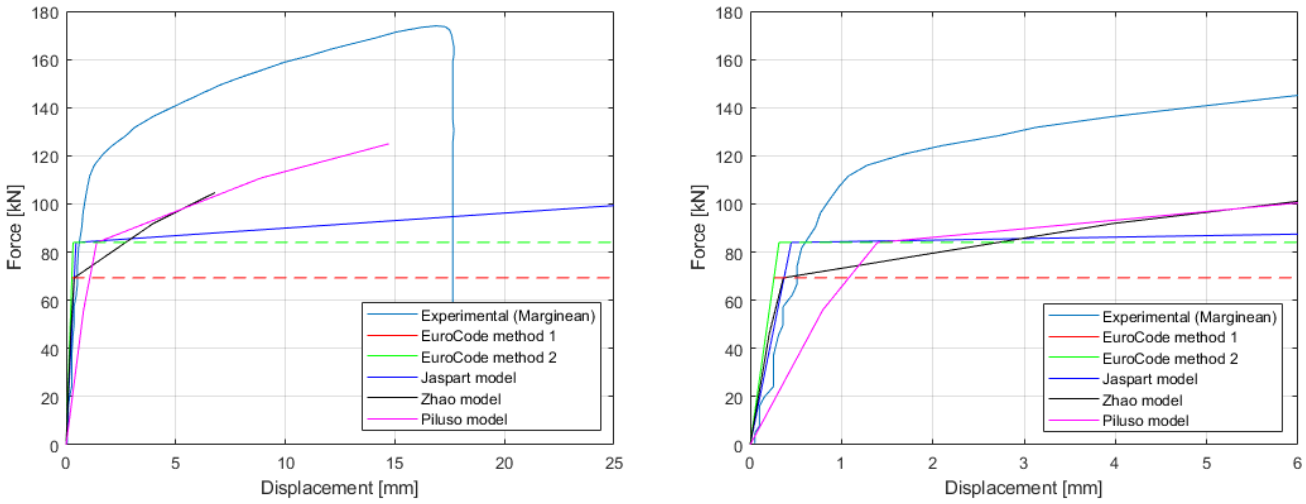

(a) Global response (b) Zoom on the elastic response

FIGURE 3.14 – Force-displacement curve of specimen T-10-16-100

Authors	mode	$K_{1stub,init}$ [kN/mm]	F_y [kN]	Rel. error [%]	F_u [kN]	Rel. error [%]	Δ_u [mm]	Rel. error [%]
Experimental	1	125.29	119.9	/	173.9	/	16.9	/
EC method 1	1	133	69.3	-42.2	/	/	/	/
EC method 2	1	133	84	-29.9	/	/	/	/
Jaspart	1	93.3	84	-29.9	110.56	-36.4	43	+155
Piluso	1	70.4	84	-29.9	124.9	-28.1	14.7	-12.8
Zhao	1-FF	219.3	69.3	-42.2	104.67	-39.8	6.8	-59.8

TABLE 3.12 – Characterisation of specimen T-10-16-100

To help the reader to interpret the results, an arbitrary color code is used. Four ranges of relative errors are proposed. The first three are 5% wide each and begin at 0 for the best, improvable and insufficient one respectively. The last one is unbounded and contains all the incorrect predictions. However, pay attention that when comparing small numbers, the relative error obtained may lead to misinterpret the results. An example of this affirmation can be found in the previous TABLE. While the ultimate displacement found by Piluso tends to be classified as insufficient, the absolute error is 2.2 [mm] which is a good prediction. By consequence, the relative error should systematically be compared to the absolute error to avoid misinterpretation of the results. Unfortunately, both could not be presented in the characterisation TABLES for sake of readability. Notice that the color code is kept for the entire thesis.

b) T-10-16-120

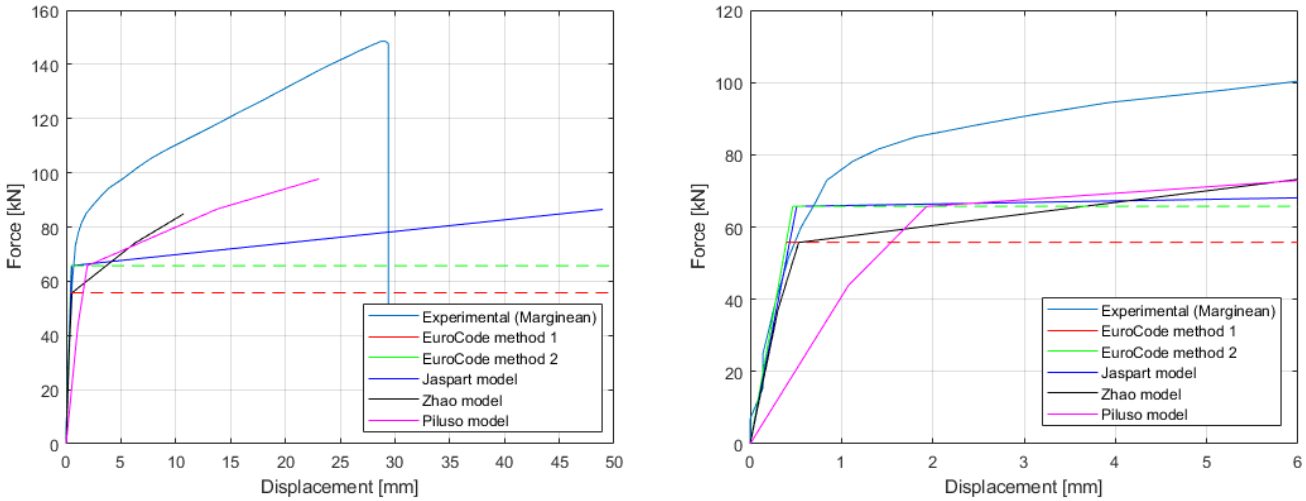

(a) Global response (b) Zoom on the elastic response

FIGURE 3.15 – Force-displacement curve of specimen T-10-16-120

Authors	mode	$K_{1stub,init}$ [kN/mm]	F_y [kN]	Rel. error [%]	F_u [kN]	Rel. error [%]	Δ_u [mm]	Rel. error [%]
Experimental	1	87.3	87.15	/	148.5	/	29.1	/
EC method 1	1	70.5	55.76	-36	/	/	/	/
EC method 2	1	70.5	65.7	-24.6	/	/	/	/
Jaspart	1	64.5	65.7	-24.6	86.5	-41.7	48.7	+67.1
Piluso	1	40.7	65.7	-24.6	97.76	-34.2	23	-20.9
Zhao	1-FF	121.9	55.7	-36	84.9	-42.8	10.7	-63.1

TABLE 3.13 – Characterisation of specimen T-10-16-120

FIGURE (3.15) and TABLE (3.13) show the results for the second specimen. Surprisingly, the tendency deduced from the first specimen can also be observed for this test.

c) T-10-16-140

Identical conclusions can be drawn of the T-10-16-140 specimen illustrated on FIGURE (3.16). A slights increase of the strength at the end of the experimental curve tends to indicate the apparition of membrane effects in this test. However, this contribution is neglected as previously explained. TABLE (3.14) summarises the performances of the models for this specimen.

Authors	mode	$K_{1stub,init}$ [kN/mm]	F_y [kN]	Rel. error [%]	F_u [kN]	Rel. error [%]	Δ_u [mm]	Rel. error [%]
Experimental	1	102	77.2	/	155	/	42.9	/
EC method 1	1	40.5	46	-40.4	/	/	/	/
EC method 2	1	40.5	53.3	-31	/	/	/	/
Jaspart	1	46.2	53.3	-31	70.12	+54.8	55.1	+28.4
Piluso	1	25.1	53.2	-31	79.2	-48.9	33.5	-21.8
Zhao	1-FF	72	46	-40.5	70.8	-54.3	15.7	-63.4

TABLE 3.14 – Characterisation of specimen T-10-16-140

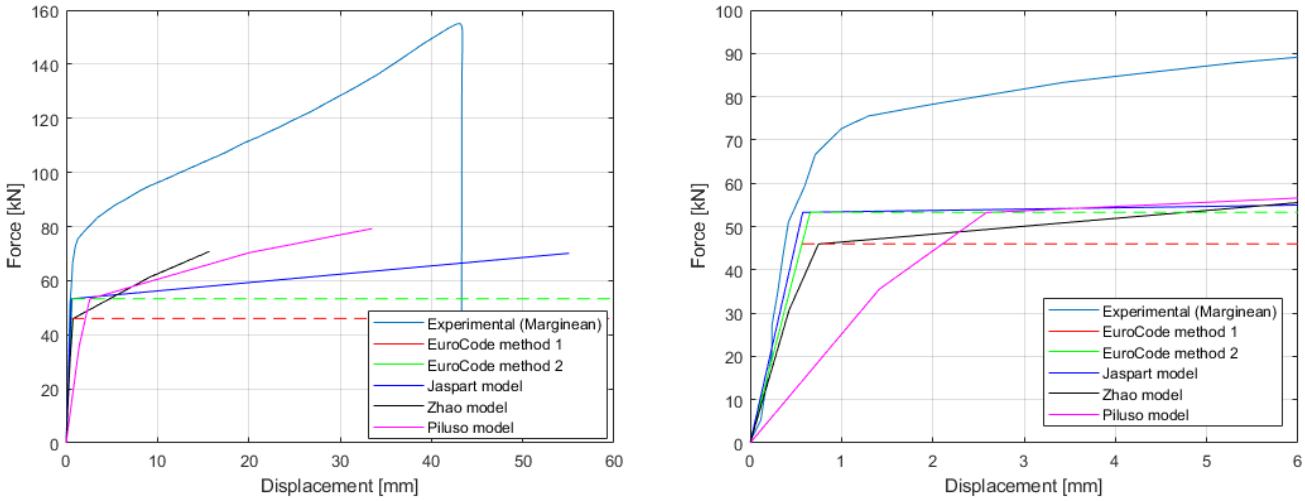

(a) Global response (b) Zoom on the elastic response

FIGURE 3.16 – Force-displacement curve of specimen T-10-16-140

d) T-12-16-100

The T-stubs of the second series have thicker flanges than in the previous tests. The narrowest of this series is illustrated on FIGURE (3.17). To begin with, Piluso is the only model to mischaracterise the current specimen as a **mode 2**. Concerning the strength, both plastic and ultimate resistances are slightly underestimated as highlighted by TABLE (3.15). Similarly to the previous tests, the assessment of the initial stiffness is well performed. Zhao model gives a good approximation of the post-yielding behaviour. In opposition to that, the same pathology as before is contemplated for Jaspart model.

Authors	mode	$K_{1stub,init}$ [kN/mm]	F_y [kN]	Rel. error [%]	F_u [kN]	Rel. error [%]	Δ_u [mm]	Rel. error [%]
Experimental	1	240	136.45	/	184.87	/	9.3	/
EC method 1	1	223.4	103.08	-24.5	/	/	/	/
EC method 2	1	223.4	124.9	-8.5	/	/	/	/
Jaspart	1	167.3	124.9	-8.5	182.2	-1.5	49.2	+426.3
Zhao	1-FF	332.4	103	-24.5	167.44	-9.4	6.5	-30.3

TABLE 3.15 – Characterisation of specimen T-12-16-100

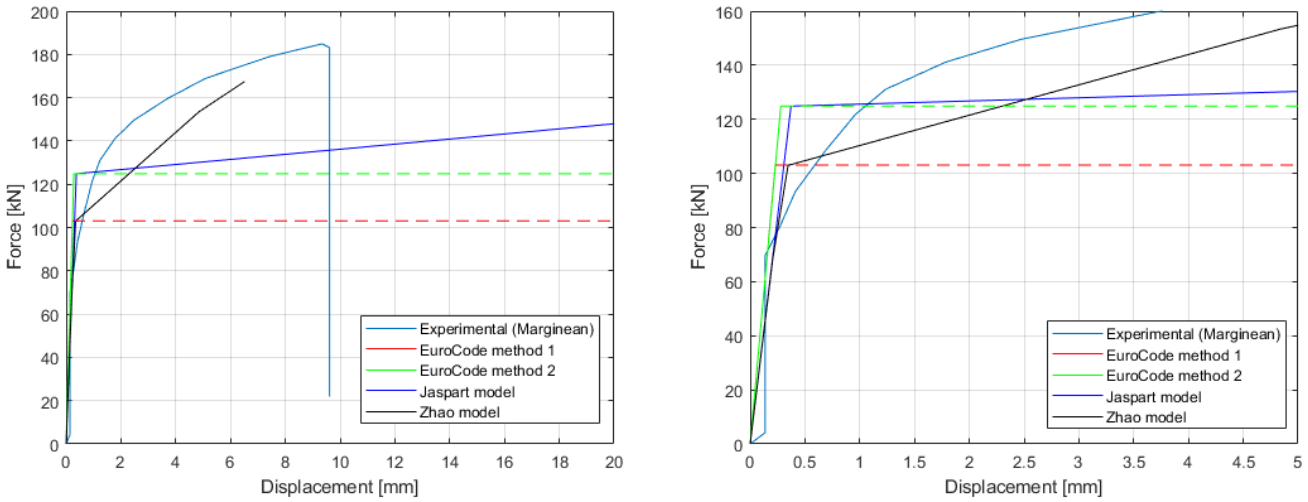

(a) Global response (b) Zoom on the elastic response

FIGURE 3.17 – Force-displacement curve of specimen T-12-16-100

e) T-12-16-120

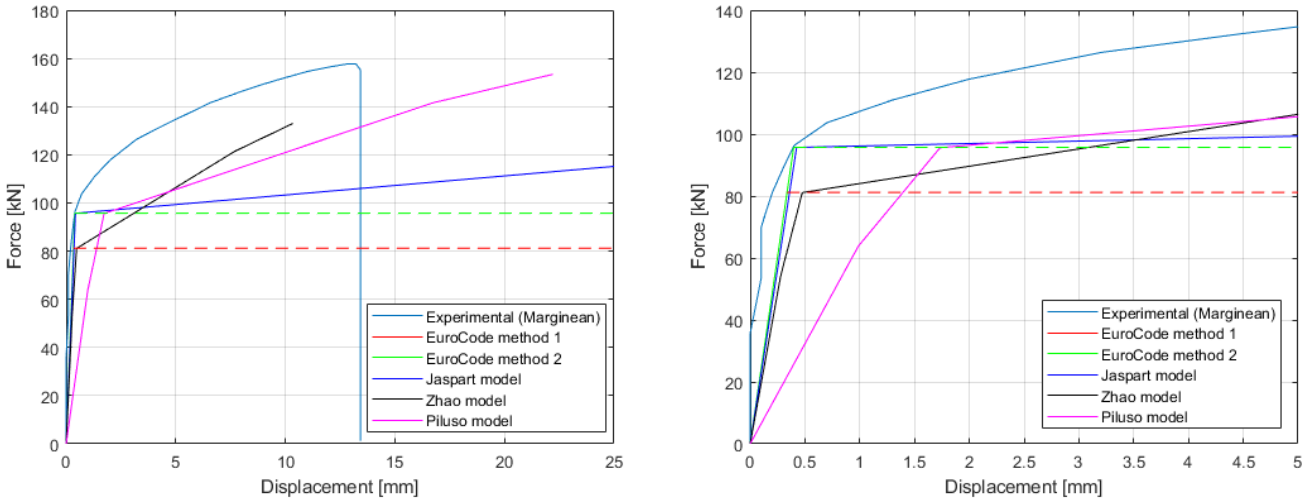

(a) Global response (b) Zoom on the elastic response

FIGURE 3.18 – Force-displacement curve of specimen T-12-16-120

Authors	mode	$K_{1stub,init}$ [kN/mm]	F_y [kN]	Rel. error [%]	F_u [kN]	Rel. error [%]	Δ_u [mm]	Rel. error [%]
Experimental	1	381.9	118.5	/	157.67	/	13.2	/
EC method 1	1	120.6	81.2	-31.5	/	/	/	/
EC method 2	1	120.6	95.7	-19.2	/	/	/	/
Jaspart	1	112.9	95.7	-19.2	139.62	-11.4	55.9	+322.3
Piluso	1	65.6	95.6	-19.2	153.4	-2.7	22.2	+67.9
Zhao	1-FF	194.3	81.1	-31.6	133	-15.7	10.3	-21.8

TABLE 3.16 – Characterisation of specimen T-12-16-120

FIGURES (3.18) and (3.19) show respectively the results obtained for the T-12-16-160 and T-12-16-140 specimens. Concerning the resistance and the initial stiffness, the exact same observations can be done. Once again, Zhao model gives a good prediction of the hardening stiffness of the T-stubs. On the other hand its prediction of the ultimate displacement tends to be too conservative. Jaspart models still overestimates the displacement reached at failure. In opposition to the previous series, the predictions made by Piluso are here unconservative. TABLES (3.16) and (3.17) summarises the results obtained for those tests.

f) T-12-16-140

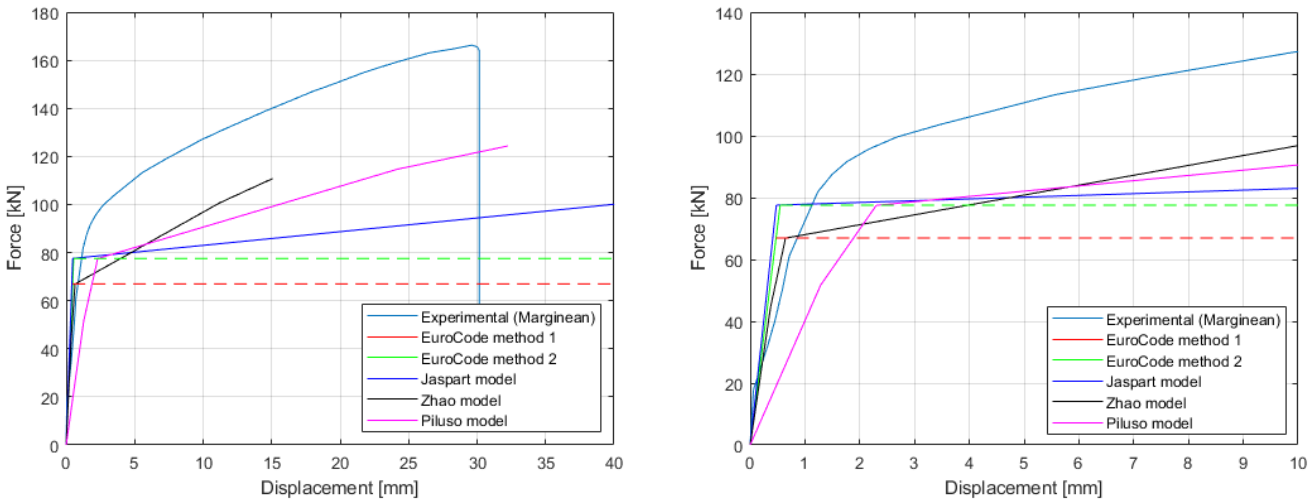

(a) Global response (b) Zoom on the elastic response

FIGURE 3.19 – Force-displacement curve of specimen T-12-16-140

Authors	mode	$K_{1stub,init}$ [kN/mm]	F_y [kN]	Rel. error [%]	F_u [kN]	Rel. error [%]	Δ_u [mm]	Rel. error [%]
Experimental	1	68.7	98	/	166.26	/	29.6	/
EC method 1	1	70.7	67	-31.7	/	/	/	/
EC method 2	1	70.7	77.6	-20.9	/	/	/	/
Jaspart	1	81.1	77.6	-20.9	113.17	-31.9	63	+112.5
Piluso	1	40.2	77.5	-20.9	124.34	-25.2	32.3	+8.8
Zhao	1-FF	119.6	66.9	-31.8	110.8	-33.4	15.1	-49.1

TABLE 3.17 – Characterisation of specimen T-12-16-140

g) T-15-16-100

The third series consists in the same geometries with 15 [mm] thick plates. The results associated to those tests can be seen in FIGURES (3.20), (3.21) and (3.22) herebelow. Those tests are at the verge of transition between collapse modes 1 and 2. Indeed, Piluso characterises all these specimens as mode 2. For specimen T15-16-100, depending if either method 1 or 2 is used, a mode 1 or 2 is respectively predicted. Otherwise, the same general observations remain valid : a good estimation is made for the initial stiffness while the resistance is underestimated. Jaspart model still provides a far overestimated ultimate displacement.

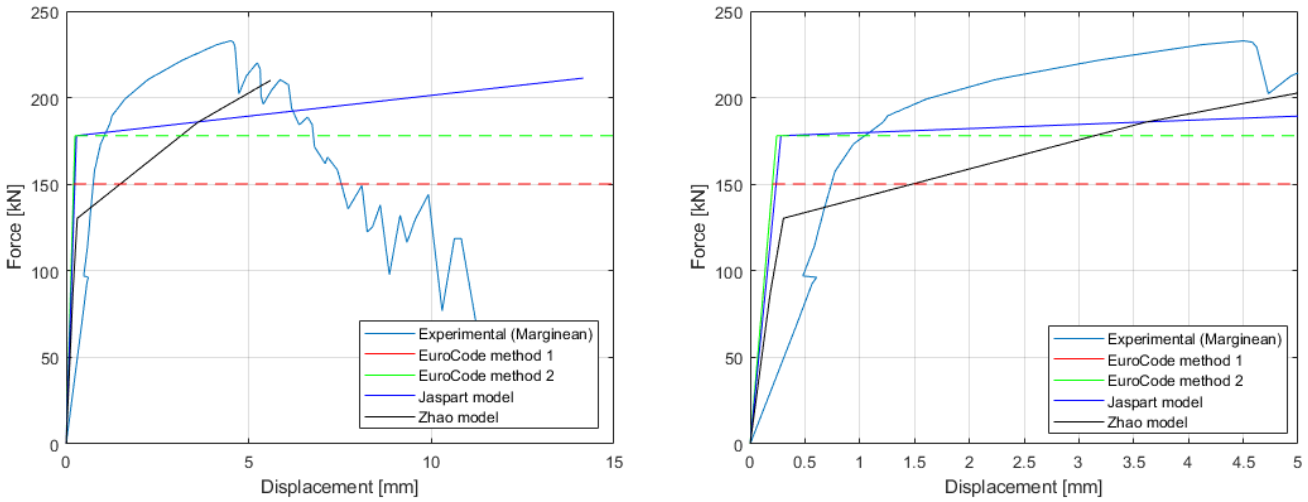

(a) Global response (b) Zoom on the elastic response

FIGURE 3.20 – Force-displacement curve of specimen T-15-16-100

Authors	mode	$K_{1stub,init}$ [kN/mm]	F_y [kN]	Rel. error [%]	F_u [kN]	Rel. error [%]	Δ_u [mm]	Rel. error [%]
Experimental	2	186.2	179.1	/	232.84	/	4.5	/
EC method 1	1-2	367	150.2	-16.1	/	/	/	/
EC method 2	2	367	178	-0.6	/	/	/	/
Jaspart	2	316.7	178	-0.6	211.31	-9.2	14.2	+214.8
Zhao	2	476.2	130.35	-27.2	210	-14.6	5.6	+24.4

TABLE 3.18 – Characterisation of specimen T-15-16-100

Similarly to what was previously done, TABLES containing all the characteristic values obtained by both models and experimental tests are proposed. For specimen T-15-16-100, the TABLE (3.18) can be found above. For the two remaining tests, their related TABLES (3.19) and (3.20) can be consulted hereafter.

h) T-15-16-120

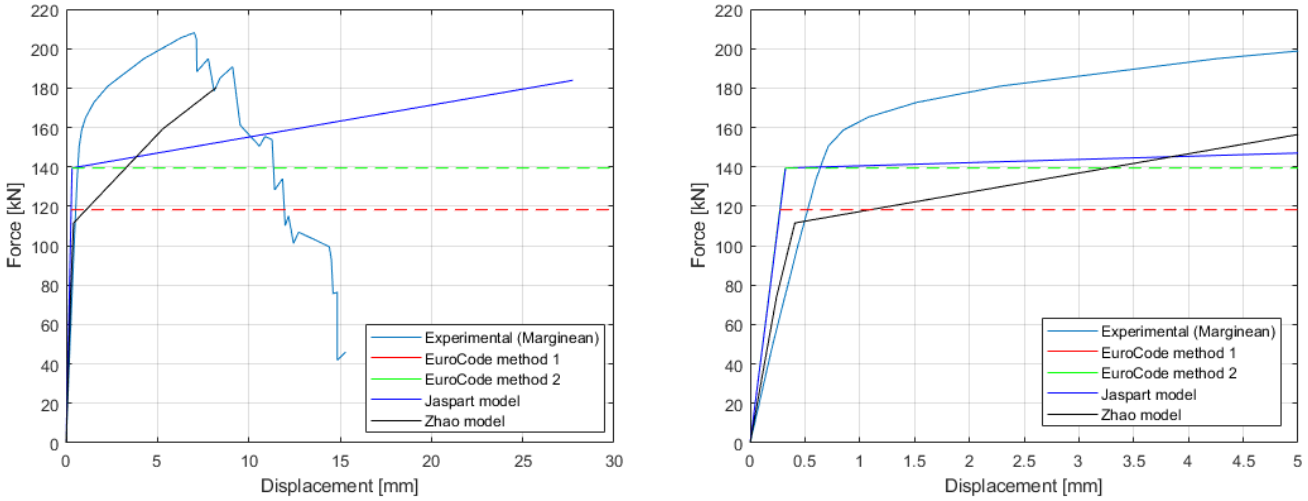

(a) Global response (b) Zoom on the elastic response

FIGURE 3.21 – Force-displacement curve of specimen T-15-16-120

Authors	mode	$K_{1stub,init}$ [kN/mm]	F_y [kN]	Rel. error [%]	F_u [kN]	Rel. error [%]	Δ_u [mm]	Rel. error [%]
Experimental	1-2	218.2	162.1	/	208.06	/	7	/
EC method 1	1	218.1	118.3	-27	/	/	/	/
EC method 2	1-2	218.1	139.4	-14	/	/	/	/
Jaspart	1-2	216	139.4	-14	183.9	-11.6	27.7	+295.2
Zhao	1-BR	307.8	111.5	-31.2	180.34	-16.2	8.2	+17.2

TABLE 3.19 – Characterisation of specimen T-15-16-120

i) T-15-16-140

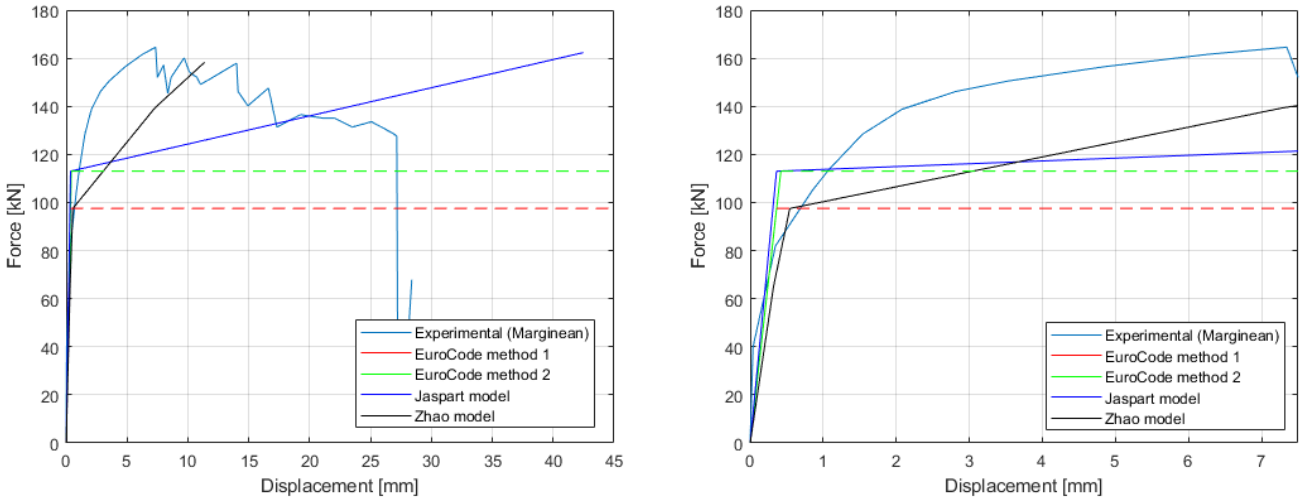

(a) Global response (b) Zoom on the elastic response

FIGURE 3.22 – Force-displacement curve of specimen T-15-16-140

Authors	mode	$K_{1stub,init}$ [kN/mm]	F_y [kN]	Rel. error [%]	F_u [kN]	Rel. error [%]	Δ_u [mm]	Rel. error [%]
Experimental	1-2	246.4	138	/	164.6	/	7.3	/
EC method 1	1	134.6	97.6	-29.3	/	/	/	/
EC method 2	1	134.6	113	-18.1	/	/	/	/
Jaspart	1	156.4	113	-18.1	162.33	-1.4	42.5	+478.2
Zhao	1-BR	203.2	97.5	-29.3	158.3	-5.6	11.4	+54.7

TABLE 3.20 – Characterisation of specimen T-15-16-140

j) T-18-16-120

In the last series, the plates thickness is increased up to 18 [mm]. Due to this reason, the failures observed was mode 2. It can be seen from FIGURES (3.23) and (3.24) that the collapse mode was correctly predicted in each model. Another property accurately assessed is the plastic resistance. However, this observation does not stand at failure, the expected failure strength is either underestimated in Zhao model, either overestimated in Jaspart model. Concerning the displacement at failure, this value is overestimated in each model. However, the post-yielding is not significant for mode 2. From a design perspective, such a failure mode is considered brittle and only the properties at yielding are required. Considering that the stiffness is correctly predicted like for the previous tests, it can be conclude that mode 2 are well predicted by the models.

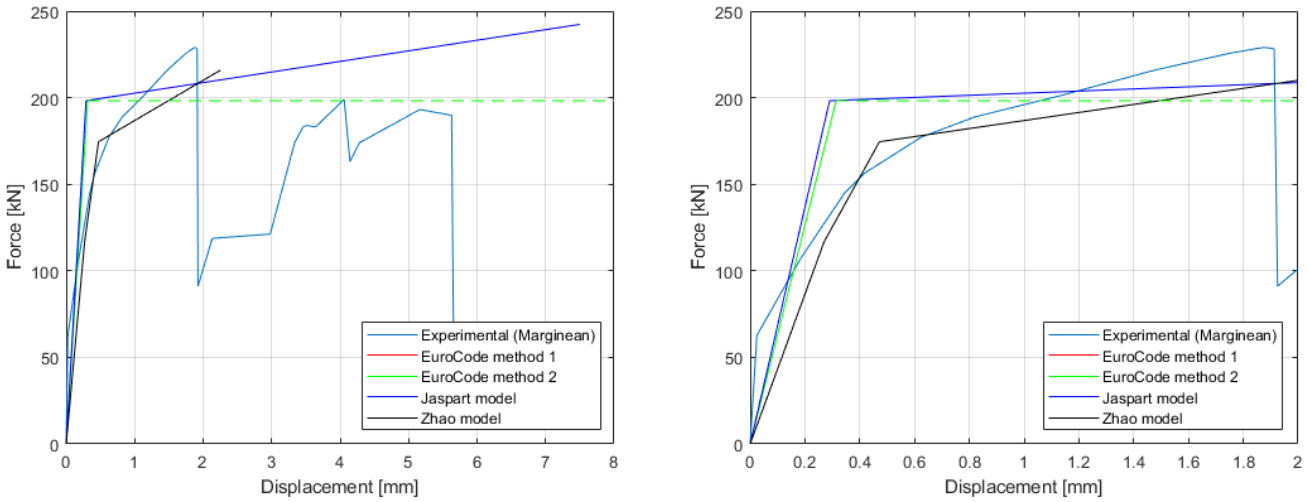

(a) Global response (b) Zoom on the elastic response

FIGURE 3.23 – Force-displacement curve of specimen T-18-16-120

Authors	mode	$K_{1stub,init}$ [kN/mm]	F_y [kN]	Rel. error [%]	F_u [kN]	Rel. error [%]	Δ_u [mm]	Rel. error [%]
Experimental	2	465.4	200	/	229.1	/	1.9	/
EC method 1	2	315.8	198.3	-0.9	/	/	/	/
EC method 2	2	315.8	198.3	-0.9	/	/	/	/
Jaspart	2	341.3	198.3	-0.9	242.35	+5.8	7.5	+299.9
Zhao	2	432.8	174.5	-12.25	215.87	-5.8	2.25	+18.4

TABLE 3.21 – Characterisation of specimen T-18-16-120

TABLES (3.21) and (3.22) illustrate the results for the narrowest and the widest T-stubs respectively. Notice that those specimens are good examples of how the relative error may lead to misinterpretation. For both tests, the ultimate displacement computed according to Zhao makes little absolute error. However, they may be considered terribly wrong when looking only at the relative error.

k) T-18-16-140

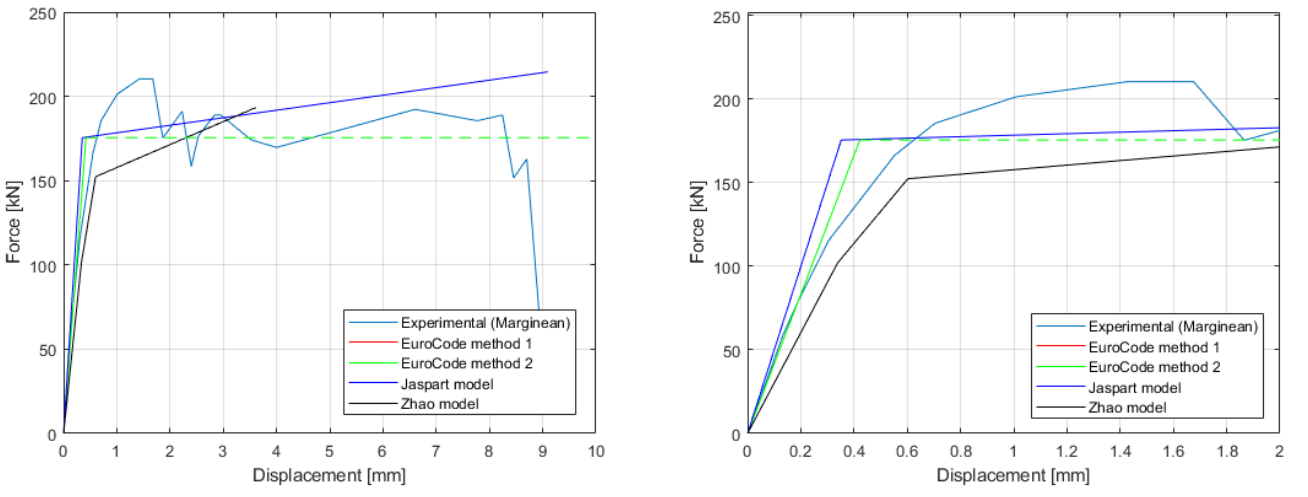

(a) Global response (b) Zoom on the elastic response

FIGURE 3.24 – Force-displacement curve of specimen T-18-16-140

Authors	mode	$K_{1stub,init}$ [kN/mm]	F_y [kN]	Rel. error [%]	F_u [kN]	Rel. error [%]	Δ_u [mm]	Rel. error [%]
Experimental	2	395.5	180	/	210.41	/	1.7	/
EC method 1	2	207.8	175.5	-2.5	/	/	/	/
EC method 2	2	207.8	175.5	-2.5	/	/	/	/
Jaspart	2	249.2	175.5	-2.5	214.52	+2	9.1	+442.8
Zhao	2	300.9	152.3	-2.2	193.4	-8.1	3.6	+111.8

TABLE 3.22 – Characterisation of specimen T-18-16-140

3.2.2 Tongji test campaign

a) T-17.5a-18

The TS series consists in four short T-stubs. The first one is illustrated in FIGURE (3.25) and TABLE (3.23). It can be seen that the initial stiffness is well estimated. Similarly, the models make a small error when assessing the strength and the mode. Zhao model is an exception to this observation and drastically underestimates the plastic strength. Concerning the ultimate displacement, none of the models makes a correct prediction.

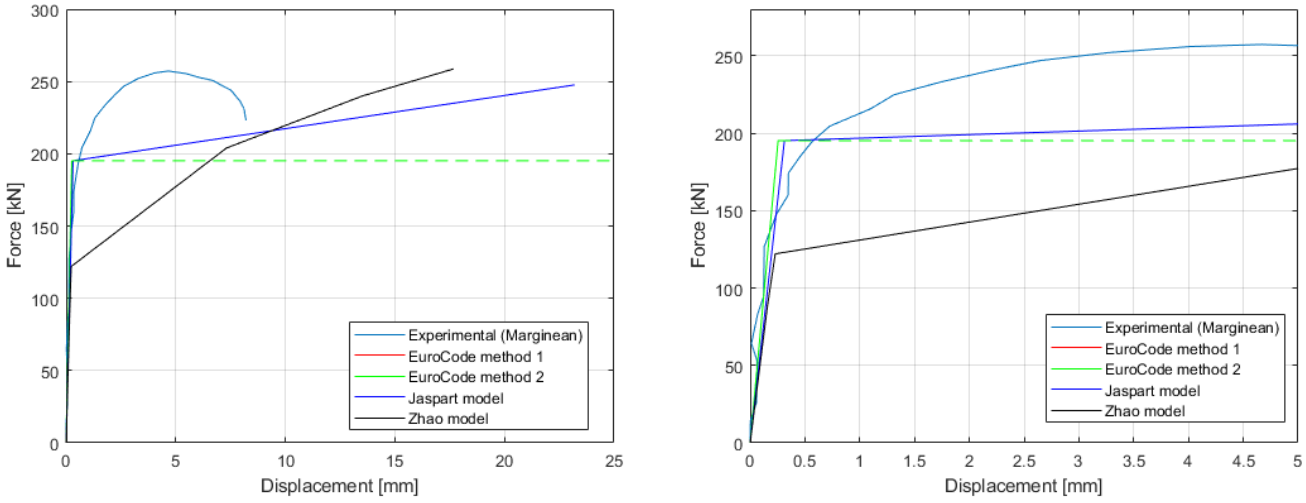

(a) Global response (b) Zoom on the elastic response

FIGURE 3.25 – Force-displacement curve of specimen T-17.5a-18

Authors	mode	$K_{1stub,init}$ [kN/mm]	F_y [kN]	Rel. error [%]	F_u [kN]	Rel. error [%]	Δ_u [mm]	Rel. error [%]
Experimental	2	572.6	200	/	257.2	/	4.7	/
EC method 1	2	381.9	195.1	-2.5	/	/	/	/
EC method 2	2	381.9	195.1	-2.5	/	/	/	/
Jaspart	2	311.5	195.1	-2.5	247.63	-3.7	23.2	+397.5
Zhao	2	560.6	122	-39	258.7	+0.6	17.7	+279.1

TABLE 3.23 – Characterisation of specimen T-17.5a-18

b) T-11.5a-18

The remaining tests are expected to be mode 1. All the results have similar tendency. Thus, a unique analysis is proposed for sake of concisely and avoid repetitions. Moreover, the tendency observed is identical to the one exhibited by Timisoara test campaign in Section (3.2.1). Models fail to give good prediction of the T-stub response both at yielding and failure. Only the initial stiffness seems to be well assessed. It is important to notice that Zhao model gives relatively good results in comparison to the other models. However, caution is required. Indeed, as explained in Section (2.3.4), it requires some hardening and necking properties of the material that can only be obtained through coupon tests. Although those values are provided by the authors in [**10**], it is not the case of the stress-strain curves of the coupons. Thus, those values could not be rigorously validated. In addition to that, the authors do not describe the procedure followed to obtain those properties.

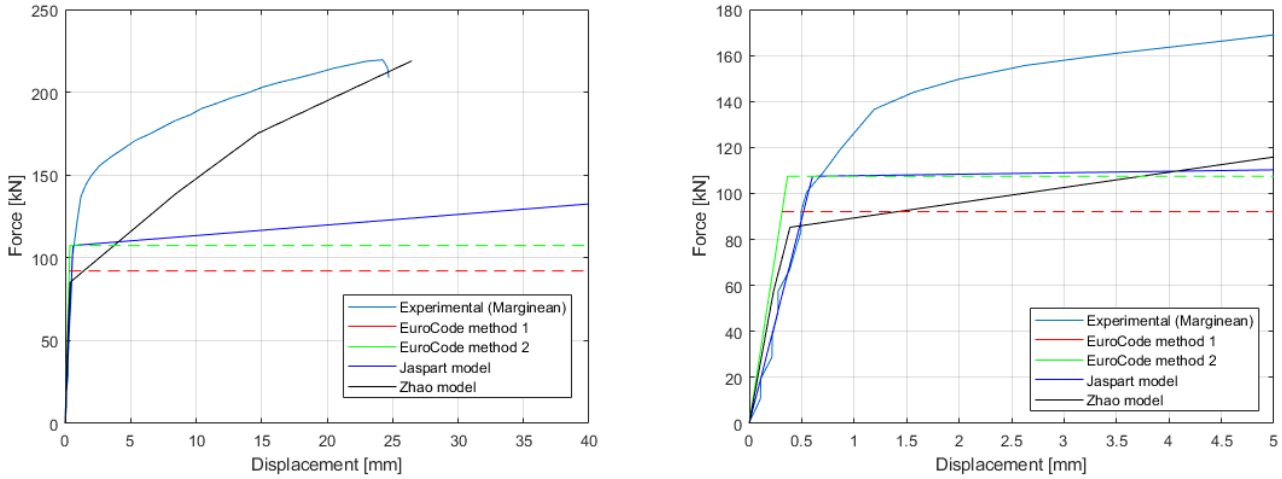

(a) Global response

(b) Zoom on the elastic response

Figure 3.26 – Force-displacement curve of specimen T-11.5a-18

Authors	mode	$K_{1stub,init}$ [kN/mm]	F_y [kN]	Rel. error [%]	F_u [kN]	Rel. error [%]	Δ_u [mm]	Rel. error [%]
Experimental	1	140.7	152.8	/	219.6	/	24.2	/
EC method 1	1	147.1	92.1	-39.7	/	/	/	/
EC method 2	1	147.1	107.5	-29.7	/	/	/	/
Jaspart	1	89.1	107.5	-29.7	168.64	-23.2	96.6	+298.4
Zhao	1-BR	247.4	85.3	-44.2	219	-0.3	26.5	+9.2

Table 3.24 – Characterisation of specimen T-11.5a-18

a) T-11.5b-18

Authors	mode	$K_{1stub,init}$ [kN/mm]	F_y [kN]	Rel. error [%]	F_u [kN]	Rel. error [%]	Δ_u [mm]	Rel. error [%]
Experimental	1	183.3	169	/	225.2	/	17.2	/
EC method 1	1	147.1	113.6	-32.8	/	/	/	/
EC method 2	1	147.1	132.6	-21.6	/	/	/	/
Jaspart	1	89.1	132.6	-21.6	195.7	-13.1	83.6	+386.4
Zhao	1-BR	249.1	96.3	-43	226.5	+0.6	22.1	+28.3

Table 3.25 – Characterisation of specimen T-11.5b-18

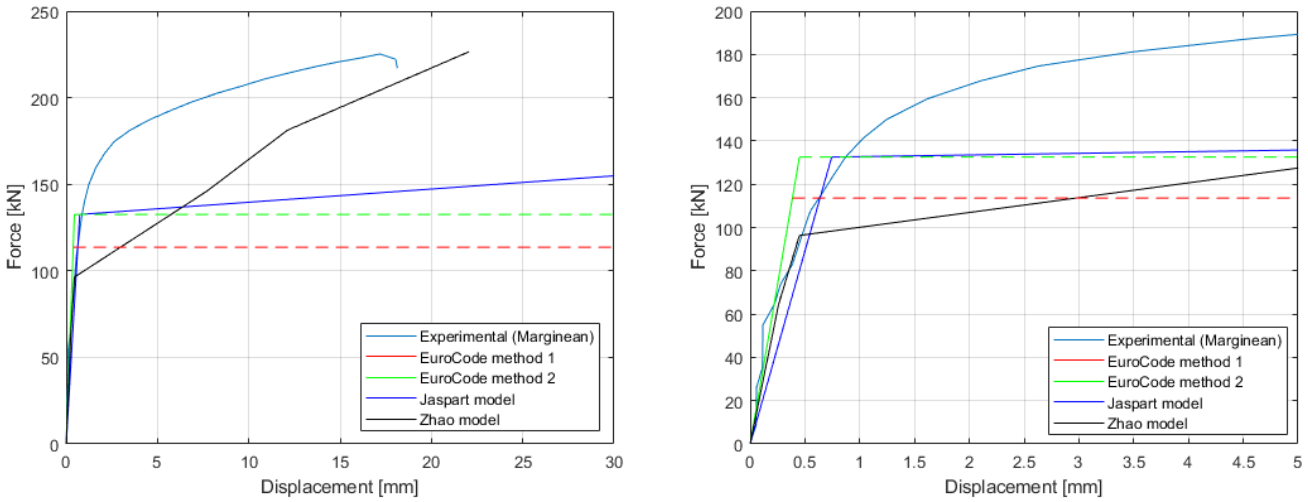

(a) Global response (b) Zoom on the elastic response

FIGURE 3.27 – Force-displacement curve of specimen T-11.5b-18

d) T-11.5b-20

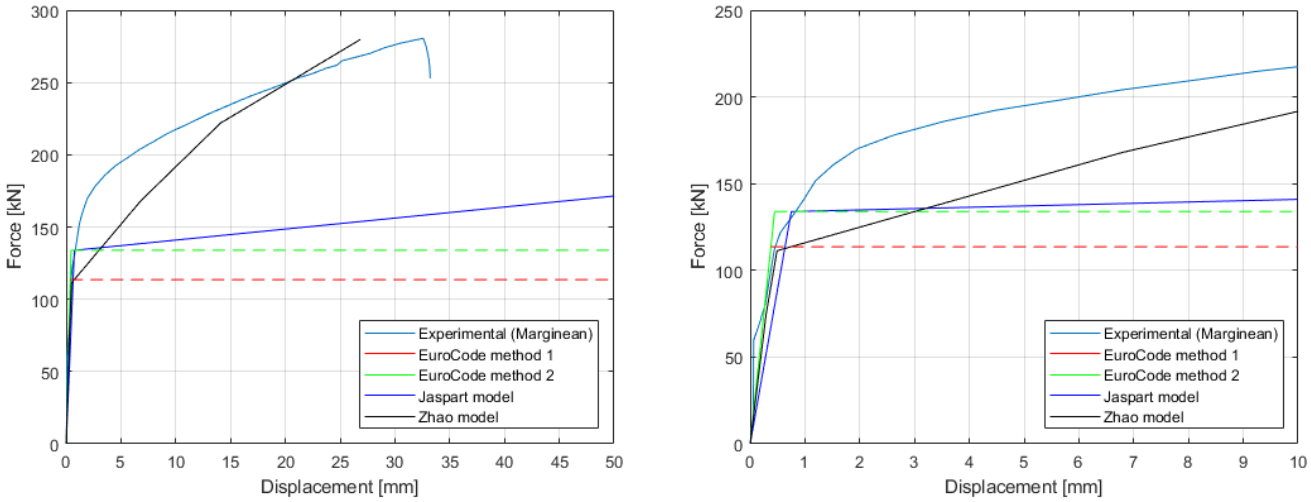

(a) Global response (b) Zoom on the elastic response

FIGURE 3.28 – Force-displacement curve of specimen T-11.5b-20

Authors	mode	$K_{1stub,init}$ [kN/mm]	F_y [kN]	Rel. error [%]	F_u [kN]	Rel. error [%]	Δ_u [mm]	Rel. error [%]
Experimental	1	145.7	181	/	280.55	/	32.6	/
EC method 1	1	150.1	113.6	-37.2	/	/	/	/
EC method 2	1	150.1	133.9	-26	/	/	/	/
Jaspart	1	89.1	133.89	-26	197.67	-29.5	84.4	+159
Zhao	1-BR	256.3	111.3	-38.5	279.76	-0.3	26.8	-17.6

TABLE 3.26 – Characterisation of specimen T-11.5b-20

3.3 Conclusions

From the six test campaigns found in the literature, only two are exploitable for the current topic. Models from SECTION (2.3) were applied to predict the response of their test specimens. Some tendencies were identified, they are listed hereafter :

— Mode 2 is correctly predicted considering that the post-yield behaviour can be neglected due to its high brittleness.

— The initial stiffness is globally well estimated.

— For **mode 1**, the plastic strength computed by the models greatly underestimates the actual one.

— None of the models is able to give a good approximation of the ultimate displacement.

— Concerning the last affirmation, Jaspart model gives the worst results. As previously said, observation is unexpected due to the conclusions made by several researchers. This can be explained easily from the components definition. In EQUATIONS (2.14) and (2.15), the Young modulus E is used to characterise the elastic response. In the post-yielding domain, the same modulus is kept for the bolt but not for the plates. For this sub-component, the hardening modulus E_h is applied. The inconsistency lies in the fact that **this modulus is tapered on the entire plate**. Indeed, in reality, the plasticity is localised at the plastic hinges while the rest of the plate remains in the elastic domain as illustrated on FIGURE (3.29).

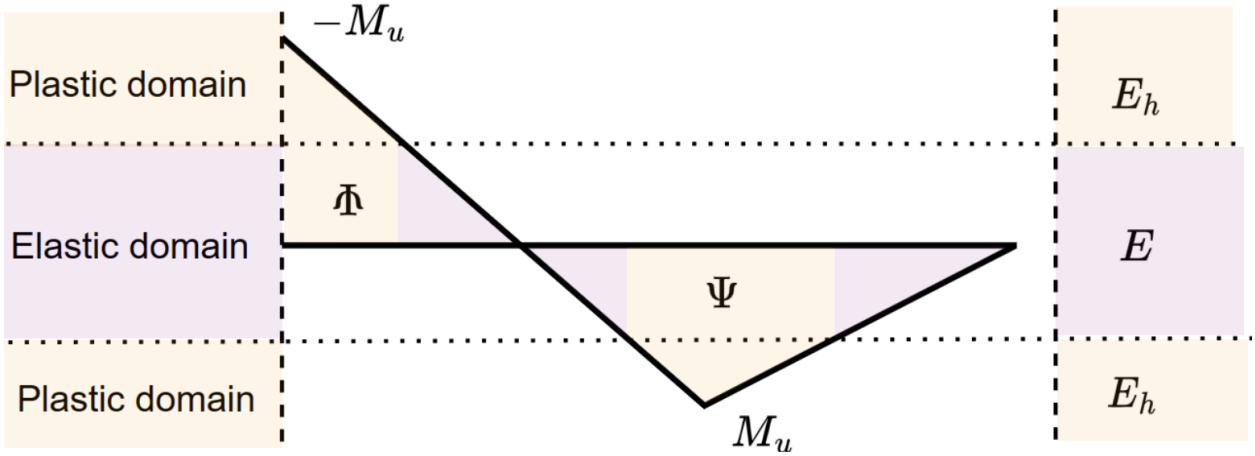

FIGURE 3.29 – Distribution of E along the length of the plate

In fact, E is function of the point considered. It should be integrated over the length of the T-stub and then pondered. The E_{mean} obtained can thus be used in the equations. In a conservative form, it consists in the experimental based $E/50$ value proposed by Jaspart in [**4**]. By this small explanation, both observations from this SECTION and [**9**] can be conciliated.

Most of the models and their added complexities try to predict the response at failure. However, the results of this SECTION clearly prove some inconsistencies in the prior steps. In consequence, it was decided that the first problem to be solved is the prediction of the plastic strength.

Chapter 4

Numerical modelling

In Chapter (3), several problems in the characterisation models were pointed out by comparing them to experimental tests. Nevertheless, the data available are quite limited. In consequence, it was decided to perform an extended parametric analysis. To do so, the non linear finite element software Abaqus© is used [**18**]. The first step of the followed procedure consists in modelling the test campaigns of Chapter (3). By proceeding this way, the modelling assumptions and the sensitivity of the mesh used can be confronted to actual cases.

From the two campaigns studied in Section (3.2), only Timisoara is partially modelled in Abaqus©. Indeed, since no coupon tests are provided for Tongji, the material laws cannot be implemented. In addition to that, only **mode 1** T-stubs are useful for the investigated problem. This means that only the T-10 and T-12 series are considered hereafter (see Table (3.1)).

4.1 Main modelling assumptions

The modelling of a T-stub can be decomposed in three mains axes. The first one concerns the implementation of the constitutive laws in the software. The second consists in modelling the bolts efficiently in such way to obtain accurate results for reasonable computational time. The last step is related to the loading procedure of the T-stub itself. Notice that in such software, the choice of the units is up to the user. To be self consistent, the mass is in tons [T], the time in seconds [s] and the lengths in millimeters [mm]. By proceeding this way, the dimensions of forces and pressures are in Newton [N] and MegaPascal [MPa] respectively.

4.1.1 Constitutive laws

In the selected specimens, four constitutive laws can be identified : one for the bolts and three for the plates. Several subtleties hide in the former. For this reason, an entire Section (4.1.2) is dedicated to those considerations. The three remaining laws are related to the webs, the 10 [mm] and 12 [mm] flanges.

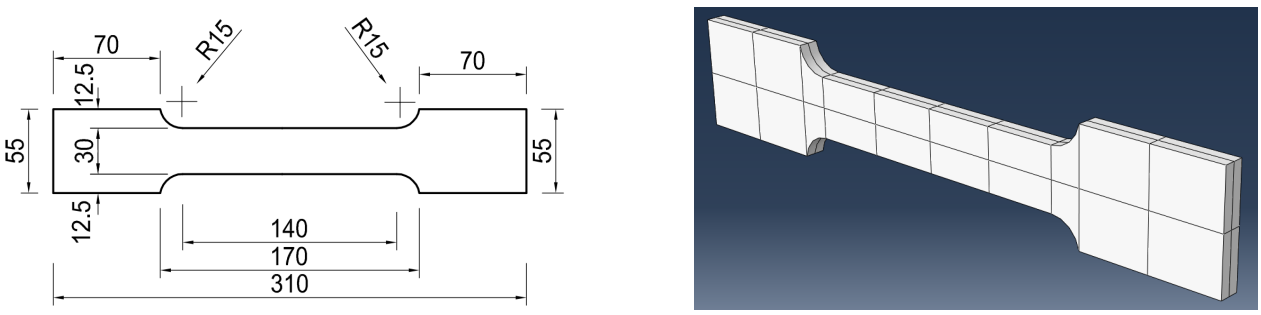

(a) Geometry (b) 3D model

Figure 4.1 – Model of the coupon

For sake of concisely, only the 10 [mm] flange material law is fully detailed herebelow. The same assumptions and modelling procedures apply to the other laws. The geometry implemented can be consulted on FIGURE (4.1)

Then, in addition to the density (taken as 0.00785 $[T/mm^3]$), the different parts of the stress-strain curve must be defined. The **elastic domain** is entirely characterised by the **Young modulus** E taken as 210,000 [MPa]. For the **plastic domain**, few manipulations are required. First, the plastic strain should be extracted from the engineering stress-strain curve. This is simply done by subtracting the elastic part as follow :

$$\varepsilon_{pl,eng} = \varepsilon_{eng} - \varepsilon_{el,eng}. \tag{4.1}$$

On the other hand, the engineering stress should not be modified unless the onset of necking is attained. Once the ultimate stress past, a perfectly plastic behaviour is assumed. The curve obtained can be seen in FIGURE (4.2). Nevertheless, this law cannot be implemented as such in ABAQUS©. To do so, the transition of engineering properties to true one must be performed with EQUATIONS (2.16) and (2.17). This correspond of the back curve of the FIGURE hereafter and must be implemented in the software.

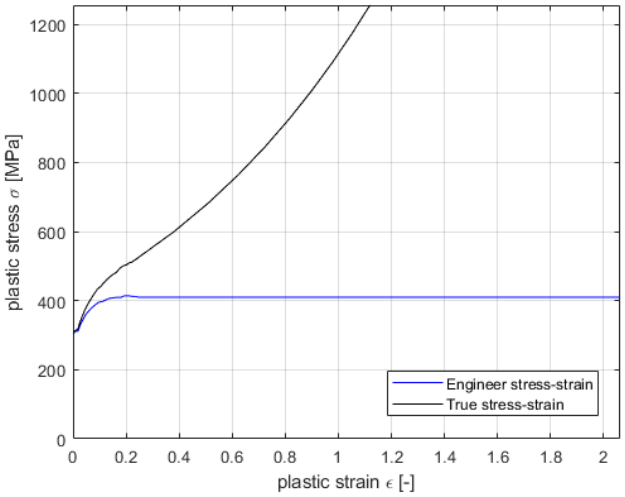

FIGURE 4.2 – Undamaged plastic law

The third and last domain of the material law is the damaged response. This phase is attained once the strain at onset of necking is reached. In this thesis, the formulation used to characterise this response is proposed by Ling in [**19**]. It consists in a weighted combination of a linear and exponential formulation as expressed in EQUATION (4.2) :

$$\sigma_{pl,true,damaged} = W(A\varepsilon_{pl,true} + b) + (1 - W)(K\varepsilon_{pl,true}^{N}) \tag{4.2}$$

with :

— A, the true stress at the onset of necking.

— N, the true strain at the onset of necking.

— $b = A(1 - N)$.

— $K = A/N^N$.

— W, the weighted coefficient to be determined.

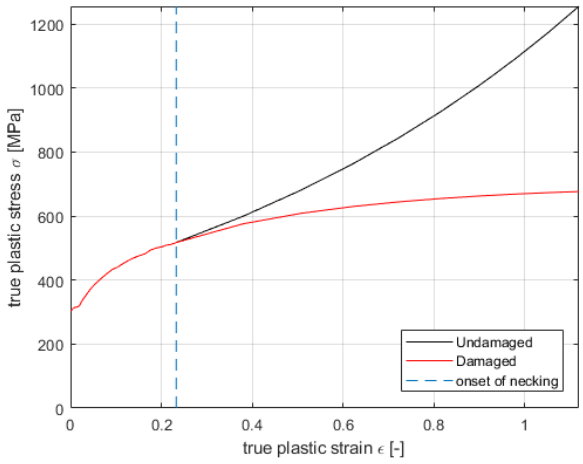

FIGURE 4.3 – Damage response law

FIGURE (4.3) illustrates the transition from the undamaged plastic response to the damaged one. In the current example, $W = -0.3$. Nevertheless, this curve cannot be implemented in ABAQUS©. Indeed, in the software, damage is modelled as growing voids, i.e. as a porosity. This dimensionless damage variable can be formulated :

$$D = 1 - \frac{\sigma_{pl,true,damaged}}{\sigma_{pl,true}}. \tag{4.3}$$

Notice that damage increases up to a certain point. Once this **critical damage** is attained, rupture occurs and leads to a complete loss of the bearing capacity. The damage at which failure appears is unknown and must be determined by trials-and-errors. For the current example, $D_{cr} = 0.3$. This law can be implemented in ABAQUS© as a function of the equivalent plastic displacement :

$$u_{pl,eq.displ} = L_{char}(\varepsilon_{pl,true} - N). \tag{4.4}$$

With L_{char} the characteristic length of the mesh. Thus, notice that a mesh sensitivity analysis must be performed. In FIGURE (4.4) can be seen the damage evolution law for the current example with $L_{char} = 4$ [mm].

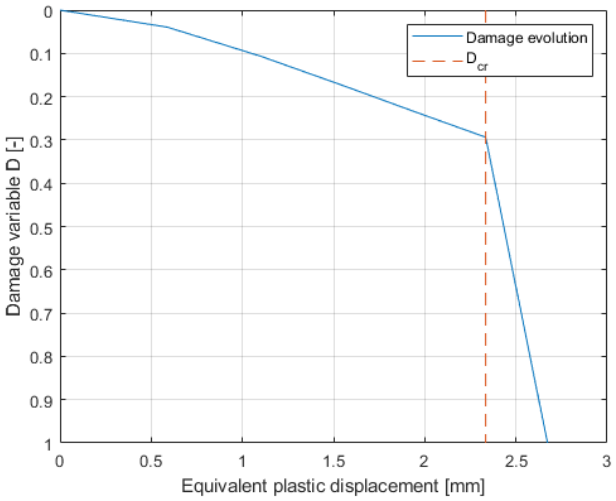

FIGURE 4.4 – Damage evolution law

In addition to that, a **damage initiation criterion** must be implemented. Thus, stress state of matter have to be evaluated. This is done by means of **triaxiality** defined as the mean stress divided by equivalent stress :

$$\theta = \frac{q}{p_{eq}} = \frac{\frac{1}{3}(\sigma_{xx} + \sigma_{yy} + \sigma_{zz})}{\sigma_{mises}} \tag{4.5}$$

For simple stress state, as the uniaxial loading applied to the coupon, some simplifications occur. In that case, $\sigma_{yy} = \sigma_{zz} = 0$, $\sigma_{Mises} = \sigma_{xx}$ and thus $\theta = 1/3$. For more complicated stress state, a criteria is proposed by Pavlović in [**20**] and [**21**]. It expresses as follow :

$$\varepsilon_{pl,true,damaged} = \alpha e^{-\beta\theta} \tag{4.6}$$

where :

— $\varepsilon_{pl,true,damaged}$ [-] is the equivalent plastic strain at damage initiation.

— β [-] is a material parameter (assumed equal to 1.5).

— θ [-] is the stress triaxiality.

— α [-] is a parameter determined as follow. For uniaxial stress state, it was proved that $\theta = 1/3$ [-] and $\varepsilon_{pl,true,damaged} = N$ [-]. Then, by rewriting Equation (4.6), a formulation can be found for α.

$$\alpha = \frac{N}{e^{-1.5 \cdot \frac{1}{3}}} = \frac{N}{e^{-0.5}} \tag{4.7}$$

This criterion is depicted on Figure (4.5) and must be implemented into Abaqus©. Notice that the strain rate was assumed to be equal to 0.01 $[s^{-1}]$.

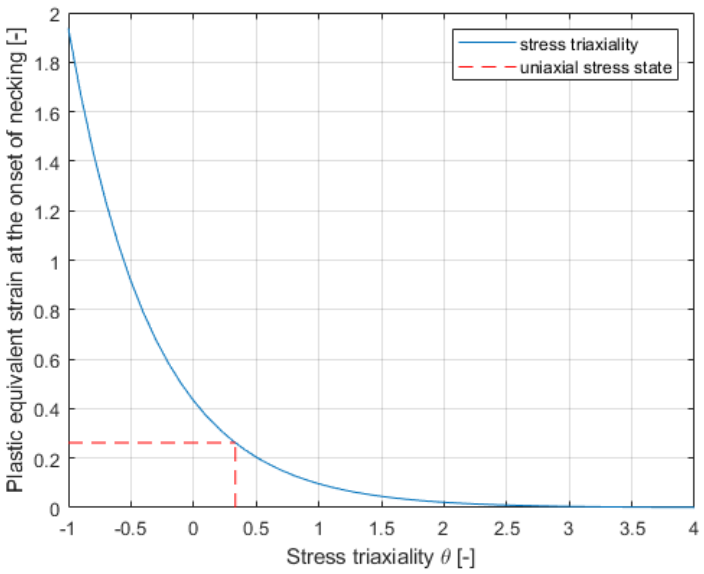

Figure 4.5 – Damage initiation criterion

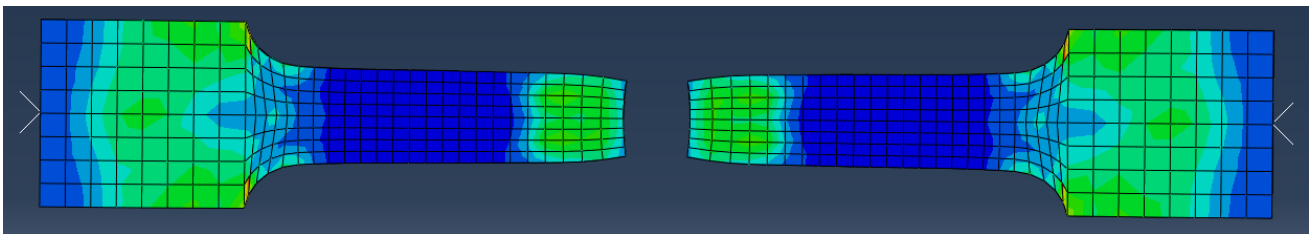

FIGURE 4.6 – Coupon tensile failure

To finalise the model and validate the constitutive law, both mesh and boundary conditions should be defined. Concerning the mesh, its characteristics length is 4 [mm] as previously explained. On the edges, a cruder mesh was applied since the failure was not expected to occur there. One extremity of the coupon is clamped while the other has all its degrees of freedom locked expect in the axial direction. The loading was performed by an imposed velocity of 0.1 [mm/s] in a dynamic implicit procedure until failure is reached. FIGURES (4.6) and (4.7) illustrate the failure and the force-displacement curve obtained by ABAQUS©.

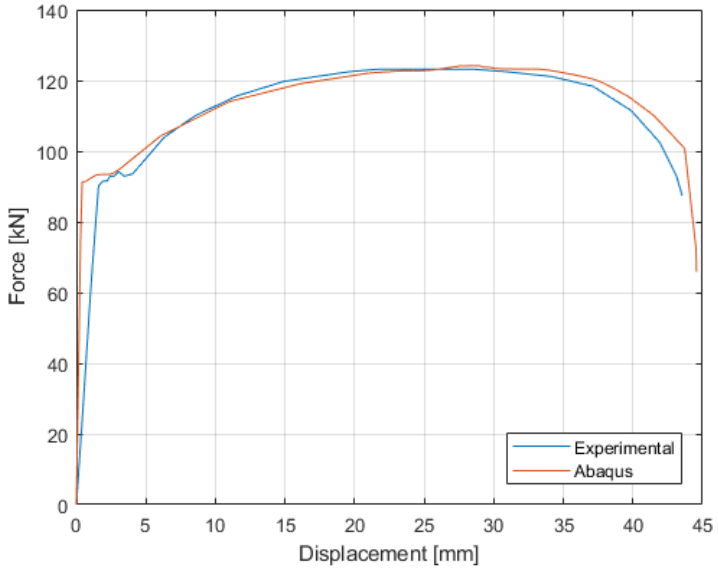

FIGURE 4.7 – Material law validation for 10 [mm] flange

It can be seen that the force-displacement curve obtained numerically approximates satisfactorily the experimental data. A slight overestimation of the initial stiffness can be noticed. However, this error can be neglected. Indeed, although the Young modulus may be overestimated, it should be noted that the unaccounted test setup stiffness influences the initial response.

A summary of all the parameters to be determined by trials-and-errors is proposed in TABLE (4.1). Similar procedure is applied to the two other coupon tests. The force-displacement curves obtained for these tests can be consulted on FIGURE (4.8). It can be concluded that the results found are satisfying

Element	A [MPa]	N [-]	W [-]	D_{cr} [-]	L_{char} [mm]
Web 10 [mm]	678.47	0.187	-1.5	0.28	4
Flange 10 [mm]	517.54	0.2328	-0.3	0.3	4
Flange 12 [mm]	560.44	0.2378	-0.8	0.3	4
Bolt M16	1,148.23	0.0112	0	0.38	2

TABLE 4.1 – Numerical parameters of the constitutive laws

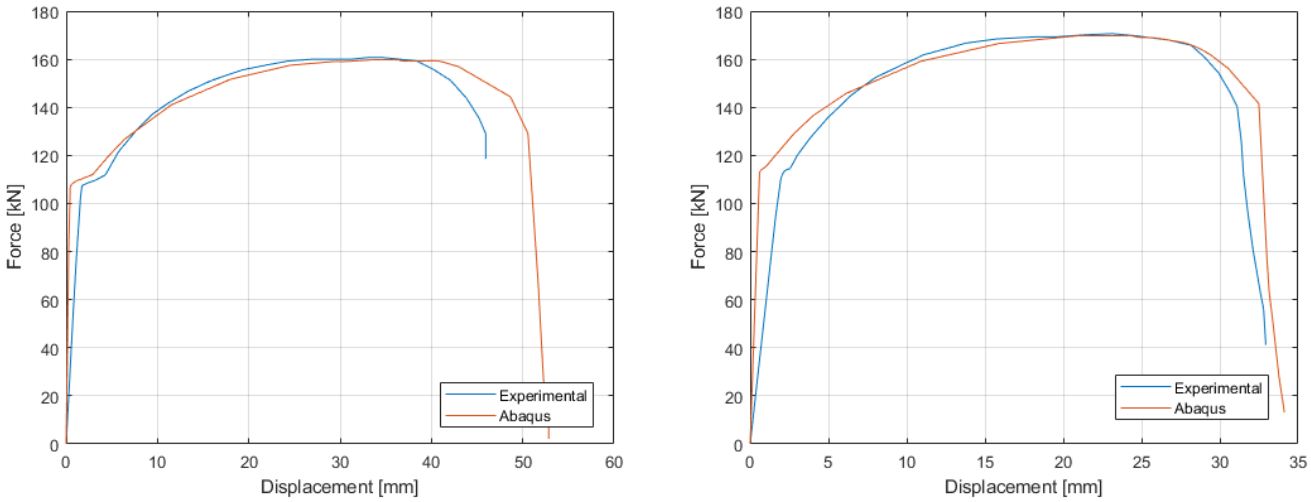

(a) 10 [mm] web (b) 12 [mm] flange

FIGURE 4.8 – Material laws validation for plates

4.1.2 Modelling of the bolts

Regarding the bolts, it was explained in SECTION (3.1.1) that although tests were performed on the bolts, the stress-strain curves were not provided. Fortunately, in [**22**] and [**23**], D'Aniello performed tension tests on M16 10.9 bolt grade. In his papers, he proved that the standard deviation of the ultimate stress and strain is negligible as illustrated on FIGURE (4.9) herebelow.

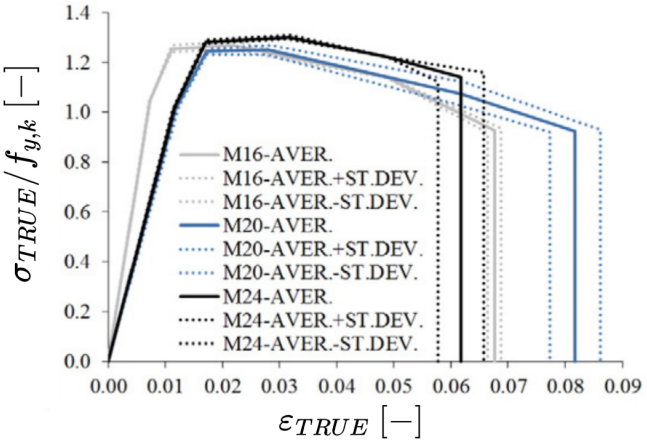

FIGURE 4.9 – Bolt properties standard deviation [**22**]

In consequence, the model of the bolt is based on those results. D'Aniello also pointed out that there exist two types of bolts on the European market : they can be HR (High Resistance) or HV (Hochfeste Bolzen mit Vorspannung) [**22**], [**23**]. The distinction is important since they show different failure modes. Indeed, while the former fails due to necking in the threaded shaft, the latter is expected to undergo thread stripping and nut slipping up to removal. In Timisoara test campaign, **the bolts are assumed to be HR**.

From this perspective, it was decided to model the threaded shaft as a cylinder. In addition to that, the head, the shaft and the nut constituting the bolt are modelled as one unique element (see FIGURE (4.10)). If the assumption is correct, those two simplifications should not influence the results obtained. Indeed, since the failure is expected to occur in the threaded part, the nut-shaft interaction can be disregarded. The geometry implemented is the nominal one found in the standards [**24**].

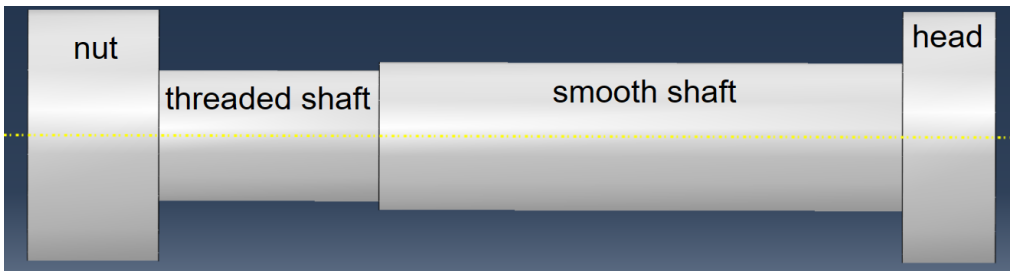

FIGURE 4.10 – Bolt 3D model

The next step of this modelling consists in defining the material law. This done by following the procedure described in SECTION (4.1.1). All the parameters to be determined can be consulted in TABLE (4.1). The loading is applied through an imposed velocity of 0.1 [mm/s] (dynamic implicit analysis) on the internal head face. All the other degrees of freedom of the head are blocked. On the other hand, the nut is considered clamped on its internal face. Those boundary conditions are imposed in such way to mimic the test setup illustrated on FIGURE (4.11).

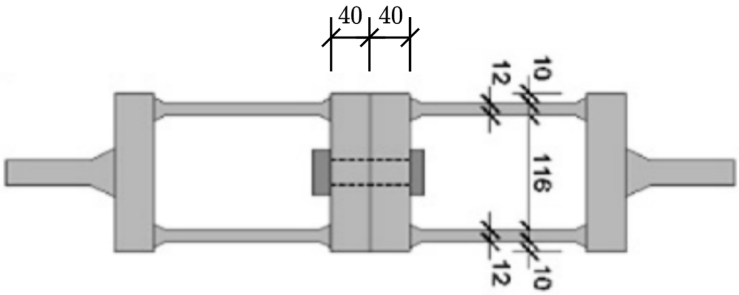

FIGURE 4.11 – Bolt test setup [**22**]

The results obtained can be consulted on FIGURES (4.12) and (4.13). It can be observed that the failure is due to necking in the threaded shaft as expected. On the first FIGURE (4.12), it can be seen that the both ultimate displacement and strength are well assessed. Similarly to the coupon tests of the previous SECTION, the initial stiffness is slightly overestimated. However, as for the plates, the error made is due to the setup stiffness not taken into account and can be considered negligible. Thus, it can be conclude that the law implemented for the bolt is sufficient.

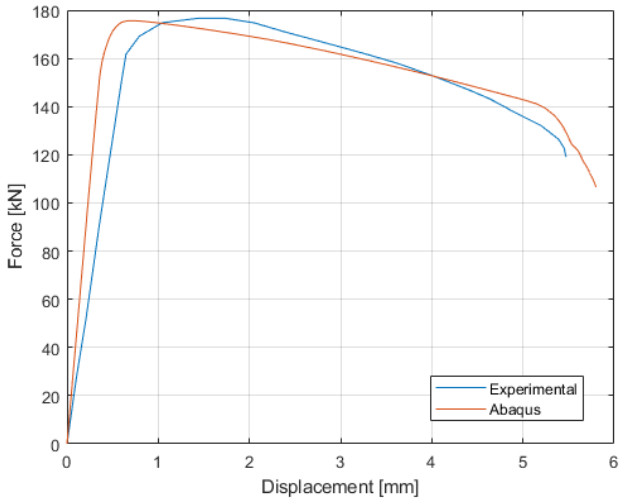

FIGURE 4.12 – Bolt material law validation

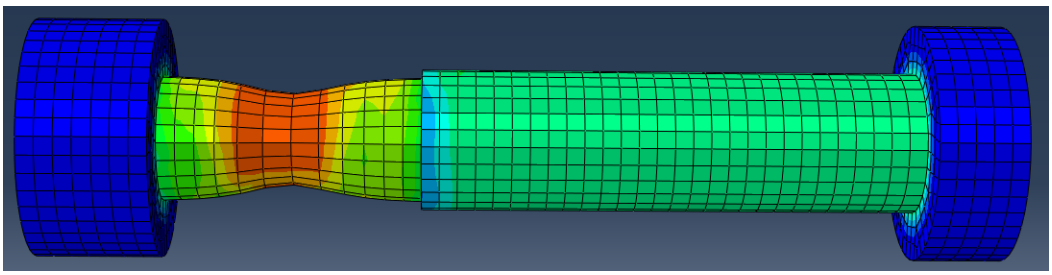

FIGURE 4.13 – Bolt tensile failure

4.1.3 Modelling of the T-stubs

The geometry modelled for the T-stubs can be found in TABLE (3.1). For the bolts, the same nominal geometry proposed in the standard [**24**] is used. Once the constitutive laws validated in SECTIONS (4.1.1) and (4.1.2) are implemented and attributed to their respective element, the assembly can be performed. An illustration is proposed on the FIGURE (4.14) hereafter.

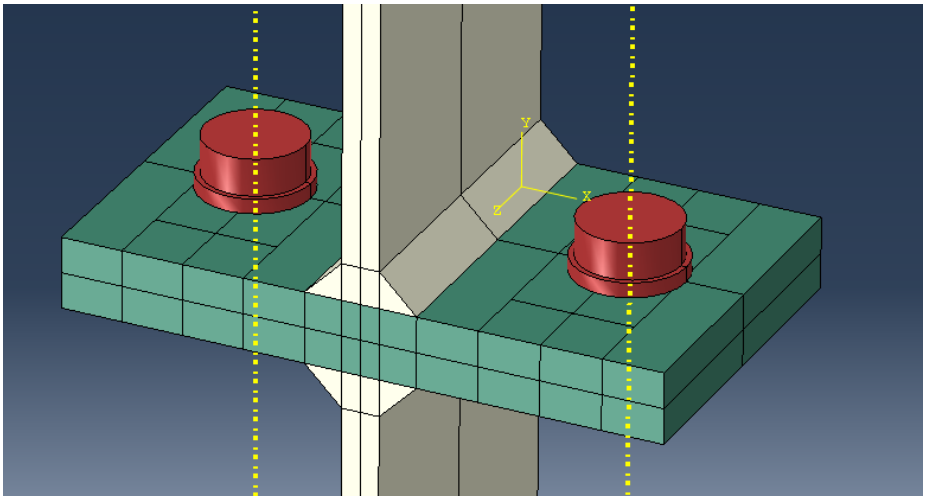

FIGURE 4.14 – T-10-16-100 T-stub 3D model (colored by material law)

To model the interaction between elements, a **contact law** must be defined in ABAQUS©. The normal contact is chosen as "**hard**" to prevent any overlapping. On the other hand, a **friction coefficient assumed at 0.2** is used to characterise the tangential contact. This law is applied to the eleven surface contact pairs identified and listed hereafter :

— Flange to flange (x1) (1)

— Nut to flange (x2) (2)

— Bolt head to flange (x2) (3)

— Bolt shaft to flange hole (x6) (4) (5) (6)

All those pairs are illustrated on FIGURE (4.15). The loading, as for the previous models, is applied by an imposed velocity of 0.1 [mm/s]. This boundary condition is imposed on the free end of the web of the upper T-stub. All the other degrees of freedom of this extremity are locked. Regarding the second T-stub, the free edge of its web is clamped. Thus, the meshes discussed in the next SECTION (4.2) are applied and the implicit dynamic analysis can be carried on. Results of the described procedure are presented in SECTION (4.3).

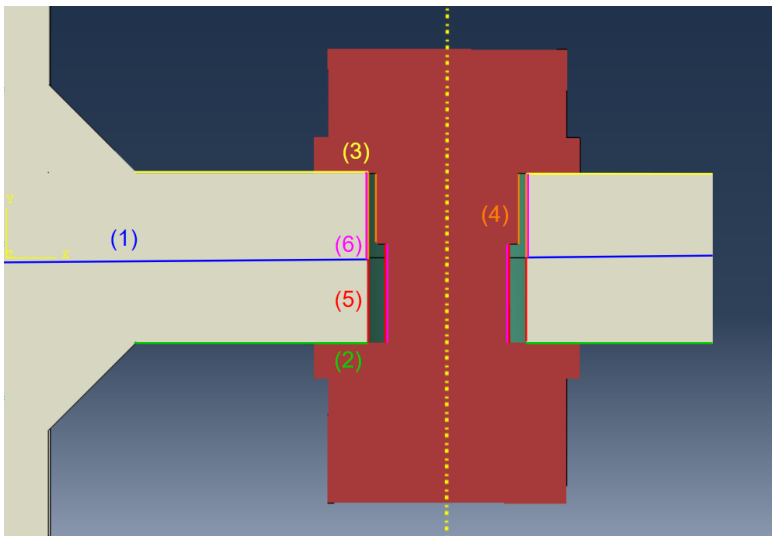

FIGURE 4.15 – Contact pairs

4.2 Mesh sensitivity analysis

As previously explained, a mesh sensitivity analysis must be performed to ensure the accuracy of the results and that the material laws are correctly implemented. The first analysis is conducted on D'Aniello's bolt presented in SECTION (4.1.2). To do so, the damage in the constitutive law is disabled. The results obtained are presented on FIGURE (4.16).

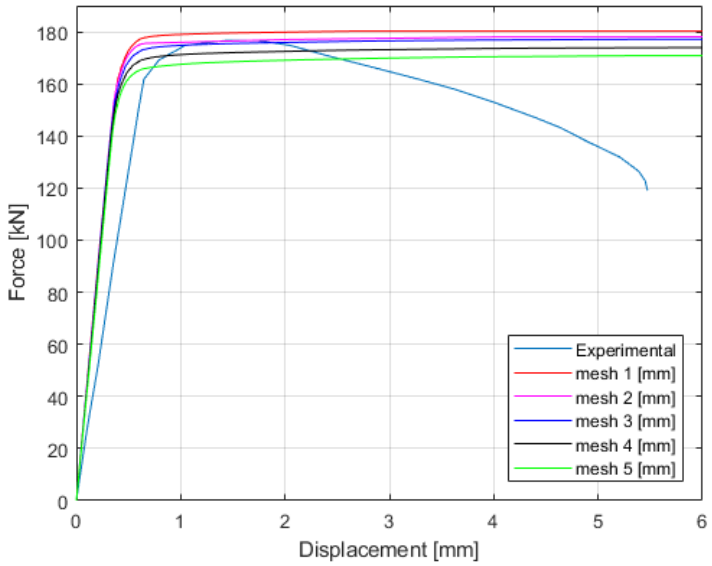

FIGURE 4.16 – Bolt mesh sensibility analysis

On this FIGURE, it can be seen that the 5 [mm] mesh and the **4 [mm] mesh** are too crude and do not provide accurate results. In opposition to that, the 1 [mm] mesh is so refined that it requires a prohibited computational time. It also leads to numerical error and convergence difficulties as suggested by the slight overestimation of the ultimate strength. It can be concluded that the 2 [mm] mesh and 3 [mm] mesh are optimal by combining a sufficient accuracy of the results with a reasonable computational time. Nevertheless, the 2 [mm] mesh is still preferred because it allows to have more elements over the head and nut depths. A comparison between those two meshes is proposed on FIGURE (4.17). The damage properties and validation of this mesh were already presented in TABLE (4.1) and FIGURE (4.12).

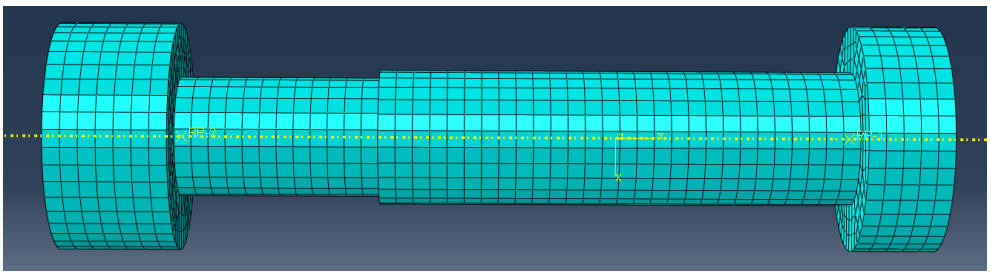

(a) 2 [mm] mesh

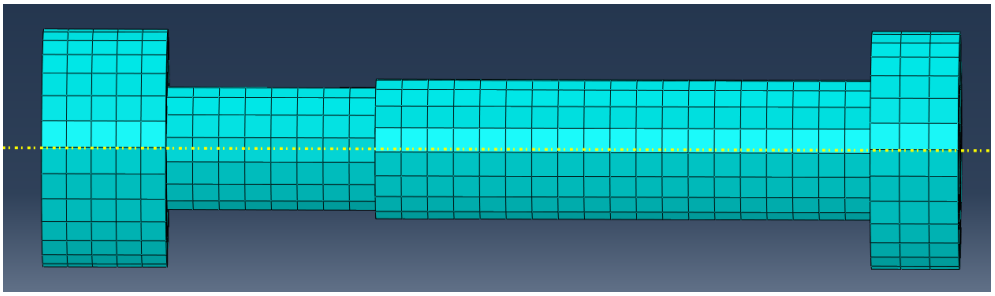

(b) 3 [mm] mesh

FIGURE 4.17 – Bolt mesh comparison

The second mesh sensitivity analysis concerns the T-stubs themselves. In a similar way, the damage was disabled for all materials. The results issued from the bolt analysis are directly implemented here and the mesh varies only in the plates. The results can be consulted on FIGURE (4.18) where the same color code as for the bolt is applied.

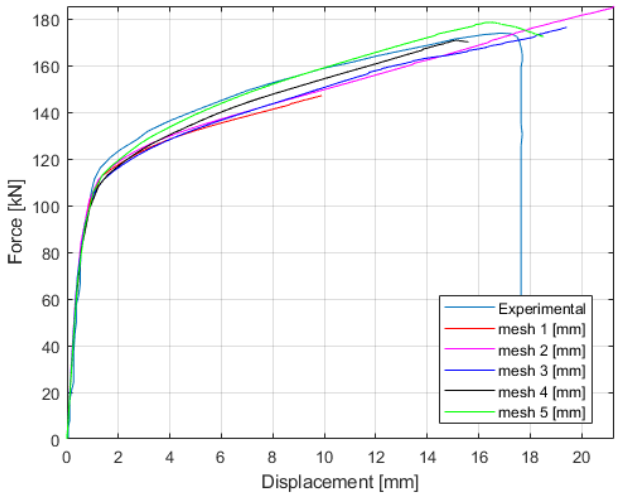

FIGURE 4.18 – T-10-16-100 T-stub mesh analysis

Identical conclusions as before can be drawn from this FIGURE. The 1 [mm] mesh is too refined and requires important computational resources. In the current example, the required time step was so small that it led the simulation to abort. The **4 [mm] mesh** and the 5 [mm] mesh are too crude which makes the results inaccurate. Although the 3 [mm] mesh gives good results, the 2 [mm] mesh is preferred since the higher number of elements along the thickness increases the accuracy of the results. An illustration of those two last meshes is proposed on FIGURE (4.19). Notice that the chosen mesh does not correspond to the one of TABLE (4.1). Thus, the damage should be re-calibrated. However, as it is demonstrated in the next SECTION, the results are not impacted since the failure is always expected in the bolt and not in the flanges. The results of this analysis are extrapolated to the five other T-stubs of the campaign.

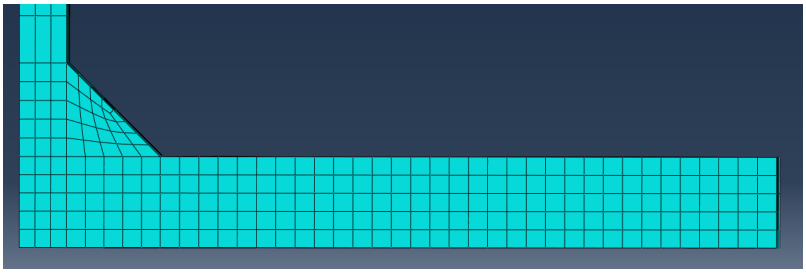

(a) 2 [mm] mesh

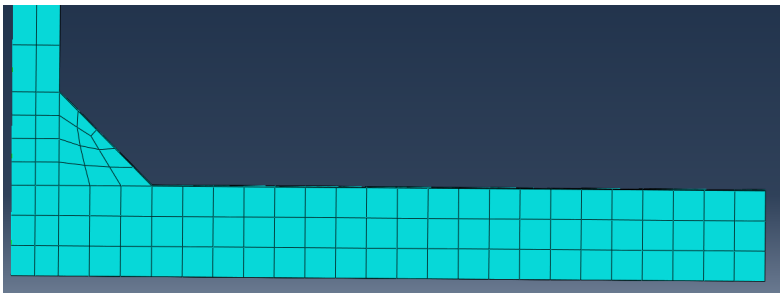

(b) 3 [mm] mesh

FIGURE 4.19 – T-10-16-100 T-stub mesh comparison

4.3 Results

In this SECTION all the assumptions, material laws and modelling procedures previously defined are applied and compared to the experimental tests. Notice that the load is measured at the web free end and the displacements are taken as the distance between the internal faces of the flanges. The results presented hereafter stand for one T-stub (the displacement is divided by 2).

FIGURE (4.20) shows that the overall T-stub response is well modelled. A slight overestimation of the ultimate displacement is observed. This error can still be considered negligible and the test is validated.

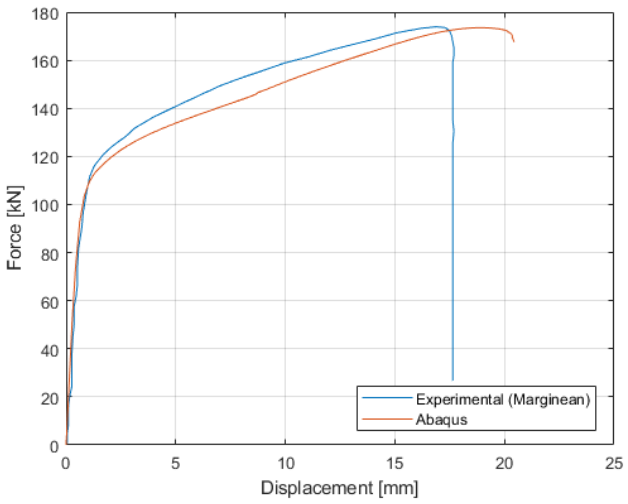

FIGURE 4.20 – T-10-16-100 validation

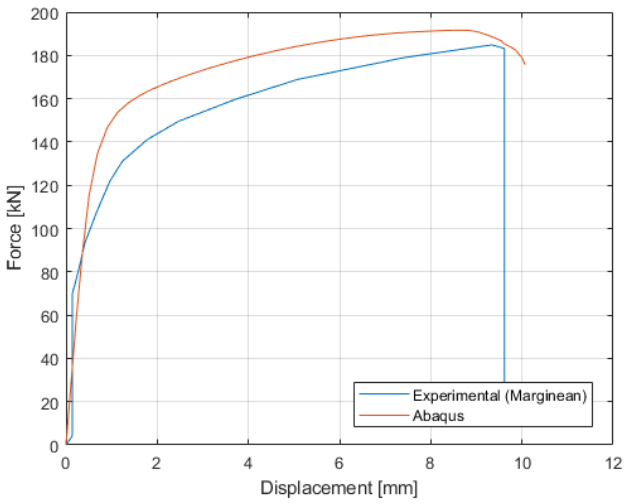

FIGURE 4.21 – T-12-16-100 validation

On the other hand, FIGURES (4.21) and (4.23) exhibits the worst results of the series. In those cases, the plastic strength is overestimated. This can be explained by the many assumptions made on the bolts material law. In addition to that, those two tests are the closest to a mode 2 and the loading procedure is idealised. However, the modelling is still considered valid.

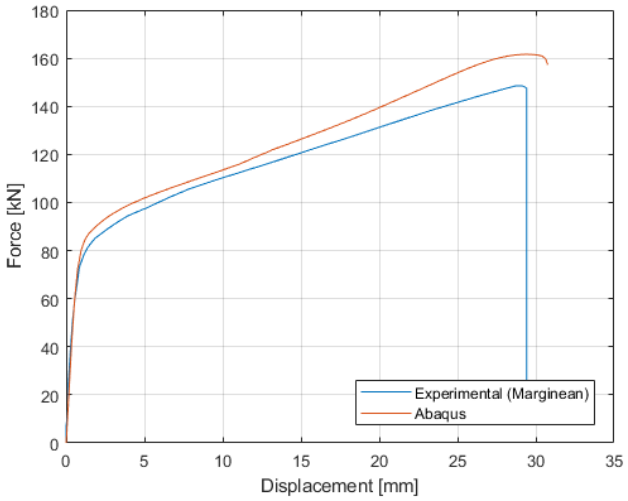

FIGURE 4.22 – T-10-16-120 validation

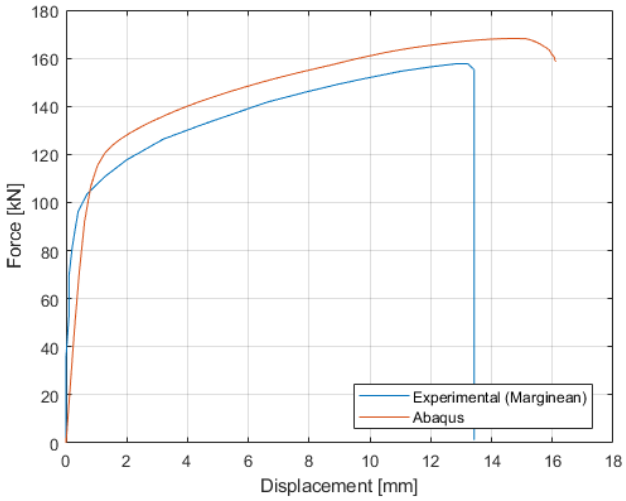

FIGURE 4.23 – T-12-16-120 validation

The last three remaining tests of the series are depicted on FIGURES (4.22), (4.24) and (4.25). Comparing the ABAQUS© results to the experimental ones gives good correspondences. Despite having small errors on the ultimate displacement, the yielding or the ultimate strength, all the specimens presented here can be considered validated.

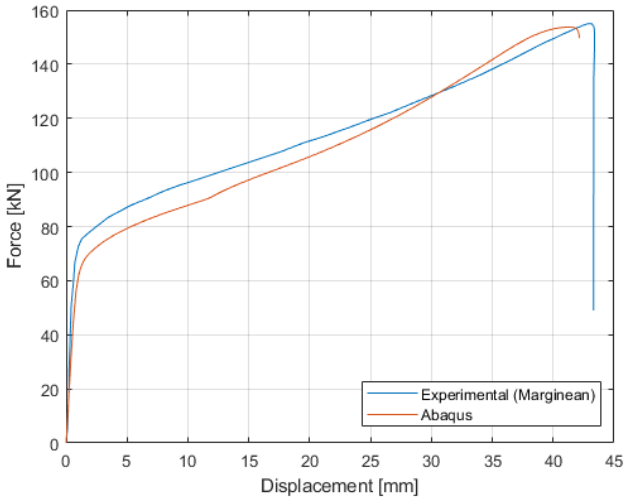

FIGURE 4.24 – T-10-16-140 validation

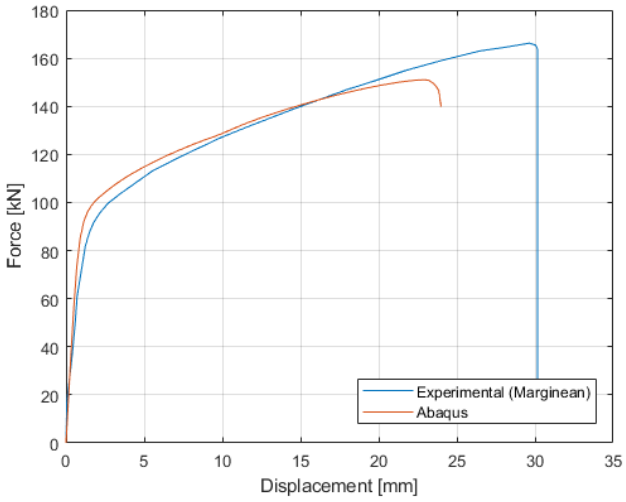

FIGURE 4.25 – T-12-16-140 validation

4.4 Conclusions

In this CHAPTER, all the material constitutive laws were modelled up to failure and validated. A simplified procedure to model the bolts was proposed based on D'Aniello tests. Thus, all the unknowns related to the bolt properties could be overridden. In addition to that, two mesh sensitivity analyses were carried out to determine that the most suited meshes for both the T-stubs and the bolts are 2 [mm] long elements. Finally, for each specimen of Timisoara campaign, a comparison between the numerical and experimental data was performed. It was concluded that the modelling procedure developed here provides good results and can be applied to an extended parametric analysis.

Chapter 5

Parametric analysis

With the modelling procedure developed in CHAPTER (4) an extended parametric analysis can be envisaged. Thus, the phenomena encountered can be studied in depth and all the limitations bound to experimental test can be overcome. To begin with, the numerical procedure developed is simplified by several assumptions. Thus, the properties of the specimens created for the analysis are presented. Afterwards, the results are analysed. Finally, conclusions are drawn on the problems that require analytical developments and those that can be disregarded.

5.1 Description and assumptions

First of all, remind that it was decided to investigate the plastic strength of the T-stub. In consequence, the damage was disabled in all the constitutive laws. In addition to that, the hardening branch of the stress-strain curve is also neglected. In other words, in this analysis, the material laws are assumed to be elastic-perfectly plastic as in the EuroCode model and represented on FIGURE (5.1a). By proceeding this way, a proper comparison can be ensured and the component response should exhibit a horizontal plateau once yielding is attained (seeFIGURE (5.1b)). This corresponds to the theoretical definition of the plastic strength. From a numerical point of view, those assumptions drastically reduce the computational time of each model. Notice that the nominal steel properties are used here and that geometrical non linearities are still considered in purpose to highlight the possible membrane effect contribution.

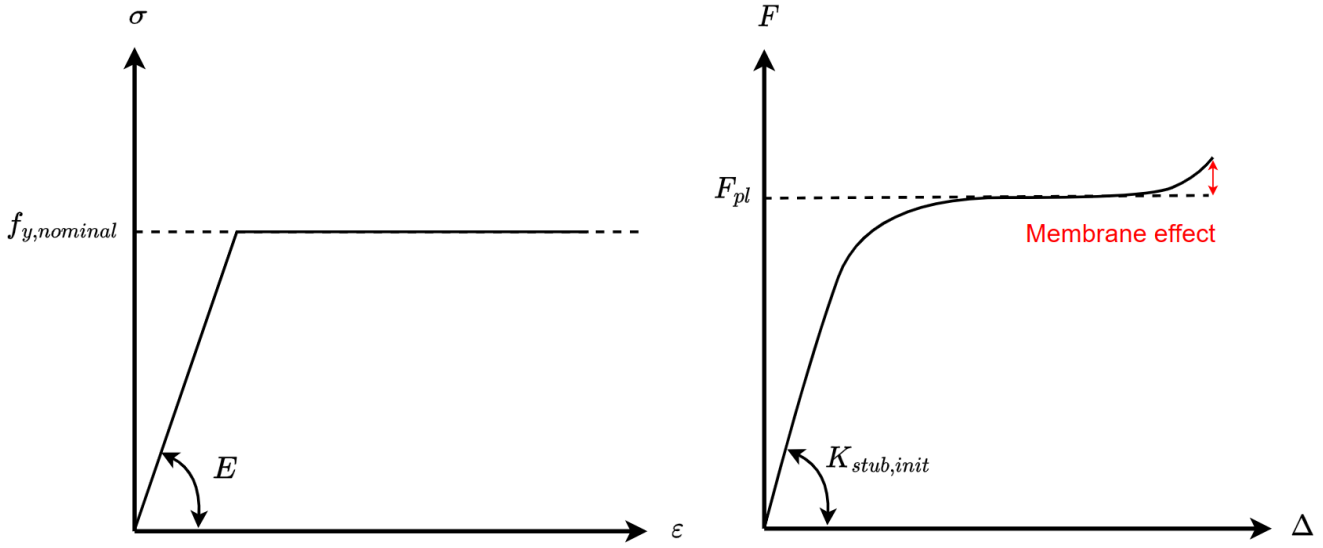

(a) Material law

(b) T-stub response

FIGURE 5.1 – Idealised response

The purpose of the current analysis is to cover as many configurations as possible from an extreme to another. To do so in the most efficient way possible, three dimensionless parameters and their respective range are proposed hereafter. The position of the specimens issued of the Timisoara campaign in the proposed parametric ranges can be consulted in TABLE (5.1).

— $t_f/C \in [0.1\,;\,0.2\,;\,0.3]$ estimates the flange flexibility (NB : C is the distance between the bolt axis and the weld toe, see FIGURE (5.4)).

— $t_f/d_b \in [0.6\,;\,0.7\,;\,0.8\,;\,0.9]$ should indicate how close to a mode 2 the specimen is.

— $e/C \in [0.5\,;\,0.8\,;\,1]$ investigates the effect of the prying forces. Notice that for all specimens $n = e$ according to EuroCode.

Notice that additional series and tests are carried out depending on the observations made. For comprehension sake, those series are presented later on when the problem they are related to is faced.

Specimen	t_f/C	t_f/d_b	e/C
T10-16-100	0.27	0.6	0.85
T10-16-120	0.21	0.61	0.67
T10-16-140	0.18	0.61	0.54
T12-16-100	0.34	0.74	0.85
T12-16-120	0.26	0.74	0.67
T12-16-140	0.21	0.74	0.54

TABLE 5.1 – Position of Timisoara campaign in the range analysis

Each specimen of the presented series is named according to the following protocol : $T - d_b - \frac{t_f}{d_b} - \frac{t_f}{C} - \frac{e}{C}$. To define the geometry, a bolt diameter d_b is **arbitrarily chosen**. Then owing the dimensionless parameters, all the main geometrical properties can be determined. It must be added that the remaining dimensions are taken identical to the Timisoara campaign. The steel grades used are S235 for the flanges and S355 for both welds and web. As for Timisoara, this choice was done to limit the influence of the web on the T-stub response.

The length of the T-stubs requires a particular attention. Indeed, on FIGURE (5.2) can be seen the T-10-16-100 specimen yield line pattern at failure. The worrying part is that a begin of transition in the yield line pattern can be observed. Indeed, the pattern should theoretically consist in two straight lines and do not have those two descending branches.

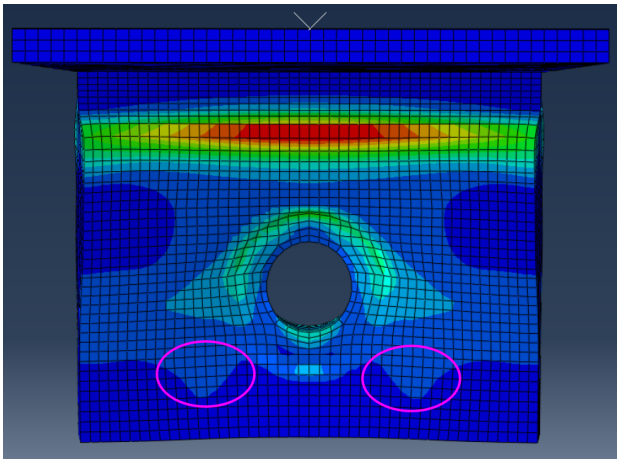

FIGURE 5.2 – T-10-16-100 yield line pattern (L = 90 [mm])

In consequence, the length of this T-stub was increased to 100 and 110 [mm]. These configurations can be seen on FIGURE (5.3). For the former case, the yield line pattern shows a clear transition mechanism between short T-stub and the latter case. Unfortunately, by using EQUATIONS (2.6) to (2.10), a non-idealised mechanism is detected at $L = 185.8$ [mm] according to EuroCode. According to Warnant A. [**1**], those values are 142.5 and 145.3 [mm] respectively for the 100 and 110 [mm] long T-stubs.

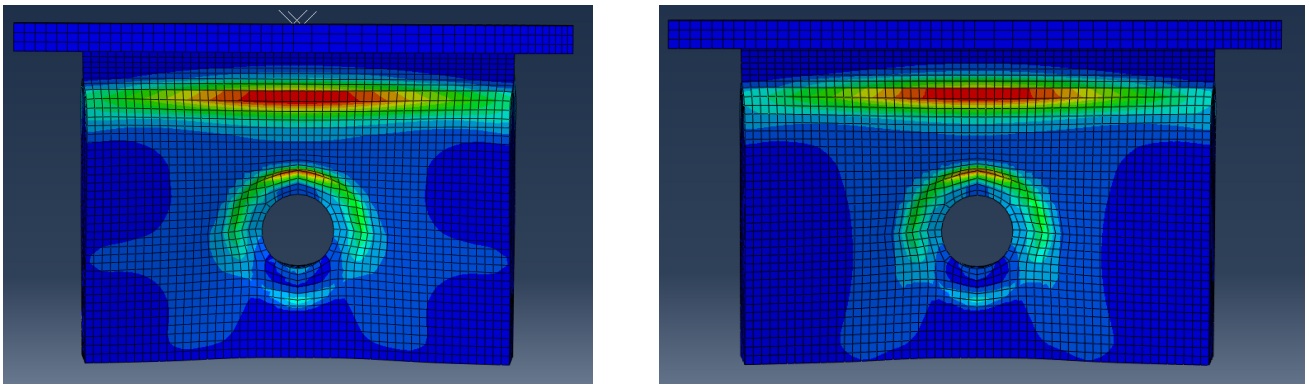

(a) L = 100 [mm] (b) L = 110 [mm]

FIGURE 5.3 – Yield line pattern of T-10-16-100 specimen with a length variation

It can be concluded that the range of application of the short T-stub theory is misjudged. Thus, EuroCode is not reliable when characterising whether the T-stub is short or not. In response to that, it was decided to set the T-stubs length at 70 [mm] in the parametric analysis. This value is arbitrary and expected to produce short T-stubs for each specimen.

A summary of the geometry considered in the first series is proposed in the following TABLE. Notice that some tests are colored in red. Those specimens are so close to a mode 2 that the bended bolts yield before reaching the plastic strength of the T-stub. However, due to the brittle behaviour of the bolts and the simplification on the material laws, those specimens should be disregarded and are no more considered later on.

Test	d_b [mm]	t_f [mm]	C [mm]	e [mm]	t_w [mm]	a_w [mm]	L [mm]	B [mm]	e_1 [mm]
T-12-09-03-1	12	10.8	36	36	10	7	70	173.8	35
T-14-09-03-08	14	12.6	42	33.6	10	7	70	181	35
T-20-09-03-05	20	18	60	30	10	7	70	209.8	35
T-12-09-02-1	12	10.8	54	54	10	7	70	245.8	35
T-12-09-02-08	12	10.8	54	43.2	10	7	70	224.2	35
T-14-09-02-05	14	12.6	63	31.5	10	7	70	218.8	35
T-12-09-01-1	12	10.8	108	108	10	7	70	461.8	35
T-12-09-01-08	12	10.8	108	86.4	10	7	70	418.6	35
T-12-09-01-05	12	10.8	108	54	10	7	70	353.8	35
T-14-08-03-1	14	11.2	37.3	37.3	10	7	70	179.1	35
T-16-08-03-08	16	12.8	42.7	34.1	10	7	70	183.4	35
T-27-08-03-05	27	21.6	72	10	7	70	36	245.8	35
T-14-08-02-1	14	11.2	56	56	10	7	70	253.8	35
T-14-08-02-08	14	11.2	56	44.8	10	7	70	231.4	35
T-16-08-02-05	16	12.8	64	32	10	7	70	221.8	35
T-14-08-01-1	14	11.2	112	112	10	7	70	477.8	35

TABLE 5.2 – Parametric study geometrical properties (part 1)

Test	d_b [mm]	t_f [mm]	C [mm]	e [mm]	t_w [mm]	a_w [mm]	L [mm]	B [mm]	e_1 [mm]
T-14-08-01-08	14	11.2	112	89.6	10	7	70	433	35
T-14-08-01-05	14	11.2	112	56	10	7	70	365.8	35
T-16-07-03-1	16	11.2	37.3	37.3	10	7	70	179.1	35
T-18-07-03-08	18	12.6	42	33.6	10	7	70	181	35
T-22-07-03-06	22	15.4	51.3	30.8	10	7	70	194.1	35
T-16-07-02-1	16	11.2	56	56	10	7	70	253.8	35
T-16-07-02-08	16	11.2	56	44.8	10	7	70	231.4	35
T-18-07-02-05	18	12.6	63	31.5	10	7	70	218.8	35
T-16-07-01-1	16	11.2	112	112	10	7	70	477.8	35
T-16-07-01-08	16	11.2	112	89.6	10	7	70	433	35
T-16-07-01-05	16	11.2	112	56	10	7	70	365.8	35
T-18-06-03-1	18	10.8	36	36	10	7	70	173.8	35
T-18-06-03-08	18	10.8	36	28.8	10	7	70	159.4	35
T-27-06-03-06	27	16.2	54	32.4	10	7	70	202.6	35
T-18-06-02-1	18	10.8	54	54	10	7	70	245.8	35
T-18-06-02-08	18	10.8	54	43.2	10	7	70	224.2	35
T-20-06-02-05	20	12	60	30	10	7	70	209.8	35
T-18-06-01-1	18	10.8	108	108	10	7	70	461.8	35
T-18-06-01-08	18	10.8	108	86.4	10	7	70	418.6	35
T-18-06-01-05	18	10.8	108	54	10	7	70	353.8	35

TABLE 5.3 – Parametric study geometrical properties (part 2)

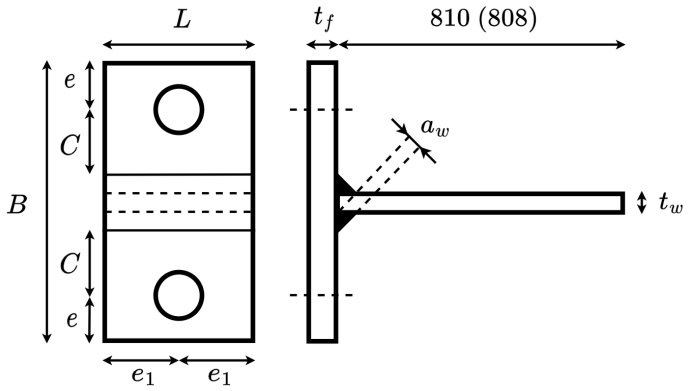

FIGURE 5.4 – Parametric study geometry

At the end, the first parametric study consists in 27 tests.

5.2 Results

First of all, the results were investigated based on the Eurocode assumptions. The latter were presented in CHATER (2) but are recalled here for sake of clarity : A mode 1 collapse occurs when two **plastic hinges** are formed. The first one is located **at 80% of the projection of the weld thickness (starting from the web)** while the second can be found **in the axis of the bolt hole**. At this point, both **MV interaction and membrane effects are neglected**. The **prying forces are located at the flange edge (or $1.25 \cdot m$ if this value is smaller)** and **the stress distribution under the bolt head is supposed uniform**. Concerning the material law, an **elastic law** is attributed to **the bolts** while **the plates** are granted an **elastic-perfectly platsic law**. For sake of clarity, only relevant results are presented in the body of the manuscript. Yet all the detailed results can be consulted in APPENDIX (C).

5.2.1 Position of the hinges

The first assumption that can be invalidated is the **position of the hinges**. It can be seen on FIGURE (5.5) that both hinges are misplaced. Similar observation can be made on each specimen. For the first hinge, it can be observed that its location is at the weld toe or even further while it should be found at 80% of the projection of the weld thickness. On the other hand, the second hinge is not localised at the bolt axis but is offset towards the web. Notice that, although this case was not encountered, the hinge could be so eccentric that the bolt may not work at all. TABLE (5.6) summarizes the correction that should be applied to the positions in addition to the plastic strength.

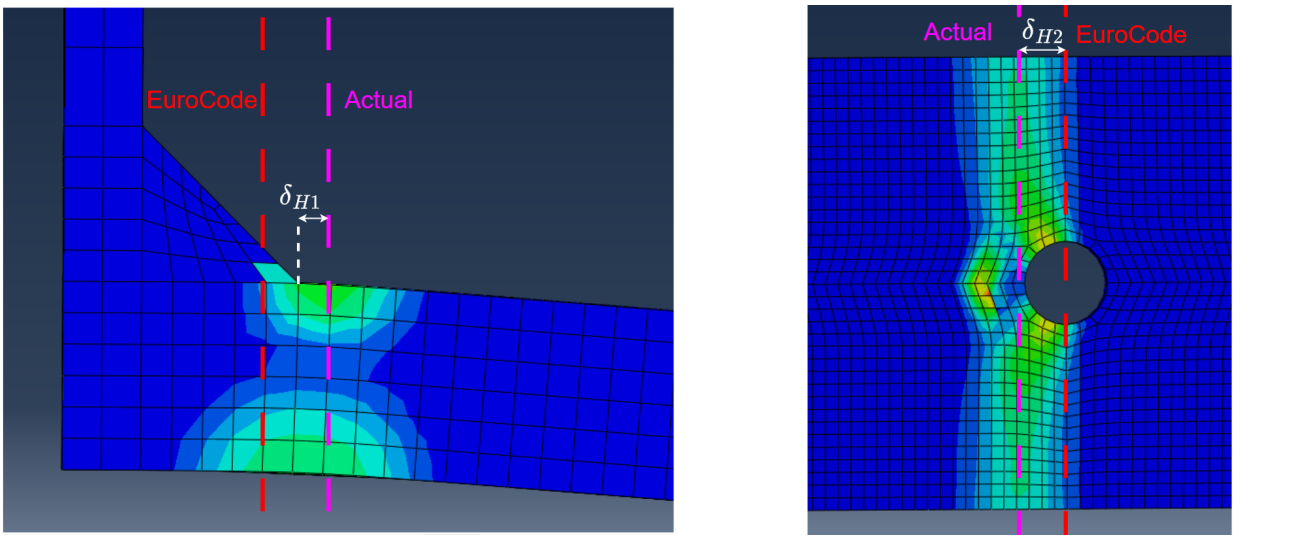

(a) Plastic hinge at the weld toe T-27-08-03-05 (b) Plastic hinge at the bolt axis T-12-09-01-05

FIGURE 5.5 – Position of the plastic hinges

5.2.2 Membrane effects

Then, to determine the contribution of the membrane effect, the force-displacement of the T-stub can be analysed. This is done on the following FIGURE (5.6). On the response can be seen a slight increase of the strength. This is due to the membrane effect. However, this contribution appears later in the post-yielding response and thus, is irrelevant at yielding.

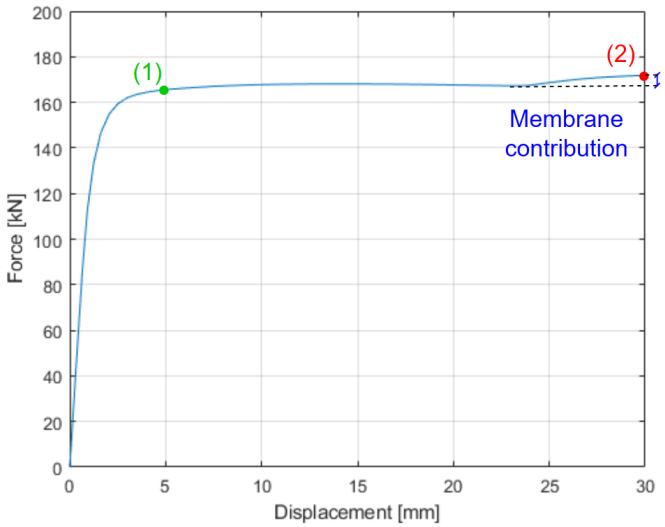

FIGURE 5.6 – Contribution of the membrane effect T-27-08-03-05

This observation seems quite logic. Indeed, membrane effect can be defined as the apparition of tensile stress in the deformed configuration. Thus, large rotations at the plastic hinges are required. FIGURE (5.7) shows the deformation of the two specific points (1) and (2) highlighted on FIGURE (5.6) hereabove. On the first one at yielding (1), the small displacement does not allow membrane effect to develop. This contrast with the second point at large displacement (2). In this configuration, the projection of the internal force perpendicularly and parallel to the flange axis shows a non negligible axial contribution.

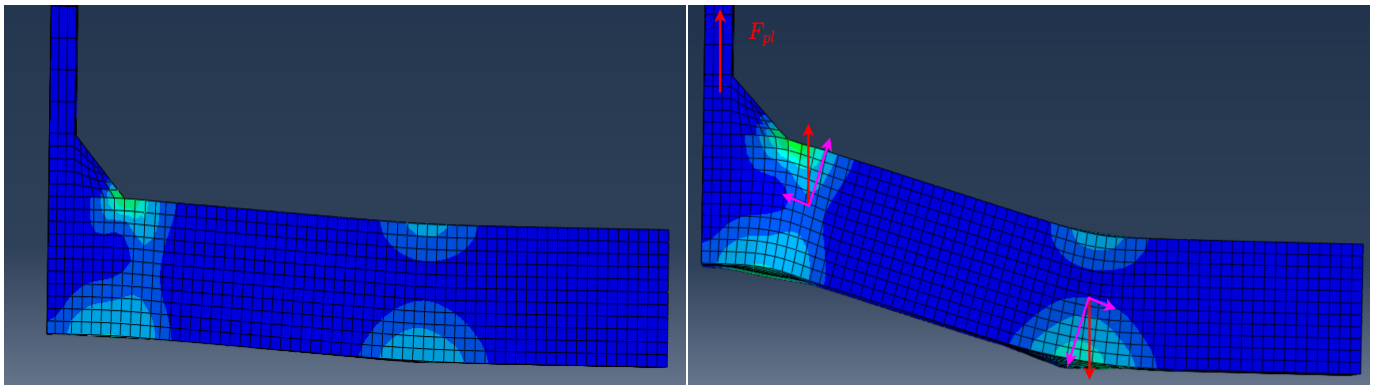

(a) Yielding (1) (b) Large displacement (2)

FIGURE 5.7 – Deformation of specimen T-27-08-03-05

5.2.3 Stress distribution under the bolt head

Afterwards, the stress distribution under the bolt head can be investigated. This can be done by looking the contact pressures in ABAQUS© which are illustrated on FIGURE (5.8). It can be observed that **the uniform distribution assumed in the EuroCode is inadequate**.

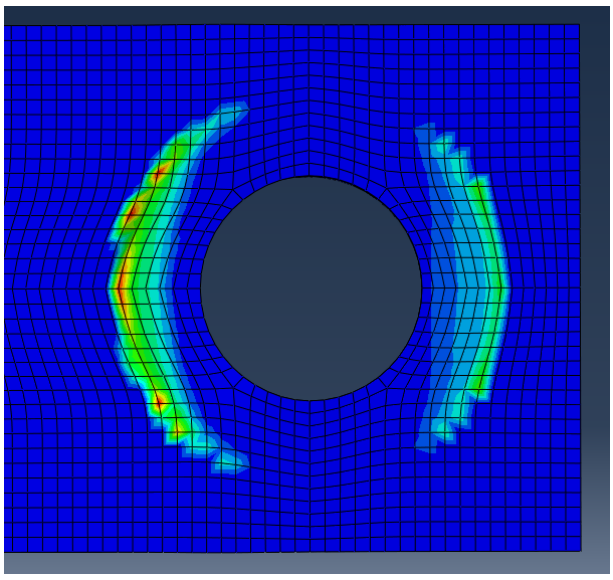

FIGURE 5.8 – Real stress distribution under the bolt head T-27-08-03-05

Indeed, due to the T-stub deformation, one side tends to move up while the other remains in place. This configuration induces **flexion in the bolts as suggested by the asymmetry of the distribution**. Another consequence is that stress concentration occurs at the washer edges. From this perspective, a uniform distribution does not make sense. **A triangular distribution** seems more suitable to idealise the contact pressure exerted by the bolt head. Those two cases are depicted on FIGURE (5.9) hereafter.

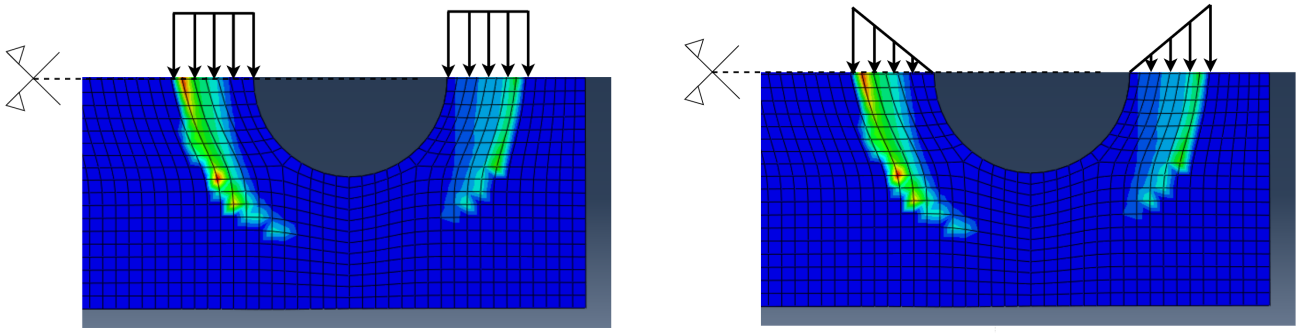

(a) Uniform distribution (b) Triangular distribution

FIGURE 5.9 – Assumed stress distribution under the bolt head

5.2.4 Position of the prying forces

Next, a focus was made on the prying forces. A first interesting observation is that all the force-displacement curves look alike when the flange edge length is the only varying parameter. However, in the studied test, the value of e was quite important. So, additional tests were performed to study the impact of this variable. Their geometry is summarised in the TABLE (5.4) herebelow.

Test	d_b [mm]	t_f [mm]	C [mm]	e [mm]	t_w [mm]	a_w [mm]	L [mm]	B [mm]	e_1 [mm]
T-14-08-02-05	14	11.2	56	28	10	7	70	197.8	35
T-14-08-02-06	14	11.2	56	33.6	10	7	70	209	35
T-14-08-01-02	14	11.2	112	22.4	10	7	70	298.6	35
T-14-08-01-025	14	11.2	112	28	10	7	70	309.8	35
T-14-08-01-03	14	11.2	112	33.6	10	7	70	321	35

TABLE 5.4 – Prying forces series geometrical properties

A conclusion drawn from this series is that the prying forces location does not impact the solution. Indeed, as it can be seen on FIGURE (5.10) that all the force-displacement curves overlap. Thus, it can be deduced that the works exerted by the bolt and the prying forces are identical for each of these specimens. However, it is not what the EuroCode model predicts as it can be seen with the two distinguished predicted strengths (see the red and blue lines in FIGURE (5.10)).

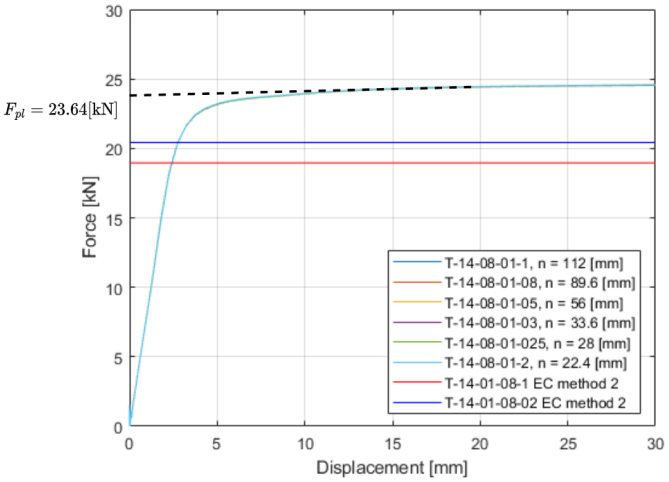

FIGURE 5.10 – T-14-08-01-XX series force-displacement curves

FIGURE (5.11) shows the contact pressures distribution between the flanges for the two extreme cases of this series. For the longest one (T-14-08-01-1), it can be seen that all the contact pressures are localised near the bolt hole and vanishes past a certain distance. In this case, the prying forces are assumed to apply at the flange edge while, if they were rigorously integrated, their location would be much closer to the hole. For the shortest specimen (T-14-08-01-02), assuming the prying forces at the flange edge is a good approximation of the true integrative process.

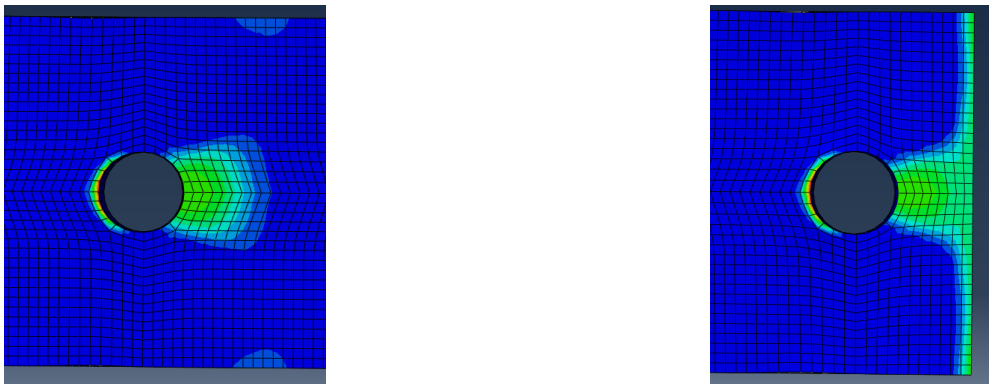

(a) Specimen T-14-08-01-1 (b) Specimen T-14-08-01-02

FIGURE 5.11 – Contact pressures distribution between the flanges for the T-14-08-01-XX series

In fact, for each specimen of the series, the prying forces should be approximately positioned at the same place according to EuroCode. This highlights that a boundary is missing in the formula of n. For mode 1 and mode 1 **only**, the criteria should write as EQUATION (5.1) hereafter. Notice that this new boundary should not apply to the mode 2 due to the definition of this failure mode.

$$n_{mode1} = \min(e; 1.25m; \text{to be found}) \tag{5.1}$$

Where the $1.25m$ criterion was proposed by [**25**] based on experimental observations. The shape of the contact pressures distribution previously shown can be attributed to the bending in the bolts as illustrated on FIGURE (5.12). Indeed, one side of the bolt undergoes a displacement while the other side does not move. Nevertheless, the bolt cannot deform freely and is blocked by the flanges. This results in the stress distribution under the bolt head presented in FIGURE (5.8). This also implies that the flanges are clamped by the bolt head and the nut. Thus, this compressing force distributes as shown in FIGURE (5.12) hereafter, which results in the illustration of FIGURE (5.11).

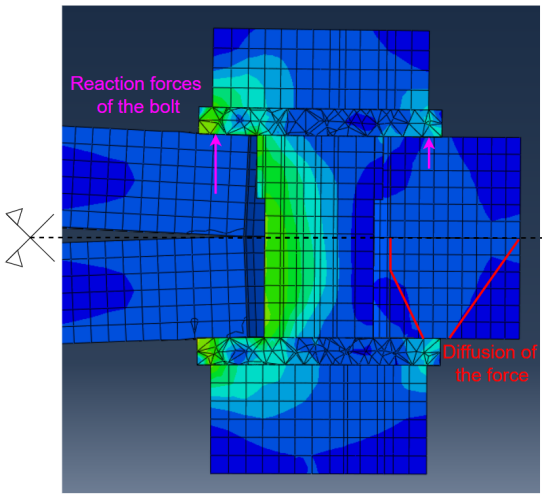

FIGURE 5.12 – Distribution of the bolt head force up to the contact pressure

5.2.5 Yield line pattern

Finally, it should be pointed out that all the T-stubs modelled do not exhibit the same yield line pattern. Indeed, some have a pattern composed of two straight lines as expected by theory for short T-stubs. On the other hand, some show an interaction between their yield lines. While the first one at the weld toe is rectilinear, the second one has a curved part mixed to a rectilinear pattern. Those configurations are represented on FIGURE (5.13).

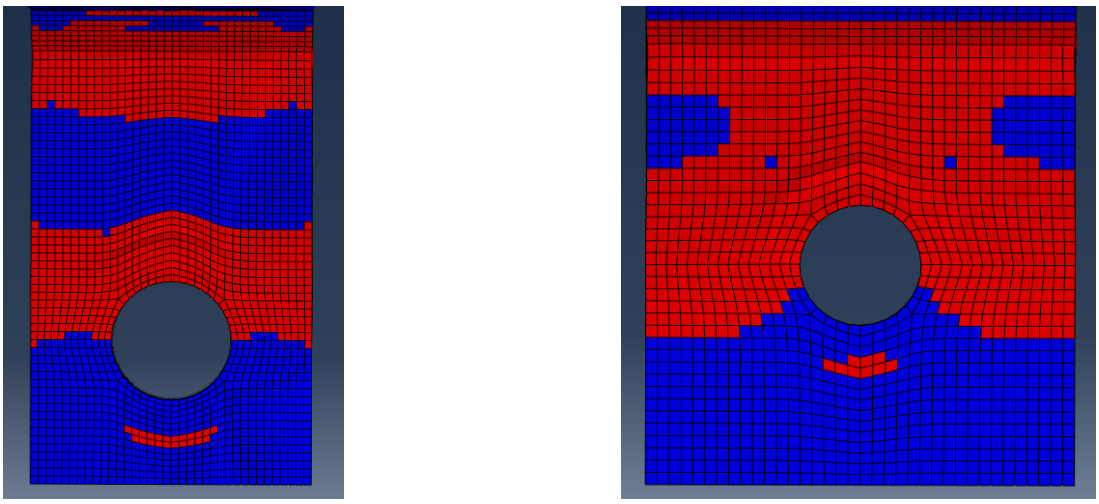

(a) Specimen T-27-08-03-05 (b) Specimen T-18-06-03-1

FIGURE 5.13 – Yield line patterns encountered

To investigate this phenomena and the transition between the two patterns, additional tests were performed. They can be identified as three different series which geometrical properties are summarised in TABLE (5.5). The first one fills the gaps in the t_f/C ratios considered and consists in the first research axis. Then, for the second series, a specimen is chosen. Its bolt diameter varies while all the dimensionless parameters remain constant. The third and last series studies the effect of the flange thickness alone. A special denomination is granted to this series since it does not follow the same philosophy as the previous specimen. Their name should read $T - d_b - t_f - C$.

Test	d_b [mm]	t_f [mm]	C [mm]	e [mm]	t_w [mm]	a_w [mm]	L [mm]	B [mm]	e_1 [mm]
T-12-09-015-1	12	10.8	72	72	10	7	70	317.8	35
T-14-08-015-1	14	11.2	74.7	74.7	10	7	70	328.5	35
T-16-07-015-1	16	11.2	74.7	74.7	10	7	70	328.5	35
T-16-07-025-1	16	11.2	44.8	44.8	10	7	70	209	35
T-18-06-015-1	18	10.8	72	72	10	7	70	317.8	35
T-18-06-025-1	18	10.8	43.2	43.2	10	7	70	202.6	35
T-22-08-03-05	22	17.6	58.7	29.3	10	7	70	205.8	35
T-24-08-03-05	24	19.2	64	32	10	7	70	221.8	35
T-30-08-03-05	30	24	80	40	10	7	70	269.8	35
T-27-14-50	27	14	50	36	10	7	70	201.8	35
T-27-14-72	27	14	72	36	10	7	70	245.8	35
T-27-16-72	27	16	72	36	10	7	70	245.8	35
T-27-17-72	27	17	72	36	10	7	70	245.8	35
T-27-18-72	27	18	72	36	10	7	70	245.8	35

TABLE 5.5 – Additional series geometrical properties

5.3 Conclusions

In this Section, a parametric study of 45 tests was performed. All the assumptions made by the EuroCode model were studied in depth :

— The membrane effect can, indeed, be neglected at yielding.

— The plastic hinges are inadequately placed. The first one is located at the weld toe or even further. The second one is offset from the bolt axis towards the web. Table (5.6) hereafter summarises the real positions of the hinges.

— The stress distribution under the bolt head was proved to wrongly be assumed uniform. A triangular distribution seems more suitable.

— The prying forces were also proved to be misplaced but for mode 1 only. In this configuration, a boundary is missing in the formulation of n.

— Even if the specimens length was fixed at 70 [mm] to ensure that all the T-stubs are short with a yield line pattern consisting of two straight lines, some tests showed another yield line pattern.

Some analytical developments proposed in the next Section try to improve the current model and correct the observed inconsistencies in purpose to improve the prediction of F_{pl}. Remind that this key value is found at the intersection of the Y axes and the tangent to the yield plateau in the force-displacement curves (see Figure (5.10)). Notice that all the force-displacement curves of the specimens presented in this study can be found in Appendix (C).

Specimens	δ_{H1} [mm]	δ_{H2} [mm]	F_{pl} [kN]
T12-09-015-1	3	6	35.11
T12-09-01-1	4	8	21.92
T12-09-01-08	4	8	21.92
T12-09-01-05	4	8	21.92
T22-08-03-05	2.5	8	132.52
T24-08-03-05	3	10	147.97
T27-08-03-05	3	12	166
T30-08-03-05	3	14	185.25
T14-08-02-08	2	6	54
T14-08-02-06	2	6	54
T14-08-02-05	2	6	54
T16-08-02-05	2	7	60.56
T14-08-015-1	3	8	37.94
T14-08-01-1	4	9	23.64
T14-08-01-08	4	9	23.64
T14-08-01-05	4	9	23.64
T14-08-01-03	4	9	23.64
T14-08-01-025	4	9	23.64
T14-08-01-02	4	9	23.64
T18-07-03-08	1.5	5	104.12
T22-07-03-06	2	8	123.35
T16-07-025-1	2	6	74.08
⋮	⋮	⋮	⋮

Specimens	δ_{H1}	δ_{H2}	F_{pl}
⋮	⋮	⋮	⋮
T16-07-02-1	2	8	56.13
T16-07-02-08	2	8	56.13
T18-07-02-05	2	9	63.43
T16-07-015-1	3	9	39.79
T16-07-01-1	4	10	24.34
T16-07-01-08	4	10	24.34
T16-07-01-05	4	10	24.34
T18-06-03-1	1	4	97.55
T18-06-03-08	1	4	97.55
T27-06-03-06	1	12	151.44
T18-06-025-1	2	6	78.13
T18-06-02-1	2	9	58.51
T18-06-02-08	2	9	58.51
T20-06-02-05	2	10	64.45
T18-06-015-1	3	11	39.94
T18-06-01-1	4	13	23.96
T18-06-01-08	4	13	23.96
T18-06-01-05	4	13	23.96
T27-14-50	3	17	132.57
T27-14-72	1	13	80.21
T27-16-72	3	16	101.38
T27-17-72	4	14	112
T27-18-72	4	14	123.42

Table 5.6 – Results of the parametric study

Chapter 6

Analytical models

Finally, the problems identified in CHAPTER (5) are investigated through analytical developments. First, an empirical formulation for the plastic hinges location is proposed. Then this aspect, in addition to the stress distribution under the bolt head, are integrated in the bolt work. Afterwards, an effective length is computed for the new yield line pattern observed. Next, MV interaction is introduced into the model to assess the validity of the assumptions made by the EuroCode. In fact, a classification criterion based on the stiffness is required to classify the T-stubs. To conclude this CHAPTER, the new proposal is summarised before being validated against the test campaigns previously developed in SECTION (3.2).

6.1 Hinges position

To study this first problematic, the influence of many parameters on the real hinges position provided by ABAQUS© in TABLE (5.6) was investigated. It appears that the most relevant one is the ratio between the bolts and plate stiffnesses of EQUATIONS (2.14) and (2.15). Notice that the m parameter issued from EuroCode is replaced by the geometrical property C (see FIGURE (5.4)).

$$k_{rel} = \frac{k_{bolt}}{k_{plate}} = \frac{\frac{1.6A_s}{L_b}}{\frac{0.9t_f^3 L}{C^3}} = \frac{1.6A_s C^3}{0.9L_b t_f^3 L} \tag{6.1}$$

FIGURE (6.1) herebelow shows the representation of the first correction factor δ_{H1} as a function of the stiffness ratio. A clear tendency in the results can be identified. However, an horizontal spreading of the tests results is still to be ascertained. Unfortunately, the parameter causing this phenomena could not be identified.

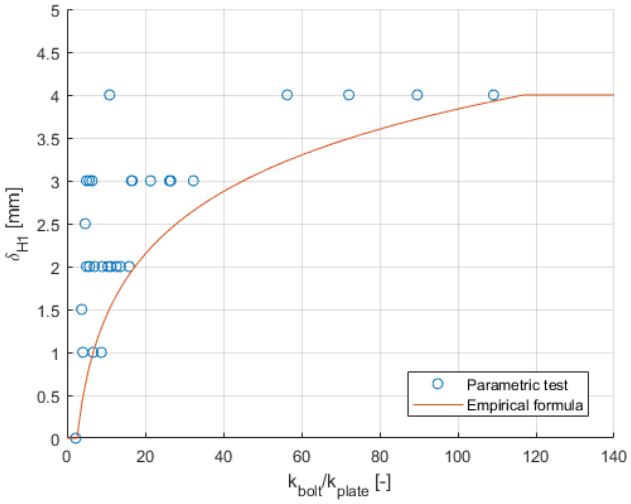

FIGURE 6.1 – Empirical fitting of the plastic hinge location at the weld toe

Moreover, an analytical formulation was not found as well. In consequence, a preliminary empirical formulation is proposed. Before fitting a curve through the parametric test represented by the blue "o", the guidelines followed must be highlighted. It was decided that the proposed formulation has to be conservative since its purpose is to be applied to real experimental tests. Owing this, the conclusion drawn in SECTION (5.2) stating that the position assumed by EuroCode is too conservative is used. In consequence, **the empirical formulation is conservative if it underestimates δ_{H1}**. Thus, EQUATION (6.2) representing the orange curve of FIGURE (6.1) is proposed hereafter. Notice that the boundary of 4 [mm] is fixed based on empirical observations.

$$\delta_{H1} = 0 \leq 1.05 \ln k_{rel} - 1 \leq 4 \text{ [mm]} \tag{6.2}$$

Critics must be emitted on this formula. Indeed, it is very inconvenient that this formulation has units. The unidentified parameter causing the horizontal spreading is likely to be the cause. Notice that the weld properties and dimensions were not studied in the parametric study and may be relevant for this problem. This also raises the question of the range of validity of the proposed EQUATION. Since all the specimens consists in welded sections, **this formula should not be applied to rolled sections** without any further study and validation.

A similar procedure was used to determine the position of the second hinge at the bolt axis. A major difference can still be noticed on FIGURE (6.2). Indeed, the horizontal spreading was here avoided by normalizing δ_{H2} by the diameter of the washer d_w.

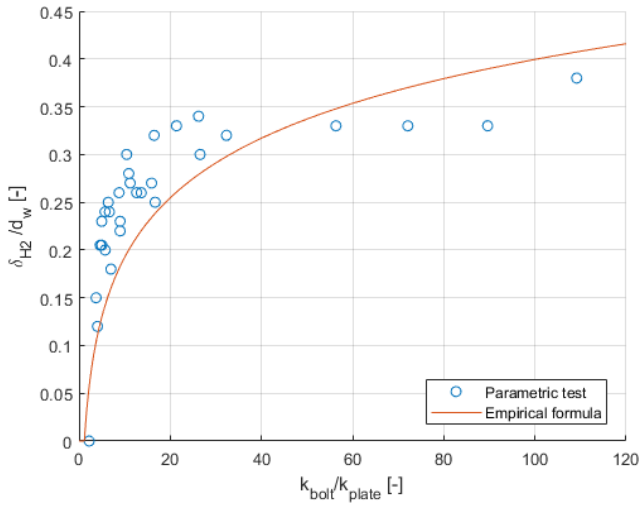

FIGURE 6.2 – Empirical fitting of the plastic hinge location at the bolt axis

As it was previously done, the curve was fitted is such way that the obtained results are conservative. In other words, it means that δ_{H2} may be underestimated and by consequence, the hinge is located closer to the conservative position assumed by EuroCode. The EQUATION of this curve is the following :

$$\delta_{H2} = (0 \leq 0.09 \ln k_{rel} - 0.015 \leq 0.5)\, d_w \text{ [mm]} \tag{6.3}$$

In comparison to the other criteria, the one proposed here does not have any coefficient with dimension which is better. It must be precised that this formula should not be used on rolled section as well since all the specimens were welded. Although further validation for that kind of section should be performed for sake of completion, it seems unlikely that the weld or such parameter influences the hinge near the bolt.

6.2 Bolt head work

Then, considering that the stress distribution under the bolt head has to be modified, the EQUATION (2.3) taking this effect into account must be rewritten. However, the position of the plastic hinge should also be integrated in the process of assessing the work of the bolt head. Indeed, as represented on FIGURE (6.3), the bolt head works more or less depending of the hinge position. If the hinge offset is such as the hinge is located further than the washer edge, the bolt should not be allowed to contribute to the strength and the formulation should degenerate in EQUATION (2.2). In fact, the reality lies between the current methods 1 and 2. In consequence, the new formulation to be developed should take into account the triangular stress distribution, the presence of the hole and the real position of the hinge in such way that it degenerates either in method 1 or 2 depending the extreme case encountered.

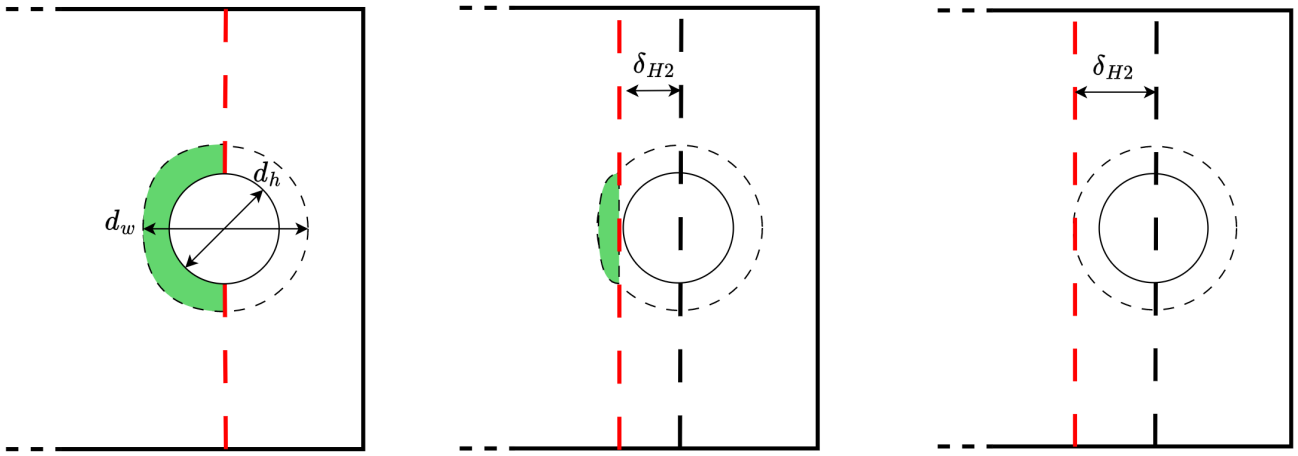

(a) Half of the head (see method 2) (b) Intermediate configuration (c) None of the head (see method 1)

FIGURE 6.3 – Part of the bolt head contributing to the virtual work

FIGURE (6.4) hereafter is a zoom on the bolt head and shows the equivalent force diagram obtained after integration of the assumed stress distribution. On the right side of the FIGURE can be seen a distinction between the part of the bolt head that undergoes a displacement and thus works, and the part that does not work.

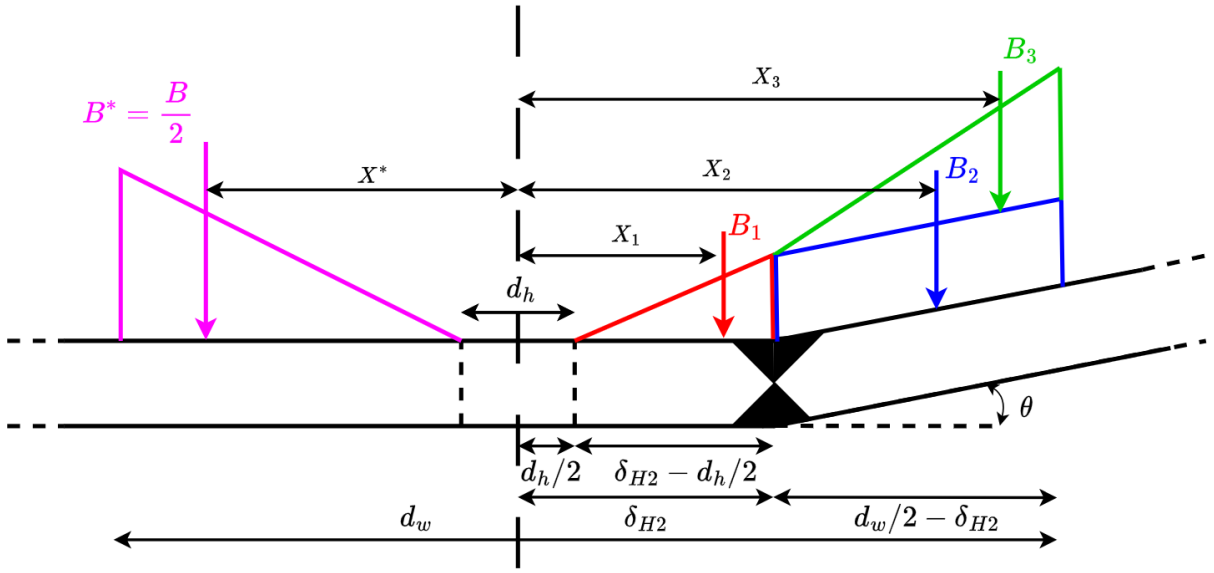

FIGURE 6.4 – Force diagram at the bolt head

The expressions of the integrated forces and their locations in respect to the hole axis are proposed herebelow.

$$B_1 = \frac{4B^*}{(d_w - d_h)^2}\left(\delta_{H2} - \frac{d_h}{2}\right)^2 \qquad X_1 = \frac{d_h}{2} + \frac{2}{3}\left(\delta_{H2} - \frac{d_h}{2}\right) \tag{6.4}$$

$$B_2 = \frac{8B^*}{(d_w - d_h)^2}\left(\delta_{H2} - \frac{d_h}{2}\right)\left(\frac{d_w}{2} - \delta_{H2}\right) \qquad X_2 = \delta_{H2} + \frac{1}{2}\left(\frac{d_w}{2} - \delta_{H2}\right) \tag{6.5}$$

$$B_3 = \frac{4B^*}{(d_w - d_h)^2}\left(\frac{d_w}{2} - \delta_{H2}\right)^2 \qquad X_3 = \delta_{H2} + \frac{2}{3}\left(\frac{d_w}{2} - \delta_{H2}\right) \tag{6.6}$$

$$B^* = B_1 + B_2 + B_3 \qquad X^* = \frac{d_w - d_h}{3} + \frac{d_h}{2} \tag{6.7}$$

Owing the set of equations previously set, three unknowns remain : B^*, Q and F_{pl}. By performing equilibria, three equations can be established and thus close the system. Equations (6.8) and (6.10) are obtained trough vertical and energy equilibrium respectively on the entire system depicted on Figure (6.5). On the other hand, the bending moment Equation (6.9) is found by writing the equilibrium of a part on the beam model (on the right side of the hinge located at the bolt axis).

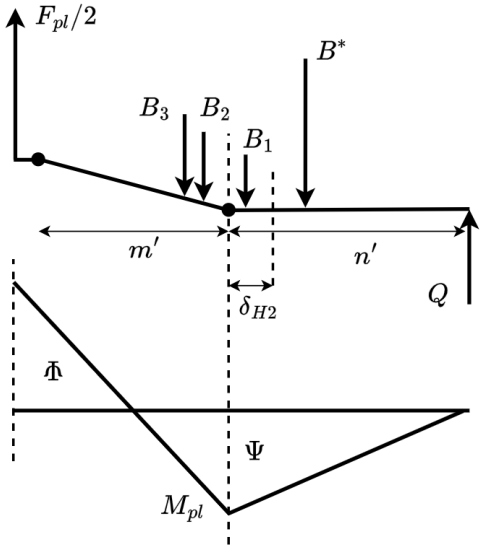

Figure 6.5 – Beam model with the new plastic hinges

$$Q = 2B^* - \frac{F_{pl}}{2} \tag{6.8}$$

$$M_{pl} + \frac{B_1}{3}\left(\delta_{H2} - \frac{d_h}{2}\right) + B^*\left(\delta_{H2} + \frac{d_h}{2} + \frac{d_w - d_h}{3}\right) = Q'n \tag{6.9}$$

$$\frac{F_{pl}m'}{2} - \frac{B_2}{2}\left(\frac{d_w}{2} - \delta_{H2}\right) - \frac{2B_3}{3}\left(\frac{d_w}{2} - \delta_{H2}\right) = 2M_{pl} \tag{6.10}$$

It can be seen from EQUATIONS (6.8) and (6.9) that the prying forces can easily be simplified by equaling those expressions. Thus, B^* is the only unknown from the obtained expression and can be isolated after few rewritings. The following formulae can be found :

$$B^* = \frac{-(3F_{pl}n' + 6M_{pl})(d_w - d_h)^2}{G} \tag{6.11}$$

$$G = (2\delta_{H2} - d_h)^3 + (d_w - d_h)^2(6\delta_{H2} + d_h + 2d_w - 12n') \tag{6.12}$$

Finally, by injecting this expression in EQUATION (6.10), the plastic strength formula can be determined. The EQUATION obtained is the following :

$$F_{pl} = \frac{2M_{pl}(2G - \zeta(d_w - 2\delta_{H2})^2)}{m'G + n'\zeta(d_w - 2\delta_{H2})^2} \tag{6.13}$$

with $\zeta = 2\delta_{H2} - 3d_h + 2d_w$, a parameter introduced for sake of readability. All the demonstration, line by line, can be consulted in APPENDIX (B). Notice that the expression degenerates in the limit cases illustrated on FIGURE (6.3) as expected. To obtain the method 1 of EuroCode, it requires that $\delta_{H2} = d_w/2$. On the other hand, a result more or less similar to the method 2 (with $e_w = d_w/3$ instead of $d_w/4$) can be found if $\delta_{H2} = 0$ and $d_h = 0$ (artificial). TABLE (6.1) illustrates the impact of this rewriting on the results of the parametric study.

Specimens	F_{EC} [mm]	$F_{Neutelers}$ [mm]	$F_{pl,Abaqus}$ [kN]
T12-09-015-1	27.67	32.09	35.11
T12-09-01-1	18.21	20.34	21.92
T12-09-01-08	18.28	20.37	21.92
T12-09-01-05	18.49	20.47	21.92
T22-08-03-05	102.25	132.61	132.52
T24-08-03-05	112.8	148.17	147.97
T27-08-03-05	127.69	166.48	166
T30-08-03-05	142.6	184.18	185.25
T14-08-02-08	39.53	47.77	54
T14-08-02-06	40.18	48.56	54
T14-08-02-05	40.72	49.23	54
T16-08-02-05	46.56	55.52	60.56
T14-08-015-1	28.89	33.93	37.94
T14-08-01-1	18.96	21.28	23.64
T14-08-01-08	19.04	21.32	23.64
T14-08-01-05	19.29	21.44	23.64
T14-08-01-03	19.77	21.66	23.64
T14-08-01-025	20.02	21.77	23.64
T14-08-01-02	20.42	21.95	23.64
T18-07-03-08	71.6	94.66	104.12
T22-07-03-06	89.81	120.47	123.35
T16-07-025-1	50.55	65.75	74.08
⋮	⋮	⋮	⋮

Specimens	F_{EC}	$F_{Neutelers}$	$F_{pl,Abaqus}$
⋮	⋮	⋮	⋮
T16-07-02-1	39.61	49.09	56.13
T16-07-02-08	40.04	51.26	56.13
T18-07-02-05	46.87	57.09	63.43
T16-07-015-1	29.13	34.65	39.79
T16-07-01-1	19.07	21.56	24.34
T16-07-01-08	19.16	21.61	24.34
T16-07-01-05	19.44	21.75	24.34
T18-06-03-1	61.73	81.9	97.55
T18-06-03-08	63.19	84.83	97.55
T27-06-03-06	100.2	140.88	151.44
T18-06-025-1	50	67.28	78.13
T18-06-02-1	38.95	49.9	58.51
T18-06-02-08	39.47	50.48	58.51
T20-06-02-05	45.74	57.4	64.45
T18-06-015-1	28.49	34.82	39.94
T18-06-01-1	18.55	21.42	23.96
T18-06-01-08	18.66	21.45	23.96
T18-06-01-05	18.99	21.55	23.96
T27-14-50	80.21	117.47	132.57
T27-14-72	53.64	69.07	80.21
T27-16-72	70.07	90.44	101.38
T27-17-72	79.1	102.71	112
T27-18-72	88.68	117.54	123.42

TABLE 6.1 – Impact of the new bolt head work formula

6.3 Yield line pattern

To conclude the previous SECTION, it was shown that the new formula for the bolt head work significantly improves the results. However, some can still be considered inaccurate. The reason behind this inconsistency is the mischaracterisation of the yield line pattern as pointed in SECTION (4.3).

FIGURE (6.6) hereafter shows the equivalent plastic strain of the T-18-06-03-01 specimen. By proceeding this way, a hybrid pattern can be identified. It is in the combination of a circular pattern and the "short T-Stub" pattern consisting of two straight lines.

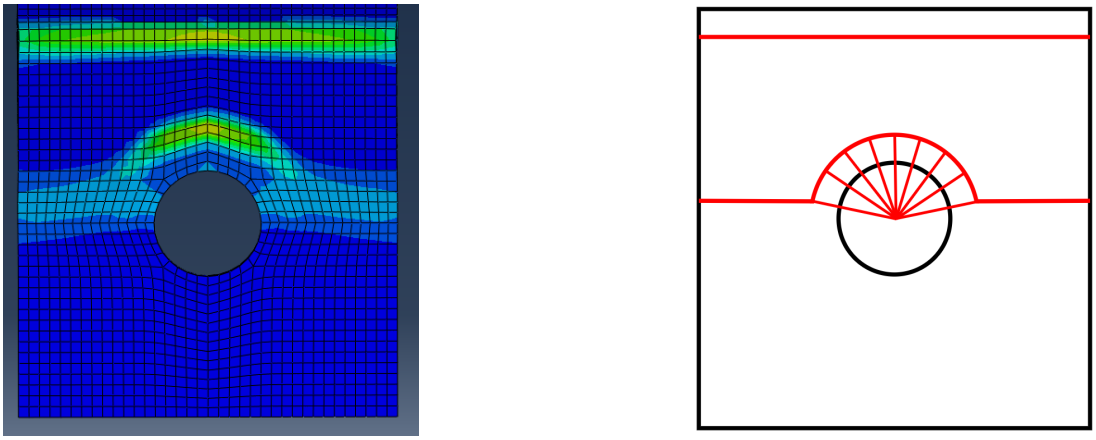

(a) Plastic equivalent strain (b) yield line pattern

FIGURE 6.6 – Identification of the new yield line pattern

As a first approach, the philosophy of the EuroCode can be followed. The idea is to use an effective length as presented in SECTION (2.2). To present this principle, the development of the internal energy term for a short T-stub is proposed (see APPENDIX (B) for additional information).

$$\Delta E = M_{pl,H1}\theta + M_{pl,H2}\theta = m_{pl}L_{H1}\theta + m_{pl}L_{H2}\theta = 2m_{pl}\left(\frac{L_{H1}+L_{H2}}{2}\right)\theta = 2m_{pl}L_{eff}\theta = 2M_{pl,mean}\theta \quad (6.14)$$

For the short T-stub, $L_{H1} = L_{H2} = L$ and thus, $L_{eff} = L$ as stated by EQUATION (2.7). The same procedure can be applied to the new yield line pattern. FIGURE (6.7) illustrates the geometry of the problem.

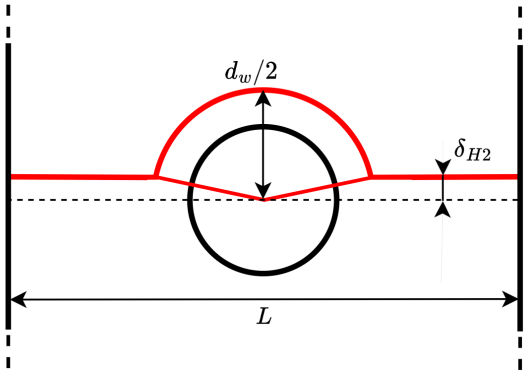

FIGURE 6.7 – Geometry of the hybrid yield line pattern

From this FIGURE can be identified the hinges lengths. Their expressions are the followings :

$$L_{H1} = L \tag{6.15}$$

$$L_{H2} = L - 2\sqrt{\frac{d_w^2}{4} - \delta_{H2}^2} + \frac{d_w}{2}\left(\pi - 2\arcsin\left(\frac{\delta_{H2}^2}{d_w/2}\right)\right) \tag{6.16}$$

Owing this, EQUATION (6.13) can be used where M_{pl} is simply $m_{pl}L_{eff}$. The results obtained with this procedure are summarised in TABLE (6.2) hereafter. Notice that this expression simplifies in $L_{H2} = L$ when the second hinge offset is $d_w/2$. In other words, when the hinge is at a distance further or equal to the washer edge.

Nevertheless, the model could be further improved. Indeed, the proposed formulation is a simple combination of two existing patterns. To be rigorous, a full integration of the real displacement and rotation at the hinges should be performed. In addition to that, it must be noticed that the work of the bolt head was not recomputed for the proposed configuration. In conclusion, to solve all these inconsistencies, the current model for the yield line pattern should be reviewed more rigorously. The results are still presented to assess the improvement done by this new pattern.

Specimens	F_{EC} [mm]	$F_{Neutelers}$ [mm]	$F_{pl,Abaqus}$ [kN]
T12-09-015-1	27.67	33.09	35.11
T12-09-01-1	18.21	20.68	21.92
T12-09-01-08	18.28	20.71	21.92
T12-09-01-05	18.49	20.81	21.92
T22-08-03-05	102.25	141.33	132.52
T24-08-03-05	112.8	157.87	147.97
T27-08-03-05	127.69	177.95	166
T30-08-03-05	142.6	197.53	185.25
T14-08-02-08	39.53	49.75	54
T14-08-02-06	40.18	50.57	54
T14-08-02-05	40.72	51.26	54
T16-08-02-05	46.56	57.91	60.56
T14-08-015-1	28.89	34.78	37.94
T14-08-01-1	18.96	21.68	23.64
T14-08-01-08	19.04	21.72	23.64
T14-08-01-05	19.29	21.84	23.64
T14-08-01-03	19.77	22.06	23.64
T14-08-01-025	20.02	21.18	23.64
T14-08-01-02	20.42	22.35	23.64
T18-07-03-08	71.6	101.84	104.12
T22-07-03-06	89.81	128.39	123.35
T16-07-025-1	50.55	69.17	74.08
⋮	⋮	⋮	⋮

Specimens	F_{EC}	$F_{Neutelers}$	$F_{pl,Abaqus}$
⋮	⋮	⋮	⋮
T16-07-02-1	39.61	50.8	56.13
T16-07-02-08	40.04	51.26	56.13
T18-07-02-05	46.87	59.37	63.43
T16-07-015-1	29.13	35.6	39.79
T16-07-01-1	19.07	22.01	24.34
T16-07-01-08	19.16	22.05	24.34
T16-07-01-05	19.44	22.2	24.34
T18-06-03-1	61.73	89.09	97.55
T18-06-03-08	63.19	92.27	97.55
T27-06-03-06	100.2	150.59	151.44
T18-06-025-1	50	71.77	78.13
T18-06-02-1	38.95	51.89	58.51
T18-06-02-08	39.47	52.5	58.51
T20-06-02-05	45.74	59.8	64.45
T18-06-015-1	28.49	35.7	39.94
T18-06-01-1	18.55	21.71	23.96
T18-06-01-08	18.66	21.74	23.96
T18-06-01-05	18.99	21.84	23.96
T27-14-50	80.21	124.59	132.57
T27-14-72	53.64	71.29	80.21
T27-16-72	70.07	93.92	101.38
T27-17-72	79.1	108.13	112
T27-18-72	88.68	123.75	123.42

TABLE 6.2 – Impact of the new yield line pattern formula

It can be observed that the results obtained are significantly better than the ones proposed by the Euro-Code. In addition to that, some results overestimate the plastic strength. This observation is not surprising considering that they were perfectly assessed in the SECTION related to the bolt head work (see the boxes in green in TABLE (6.1). This means that these tests have an effective length which consist in their real dimension. This length corresponds to the definition of a short T-stub proposed by the Eurocode (see SECTION (2.2)) and is shorter than the one developed in the present SECTION.

6.4 MV interaction

In SECTION (5.2), it was explained that according to EuroCode, MV interaction may be neglected. This assumption was still unchecked. To solve this problem, a simple model taking this effect into account is developed. The results obtained with this model can thus be compared to the results without the interaction and the assumption may be be validated or not. This phenomena is applied through a penalisation coefficient ρ which can be defined as follows :

$$\rho = \left(\frac{2v_{ed}}{v_{Rd}} - 1\right)^2 \tag{6.17}$$

Where v_{ed} and v_{Rd} are the applied shear force and the shear resistance respectively. If the former is at least bigger than half the latter, then MV interaction should be considered when assessing the yield strength. Introduced in the plastic bending moment by units of length m_{pl}, it comes :

$$m_{pl}^{MV} = \frac{t_f^2 f_y^{MV}}{4} = (1-\rho)\frac{t_f^2 f_y}{4} = (1-\rho)m_{pl} \tag{6.18}$$

Then, this expression can be injected in EQUATION (6.14) assessing the internal energy of deformation of the mechanism. Notice that the penalisation should only be applied on the first hinge and the curved part of the second one.

$$\Delta E = (1-\rho_{H1})m_{pl}L\theta + m_{pl}\theta\left(L - 2\sqrt{\frac{d_w^2}{4} - \delta_{H2}^2}\right) + \frac{d_w}{2}\left(\pi - 2\arcsin\left(\frac{\delta_{H2}^2}{d_w/2}\right)\right)(1-\rho_{H2})m_{pl}\theta \tag{6.19}$$

Afterwards, the shear applied force and resistance must still be defined. The latter is the simplest and simply consists in the following expression :

$$v_{Rd} = \frac{t_f f_y}{\sqrt{3}} \tag{6.20}$$

Notice that this resistance is expressed by unit of length. The reason of this choice will appear clearly when focusing on the hinge near the bolt. The shear force by unit of length that has to be transferred by the plastic hinge at the weld toe is simply half of the plastic strength over its entire length :

$$v_{ed,H1} = \frac{F_{pl}/2}{L} \tag{6.21}$$

Concerning the second hinge, the force that must be transmitted is only a fraction of the bolt force. To be conservative, this force is assumed to be the half. In other words, it corresponds to B^* of EQUATION (6.11) previously established. This load is supposed to be applied on the perimeter of the washer located on the yielding mechanism.

$$v_{ed,H2} = \frac{B^*}{\frac{d_w}{2}\left(\pi - 2\arcsin\left(\frac{\delta_{H2}^2}{d_w/2}\right)\right)} \tag{6.22}$$

From this simple model, it appears that none of the specimens of the parametric study undergoes MV interaction at the hinge located at the weld toe. On the other hand, MV interaction is sometimes detected near the bolt. However, as illustrated in TABLE (6.3), it can be considered negligible. In consequence, the assumption made by the EuroCode to neglect the MV interaction seems to be correct.

Specimens	F_{hybrid} [mm]	F_{MV} [mm]	Penalisation [%]
T12-09-015-1	33.09	33.09	0
T12-09-01-1	20.68	20.68	0
T12-09-01-08	20.71	20.71	0
T12-09-01-05	20.81	20.81	0
T22-08-03-05	141.33	137.37	2.9
T24-08-03-05	157.87	154.65	2
T27-08-03-05	177.95	176.22	1
T30-08-03-05	197.53	196.87	0.3
T14-08-02-08	49.75	49.75	0
T14-08-02-06	50.57	50.45	0.3
T14-08-02-05	51.26	50.87	0.8
T16-08-02-05	57.91	57.77	0.2
T14-08-015-1	34.78	34.78	0
T14-08-01-1	21.68	21.68	0
T14-08-01-08	21.72	21.72	0
T14-08-01-05	21.84	21.84	0
T14-08-01-03	22.06	22.06	0
T14-08-01-025	21.18	22.17	0
T14-08-01-02	22.35	22.25	0.4
T18-07-03-08	101.94	100.94	0
T22-07-03-06	128.39	125.53	2.2
T16-07-025-1	69.17	69.08	0.1
⋮	⋮	⋮	⋮

Specimens	F_{hybrid}	F_{MV}	Penalisation
⋮	⋮	⋮	⋮
T16-07-02-1	50.8	50.8	0
T16-07-02-08	51.26	51.25	0
T18-07-02-05	59.37	59.18	0.3
T16-07-015-1	35.6	35.6	0
T16-07-01-1	22.01	22.01	0
T16-07-01-08	22.05	22.05	0
T16-07-01-05	22.2	22.2	0
T18-06-03-1	89.09	88.6	0.6
T18-06-03-08	92.27	90.87	1.5
T27-06-03-06	150.59	146.48	2.7
T18-06-025-1	71.77	71.75	0
T18-06-02-1	51.89	51.89	0
T18-06-02-08	52.5	52.48	0
T20-06-02-05	59.8	59.56	0.4
T18-06-015-1	35.7	35.07	0
T18-06-01-1	21.71	21.71	0
T18-06-01-08	21.74	21.71	0
T18-06-01-05	21.84	21.84	0
T27-14-50	124.59	122.23	1.9
T27-14-72	71.29	71.13	0.2
T27-16-72	93.92	93.45	0.5
T27-17-72	108.13	107.88	0.2
T27-18-72	123.75	123.16	0.5

TABLE 6.3 – Influence of the MV interaction

6.5 Stiffness classification

In the previous SECTIONS, models with different yield line patterns were developed. When they are applied to the T-stubs of the parametric study, it can be easily seen which one is the most suited in TABLES (6.1) and (6.2). Those results agree with the plastic mechanisms obtained with ABAQUS©. According to EuroCode, the same conclusions should be acheived by computing the effective lengths of both mechanisms for each T-stubs. The computed results can be consulted in TABLE (6.4) hereafter.

The results found in this TABLE are unexpected. Indeed, according to EuroCode, none of these T-stubs should be considered long, neither have a yield line mechanism different of the two straight lines. This conclusion is the complete opposite of the observation made in the parametric study. In consequence, two problems arise.

The first one is that a new definition of a short T-stub is required. A proposition made in this thesis is : "**a T-stub can be characterised as short if its yield line pattern consists in two straight lines**". It must be noticed that this definition is independent of the notion of effective length and allows the hinges to be offset (see SECTION (6.1)).

Specimens	L_{short} [mm]	L_{hybrid} [mm]	Selected model
T12-09-015-1	70	74.3	short
T12-09-01-1	70	72.3	short
T12-09-01-08	70	72.3	short
T12-09-01-05	70	72.3	short
T22-08-03-05	70	71.3	short
T24-08-03-05	70	75	short
T27-08-03-05	70	78.3	short
T30-08-03-05	70	80	short
T14-08-02-08	70	75.8	short
T14-08-02-06	70	75.8	short
T14-08-02-05	70	75.8	short
T16-08-02-05	70	76	short
T14-08-015-1	70	73.5	short
T14-08-01-1	70	72.6	short
T14-08-01-08	70	72.6	short
T14-08-01-05	70	72.6	short
T14-08-01-03	70	72.6	short
T14-08-01-025	70	72.6	short
T14-08-01-02	70	72.6	short
T18-07-03-08	70	75.4	short
T22-07-03-06	70	73.3	short
T16-07-025-1	70	75.8	short
⋮	⋮	⋮	⋮

Specimens	L_{short}	L_{hybrid}	Select. model
⋮	⋮	⋮	⋮
T16-07-02-1	70	74.8	short
T16-07-02-08	70	74.8	short
T18-07-02-05	70	73.8	short
T16-07-015-1	70	73.8	short
T16-07-01-1	70	72.9	short
T16-07-01-08	70	72.9	short
T16-07-01-05	70	72.9	short
T18-06-03-1	70	78.1	short
T18-06-03-08	70	78.1	short
T27-06-03-06	70	76.6	short
T18-06-025-1	70	78.8	short
T18-06-02-1	70	75.6	short
T18-06-02-08	70	75.6	short
T20-06-02-05	70	74.7	short
T18-06-015-1	70	73.6	short
T18-06-01-1	70	71.9	short
T18-06-01-08	70	71.9	short
T18-06-01-05	70	71.9	short
T27-14-50	70	76.8	short
T27-14-72	70	74.5	short
T27-16-72	70	75.1	short
T27-17-72	70	76.8	short
T27-18-72	70	77.1	short

TABLE 6.4 – Characterisation of the yield line pattern according to EuroCode definition

The second problem is that a criterion is necessary to distinguish the two yield lines patterns. By performing the ratio of bending stiffness of the plate to the axial stiffness of the bolt, two ranges can be identified to characterise the T-stubs. This criterion can be written as follows :

$$\Psi = \frac{\frac{EI_{plate}}{m'}}{\frac{EA_{bolt}}{L_b}} = \frac{\frac{ELt_f^3}{12m'}}{\frac{EA_s}{L_b}} = \frac{Lt_f^3 L_b}{12m'A_s} \tag{6.23}$$

As it can be seen in TABLE (6.5) herebelow, the transition between the two models occurs when $\psi = 90$ $[mm^2]$. Below this boundary, the hybrid yield line pattern should be used and the T-stub is characterised as **flexible** (mode 1-F). On the other hand, the T-stub is defined as **rigid** (mode 1-R) if Ψ lies above this boundary and the two straight lines pattern is used.

It is important to highlight that this criterion is a first preliminary proposition. Indeed, it is very unfortunate and inconvenient that the boundary found has units. In consequence, this criterion should be reviewed in purpose to find a dimensionless criterion. Nevertheless, those critics should not discredit the real discovery of this SECTION. **Stiffness is a relevant key parameter when characterising the T-stub yield line pattern**. This conclusion is something completely new in comparison to the procedure proposed by EuroCode.

Specimens	Ψ $[mm^2]$	Classification
T12-09-015-1	50.6	Flexible
T12-09-01-1	33.2	Flexible
T12-09-01-08	33.2	Flexible
T12-09-01-05	33.2	Flexible
T22-08-03-05	129.1	Rigid
T24-08-03-05	146.8	Rigid
T27-08-03-05	163.8	Rigid
T30-08-03-05	181.5	Rigid
T14-08-02-08	57.7	Flexible
T14-08-02-06	57.7	Flexible
T14-08-02-05	57.7	Flexible
T16-08-02-05	64.7	Flexible
T14-08-015-1	43.5	Flexible
T14-08-01-1	28	Flexible
T14-08-01-08	28	Flexible
T14-08-01-05	28	Flexible
T14-08-01-03	28	Flexible
T14-08-01-025	28	Flexible
T14-08-01-02	28	Flexible
T18-07-03-08	79.6	Flexible
T22-07-03-06	93.32	Rigid
T16-07-025-1	60.2	Flexible
⋮	⋮	⋮

Specimens	Ψ	Classification
⋮	⋮	⋮
T16-07-02-1	48.2	Flexible
T16-07-02-08	48.2	Flexible
T18-07-02-05	54.3	Flexible
T16-07-015-1	35.3	Flexible
T16-07-01-1	22.6	Flexible
T16-07-01-08	22.6	Flexible
T16-07-01-05	22.6	Flexible
T18-06-03-1	52.9	Flexible
T18-06-03-08	52.9	Flexible
T27-06-03-06	81.9	Flexible
T18-06-025-1	46.6	Flexible
T18-06-02-1	38.2	Flexible
T18-06-02-08	38.2	Flexible
T20-06-02-05	40	Flexible
T18-06-015-1	28.3	Flexible
T18-06-01-1	18	Flexible
T18-06-01-08	18	Flexible
T18-06-01-05	18	Flexible
T27-14-50	55.9	Flexible
T27-14-72	38.7	Flexible
T27-16-72	60.6	Flexible
T27-17-72	73.7	Flexible
T27-18-72	90	Flexible

TABLE 6.5 – T-stub characterisation based on the stiffness criterion

6.6 Neutelers model

At this point, many formulae have been developed, some assumptions have been either made or lifted. A summary of the Neutelers model is required. The first part mainly focuses on the assumptions of the model while the second presents the procedure to be followed.

To begin with, the presented model uses the same material law as the EuroCode. In other words, elastic-perfect plastic engineering stress-strain law of the plates and an elastic engineering law for the bolts. It is not the only similarity those two models share. Both MV interaction and the geometrical non linearities were proved to be negligible. Moreover, the 3D effects are still neglected and the bolts are assumed to be loaded in tension only. In addition to that, the prying forces are positioned according to McGuire formula [**25**] although a missing boundary was identified.

In opposition with EuroCode, the stress distribution under the bolt head is assumed to be triangular. Concerning the plastic hinges, both their location and shape are not known prior an appropriate evaluation. Notice that the proposed model can only be applied for unstiffened back-to-back T-stub made of mild steel welded plated and which are characterised as short by the EuroCode. Otherwise, the T-stub is out of the range of validity of the new model.

As explained, if the T-stub is short according to EuroCode and fulfills the other conditions, the procedure illustrated on FIGURE (6.8) can be followed. The first step is to determine the real position of the hinges with EQUATIONS (6.2) and (6.3). Owing the geometric properties of the plastic mechanism, the T-stub can be classified according to its stiffness. Thus, the effective length can be assessed. Then, the plastic strength can be evaluated. Finally, this resistance should be compared to the other failure mode to ensure which one will occur in reality.

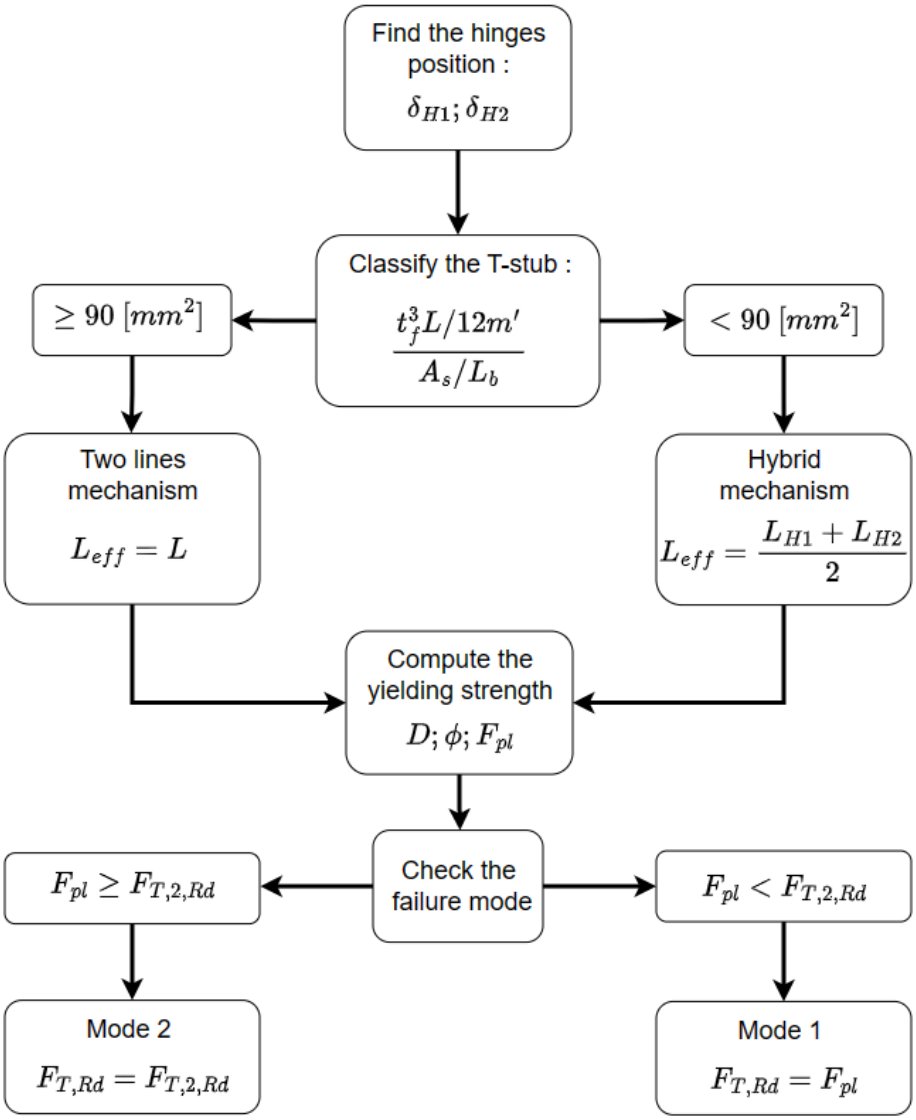

FIGURE 6.8 – Diagram of the Neutelers model

6.7 Validation of the models

Initially, the purpose of this thesis was to propose a model that improves the models currently available in the scientific literature and presented in SECTION (2.3). In this SECTION, the Neutelers model is confronted to experimental data to quantify the progress realised. To do so, the model is applied to both Timisoara and Tongji test campaigns (see SECTION (3.2)) and compared to the EuroCode. Notice that a graphical determination of the plastic strength is performed on all the tests in this SECTION. This was not shown previously for sake of readability. Additional numerical validations are proposed in APPENDIX (C).

The results shown on FIGURE (6.9) present a significant improvement when assessing the plastic strength with the new model. The T-stub is classified as flexible which seems coherent with the discussion made about this specimen on FIGURE (5.2) at the beginning of CHAPTER (5). However, a slight underestimation of F_{pl} can be noticed. It is likely to be due to the conservative aspect of the EQUATIONS assessing the hinges position. On the other hand, FIGURE (6.10) exhibits an accurate estimation of the plastic strength. In that case, the T-stub is considered rigid due to its thicker flange.

The two next specimens presented on FIGURES (6.11) and (6.12) are both characterised as flexible. They also both show that the Neutelers model significantly improves the prediction made of the plastic strength.

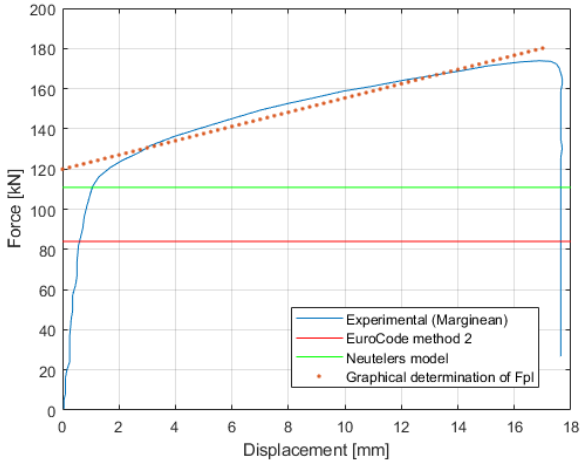

FIGURE 6.9 – T-10-16-100 model validation

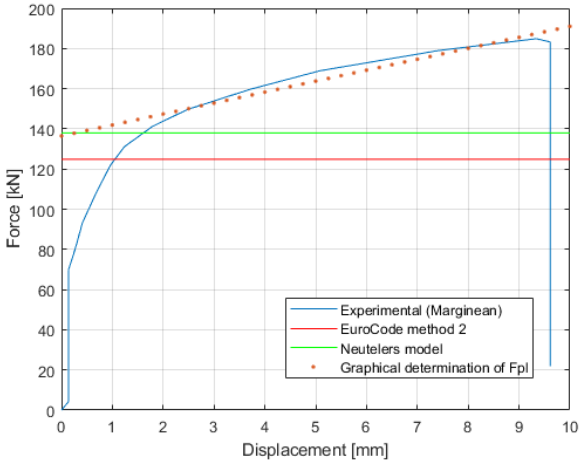

FIGURE 6.10 – T-12-16-100 model validation

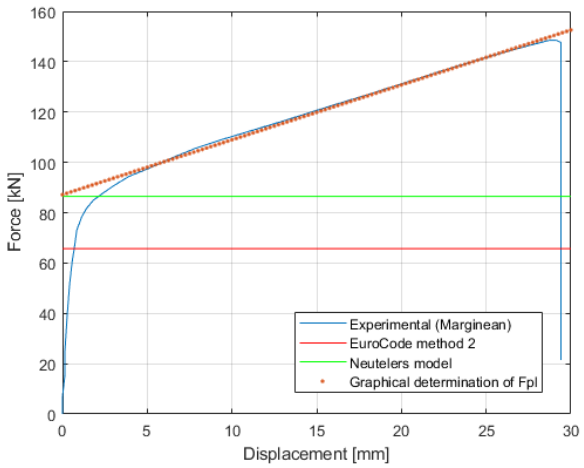

FIGURE 6.11 – T-10-16-120 model validation

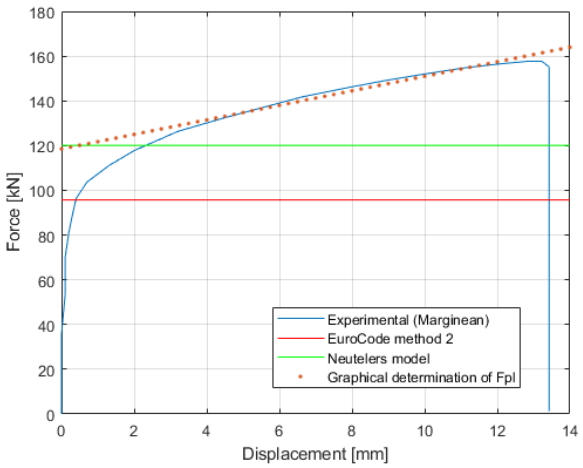

FIGURE 6.12 – T-12-16-120 model validation

Similar conclusions can be drawn for the T-12-16-140 specimen depicted on FIGURE (6.14). Concerning the T-10-16-140 specimen on FIGURE (6.13), an important improvement can still be ascertained. However, it can also be seen that the plastic strength is here underestimated. As for the T-10-16-100 specimen, it is assumed that the position found for the plastic hinge are a bit too conservative.

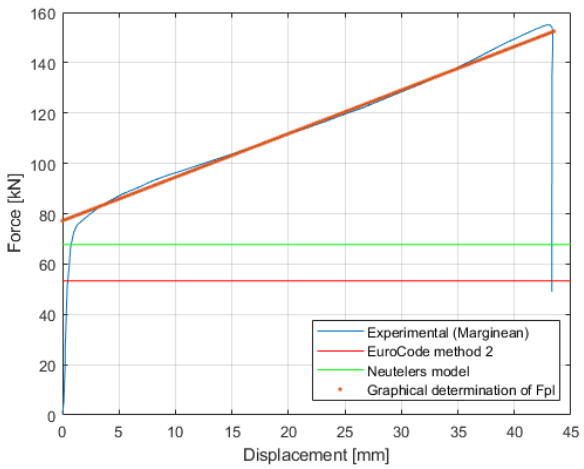

FIGURE 6.13 – T-10-16-140 model validation

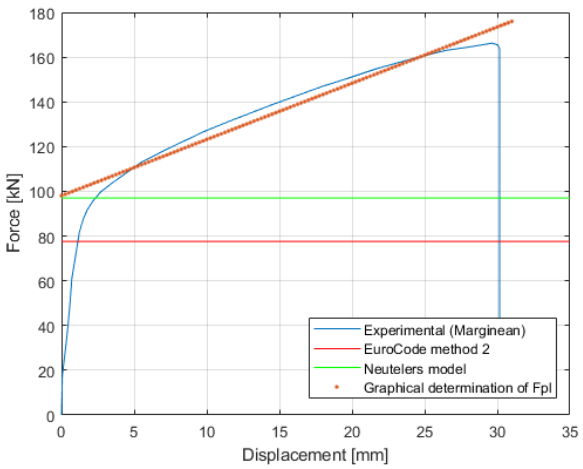

FIGURE 6.14 – T-12-16-140 model validation

FIGURE (6.15) hereafter represents the first test of the campaign which collapse is a mode 2. In that case, both EuroCode and Neutelers model succeed in detecting the correct failure mode. Notice that the small difference between those models in the predicted plastic strength is due to the plastic hinge position.

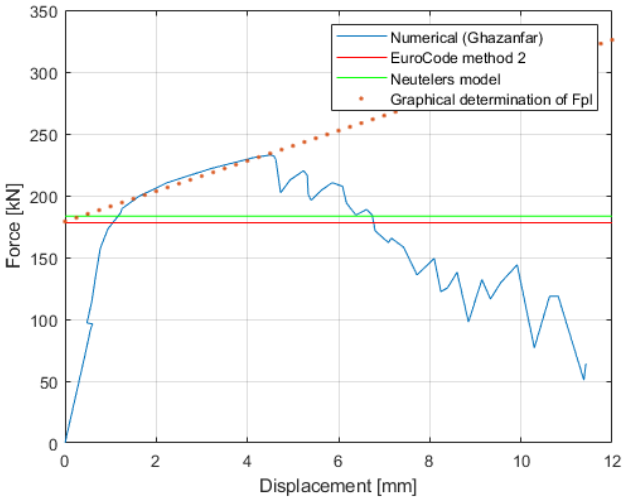

FIGURE 6.15 – T-15-16-100 model validation

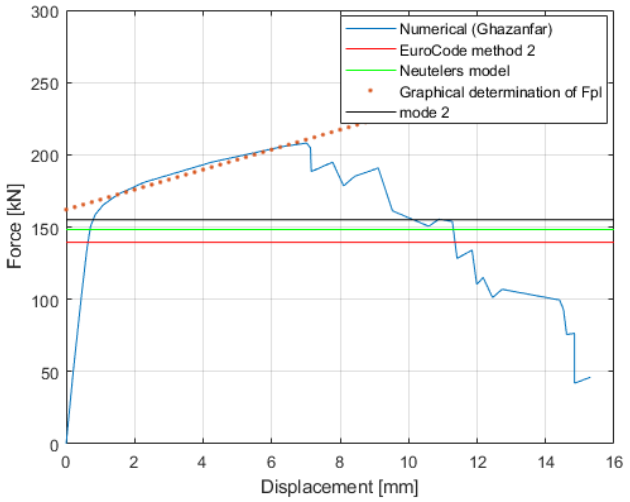

FIGURE 6.16 – T-15-16-120 model validation

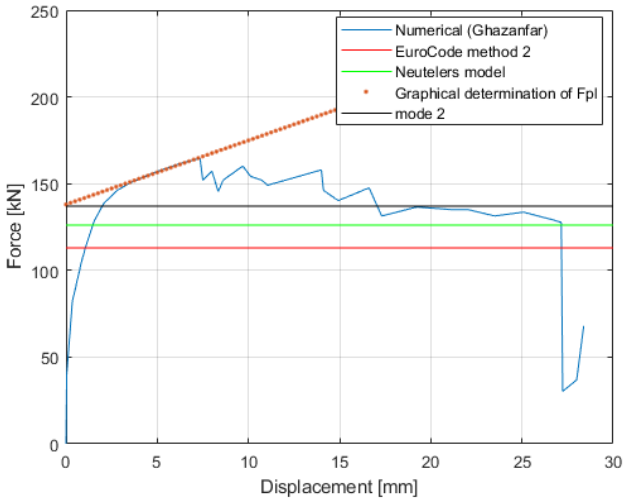

FIGURE 6.17 – T-15-16-140 model validation

Unfortunately, the two next specimens on FIGURES (6.16) and (6.17) are mischaracterised. Indeed, although they are both considered rigid and improve the predicted plastic strength, a mode 1 is still detected instead of a mode 2. For such T-stubs making the transition between mode 1 and 2, both EuroCode and the Neutelers model show the same pathology and wrongly predict the failure mode. On the other hand, this pathology is not observed in the T-18 series illustrated on FIGURES (6.18) and (6.19). For those cases, a mode 2 is detected and it can be concluded that the plastic strength is well estimated.

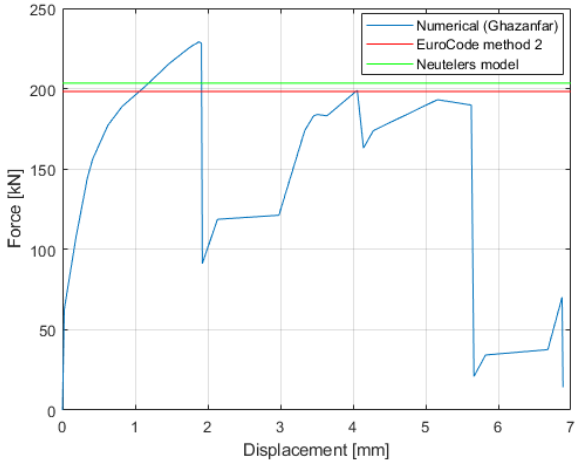

FIGURE 6.18 – T-18-16-120 model validation

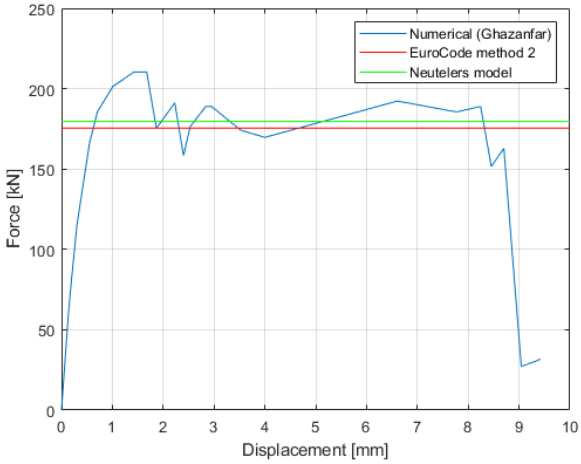

FIGURE 6.19 – T-18-16-140 model validation

Concerning the Tongji test campaign, its first specimen is a mode 2 which was already well assessed (see FIGURE (6.20)). Thus, the Neutelers model shows similar results for this rigid T-stub. This contrasts with the three remaining tests on FIGURES (6.21), (6.22) and (6.23). Indeed, all these specimens are characterised as flexible and significant improvements were performed. It still must be noticed that one of them, the T11.5a-18 may have its hinges placed too conservatively. This can explain the underestimation made for this test in particular.

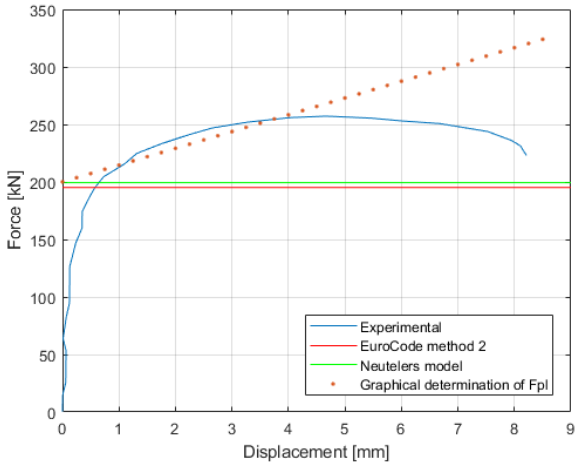

FIGURE 6.20 – T-17.5a-18 model validation

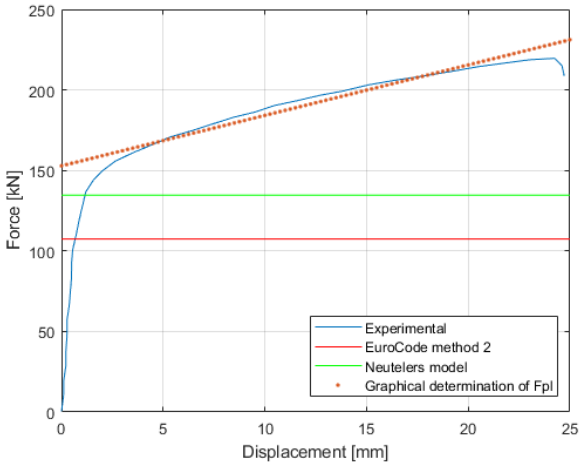

FIGURE 6.21 – T-11.5a-18 model validation

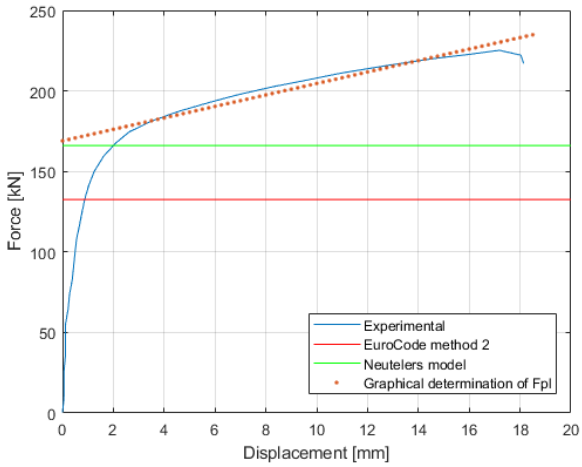

FIGURE 6.22 – T-11.5b-18 model validation

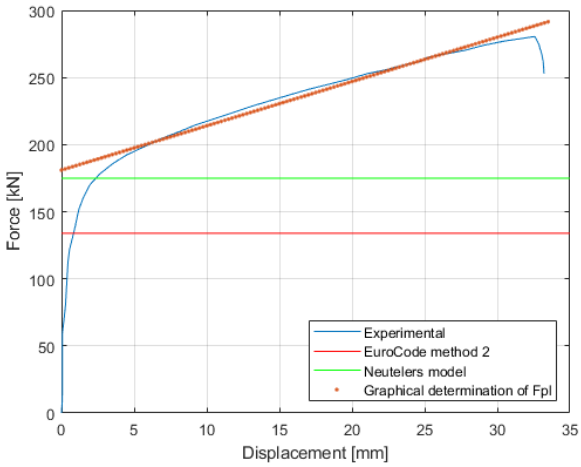

FIGURE 6.23 – T-11.5b-20 model validation

A summary of the so-obtained results can be consulted in Table (6.6) hereafter. The relative errors are also computed to assess the improvement realized. However, to relativize those values, the absolute errors are also proposed in the Table. The color code used for the former is the same as previously : the first three are 5% wide each and begin at 0 for the best, improvable and insufficient ones respectively. The last one is unbounded and contains all the incorrect predictions. The same definition can be kept for the **absolute error** but the ranges considered are now : [0 , 5], [5 , 10], [10 , 20], [20 , inf].

Experimental			EuroCode				Neutelers			
Test	F_{pl} [kN]	mode	F_{pl} [kN]	mode	Rel. error [%]	Abs. error [kN]	F_{pl} [kN]	mode	Rel. error [%]	Abs. error [kN]
T-10-16-100	119.91	1	84	1	-29.95	-35.91	110.85	1-F	-7.56	-9.06
T-10-16-120	87.15	1	65.72	1	-24.59	-21.43	86.47	1-F	-0.78	-0.68
T-10-16-140	77.2	1	53.27	1	-31	-23.93	67.77	1-F	-12.21	-9.43
T-12-16-100	136.45	1	124.87	1	-8.49	-11.58	137.94	1-R	+1.09	+1.49
T-12-16-120	118.5	1	95.69	1	-19.25	-22.81	120.08	1-F	+1.33	+1.58
T-12-16-140	98.04	1	77.57	1	-20.88	-20.47	97.05	1-F	-1.01	-0.99
T-15-16-100	179.08	2	178.03	2	-0.59	-1.05	183.45	2	+2.43	+4.36
T-15-16-120	162.06	2	139.42	1	-13.97	-22.64	148.3	1-R	-8.49	-13.76
T-15-16-140	138	2	113.01	1	-18.11	-24.99	126.11	1-R	-8.61	-11.89
T-18-16-120	200	2	198.26	2	-0.87	-1.74	203.48	2	+1.74	+3.48
T-18-16-140	180	2	175.49	2	-2.51	-4.51	179.57	2	-0.24	-0.43
T-17.5a-18	200.04	2	195.13	2	-2.45	-4.91	199.31	2	-0.36	-0.73
T-11.5a-18	152.84	1	107.46	1	-29.69	-45.38	134.64	1-F	-11.91	-18.2
T-11.5b-18	168.99	1	132.56	1	-21.56	-36.43	166.09	1-F	-1.72	-2.9
T-11.5b-20	181	1	133.89	1	-26.03	-47.11	174.95	1-F	-3.34	-6.05

Table 6.6 – Validation of the model on Timisoara and Tongji test campaigns

All computation done, it appears that the mean relative error performed by the EuroCode is 16.7 [%]. For the model developed in this thesis, this value is 4.2 [%]. This highlights the major improvement made by the model. Notice that for completion sake a Table (6.7) summarising all the key parameters and values is proposed hereafter. Thus, a clear comparison between both rigid and flexible models can be done. In addition to that, an emphases is made on the assumed conservative plastic hinges positions.

Test	δ_{H1} [mm]	δ_{H2} [mm]	Ψ [mm^2]	mode	L [mm]	F_{Rigid} [kN]	L_{hybrid} [mm]	F_{Hybrid} [kN]
T-10-16-100	0.36	3.06	52.36	Flexible	90	104.15	95.8	110.85
T-10-16-120	1.12	5	44.11	Flexible	90	82.51	94.3	86.48
T-10-16-140	1.75	6.62	36.8	Flexible	90	65.41	93.25	67.77
T-12-16-100	0	1.12	100.79	Rigid	90	137.94	97.48	149.41
T-12-16-120	0.4	3.15	82.43	Flexible	90	112.9	97.73	120.08
T-12-16-140	1.03	4.77	69.48	Flexible	90	92.44	94.5	97.05
T-15-16-100	0	0	229.85	Rigid	90	186	98.6	204.13
T-15-16-120	0	0.85	182.32	Rigid	90	148.3	97.7	161.05
T-15-16-140	0.14	2.47	153.69	Rigid	90	126.11	96.3	134.92
T-18-16-120	0	0	346.17	Rigid	90	311.43	98.56	341.06
T-18-16-140	0	0.7	286.99	Rigid	90	259.37	97.9	282.07
T-17.5a-18	0	0	347.47	Rigid	120	244.33	129.7	264.09
T-11.5a-18	0.39	3.53	84.96	Flexible	120	127.71	126.5	134.64
T-11.5b-18	0.39	3.53	84.96	Flexible	120	157.54	126.52	166.09
T-11.5b-20	0.6	4.53	70.81	Flexible	120	165.9	126.55	174.95

Table 6.7 – Key values of the Neutelers model

6.8 Conclusions

In this Chapter, many analytical developments were carried out to solve the problems identified in the parametric study. For the plastic hinges, two empirical formulations were proposed. They were developed with the purpose to be conservative. However, they still need to be improved or analytically proved. Remind that their range of validity concerns only the T-stubs made of welded plates.

Then, the bolt head work formula was rewritten to take into account both this new feature and an **assumed** triangular stress distribution. This first modification drastically improved the prediction of the plastic strength. However, this contribution alone reveals to be insufficient for some T-stubs.

In consequence, a formula for the new yield line pattern identified in Section (5.2) was proposed. For some reasons previously explained, the effective length found should be reviewed and be rigorously proved. Unexpectedly, it was observed that this mechanism should never appear according to the current definition of a short T-stub. Thus, a new definition was proposed to correct that inconsistency.

Afterwards, MV interaction was introduced into the model to validate or not the assumption made by the EuroCode. From the developed model, it appears that the MV interaction can be neglected when assessing the plastic strength.

Since the Eurocode criterion to identify a T-stub as short was invalidated, a new one to distinguish the models was sought. A first preliminary criterion based on a stiffness ratio was found. Unfortunately, due to a units dependency, this criterion should be reviewed and improved. Nevertheless, the influence of stiffness in the process of characterising the yield mechanism was proved.

Finally, the model was confronted to experimental data and compared to the EuroCode. A significant improvement in the prediction of the plastic strength was ascertained. Indeed, the mean relative error of the current models is 16.7 [%] while the model developed in this thesis has a mean relative error of 4.2 [%]. This error is mainly due to the conservative positioning of the plastic hinges.

Chapter 7

Conclusions

To sum up, in the robustness field, the loss of a column in a building could be contemplated. To achieve a new state of equilibrium and avoid progressive collapse of the structure, catenary effects need to be activated in the deformed configuration. This phenomenon requires large rotation at the joints. Naturally, a focus was made on the T-stub component which exhibits a significant reserve of ductility.

Thus, several models of characterisation were gathered from the literature. Their range of application extends from the simplest model in the design standard to the most complex one relaxing as much assumptions as possible.

To assess their accuracy and confront them to reality, many test campaigns available in the literature were collected. Two campaigns were studied especially for the properties of their specimens. Indeed, due to the wide number of possible configurations , a focus was made on the **unstiffened short back-to-back T-stubs with one bolt row and made of mild steel welded plates**. Applying the models on these specimens, the assessment of the initial stiffness was deemed satisfying. On the other hand, none of the models was able to predict accurately both ultimate strength and displacement. Regarding the prediction of the plastic strength, some heterogeneous results were obtained : for mode 2, they were well predicted while it was not the case for mode 1. In consequence, prior studying either the ultimate strength or rotation capacity, the plastic strength was first investigated.

Thus, a numerical procedure was set up to model T-stubs in Abaqus©. A full modelling of the material law up to failure was done. In addition to that, mesh sensitivity analysis was performed. To ensure the quality of the results, a rigorous validation was performed with the specimens of the Timisoara test campaign.

The next step was to extend the database through a parametric analysis. The range of configuration studied was quite large from one extreme case to another. Some assumptions already made by the current models were verified as for neglecting the membrane effect. On the other hand, several others were invalidated. Indeed, the plastic hinges were proved to be offset to their assumed position. The stress distribution under the bolt head was shown to be more triangular than uniform and to be asymmetric. This asymmetry is due to bending in the bolt that induces the plate to be clamped. This effect was proved to be a missing boundary in the formula locating the prying forces. In addition to that, a new yield line pattern unattended was identified.

In reaction to that, analytical developments were performed. Two empirical formulations for the plastic hinges offsets were derived from the parametric study. This aspect was introduced in the process of assessing the work of the bolt head as well as the triangular stress distribution observed. This new formulation produces very satisfying results for T-stubs with a two lines mechanism and constitutes a major improvement in itself. In addition to that, a new effective length was computed for the hybrid mechanism and MV interaction was proved to be negligible. However, with the current definition of a short T-stub, this mechanism is bound to never happen. A new definition stating that "**a T-stub is short only if its yield mechanism consists in two straight lines**" was thus proposed. A first preliminary stiffness based criterion was found to solve

this problem. Unfortunately, this criterion is units dependant and thus should be improved. However, the influence of stiffness on the yield line pattern characterisation was proved. This also permitted to apply the Neutelers model on the experimental test campaigns and compare its accuracy to the EuroCode. Finally, a mean relative error of 16.7 [%] was computed for the EuroCode in opposition to 4.2 [%] for the new model. It can be concluded that the initial goal of this thesis is fulfilled.

Nevertheless, as research perspectives, the lacks of this model should be solved first before looking at the post-yielding behaviour. Indeed, the hinges position was proved to be the heart of the inconsistencies of the current models. However, the formulae proposed are empirical and valid only for welded T-stubs. Further extended parametric studies could investigate this behaviour and perhaps, lead to a more accurate formulation or a larger range of validity. Otherwise, both the new yield line pattern and prying forces positioning were also deemed to be improvable. Thus, rigorous demonstrations might be necessary. A consequence to better formulations could lead to more satisfying stiffness characterisation criterion.

Once all these problems are solved, a further investigation out of the current topic might be envisaged. All the relevant parameters can be found simply by looking at the studied configuration : the unstiffened short back-to-back T-stub with a single bolt row and made of mild steel welded plates. By studying those parameters either individually or several at one time, the characterisation of the plastic strength will be extended and validated to a wide range of configurations.

The next step, once the yielding behaviour is fully characterised, is to focus on the post-yielding response. First, additional contributions as the membrane effect could be introduced into the models. Indeed, while this contribution was proved to be negligible at yielding, it significantly influences the ultimate strength.

To evaluate the ultimate displacement, the Zhao model seems to be the most efficient and closest to the reality. However, this model requires an important number of inputs, often unknown, on the material laws. A simpler model is the one proposed by Jaspart. Nevertheless, this model is too conservative with its 1/50 assumption for the hardening stiffness. A significant improvement without requiring much effort could consist in integrating the stiffness modulus E along the flange width and pondering it in such way to have a mean value of E_{st} for the post-yielding behavior.

In conclusion, this thesis is an humble contribution to this vast and interesting research field.

Bibliography

[1] Warnant, A., Contribution à l'étude des assemblages de construction métallique sous charges exceptionnelles, Université de Liège, Liège, Belgique, 2010

[2] Leruth, B., Résistance ultime et capacité de déformation d'assemblages boulonnés, Université de Liège, Liège, Belgique, 2017

[3] CEN, EN, 1-8 Eurocode 3 : Design of Steel Structures–Part 1–8 : Design of Joints, European committee for standardization, Brussels, 2005

[4] Jaspart, J.-P., Recent advances in the field of steel joints—column bases and further configurations for beam-to-column joints and beam splices, Universite de Liege, Faculte des Sciences Appliques, 1997

[5] Zoetemeijer, P., A design method for the tension side of statically loaded, bolted beam-to-column connections, Citeseer, HERON, 20 (1), 1974

[6] Johansen, K. W., Yield-line theory, Cement and Concrete Association, 1962

[7] Piluso and al, Ultimate behavior of bolted T-stubs. I : Theoretical model, P 686-693, No 6, Journal of structural engineering, American Society of Civil Engineers, 2001

[8] Piluso and al, Ultimate behavior of bolted T-stubs. II : Model validation, P 694-704, No 6, Journal of structural engineering, American Society of Civil Engineers, 2001

[9] Zhao and al, Full-range behaviour of T-stubs with various yield line patterns, volume 186, Journal of Constructional Steel Research, Elsevier, 2021

[10] Zhao and al, Mechanical model for the full range behaviour of bolted T-stubs, volume 200, Journal of Constructional Steel Research, Elsevier, 2023

[11] Francavilla and al, Ultimate behaviour of bolted T-stubs under large displacements : A mechanical model, volume 195, Journal of Constructional Steel Research, Elsevier, 2022

[12] Marginean I. M., Robustness of moment steel frames under column loss scenarios, Timişoara : Editura Politehnica, 2017

[13] Anwar G. A., Ultimate deformation and resistance capacity of bolted T-Stub connections under different loading conditions, České vysoké učení technické v Praze. Vypočetní a informační centrum, 2017

[14] Khulmann U. and al., High strength steel in seismic resistant building frames (HSS-SERF) REPORT ON PERFORMANCE OF WELDED DETAILS AND T-STUBS ; RECOMMENDATIONS OF WELDING PROCEDURES TO BE USED IN DUAL-STEEL STRUCTURES FOR WELDED CONNECTIONS BETWEEN HSS AND MCS, Commission Européenne, Bruxelles, Belgium, 2013

[15] Baldassino N. and al., Experimental test on steel and concretebeam-to-column joint components, Trento, 2007

[16] Yuan H.X. and al., Experimental behaviour of stainless steel bolted T-stub connections under monotonic loading, volume 152, pages 213-224, Journal of Constructional Steel Research, Elsevier, 2019

[17] Faralli A.C. and al., Experimental investigation and modelling of T-stubs undergoing large displacements, volume 180, Journal of Constructional Steel Research, Elsevier, 2021

[18] Dassault Inc., ABAQUS Theory guide version 6.10, Dassault Systèmes, 2010, http ://130.149.89.49 :2080/v6.10/books/usb/default.htm ?startat=pt04ch11s04abo12.html

[19] Ling Y., Uniaxial True Stress-Strain after Necking, AMP J. Technol., volume 5, pages 37–48, 1996.

[20] Pavlović M. and al., Bolted shear connectors vs. headed studs behaviour in push-out tests, volume 88, pages 134-149, Journal of Constructional Steel Research, Elsevier, 2013

[21] Pavlović M. and al., Connections in towers for wind converters, part I : Evaluation of down-scaled experiments, volume 115, pages 445-457, Journal of Constructional Steel Research, Elsevier, 2015

[22] D'Aniello M. and al., Monotonic and cyclic inelastic tensile response of European preloadable gr10. 9 bolt assemblies, volume 124, pages 77-90, Journal of Constructional Steel Research, Elsevier, 2016

[23] D'Aniello M. and al., Simplified criteria for finite element modelling of European preloadable bolts, volume 24, pages 643-658, Steel and Composite Structures, Techno-Press, 2017

[24] British standard, High-strength structural bolting assemblies for preloading, 2005

[25] McGuire, W., & Winter, G., Steel structures, 1968

Table of Figures

Table of Tables

Appendix A

Hand written validations

In this APPENDIX, all the computation models presented in CHAPTER (2) are successively applied to the TS-10-16-100 T-stub of the Timisoara test campaign that can be found in SECTION (3.1). These hand written validations allow to assess that the EXCEL file created for this thesis is correctly implemented. By consequence, the accuracy of the results shown in SECTION (3.2.1) are ensured. The complete geometry of the T-stub is represented on FIGURE (A.1) herebelow.

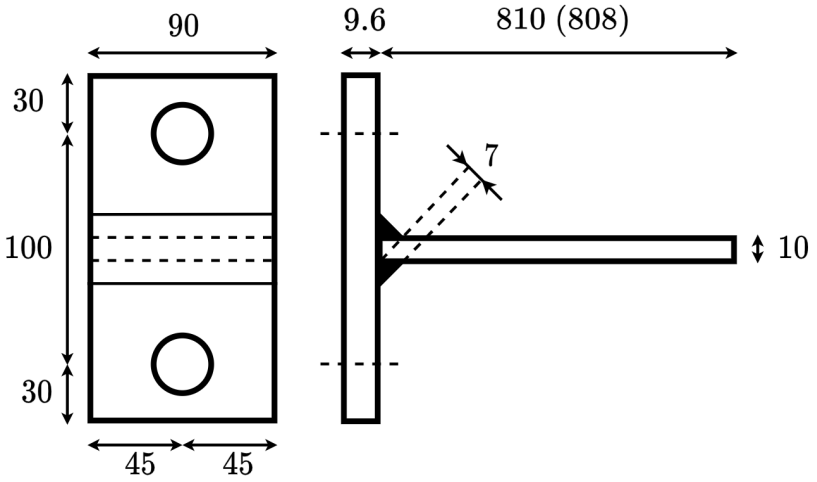

FIGURE A.1 – TS-10-16-100 full geometry (all dimensions in [mm])

Additional geometrical parameters required for each characterisation models can be computed as follows :

$$m = \frac{b - t_w}{2} - 0.8 a_w \sqrt{2} = \frac{160 - 10}{2} - 0.8 \times 7 \times \sqrt{2} = 37.08 \text{ [mm]}$$
$$n = \min(e; 1.25m) = \min(30; 1.25 \times 37.08) = 30 \text{ [mm]}$$

The steel nominal properties can be obtained by the test performed on the coupon. They are listed hereafter :

$$E = 210,000 \text{ [MPa]} \qquad f_y = 310 \text{ [MPa]} \qquad f_u = 408 \text{ [MPa]}$$
$$E_h = 1,735.9 \text{ [MPa]} \qquad \varepsilon_h = 0.03473 \text{ [-]} \qquad \varepsilon_u = 0.17586 \text{ [-]}$$

Concerning the M16 10.9 non-preloaded bolts, the nominal geometry can be found in the standards [**24**].

$$d_{bolt} = 16 \text{ [mm]} \qquad d_{hole} = 18 \text{ [mm]} \qquad d_{head} = 27 \text{ [mm]}$$
$$L_{head} = 10 \text{ [mm]} \qquad d_{nut} = 27 \text{ [mm]} \qquad L_{nut} = 14.1 \text{ [mm]}$$
$$d_{washer} = 30 \text{ [mm]} \qquad L_{washer} = 4 \text{ [mm]} \qquad L_{bolt} = 45 \text{ [mm]}$$
$$L_{shank,min} = 8 \text{ [mm]} \qquad L_{shank,max} = 14 \text{ [mm]}$$

$$L_{thread} = L_{bolt} - L_{shank,max} = 45 - 14 = 31 \text{ [mm]}$$
$$A_{bolt,nom} = \frac{\pi d_{bolt}^2}{4} = \frac{\pi \times 16^2}{4} = 201.06 \ [mm^2]$$
$$A_s = 0.78\frac{\pi d_{bolt}^2}{4} = 0.78\frac{\pi \times 16^2}{4} = 157 \ [mm^2]$$
$$e_w = d_{washer}/4 = 30/4 = 7.5 \text{ [mm]}$$
$$L_b = 2 \times (t_f + L_{washer}) + \frac{L_{head} + L_{nut}}{2} = 2 \times (9.6 + 4) + \frac{10 + 14.1}{2} = 39.25 \text{ [mm]}$$

In addition to that, its material properties were provided in [**12**] and [**13**]. A listing of them can be found herebelow.

$$E = 210,000 \text{ [MPa]} \qquad f_{b,y} = 965 \text{ [MPa]} \qquad f_{b,u} = 1,080 \text{ [MPa]} \qquad \varepsilon_{b,u} = 0.05 \text{ [MPa]}$$

$$\varepsilon_{b,y} = f_y/E = 965/210,000 = 4.5952 \times 10^{-3} \text{ [-]}$$
$$B_{t,Rd} = 0.9 f_u \times A_{thread} = 0.9 \times 1080 \times 157 = 152.63 \text{ [kN]}$$
$$B_{u,Rd} = f_u \times A_{thread} = 1080 \times 157 = 169.592 \text{ [kN]}$$

A.1 EuroCode models

The first model presented in Chapter (2) was the EuroCode model. The first step to perform in this procedure is to characterise the effective length of the T-stub. To do so, only the commonly accepted yield line patterns are investigated.

$$L_{eff,cp} = 2\pi m = 2 \times \pi \times 37.08 = 232.98 \text{ [mm]} \tag{A.1}$$
$$L_{eff,nc1} = 4m + 1.25e = 4 \times 37.08 + 1.25 \times 30 = 185.82 \text{ [mm]} \tag{A.2}$$
$$L_{eff,nc2} = L = 90 \text{ [mm]} \tag{A.3}$$

The mechanism that will occur first is the one that minimises the required energy. In other words, the minimum of the effective lengths. Notice that, due to the definition of its collapse, the circular yield line pattern cannot appear in such case.

$$L_{eff,mode1} = \min(L_{eff,cp}\,;\, L_{eff,nc1}\,;\, L_{eff,nc2}) = \min(232.98\,;\, 185.82\,;\, 90) = 90 \text{ [mm]} \tag{A.4}$$
$$L_{eff,mode2} = \min(L_{eff,nc1}\,;\, L_{eff,nc2}) = \min(185.82\,;\, 90) = 90 \text{ [mm]} \tag{A.5}$$

Then, it can be checked that prying effects indeed appear with this formula :

$$L_b^* = \frac{8.8 m^3 A_s}{t_f^3 L_{eff}} = \frac{8.8 \times 37.08^3 \times 157}{9.6^3 \times 90} = 884.8 \text{ [mm]} > 39.25 \text{ [mm]} = L_b \tag{A.6}$$

In consequence, the followings equations can be used to assess the failure modes strength. Notice that EuroCode proposes two methods to evaluate the resistance of mode 1. As it was done in the main text, both are developed.

$$M_{pl,Rd1} = \frac{f_y t_f^2 L_{eff,mode1}}{4} = \frac{310 \times 9.6^2 \times 90}{4} = 642,816 \text{ [Nmm]} \tag{A.7}$$
$$F_{T,Rd1,method1} = \frac{4 M_{pl,Rd1}}{m} = \frac{4 \times 642,816}{37.08} = 69.343 \text{ [kN]} \tag{A.8}$$
$$F_{T,Rd1,method2} = \frac{(8n - e_w) M_{pl,Rd1}}{2mn - e_w(m+n)} = \frac{(8 \times 30 - 7.5) \times 642,816}{2 \times 37.08 \times 30 - 7.5 \times (37.08 + 30)} = 84 \text{ [kN]} \tag{A.9}$$

$$M_{pl,Rd2} = \frac{f_y t_f^2 L_{eff,mode2}}{4} = \frac{310 \times 9.6^2 \times 90}{4} = 642,816 \text{ [Nmm]} \tag{A.10}$$
$$F_{T,Rd2} = \frac{2 M_{pl,Rd2} + n_{t,Rd}}{m+n} = \frac{2 \times 642,816 + 30 \times 2 \times 152,630}{37.08 + 30} = 155.69 \text{ [kN]} \tag{A.11}$$

$$F_{t,Rd3} = \sum B_{t,Rd} = 2 \times 152,630 = 305.27 \text{ [kN]} \tag{A.12}$$

The resistance and the failure mode that will occur first is the weakest one :

$$F_{Rd,method1} = \min(F_{T,Rd1,method1}\,;\, F_{T,Rd2}\,;\, F_{T,Rd,3}) = \min(69.343\,;\, 155.69\,;\, 305.27) = 69.343 \text{ [kN]} \tag{A.13}$$
$$F_{Rd,method2} = \min(F_{T,Rd1,method2}\,;\, F_{T,Rd2}\,;\, F_{T,Rd,3}) = \min(84\,;\, 155.69\,;\, 305.27) = 84 \text{ [kN]} \tag{A.14}$$

In both case, the collapse is characterised as a mode 1. After that, the stiffness of the sub-components can be evaluated.

$$K_{plate,init} = \frac{0.9 L_{eff} t_f^3}{m^3} E = \frac{0.9 \times 90 \times 9.6^3}{37.08^3} 210,000 = 295.188 \text{ [kN/mm]} \tag{A.15}$$
$$K_{bolt,init} = \frac{1.6 A_s}{L_b} E = \frac{1.6 \times 157}{39.45} 210,000 = 1,337.44 \text{ [kN/mm]} \tag{A.16}$$

Notice that, like it was explained above, the expression of the plate stands for one plate only while the formula for the bolt stiffness stands for one row of two bolts. Thus, the assembly of these sub-components should write :

$$K_{2stubs,init} = \frac{1}{\frac{1}{K_{plate,init}} + \frac{1}{K_{bolt,init}} + \frac{1}{K_{plate,init}}} = \frac{1}{\frac{1}{295.188} + \frac{1}{1337.44} + \frac{1}{295.188}} = 132.952 \text{ [kN]} \tag{A.17}$$

Which correspond to the stiffness of the two back-to-back T-stubs. For the final step, consisting in building the force displacement curve, the displacement is expressed for one T-stub. In consequence, a factor 2 is applied on the displacement. EuroCode gives the choice either to build a bilinear or a trilinear force-displacement response. This combined with the possibility to use either method 1 or 2, gives four combinations. For sake of concisely, the formulae used are proposed hereafter and the computed points are summarised in Table (A.1). For a bilinear curve, the equations that should be used are :

$$\begin{array}{lll} F_0 = 0 & F_1 = F_{T,Rd} & F_2 = F_1 \\ \Delta_0 = 0 & 2\Delta_1 = \dfrac{F_1}{K_{2stubs,init}} & \Delta_2 = \infty \end{array}$$

For the trilinear model, the following set of formulae must be used :

$$\begin{array}{llll} F_0 = 0 & F_1 = \dfrac{2F_{T,Rd}}{3} & F_2 = F_{T,Rd} & F_3 = F_2 \\ \Delta_0 = 0 & 2\Delta_1 = \dfrac{F_1}{K_{2stubs,init}} & 2\Delta_2 = \dfrac{F_2}{K_{2stubs,init}/3} & \Delta_3 = \infty \end{array}$$

Method 1 bilinear		
Point	Δ $[mm]$	F [kN]
0	0	0
1	0.261	69.343
2	∞	69.343

Method 1 trilinear		
Point	Δ $[mm]$	F [kN]
0	0	0
1	0.174	46.23
2	0.783	69.343
3	∞	69.343

Method 2 bilinear		
Point	Δ $[mm]$	F [kN]
0	0	0
1	0.316	84
2	∞	84

Method 2 trilinear		
Point	Δ $[mm]$	F [kN]
0	0	0
1	0.211	56
2	0.948	84
3	∞	84

Table A.1 – Force-displacement curve of the EuroCode model

A.2 Jaspart model

Since most of the EuroCode model is the Jaspart model, either as such or simplified, the procedure is mostly similar. In consequence, to avoid to be redundant, the computation of the effective lengths and the resistances at yielding is omitted. Indeed, the computations are exactly the same from Equation (A.1) to (A.14). Notice that method 1 should be disregarded in profit to method 2 initially introduced by the Jaspart model.

Due to the hardening branch assumed in the plate constitutive law, the ultimate resistance should be computed as well. Equations (A.7) to (A.14) can be used with f_u instead of f_y.

$$M_{u,1} = \frac{f_u t_f^2 L_{eff,mode1}}{4} = \frac{408 \times 9.6^2 \times 90}{4} = 846,028 \text{ [Nmm]} \tag{A.18}$$

$$F_{u,1} = \frac{(8n - e_w)M_{u,1}}{2mn - e_w(m+n)} = \frac{(8 \times 30 - 7.5) \times 846,028}{2 \times 37.08 \times 30 - 7.5 \times (37.08 + 30)} = 110.56 \text{ [kN]} \tag{A.19}$$

$$M_{u,2} = \frac{f_u t_f^2 L_{eff,mode2}}{4} = \frac{408 \times 9.6^2 \times 90}{4} = 846,028 \text{ [Nmm]} \tag{A.20}$$

$$F_{u,2} = \frac{2M_{u,2} + n_{u,Rd}}{m+n} = \frac{2 \times 846,028 + 30 \times 2 \times 169,592}{37.08 + 30} = 176.92 \text{ [kN]} \tag{A.21}$$

$$F_{u,3} = \sum B_{u,Rd} = 2 \times 169,592 = 339.19 \text{ [kN]} \tag{A.22}$$

$$F_u = \min(F_{u,1}\,;\, F_{u,2}\,;\, F_{u,3}) = \min(110.56\,;\, 176.92\,;\, 339.19) = 110.56 \text{ [kN]} \tag{A.23}$$

$$\tag{A.24}$$

For this specimen, both yielding and failure are characterised as mode 1. For the stiffness, additional parameters are defined according to the following FIGURE (A.2).

$$L_t = L_{shank,min} + L_{washer} = 8 + 4 = 12 \text{ [mm]} \tag{A.25}$$

$$L_s = 2t_f + L_{washer} - L_{shank,min} = 2 \times 9.6 + 4 - 8 = 15.2 \text{ [mm]} \tag{A.26}$$

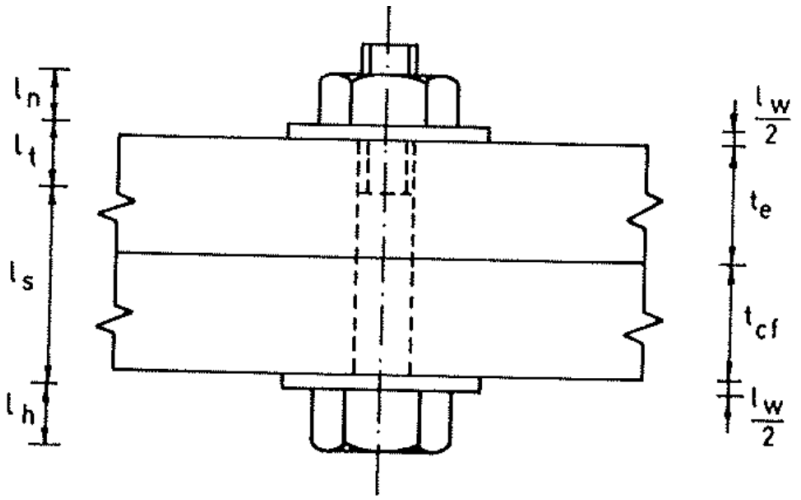

FIGURE A.2 – Bolt geometry according to Jaspart model [**4**]

Next, several parameters defined in [**4**] are computed. Notice that no distinction is made between the column flange and the end-plate due to the symmetry of the current configuration.

$$w_{cf} = w_e = b_e/2 = 160/2 = 80 \text{ [mm]} \tag{A.27}$$

$$l_{cf} = l_e = 2(m_e + 0.75n_e) = 2(37.08 + 0.75 \times 30) = 119.16 \text{ [mm]} \tag{A.28}$$

$$Z_{cf} = Z_e = \frac{l_e^3}{w_e t_e^3} = \frac{119.16^3}{80 \times 9.6^3} = 23.905 \text{ [mm}^{-1}\text{]} \tag{A.29}$$

$$\alpha_{cf} = \alpha_e = 0.75n_e/l_e = 0.75 \times 30/119.16 = 0.1888 \text{ [-]} \tag{A.30}$$

$$\alpha_{cf1} = \alpha_{e1} = 1.5\alpha_e - 2\alpha_e^3 = 1.5 \times 0.1888 - 2 \times 0.1888^3 = 0.2698 \text{ [-]} \tag{A.31}$$

$$\alpha_{cf2} = \alpha_{e2} = 6\alpha_e^2 - 8\alpha_e^3 = 6 \times 0.1888^2 - 8 \times 0.1888^3 = 0.16 \text{ [-]} \tag{A.32}$$

$$k_1 = L_s + 1.43L_t + 0.71L_n = 15.2 + 1.43 \times 12 + 0.71 \times 14.1 = 43.747 \text{ [mm]} \tag{A.33}$$

$$k_4 = 0.1L_n + 0.2L_w = 0.1 \times 14.1 + 0.2 \times 4 \times 2 = 3.01 \text{ [mm]} \tag{A.34}$$

$$q = \frac{Z_e\alpha_{e1} + Z_{cf}\alpha_{cf1}}{Z_e\alpha_{e2} + Z_{cf}\alpha_{cf2} + \frac{k_1+2k_4}{2A_s}} = \frac{2 \times 23.905 \times 0.2698}{2 \times 23.905 \times 0.16 + \frac{43.747+2\times3.01}{2\times157}} = 1.6512 \text{ [-]} \tag{A.35}$$

Owing this, the stiffness can be assessed as follows. Notice that this expression stands for one T-stub. In consequence, the assembly step is not required here since the force-displacement curve is built for one T-stub and not the entire system.

$$K_{i,cf} = K_{i,e} = E\left[Z_e\left(\frac{1}{8} - \frac{1}{4}q\alpha_e\right)\right]^{-1} = 210,000\left[23.905\left(\frac{1}{8} - \frac{1}{4}1.6512 \times 0.1888\right)\right]^{-1} = 186.686 \text{ [kN/mm]} \tag{A.36}$$

Concerning the post-yielding behaviour, the same equation can be used but with the hardening stiffness modulus E_h instead of the Young modulus E.

$$K_{st,cf} = K_{st,e} = E_{st}\left[Z_e\left(\frac{1}{8} - \frac{1}{4}q\alpha_e\right)\right]^{-1} = 1,735.9\left[23.905\left(\frac{1}{8} - \frac{1}{4}1.6512 \times 0.1888\right)\right]^{-1} = 0.617 \text{ [kN/mm]} \tag{A.37}$$

Notice that $E/E_{st} = 8.26 \times 10^{-3}$ [-] which is very far away of the 0.02 [-] value assumed by Jaspart. The reason of this difference is explained in the main text and so, is not repeated here.

To conclude this model, the force-displacement curve can be built either with a bilinear model, either with a trilinear one. The formulae that must be used for the former can be found hereafter :

$$F_0 = 0 \text{ [kN]} \qquad F_1 = F_{T,Rd} = 84 \text{ [kN]} \qquad F_2 = F_u = 110.56 \text{ [kN]}$$

$$\Delta_0 = 0 \text{ [mm]} \qquad \Delta_1 = \frac{F_1}{K_i} = 0.45 \text{ [mm]} \qquad \Delta_2 = \frac{F_2 - F_1}{K_{st}} = 43.05 \text{ [mm]}$$

The set of equations that must be used for the trilinear model are the followings :

$$F_0 = 0 \text{ [kN]} \quad F_1 = \frac{2F_{T,Rd}}{3} = 56 \text{ [kN]} \quad F_2 = \Delta_2 K_{st} + F_2 = 84.83 \text{ [kN]} \quad F_3 = F_u = 110.56 \text{ [kN]}$$

$$\Delta_0 = 0 \text{ [mm]} \quad \Delta_1 = \frac{F_{T,Rd}}{K_i} = 0.3 \text{ [mm]} \quad \Delta_2 = \frac{F_2}{K_i/3} = 1.35 \text{ [mm]} \quad \Delta_3 = \frac{F_3 - F_{T,Rd}}{K_{st}} = 41.7 \text{ [mm]}$$

A.3 Piluso model

In this model, the first step of the procedure is to convert the nominal steel properties into true ones.

$$\varepsilon_y = f_y/E = 310/210,000 = 0.0014667 \text{ [-]} \tag{A.38}$$
$$\varepsilon_{h,true} = \ln(1+\varepsilon_h) = \ln(1+0.03473) = 0.03414 \text{ [-]} \tag{A.39}$$
$$f_{m,true} = f_u(1+\varepsilon_u) = 408 \times (1+0.17586) = 479.75 \text{ [MPa]} \tag{A.40}$$
$$\varepsilon_{m,true} = \ln(1+\varepsilon_u) = \ln(1+0.17586) = 0.162 \text{ [-]} \tag{A.41}$$
$$E_{h,true} = \frac{f_{m,true} - f_y}{\varepsilon_{m,true} - \varepsilon_{h,true}} = \frac{479.75 - 310}{0.162 - 0.03414} = 1,327.61 \text{ [MPa]} \tag{A.42}$$

Two additional properties are needed to complete the set of required inputs. Those are listed hereafter and are obtained from the coupon test true stress-true strain curve.

$$E_{u,true} = 510.88 \text{ [MPa]} \qquad \varepsilon_{u,true} = 0.2443 \text{ [-]} \tag{A.43}$$

Then, the next step consists in building the bending moment-curvature relationship of the steel. This can be done by computing the curvatures first.

$$\chi_y = \frac{2\varepsilon_y}{t_f} = \frac{2 \times 0.0014667}{9.6} = 0.0003075 \text{ [rad/mm]} \tag{A.44}$$
$$\chi_h = \frac{2\varepsilon_{h,true}}{t_f} = \frac{2 \times 0.03414}{9.6} = 0.007112 \text{ [rad/mm]} \tag{A.45}$$
$$\chi_m = \frac{2\varepsilon_{m,true}}{t_f} = \frac{2 \times 0.162}{9.6} = 0.03375 \text{ [rad/mm]} \tag{A.46}$$
$$\chi_u = \frac{2\varepsilon_{u,true}}{t_f} = \frac{2 \times 0.2443}{9.6} = 0.0.0509 \text{ [rad/mm]} \tag{A.47}$$
$$\tag{A.48}$$

Then, with a formula developed by Piluso, all the bending moment can be expressed as a function of bending moment at yielding.

$$\frac{M_h}{M_y} = \frac{\chi_h}{\chi_y} + \frac{1}{2}\left[3 - 2\frac{\chi_h}{\chi_y} - \left(\frac{\chi_y}{\chi_h}\right)^2\right] = 1.499 \text{ [-]} \tag{A.49}$$

$$\frac{M_m}{M_y} = \frac{\chi_m}{\chi_y} + \frac{1}{2}\left[3 - 2\frac{\chi_m}{\chi_y} - \left(\frac{\chi_y}{\chi_m}\right)^2\right] + \frac{1}{2}\frac{E_{h,true}}{E}\left(\frac{\chi_m - \chi_h}{\chi_y}\right)\left(1 - \frac{\chi_h}{\chi_m}\right)\left(2 + \frac{\chi_h}{\chi_m}\right) = 1.9777 \text{ [-]} \tag{A.50}$$

$$\frac{M_u}{M_y} = \frac{\chi_u}{\chi_y} + \frac{1}{2}\left[3 - 2\frac{\chi_u}{\chi_y} - \left(\frac{\chi_y}{\chi_u}\right)^2\right] + \frac{1}{2}\frac{E_{h,true}}{E}\left(\frac{\chi_u - \chi_h}{\chi_y}\right)\left(1 - \frac{\chi_h}{\chi_u}\right)\left(2 + \frac{\chi_h}{\chi_u}\right) \tag{A.51}$$
$$- \frac{1}{2}\frac{E_{h,true} - E_{u,true}}{E}\left(\frac{\chi_u - \chi_m}{\chi_y}\right)\left(1 - \frac{\chi_m}{\chi_u}\right)\left(2 + \frac{\chi_m}{\chi_u}\right) = 2.231 \text{ [-]} \tag{A.52}$$

Owing this, the bending moments at relevant points can be easily be derived. Notice that according to Piluso, the effective length to be used is the one following, proposed by Faella :

$$L_{eff} = \min(d_{hole} + 2m\,;\, L) = \min(18 + 2 \times 37.08\,;\, 90) = \min 92.16\,;\, 90) = 90 \text{ [mm]} \tag{A.53}$$

$$M_y = \frac{L_{eff} t_f^2 f_y}{6} = \frac{90 \times 9.6^2 \times 310}{6} = 428,544 \text{ [Nmm]} \tag{A.54}$$

$$M_h = M_y \frac{M_h}{M_y} = 428,544 \times 1.499 = 642,387 \text{ [Nmm]} \tag{A.55}$$

$$M_m = M_y \frac{M_m}{M_y} = 428,544 \times 1.9777 = 847,531 \text{ [Nmm]} \tag{A.56}$$

$$M_u = M_y \frac{M_u}{M_y} = 428,544 \times 2.231 = 956,081 \text{ [Nmm]} \tag{A.57}$$

Afterwards, some constants must be computed in purpose to assess the rotations at both plastic hinges.

$$\xi_1 = \frac{M_y}{M_u} = \frac{428,544}{956,081} = 0.448 \text{ [-]} \tag{A.58}$$

$$\xi_2 = \frac{M_h}{M_u} = \frac{642,387}{956,081} = 0.6719 \text{ [-]} \tag{A.59}$$

$$\xi_3 = \frac{M_m}{M_u} = \frac{847,531}{956,081} = 0.8864 \text{ [-]} \tag{A.60}$$

$$D_{(\xi_2)} = \varepsilon_y \left(2\frac{\chi_h}{\chi_y} - \frac{\xi_1}{\xi_2} \left(3\frac{\chi_h}{\chi_y} + \frac{\chi_y}{\chi_h} - 3 \right) - 1 \right) = 0.001393 \text{ [-]} \tag{A.61}$$

$$F_{(\xi_3)} = \varepsilon_y \left(2\frac{\chi_m}{\chi_y} - \frac{\xi_1}{\xi_3} \left(3\frac{\chi_m}{\chi_y} + \frac{\chi_y}{\chi_m} - 3 + \frac{E_{h,true}}{E} \frac{(\chi_m - \chi_h)^3}{\chi_m \chi_y^2} \right) - 1 \right) = 0.05107 \text{ [-]} \tag{A.62}$$

$$G_h = \frac{\chi_m^3}{\chi_u \chi_y} + 3\frac{\chi_m \chi_u}{\chi_y^2} - 3\frac{\chi_m^2}{\chi_y^2} + 3\frac{\chi_h^2}{\chi_y^2} - 3\frac{\chi_h \chi_u}{\chi_y^2} - \frac{\chi_h^3}{\chi_u \chi_y^2} = 16,389 \text{ [-]} \tag{A.63}$$

$$G_u = \frac{\chi_u^2}{\chi_y^2} + 3\frac{\chi_m^2}{\chi_y^2} - 3\frac{\chi_m \chi_u}{\chi_y^2} - \frac{\chi_m^3}{\chi_u \chi_y^2} = 1,047 \text{ [-]} \tag{A.64}$$

$$C = G_{(1)} = \varepsilon_y \left(2\frac{\chi_u}{\chi_y} - \xi_1 \left(3\frac{\chi_u}{\chi_y} + \frac{\chi_y}{\chi_u} - 3 + \frac{E_{h,true}}{E} G_h + \frac{E_{u,true}}{E} G_u \right) - 1 \right) = 0.09037 \text{ [-]} \tag{A.65}$$

Then, the T-stub can be classified and the failure mode determined. To do so, the two followings expressions must be compared to each other.

$$\beta_u = \frac{2M_u}{B_{u,Rd} m} = \frac{2 \times 956.081}{169.592 \times 37.08} = 0.3041 \text{ [-]} \tag{A.66}$$

$$\lambda = \frac{n}{m} = \frac{30}{37.08} = 0.8091 \text{ [mm]} \tag{A.67}$$

$$\beta_{u,lim} = \frac{2\lambda}{1+2\lambda}\left(1-(1+\lambda)\frac{d_w}{8n}\right) = \frac{2\times 0.8091}{1+2\times 0.8091}\left(1-(1+0.8091)\frac{30}{8\times 30}\right) = 0.4783 \text{ [-]} \tag{A.68}$$

Since $\beta_u < \beta_{u,lim}$, the T-stub is characterised as a mode 1. In consequence, the followings expressions can be used to determine the resistances :

$$F_y = \frac{(32n-2d_w)M_y}{8mn-(m+n)d_w} = \frac{(32\times 30-2\times 30)428,544}{8\times 30\times 37.08-(37.08+30)\times 30} = 56 \text{ [kN]} \tag{A.69}$$

$$F_h = F_y\frac{M_h}{M_y} = 56\times 1.499 = 83.95 \text{ [kN]} \tag{A.70}$$

$$F_m = F_y\frac{M_m}{M_y} = 56\times 1.9777 = 110.76 \text{ [kN]} \tag{A.71}$$

$$F_u = F_y\frac{M_u}{M_y} = 56\times 2.231 = 124.95 \text{ [kN]} \tag{A.72}$$

Another consequence of this classification is that both plastic hinges undergo the same rotations. The plate stiffness can be obtained with those formulations :

$$\zeta = 0.16\frac{m+0.8a_w\sqrt{2}}{t_f} - 0.08 = 0.16\frac{37.08+0.8\times 7\times\sqrt{2}}{9.6} - 0.08 = 0.67 \text{ [-]} \tag{A.73}$$

$$m' = m+(0.8-\zeta)a_w\sqrt{2} = 37.08+(0.8-0.67)\times 7\times\sqrt{2} = 37.367 \text{ [mm]} \tag{A.74}$$

$$K = 0.5\frac{EL_{eff}T_f^3}{m'^3} = 0.5\frac{210,000\times 90\times 9.6^3}{38.367^3} = 148.04 \text{ [kN/mm]} \tag{A.75}$$

This was done in purpose to assess the T-stub displacement at first yielding. Another required contribution to do so is the bolt elongation. It can be evaluated as follows :

$$B_y = \frac{F_y}{2}+\frac{M_y}{n} = \frac{56}{2}+\frac{428.544}{30} = 42.285 \text{ [kN]} \tag{A.76}$$

$$\delta_{b,y} = \frac{B_yL_b}{EA} = \frac{42,285\times 39.45}{210,000\times 201.06} = 0.0395 \text{ [mm]} \tag{A.77}$$

Owing this and the plate stiffness, the T-stub displacement at first yielding can be evaluated and the initial stiffness of the T-stub can be deduced.

$$\delta_y = \frac{2F_y}{K}+\delta_{b,y} = \frac{2\times 56}{148.04}+0.0395 = 0.796 \text{ [mm]} \tag{A.78}$$

$$K_i = \frac{F_y}{\delta_y} = \frac{56}{0.796} = 70.361 \text{ [kN/mm]} \tag{A.79}$$

Once the yielding past, the displacement is seen as the sum of an elastic and plastic contribution. The former can be obtained with the stiffness computed above while the latter can be found with the constants previously assessed. By summing those terms and proceeding like this for each relevant bending moment, the entire force-displacement curve can be built. Notice that all the displacements found should be divided by 2 to obtain the response of one T-stub.

$$\delta_{eh} = \frac{F_h}{K_i} = \frac{83.95}{70.361} = 1.19 \text{ [mm]} \tag{A.80}$$

$$\delta_{ph} = \frac{m^2}{2t_f} D_{(\xi_2)} = \frac{37.08^2}{2 \times 9.6} \times 0.001393 = 0.1 \text{ [mm]} \tag{A.81}$$

$$\delta_h = \delta_{eh} + 2\delta_{ph} = 1.19 + 2 \times 0.1 = 1.39 \text{ [mm]} \tag{A.82}$$

$$\delta_{em} = \frac{F_m}{K_i} = \frac{110.76}{70.361} = 1.574 \text{ [mm]} \tag{A.83}$$

$$\delta_{pm} = \frac{m^2}{2t_f} F_{(\xi_3)} = \frac{37.08^2}{2 \times 9.6} \times 0.05107 = 3.657 \text{ [mm]} \tag{A.84}$$

$$\delta_m = \delta_{em} + 2\delta_{pm} = 1.574 + 2 \times 3.657 = 8.89 \text{ [mm]} \tag{A.85}$$

$$\delta_{eu} = \frac{F_u}{K_i} = \frac{124.95}{70.361} = 1.77 \text{ [mm]} \tag{A.86}$$

$$\delta_{ph} = \frac{m^2}{2t_f} C = \frac{37.08^2}{2 \times 9.6} \times 0.09037 = 6.472 \text{ [mm]} \tag{A.87}$$

$$\delta_u = \delta_{eu} + 2\delta_{pu} = 1.77 + 6.472 = 14.72 \text{ [mm]} \tag{A.88}$$

A.4 Zhao model

This model is based on the Piluso model and consists in an improvement of this one. In consequence, the beginning of the procedure is equivalent. The same goes for the required inputs. So, by sake of concisely, Equations (A.38) to (A.58) are not repeated and their results are taken as such.

Then, the collapse mode of the t-stub can be classified.

$$\lambda = \frac{n}{m} = \frac{30}{37.08} = 0.8091 \text{ [mm]} \tag{A.89}$$

$$\xi = \frac{M_h}{M_u} = \frac{642,387}{956,081} = 0.6719 \text{ [-]} \tag{A.90}$$

$$\eta = \frac{1-\xi}{\xi} = \frac{1-0.6719}{0.6719} = 0.488 \text{ [-]} \tag{A.91}$$

$$\beta_{lim,FF} = \frac{2\lambda\xi}{1+2\lambda} = \frac{2 \times 0.8091 \times 0.6719}{1+2 \times 0.8091} = 0.415 \text{ [mm]} \tag{A.92}$$

$$\beta_{lim,BR} = \frac{1}{\eta}\left(\sqrt{1+\frac{4\lambda\eta}{1+2\lambda}} - 1\right) = \frac{1}{0.488}\left(\sqrt{1+\frac{4 \times 0.8091 \times 0.488}{1+2 \times 0.8091}} - 1\right) = 0.545 \text{ [-]} \tag{A.93}$$

$$\beta = \frac{2M_h}{B_{t,Rd}m} = \frac{2 \times 642.387}{152.63 \times 37.08} = 0.227 \text{ [-]} \tag{A.94}$$

Since $\beta < \beta_{lim,FF} : \Psi = 1$, the T-stub is a mode 1 and is expected to fail due to a fracture in the flange. The ultimate strength that will be find at the end of this procedure is expected to be :

$$F_{u,1FF} = 2B_{u,Rd}\frac{\beta}{\xi} = 2 \times 169.592 \times \frac{0.227}{0.6719} = 114.6 \text{ [kN]} \tag{A.95}$$

In this model, the plate and bolt force-displacement curves are computed independently and are combined at the end of the procedure. The first element to be computed is the plate. To do so, a similar procedure to Piluso is applied and the plastic rotation at the hinges are assessed as follow :

$$C_h = \frac{\chi_h^3}{2\chi_h\chi_y} - \frac{(\chi_h - \chi_y)^3}{2\chi_h\chi_y} = 0.0102 \text{ [rad/mm]} \tag{A.96}$$

$$C_m = \frac{\chi_m^3}{2\chi_m\chi_y} - \frac{(\chi_m - \chi_y)^3}{2\chi_m\chi_y} + \frac{E_{h,true}(\chi_m - \chi_h)^3}{2E\chi_m\chi_y} = 0.559 \text{ [rad/mm]} \tag{A.97}$$

$$C_u = \frac{\chi_u^3}{2\chi_u\chi_y} - \frac{(\chi_u - \chi_y)^3}{2\chi_u\chi_y} + \frac{E_{h,true}(\chi_u - \chi_h)^3}{2E\chi_u\chi_y} - \frac{(E_{h,true} - E_{u,true})(\chi_u - \chi_m)^3}{2E\chi_u\chi_y} = 0.0922 \text{ [rad/mm]} \tag{A.98}$$

$$\theta_{h,p} = \frac{m}{1+\psi}\left(\chi_h - \frac{M_y}{M_h}C_h - \frac{1}{2}\chi_y\frac{M_h}{M_y}\right) = 0.001267 \text{ [rad]} \tag{A.99}$$

$$\theta_{m,p} = \frac{m}{1+\psi}\left(\chi_m - \frac{M_y}{M_m}C_m - \frac{1}{2}\chi_y\frac{M_m}{M_y}\right) = 0.09585 \text{ [rad]} \tag{A.100}$$

$$\theta_{u,p} = \frac{m}{1+\psi}\left(\chi_u - \frac{M_y}{M_u}C_u - \frac{1}{2}\chi_y\frac{M_u}{M_y}\right) = 0.171 \text{ [rad]} \tag{A.101}$$

On the other hand, the resistance can be computed for each relevant bending moment. Notice that those expression are based on the method 1 of EuroCode. The method 2 can also be applied with other equations but this is not done in the current thesis.

$$F_y = \frac{2M_y(1+\psi)}{m} = \frac{2 \times 428.544 \times (1+1)}{37.08} = 46.23 \text{ [kN]} \tag{A.102}$$

$$F_h = \frac{2M_h(1+\psi)}{m \cdot \cos\theta_{h,p}} = \frac{2 \times 642.387 \times (1+1)}{37.08 \times \cos 0.001267} = 69.3 \text{ [kN]} \tag{A.103}$$

$$F_m = \frac{2M_m(1+\psi)}{m \cdot \cos\theta_{m,p}} = \frac{2 \times 847.531 \times (1+1)}{37.08 \times \cos 0.09585} = 91.85 \text{ [kN]} \tag{A.104}$$

$$F_u = \frac{2M_u(1+\psi)}{m \cdot \cos\theta_{u,p}} = \frac{2 \times 956.081 \times (1+1)}{37.08 \times \cos 0.171} = 104.67 \text{ [kN]} \tag{A.105}$$

Concerning the displacement of the plate, as it was done for Piluso, the displacement is simply the sum of an elastic and a plastic contribution :

$$\Delta_y = \Delta_{y,e} + \Delta_{y,p} = \frac{1.18m^3F_y}{EL_{eff}t_f^3} = \frac{1.18 \times 37.08^3 \times 46,230}{210,000 \times 90 \times 9.6^3} = 0.166 \text{ [mm]} \tag{A.106}$$

$$\Delta_h = \Delta_{h,e} + \Delta_{h,p} = \frac{1.18m^3F_h}{EL_{eff}t_f^3} + m\sin\theta_{h,p} = \frac{1.18 \times 37.08^3 \times 69,300}{210,000 \times 90 \times 9.6^3} + 37.08 \times \sin 0.001267 = 0.296 \text{ [mm]} \tag{A.107}$$

$$\Delta_m = \Delta_{m,e} + \Delta_{m,p} = \frac{1.18m^3F_m}{EL_{eff}t_f^3} + m\sin\theta_{m,p} = \frac{1.18 \times 37.08^3 \times 91,850}{210,000 \times 90 \times 9.6^3} + 37.08 \times \sin 0.09585 = 3.88 \text{ [mm]} \tag{A.108}$$

$$\Delta_u = \Delta_{u,e} + \Delta_{u,p} = \frac{1.18m^3F_u}{EL_{eff}t_f^3} + m\sin\theta_{u,p} = \frac{1.18 \times 37.08^3 \times 104,670}{210,000 \times 90 \times 9.6^3} + 37.08 \times \sin 0.171 = 6.687 \text{ [mm]} \tag{A.109}$$

With an identical philosophy, the force-displacement curve of the bolt can be built. Concerning the displacement, it simply consists in the axial elongation of the bolt. Notice that the necking domain was neglected due to the lack of information.

$$\Delta_{y,b} = \varepsilon_{y,b}L_b = 4.5952 \times 10^{-3} \times 39.45 = 0.181 \text{ [mm]} \tag{A.110}$$

$$\Delta_{u,b} = \varepsilon_{u,b}L_b = 0.05 \times 39.45 = 1.9725 \text{ [mm]} \tag{A.111}$$

For the resistance, the next equations can be used :

$$F_{y,b} = \frac{2\lambda(1+\psi)}{\lambda(1+\psi)+\psi}B_{y,Rd} = \frac{2 \times 0.8091(1+1)}{0.8091(1+1)+1} \times 152.63 = 187.31 \text{ [kN]} \tag{A.112}$$

$$F_{u,b} = \frac{2\lambda(1+\psi)}{\lambda(1+\psi)+\psi}B_{u,Rd} = \frac{2 \times 0.8091(1+1)}{0.8091(1+1)+1} \times 169.592 = 209.63 \text{ [kN]} \tag{A.113}$$

To conclude, the assembly of both flanges and bolts can be performed. Since $F_u < F_{y,b}$ it can easily be deduced that the T-stub indeed fails due to flange fracture. In consequence the following equations can be used since the bolts remain in the elastic domain. Notice that the proposed values stands for one T-stub.

$$F_0 = 0 \text{ [kN]} \qquad \Delta_0 = 0 \text{ [mm]} \tag{A.114}$$

$$F_1 = F_y = 46.23 \text{ [kN]} \qquad \Delta_1 = \Delta_y + \frac{F_y}{F_{y,b}} = 0.166 + \frac{46.23}{187.31} = 0.211 \text{ [mm]} \tag{A.115}$$

$$F_2 = F_h = 69.3 \text{ [kN]} \qquad \Delta_2 = \Delta_h + \frac{F_h}{F_{y,b}} = 0.296 + \frac{69.3}{187.31} = 0.363 \text{ [mm]} \tag{A.116}$$

$$F_3 = F_m = 91.85 \text{ [kN]} \qquad \Delta_3 = \Delta_m + \frac{F_m}{F_{y,b}} = 3.88 + \frac{91.85}{187.31} = 3.968 \text{ [mm]} \tag{A.117}$$

$$F_4 = F_u = 104.67 \text{ [kN]} \qquad \Delta_4 = \Delta_u + \frac{F_u}{F_{y,b}} = 6.687 + \frac{101.67}{187.31} = 6.788 \text{ [mm]} \tag{A.118}$$

Appendix B

Demonstration of the yield line patterns

In this Chapter, the demonstrations of each yield line patterns relevant for this thesis are carried out. They consists in the plastic mechanism of the short T-stub either taking into account the work of head or not. Then, the circular pattern of the EuroCode is proved as well. Finally, the full proof a the new yield line pattern presented in Section (6.2) is developed. Notice that the hybrid yield line pattern discovered is not covered here since it can be seen as a combination of two others mechanisms and was not rigorously demonstrated.

B.1 Short yield line pattern method 1

The first plastic mechanism studied can be consulted on Figure (B.1).

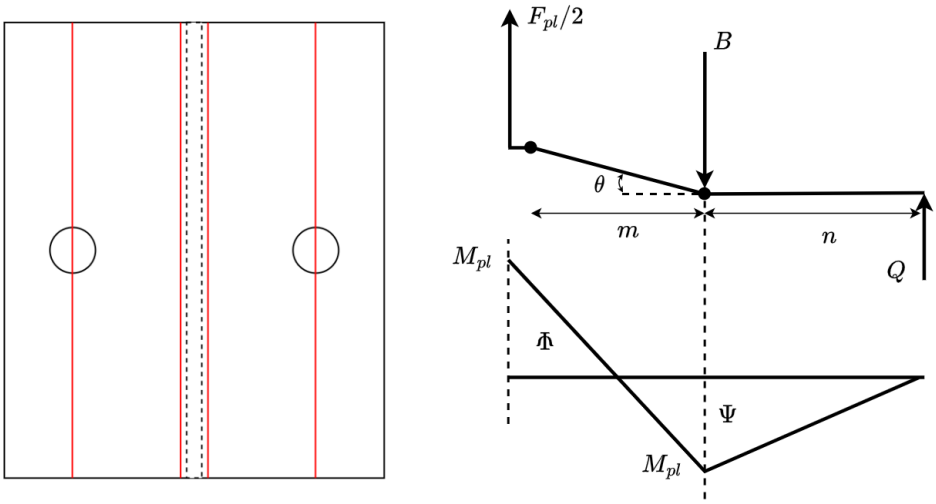

Figure B.1 – Short plastic mechanism without the bolt head work

To solve this problem, a simple energy balance can be performed. In this configuration, the bolt force B does not undergo any displacement and thus, does not contribute to the virtual work. Both internal energy of deformation and the virtual work can be written as follows :

$$\Delta E = m_{pl} L\theta - m_{pl} L(-\theta) = 2m_{pl} L\theta \tag{B.1}$$

$$\Delta W = \frac{F_{pl}}{2} m\theta \tag{B.2}$$

By equaling those terms and rewriting the equation, the plastic strength can be isolated. The EQUATION obtained is the method 1 proposed by EuroCode.

$$\Leftrightarrow \frac{F_{pl}}{2} m\theta = m_{pl} L\theta - m_{pl} L(-\theta) = 2m_{pl} L\theta \tag{B.3}$$

$$\Leftrightarrow F_{pl} = \frac{4m_{pl} L}{m} \tag{B.4}$$

B.2 Short yield line pattern method 2

The second plastic mechanism studied can be consulted on FIGURE (B.2). It consists in the same geometry as previously. However, the modelling of the bolt force is different in this configuration.

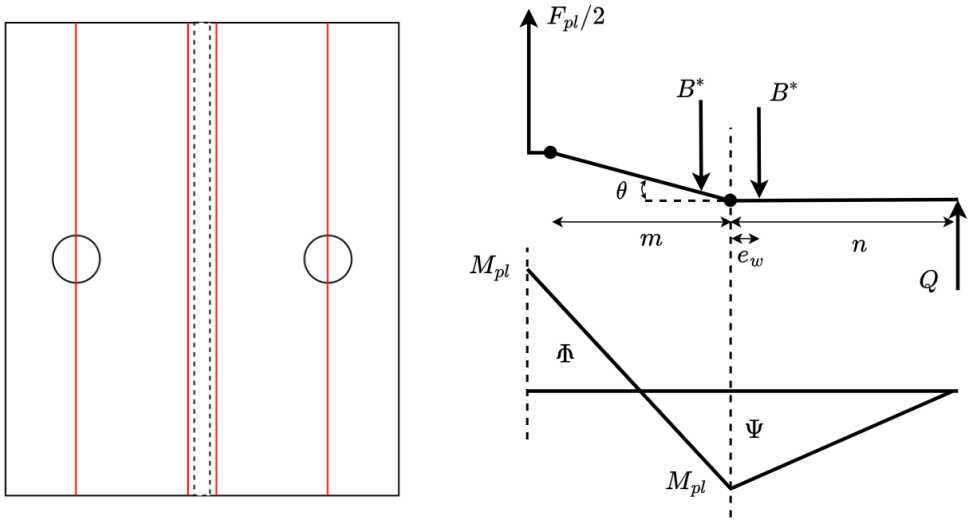

FIGURE B.2 – Short plastic mechanism with the bolt head work

To solve this problem, as it was previously done, an energy balance can be performed.

$$\Leftrightarrow \Delta W = \Delta E \tag{B.5}$$

$$\Leftrightarrow \frac{F_{pl}}{2} m\theta - B^* e_w \theta = m_{pl} L\theta - m_{pl} L(-\theta) \tag{B.6}$$

$$\Leftrightarrow \frac{F_{pl}}{2} m = 2m_{pl} L + B^* e_w \tag{B.7}$$

It can be seen that B^* is an unknown and thus, must be eliminated. To do so, both vertical (B.8) and bending moment equilibria are required (B.9). Notice that the bending moment equation is written taking the plastic hinge at the bolt axis as the pivot point. In addition to that, a cut is made in the beam model and only the part at the right of the plastic hinge is considered.

$$2B^* - \frac{F_{pl}}{2} = Q \tag{B.8}$$

$$m_{pl} L + Be_w = Qn \tag{B.9}$$

It can be observed that the prying forces Q can be easily eliminated from those two EQUATIONS. After few rewriting, the bolt force B^* can be isolated.

$$\Leftrightarrow \; 2B^* - \frac{F_{pl}}{2} = \frac{m_{pl}L}{n} + \frac{B^* e_w}{n} \tag{B.10}$$
$$\Leftrightarrow \; 4B^* n - F_{pl} n = 2m_{pl}L + 2B^* e_w \tag{B.11}$$
$$\Leftrightarrow \; 2B^*(e_w - 2n) = -2m_{pl} - F_{pl} n \tag{B.12}$$
$$\Leftrightarrow \; B^* = \frac{-2m_{pl} - F_{pl} n}{2(e_w - 2n)} \tag{B.13}$$

Finally, the solution can be obtained by injecting the last results in (B.7) and isolating F_{pl}.

$$\Leftrightarrow \; \frac{F_{pl}}{2} m = 2m_{pl}L - \frac{2m_{pl}F_{pl}n}{2(e_w - 2n)} e_w \tag{B.14}$$
$$\Leftrightarrow \; F_{pl} m(e_w - 2n) + e_w(F_{pl} + 2m_{pl}L) = 4m_{pl}L(e_w - 2n) \tag{B.15}$$
$$\Leftrightarrow \; F_{pl} m(e_w - 2n) + F_{pl} e_w n + 2m_{pl} L e_w = 4m_{pl}L(e_w - 2n) \tag{B.16}$$
$$\Leftrightarrow \; F_{pl}\left(m e_w - 2mn + e_w n\right)) = m_{pl}L(4e_w - 8n - 2e_w) \tag{B.17}$$
$$\Leftrightarrow \; F_{pl}(-2mn + e_w(m+n)) = m_{pl}L(-8n + e_w) \tag{B.18}$$
$$\Leftrightarrow \; F_{pl} = \frac{m_{pl}L(8n - 2e_w)}{2mn - e_w(m+n)} \tag{B.19}$$

The last line obtained indeed correspond to the method 2 proposed by the EuroCode. In that model, the stress distribution under the bolt head is assumed uniform. That means B^* is located at half the washer radius. In other words, $e_w = d_w/4$. In case of triangular distribution (and not taking into account the real hinge position), B^* is located at two third of the washer radius : $e_w = d_w/3$.

B.3 Neutelers short yield line pattern

As it was done in the main text, additional contributions as the triangular stress distribution or the plastic hinges offset can still be introduced in the model to increase its complexity and accuracy. The first step is to model the stress distribution and integrate it. This process can be observed on FIGURE (B.3) herebelow.

The maximum stress that can be attained in this distribution is b. For sake of simplicity, this parameter is expressed as a function of half of the bolt force B^*.

$$B^* = \frac{b}{2}\left(\frac{d_w - d_h}{2}\right) \;\Leftrightarrow\; b = \frac{4B^*}{d_w - d_h} \tag{B.20}$$

Another useful parameter that can be found from the stress distribution is the value of the stress b^* where the partitioning occurs. It formulation is simply :

$$b^* = \frac{2b}{d_w - d_h}\left(\delta_{H2} - \frac{d_h}{2}\right) \tag{B.21}$$

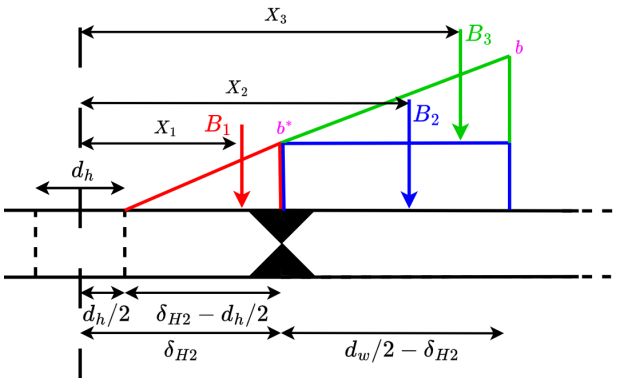

FIGURE B.3 – Zoom on the stress distribution under the bolt head

Owing those two expressions, the colored stress distributions can be integrated. Thus, EQUATIONS (6.4) to (6.6) can be obtained.

$$B_1 = \frac{b^*}{2}\left(\delta_{H2} - \frac{d_h}{2}\right) = \frac{b}{d_w - d_h}\left(\delta_{H2} - \frac{d_h}{2}\right)^2 = \frac{4B^*}{(d_w - d_h)^2}\left(\delta_{H2} - \frac{d_h}{2}\right)^2 \tag{B.22}$$

$$B_2 = b^*\left(\frac{d_w}{2} - \delta_{H2}\right) = \frac{2b}{d_w - d_h}\left(\delta_{H2} - \frac{d_h}{2}\right)\left(\frac{d_w}{2} - \delta_{H2}\right) = \frac{8B^*}{(d_w - d_h)^2}\left(\delta_{H2} - \frac{d_h}{2}\right)\left(\frac{d_w}{2} - \delta_{H2}\right) \tag{B.23}$$

$$B_3 = \frac{b - b^*}{2}\left(\frac{d_w}{2} - \delta_{H2}\right) = \frac{2B^*}{d_w - d_h}\left(1 - \frac{2}{d_w - d_h}\left(\delta_{H2} - \frac{d_h}{2}\right)\right)\left(\frac{d_w}{2} - \delta_{H2}\right) \tag{B.24}$$

$$= \frac{2B^*}{(d_w - d_h)^2}\left(d_w - d_h - 2\left(\delta_{H2} - \frac{d_h}{2}\right)\right)\left(\frac{d_w}{2} - \delta_{H2}\right) = \frac{2B^*}{(d_w - d_h)^2}\left(d_w - 2\delta_{H2}\right)\left(\frac{d_w}{2} - \delta_{H2}\right) \tag{B.25}$$

$$= \frac{4B^*}{(d_w - d_h)^2}\left(\frac{d_w}{2} - \delta_{H2}\right)^2 \tag{B.26}$$

A simple way to validate the performed developments is to check that the sum of those loads indeed gives B^*. In other words, that the load decomposition was correctly without adding or substracting any contribution.

$$B^* = B_1 + B_2 + B_3 \tag{B.27}$$

$$= \frac{4B^*}{(d_w - d_h)^2}\left(\delta_{H2} - \frac{d_h}{2}\right)^2 + \frac{8B^*}{(d_w - d_h)^2}\left(\delta_{H2} - \frac{d_h}{2}\right)\left(\frac{d_w}{2} - \delta_{H2}\right) + \frac{4B^*}{(d_w - d_h)^2}\left(\frac{d_w}{2} - \delta_{H2}\right)^2 \tag{B.28}$$

$$= \frac{4B^*}{(d_w - d_h)^2}\left(\left(\delta_{H2} - \frac{d_h}{2}\right)^2 + 2\left(\delta_{H2} - \frac{d_h}{2}\right)\left(\frac{d_w}{2} - \delta_{H2}\right) + \left(\frac{d_w}{2} - \delta_{H2}\right)^2\right) \tag{B.29}$$

$$= \frac{4B^*}{(d_w - d_h)^2}\left(\delta_{H2} - \frac{d_h}{2} + \frac{d_w}{2} - \delta_{H2}\right)^2 \tag{B.30}$$

$$= \frac{4B^*}{(d_w - d_h)^2}\frac{(d_w - d_h)^2}{4} = B^* \tag{B.31}$$

In addition to that, the distance at which the loads are applied can simply be deduced from the FIGURE.

$$X_1 = \frac{d_h}{2} + \frac{2}{3}\left(\delta_{H2} - \frac{d_h}{2}\right) \tag{B.32}$$

$$X_2 = \delta_{H2} + \frac{1}{2}\left(\frac{d_w}{2} - \delta_{H2}\right) \tag{B.33}$$

$$X_3 = \delta_{H2} + \frac{2}{3}\left(\frac{d_w}{2} - \delta_{H2}\right) \tag{B.34}$$

$$X^* = \frac{d_w - d_h}{2} + \frac{d_h}{2} \tag{B.35}$$

Owing these expressions, a similar procedure to the one used in the previous SECTION can be used. The mechanism studied is represented on FIGURE (B.4) hereafter.

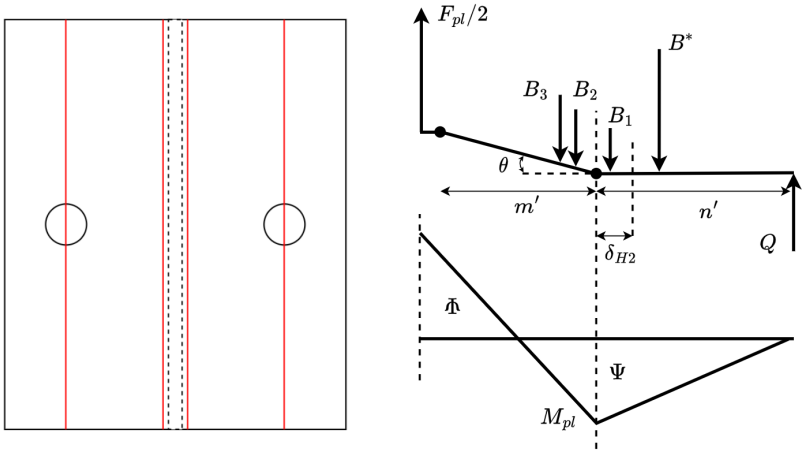

FIGURE B.4 – Short plastic mechanism with the bolt head work and the hinge offset

Next, the energy balance can be written :

$$\Leftrightarrow \Delta W = \Delta E \tag{B.36}$$

$$\Leftrightarrow \frac{F_{pl}m'\theta}{2} - \frac{B-2}{2}\left(\frac{d_w}{2} - \delta_{H2}\right)\theta - \frac{2B_3}{3}\left(\frac{d_w}{2} - \delta_{H2}\right)\theta = m_{pl}L\theta - m_{pl}L(-\theta) \tag{B.37}$$

$$\Leftrightarrow F_{pl}m' - \frac{8B^*}{(d_w - d_h)^2}\left(\delta_{H2} - \frac{d_h}{2}\right)\left(\frac{d_w}{2} - \delta_{H2}\right)^2 - \frac{16B^*}{3(d_w - d_h)^2}\left(\frac{d_w}{2} - \delta_{H2}\right)^3 = 4m_{pl}L \tag{B.38}$$

Similarly, both vertical and bending moment equilibria are required to solve this problem. Their expressions are respectively the followings. Notice that the pivot point of the bending moment equilibrium is once again the plastic hinge. A cut is performed in the beam where the plastic hinge lies and the equilibrium is made on its right side.

$$Q = 2B^* - \frac{Fpl}{2} \tag{B.39}$$

$$m_{pl}L + \frac{B_1}{3}\left(\delta_{H2} - \frac{d_h}{2}\right) + B^*\left(\delta_{H2} + \frac{d_h}{2} + \frac{d_w - d_h}{3}\right) = Qn' \tag{B.40}$$

In an identical manner, the prying forces can be eliminated from those EQUATIONS by equaling them.

$$\Leftrightarrow\ 4B^*n' - F_{pl}n' = 2m_{pl}L + \frac{8B^*}{3(d_w - d_h)^2}\left(\delta_{H2} - \frac{d_h}{2}\right)^3 + 2B^*\left(\delta_{H2} + \frac{d_h}{2} + \frac{d_w}{3} - \frac{d_h}{3}\right) \tag{B.41}$$

$$\Leftrightarrow\ -F_{pl}n' - 2m_{pl}L = \frac{8B^*}{3(d_w - d_h)^2}\left(\delta_{H2} - \frac{d_h}{2}\right)^3 + 2B^*\left(\delta_{H2} + \frac{d_h}{6} + \frac{d_w}{3}\right) - 4B^*n \tag{B.42}$$

$$\Leftrightarrow\ -(F_{pl}n' + 2m_{pl}L)3(d_w - d_h)^2 = 8B^*\left(\delta_{H2} - \frac{d_h}{2}\right)^3 + 6B^*\left(\delta_{H2} + \frac{d_h}{6} + \frac{d_w}{3}\right)(d_w - d_h)^2 - 12B^*n'(d_w - d_h)^2 \tag{B.43}$$

$$\Leftrightarrow\ -(3F_{pl}n' + 6m_{pl}L)(d_w - d_h)^2 = B^*\left(8\left(\delta_{H2} - \frac{d_h}{2}\right)^3 + 6\left(\delta_{H2} + \frac{d_h}{6} + \frac{d_w}{3}\right)(d_w - d_h)^2 - 12n'(d_w - d_h)^2\right) \tag{B.44}$$

$$\Leftrightarrow\ -(3F_{pl}n' + 6m_{pl}L)(d_w - d_h)^2 = B^*G \tag{B.45}$$

$$\Leftrightarrow\ B^* = \frac{-(3F_{pl}n' + 6m_{pl}L)(d_w - d_h)^2}{G} \tag{B.46}$$

Which corresponds to EQUATION (6.11) presented in SECTION (6.2). Notice that the equation G is the following and was also presented in the same SECTION.

$$G = 8\left(\delta_{H2} - \frac{d_h}{2}\right)^3 + 6\left(\delta_{H2} + \frac{d_h}{6} + \frac{d_w}{3}\right)(d_w - d_h)^2 - 12n'(d_w - d_h)^2 \tag{B.47}$$

By injecting EQUATION (B.46) in (B.38), the plastic strength can be isolated and the problem solved.

$$\Leftrightarrow\ F_{pl}m' + \frac{8}{G}(3F_{pl}n' + 6m_{pl}L)\left(\delta_{H2} - \frac{d_h}{2}\right)\left(\frac{d_w}{2} - \delta_{H2}\right)^2 + \frac{16}{G}(F_{pl}n' + 2m_{pl}L)\left(\frac{d_w}{2} - \delta_{H2}\right)^3 = 4m_{pl}L \tag{B.48}$$

$$\Leftrightarrow\ F_{pl}m'G + (24F_{pl}n' + 48m_{pl}L)\left(\delta_{H2} - \frac{d_h}{2}\right)\left(\frac{d_w}{2} - \delta_{H2}\right)^2 + (16F_{pl}n' + 32m_{pl}L)\left(\frac{d_w}{2} - \delta_{H2}\right)^3 = 4m_{pl}LG \tag{B.49}$$

$$\Leftrightarrow\ F_{pl} = \frac{m_{pl}L\left(4G - 48\left(\delta_{H2} - \frac{d_h}{2}\right)\left(\frac{d_w}{2} - \delta_{H2}\right)^2 - 32\left(\frac{d_w}{2} - \delta_{H2}\right)^3\right)}{m'G + 24n'\left(\delta_{H2} - \frac{d_h}{2}\right)\left(\frac{d_w}{2} - \delta_{H2}\right)^2 + 16n'\left(\frac{d_w}{2} - \delta_{H2}\right)^3} \tag{B.50}$$

$$\Leftrightarrow\ F_{pl} = \frac{m_{pl}L\left(4G - \left(\frac{d_w}{2} - \delta_{H2}\right)^2(24(2\delta_{H2} - d_h) + 16(d_w - 2\delta_{H2}))\right)}{m'G + n'\left(\frac{d_w}{2} - \delta_{H2}\right)^2(12(2\delta_{H2} - d_h) + 8(d_w - 2\delta_{H2}))} \tag{B.51}$$

$$\tag{B.52}$$

$$\Leftrightarrow \quad F_{pl} = \frac{m_{pl}L\left(4G - 2\left(d_w - 2\delta_{H2}\right)^2\left(3(2\delta_{H2} - d_h) + 2(d_w - 2\delta_{H2})\right)\right)}{m'G + n'\left(d_w - \delta_{H2}\right)^2\left(3(2\delta_{H2} - d_h) + 2(d_w - 2\delta_{H2})\right)} \tag{B.53}$$

$$\Leftrightarrow \quad F_{pl} = \frac{m_{pl}L\left(4G - 2\left(d_w - 2\delta_{H2}\right)^2\left(6\delta_{H2} - 3d_h + 2d_w - 4\delta_{H2}\right)\right)}{m'G + n'\left(d_w - \delta_{H2}\right)^2\left(6\delta_{H2} - 3d_h + 2d_w - 4\delta_{H2}\right)} \tag{B.54}$$

$$\Leftrightarrow \quad F_{pl} = \frac{m_{pl}L\left(4G - 2\left(d_w - 2\delta_{H2}\right)^2\left(2\delta_{H2} - 3d_h + 2d_w\right)\right)}{m'G + n'\left(d_w - \delta_{H2}\right)^2\left(2\delta_{H2} - 3d_h + 2d_w\right)} \tag{B.55}$$

$$\Leftrightarrow \quad F_{pl} = \frac{m_{pl}L\left(4G - 2\zeta\left(d_w - 2\delta_{H2}\right)^2\right)}{m'G + n'\zeta\left(d_w - \delta_{H2}\right)^2} \tag{B.56}$$

$$\tag{B.57}$$

Which indeed correspond to the presented expression in the main text. Notice that ζ is a simplification parameter which expression is :

$$\zeta = 2\delta_{H2} - 3d_h + 2d_w \tag{B.58}$$

Notice that if $\delta_{H2} = d_w/2$, the results of Section (B.1) can be found. Similarly, if d_h is artificially taken to 0 and $\delta_{H2} = 0$, the formula of Section (B.2) can be obtained with $e_w = d_w/3$.

B.4 Circular yield line pattern

The last yield line pattern to be proved is the circular one. This mechanism is illustrated on Figure (B.5) and also available in the EuroCode.

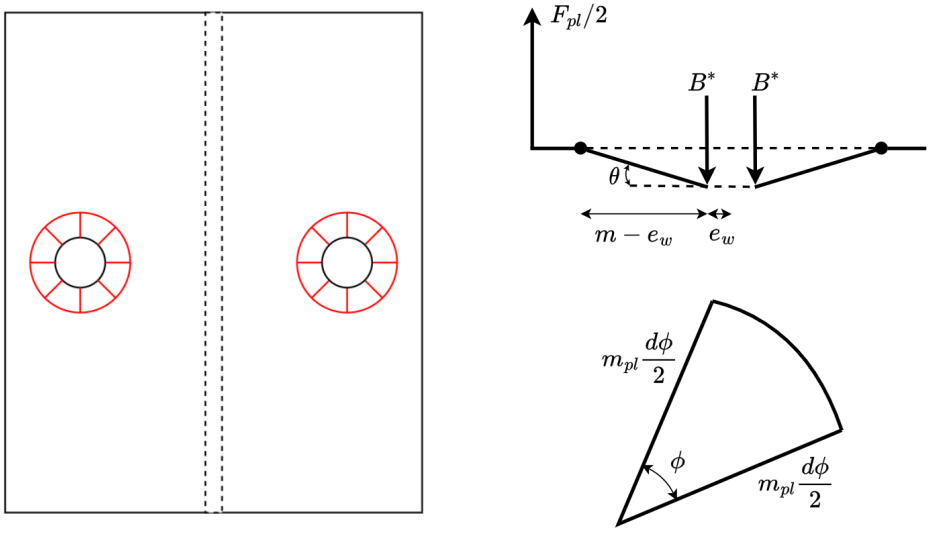

Figure B.5 – Circular plastic mechanism

For this mechanism, the virtual work can simply be assessed as following :

$$\Delta W = \frac{F_{pl}}{2}\left(m - e_w\right)\theta \tag{B.59}$$

For the internal energy, two contributions can be identified. The first one comes from the external plastic hinge while the second consists in the fan shaped lines. The integration of these internal energies of deformation gives :

$$\Leftrightarrow \ \Delta E = \int_0^{2\pi} m_{pl} m\theta d\phi + 2\int_0^{2\pi} m_{pl} m\theta \frac{d\phi}{2} \tag{B.60}$$

$$\Leftrightarrow \ \Delta E = 2\pi m_{pl} m\theta + 2\pi m_{pl} m\theta \tag{B.61}$$

$$\Leftrightarrow \ \Delta E = 4\pi m_{pl} m\theta \tag{B.62}$$

Thus, the final expression can be found.

$$F_{pl} = \frac{8\pi m_{pl} m}{m - e_w} = \frac{8\pi m_{pl}}{1 - \frac{e_w}{m}} \tag{B.63}$$

Notice that a difference of factor 2 can be observed with the results obtain through the EuroCode formula. This is due to the fact that introducing the effective length of the circular pattern in the method 2 formula implies that only half of the bolt head works (i.e. $n \to \infty$). In opposition to that, the entire bolt head here contributes to the plastic strength in the developed formula.

Appendix C

Validation of the model

In this Chapter, all the results of the parametric study can be found. On each specimen is applied the two developed models. **Rigid** stands for the model with $L_{eff} = L$. Otherwise, if $L_{eff} = L_{hybrid}$, the denomination **Flexible** is used.

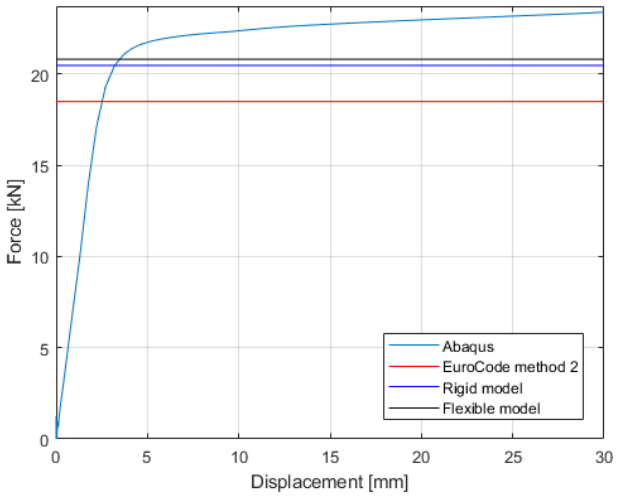

Figure C.1 – T-12-09-10-05 model validation

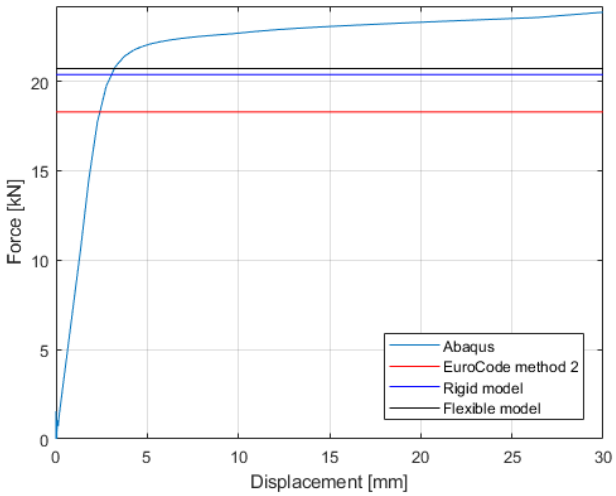

Figure C.2 – T-12-09-10-08 model validation

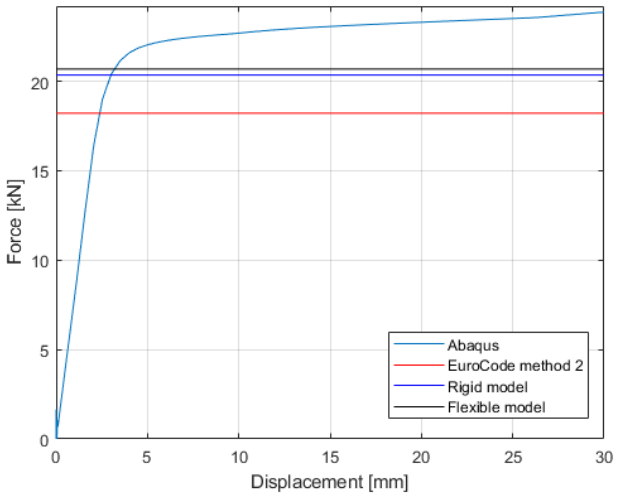

Figure C.3 – T12-09-10-1 model validation

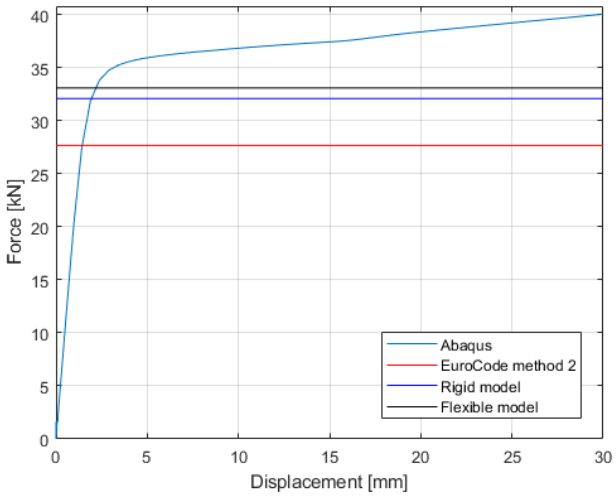

Figure C.4 – T12-09-15-1 model validation

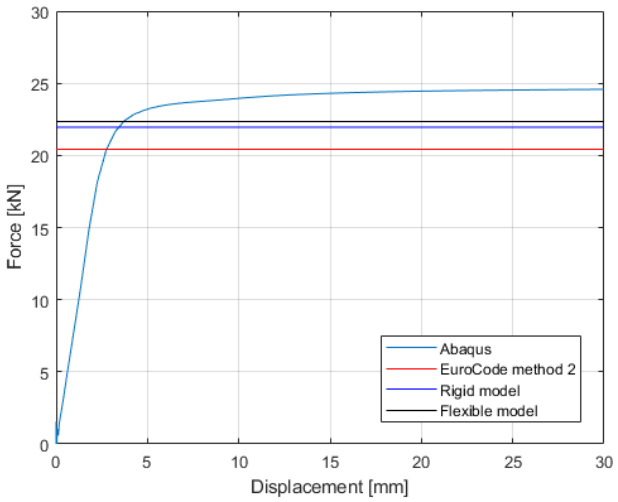

FIGURE C.5 – T14-08-10-02 model validation

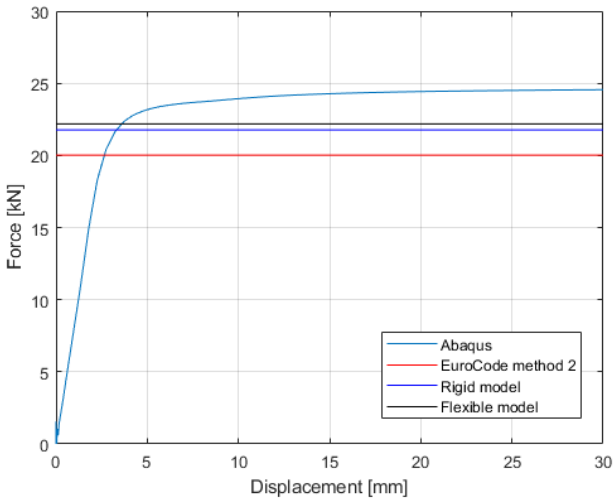

FIGURE C.6 – T14-08-10-025 model validation

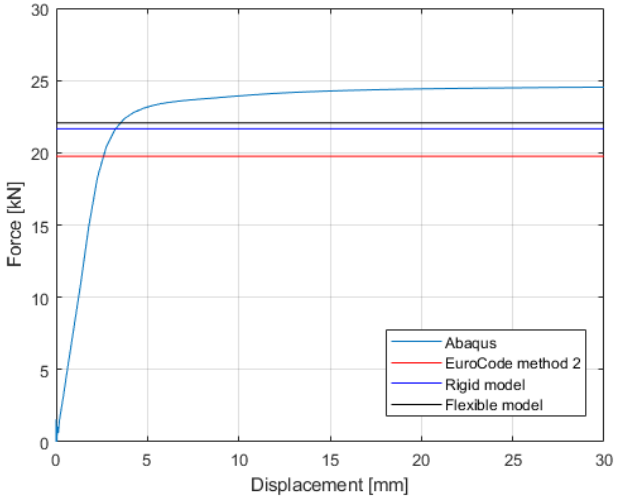

FIGURE C.7 – T14-08-10-03 model validation

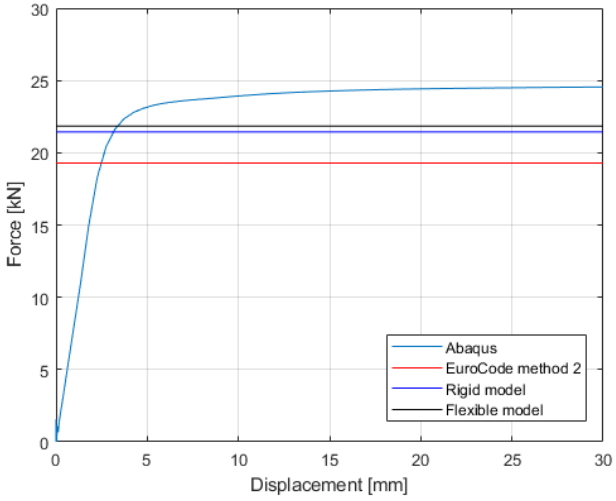

FIGURE C.8 – T14-08-10-05 model validation

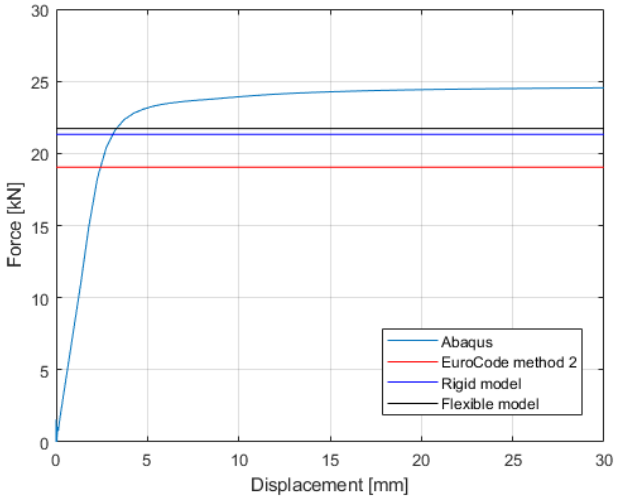

FIGURE C.9 – T14-08-10-08 model validation

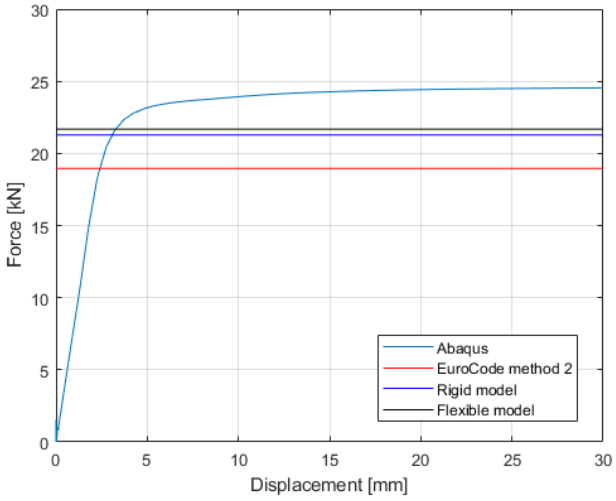

FIGURE C.10 – T14-08-10-1 model validation

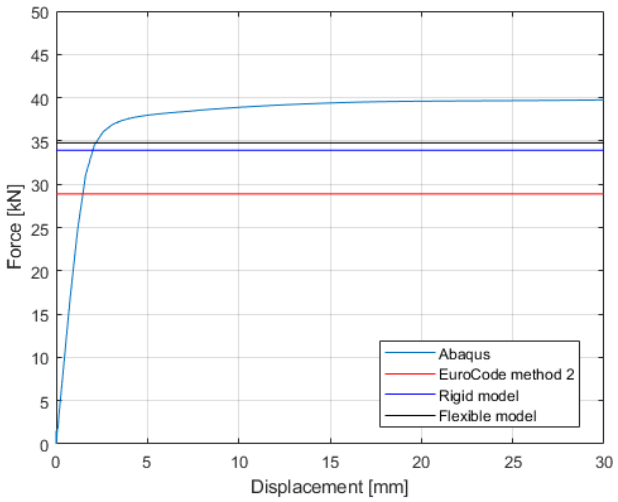

FIGURE C.11 – T14-08-15-1 model validation

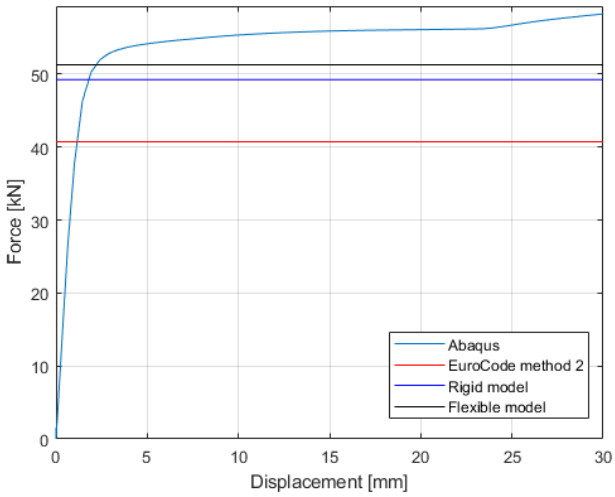

FIGURE C.12 – T14-08-20-05 model validation

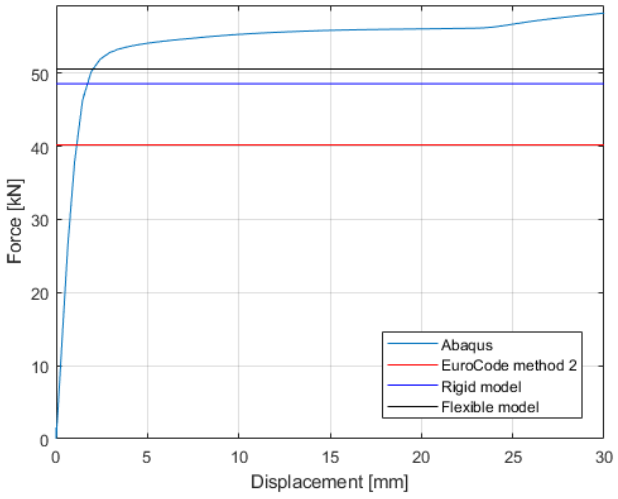

FIGURE C.13 – T14-08-20-06 model validation
14-08-20-06 model validation

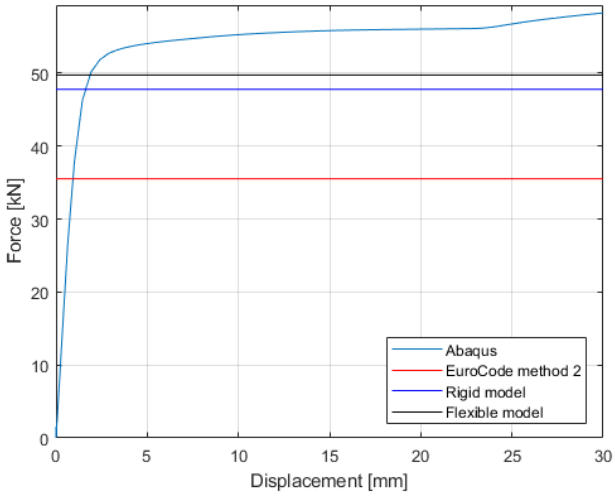

FIGURE C.14 – T14-08-20-08 model validation

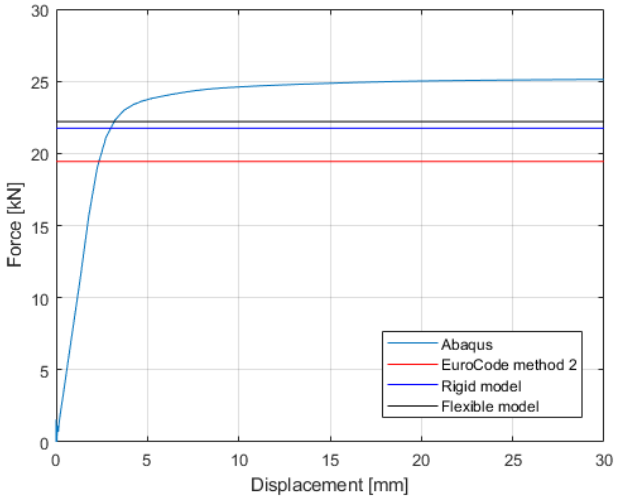

FIGURE C.15 – T16-07-10-05 model validation
T16-07-10-05 model validation

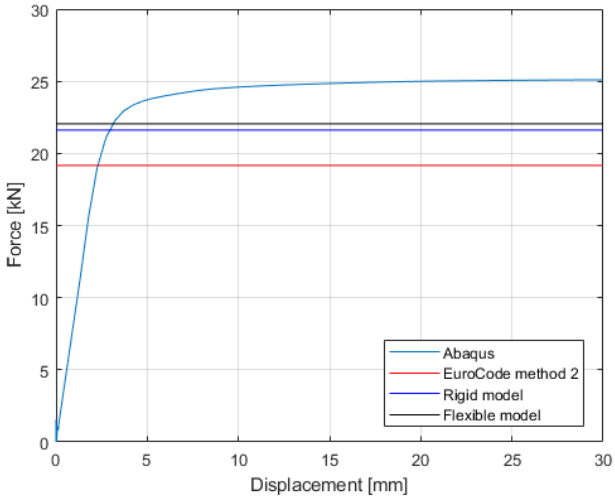

FIGURE C.16 – T16-07-10-08 model validation

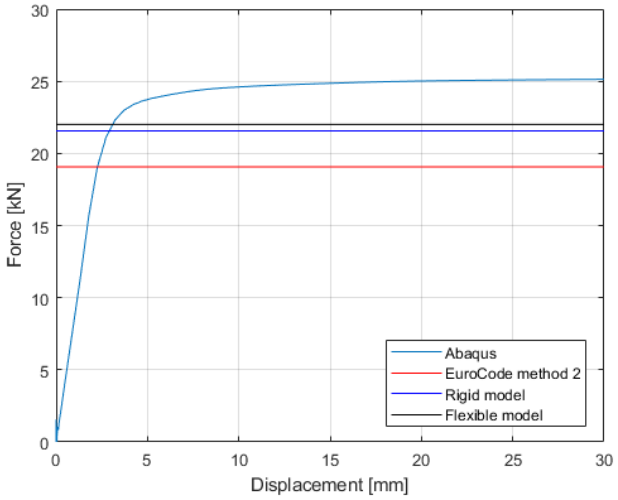

FIGURE C.17 – T16-07-10-1 model validation
T16-07-10-1 model validation

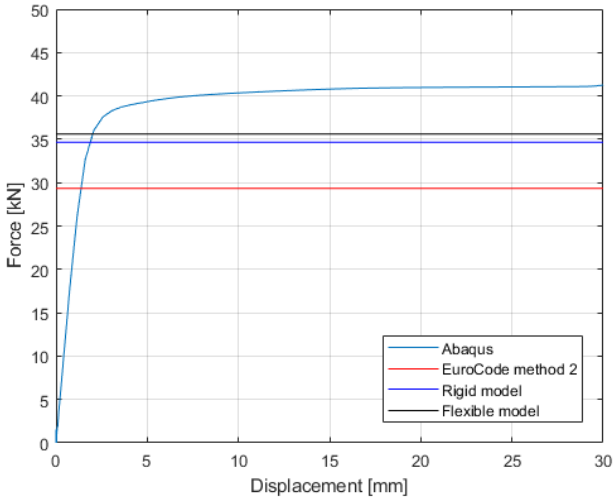

FIGURE C.18 – T16-07-15-1 model validation

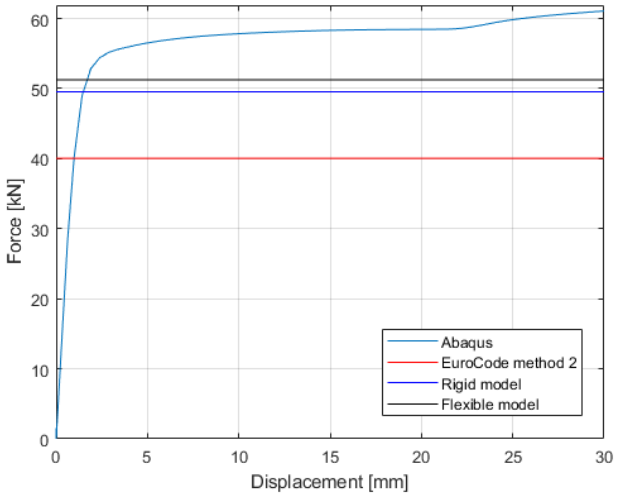

FIGURE C.19 – T16-07-20-08 model validation
T16-07-20-08 model validation

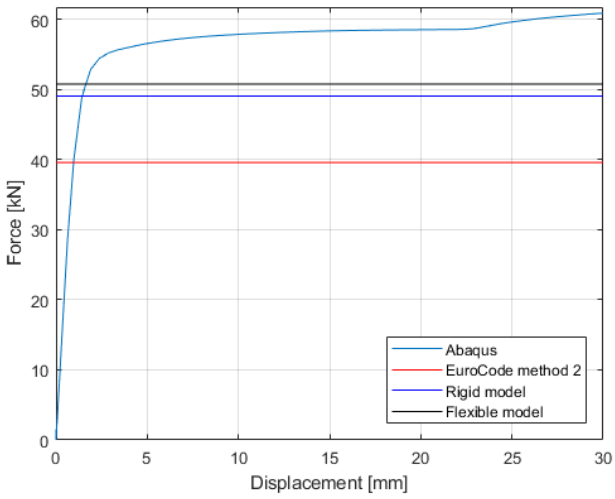

FIGURE C.20 – T16-07-20-1 model validation

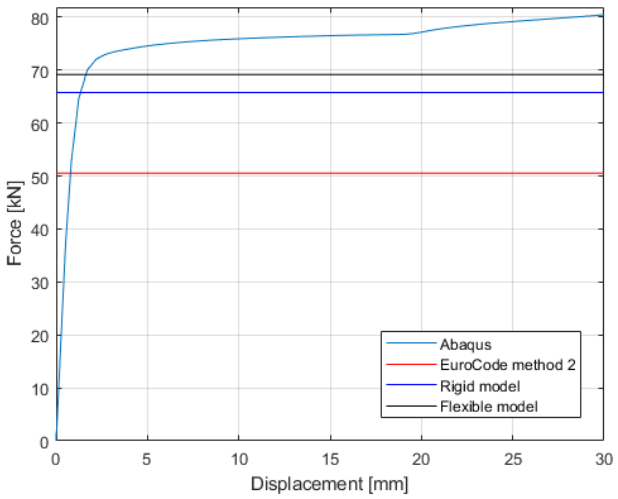

FIGURE C.21 – T16-07-25-1 model validation

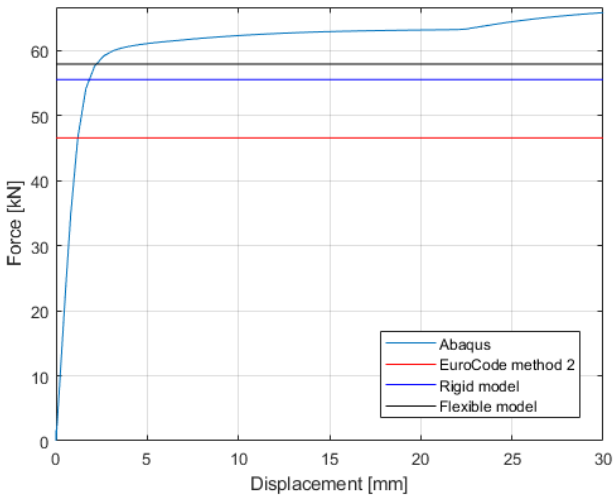

FIGURE C.22 – T16-08-20-05 model validation

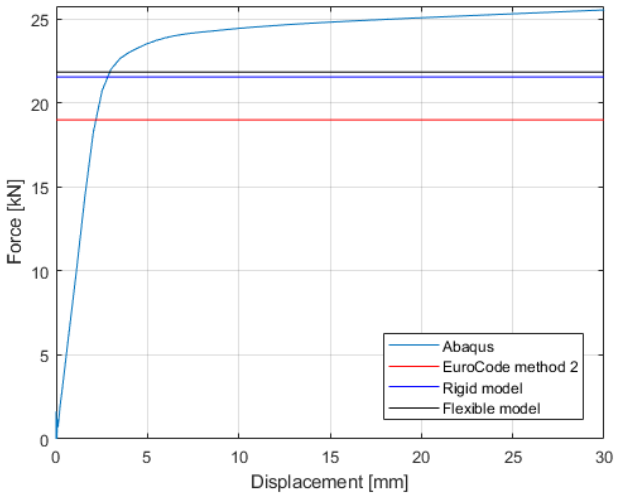

FIGURE C.23 – T18-06-10-05 model validation

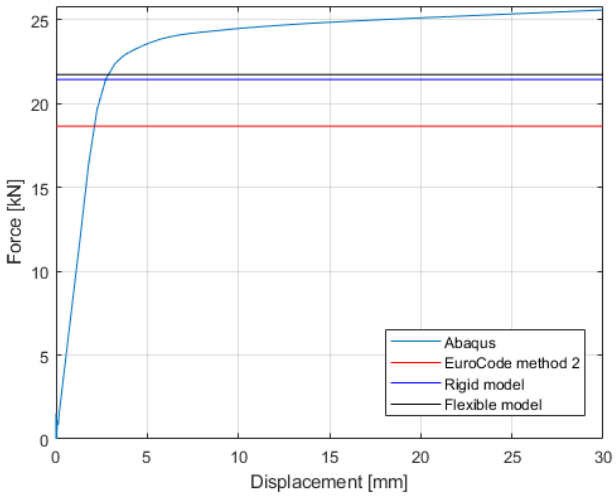

FIGURE C.24 – T18-06-10-08 model validation

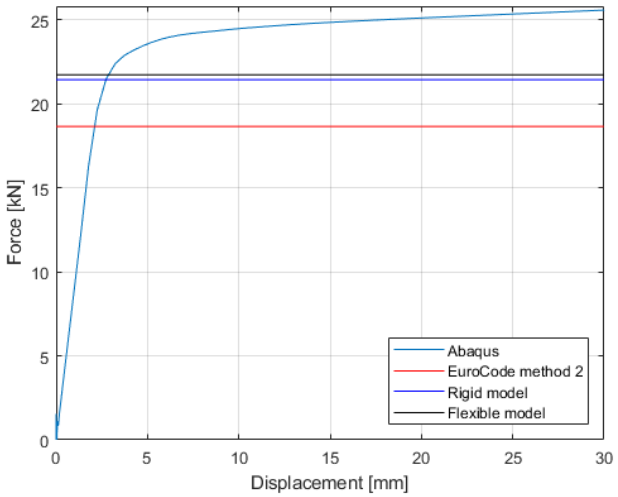

FIGURE C.25 – T18-06-10-1 model validation

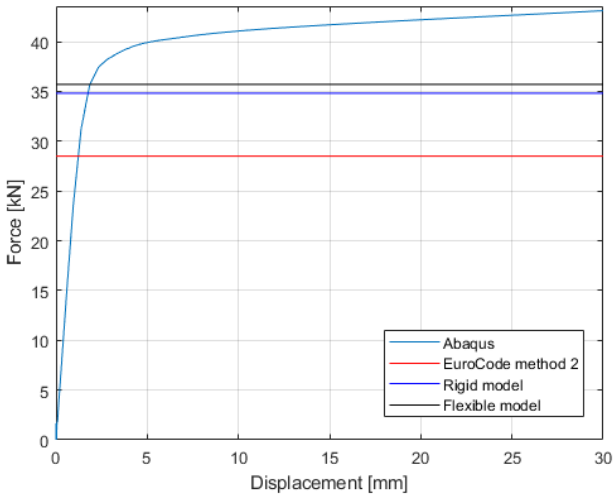

FIGURE C.26 – T18-06-15-1 model validation

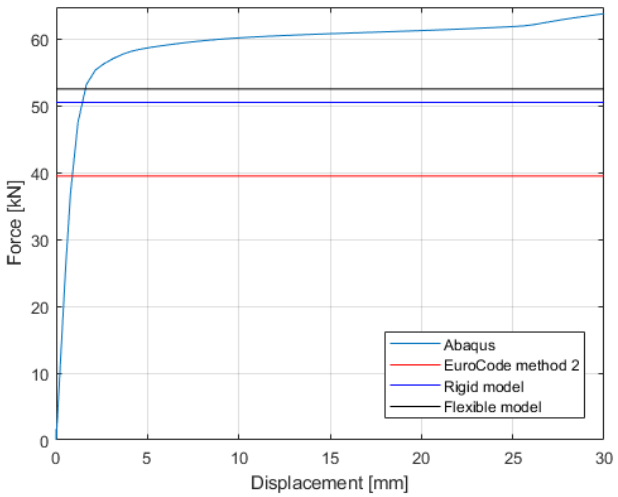

FIGURE C.27 – T18-06-20-08 model validation

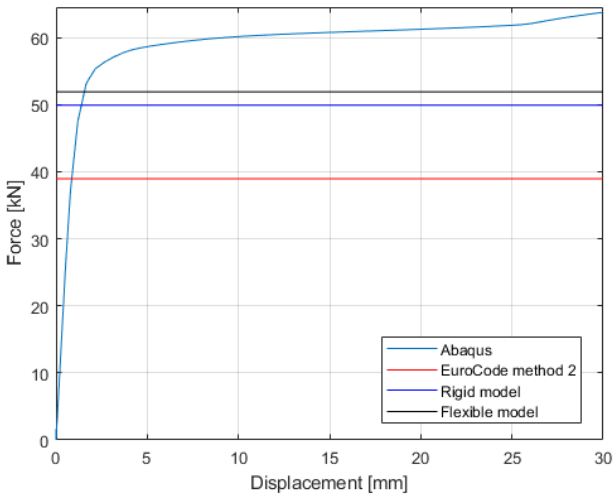

FIGURE C.28 – T18-06-20-1 model validation

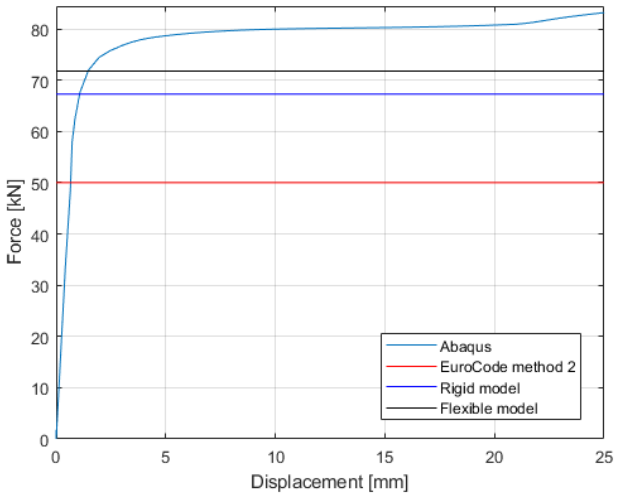

FIGURE C.29 – T18-06-25-1 model validation

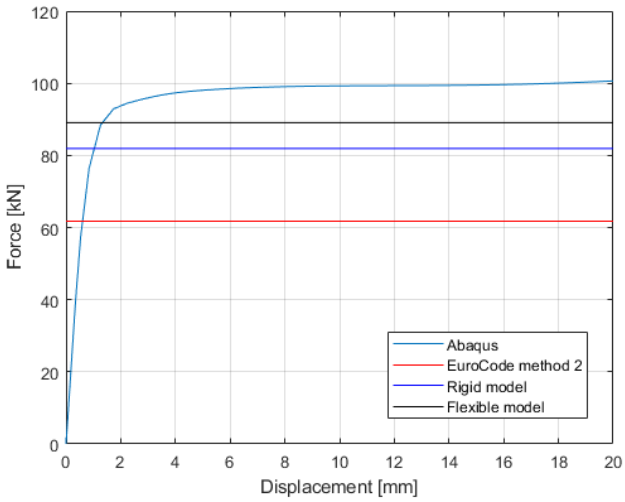

FIGURE C.30 – T18-06-30-08 model validation

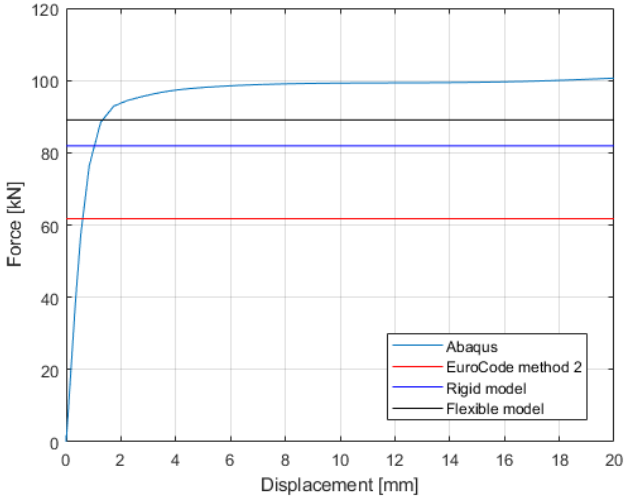

FIGURE C.31 – T18-06-30-1 model validation

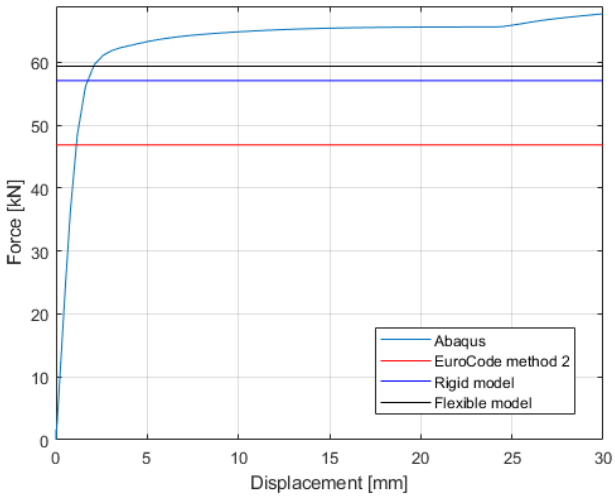

FIGURE C.32 – T18-07-20-05 model validation

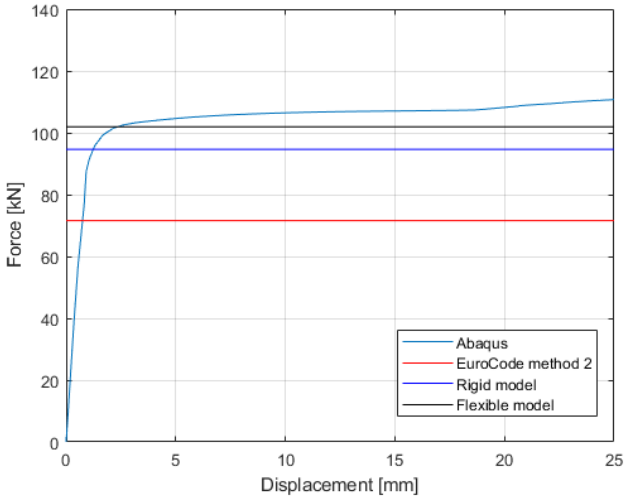

FIGURE C.33 – T18-07-30-08 model validation

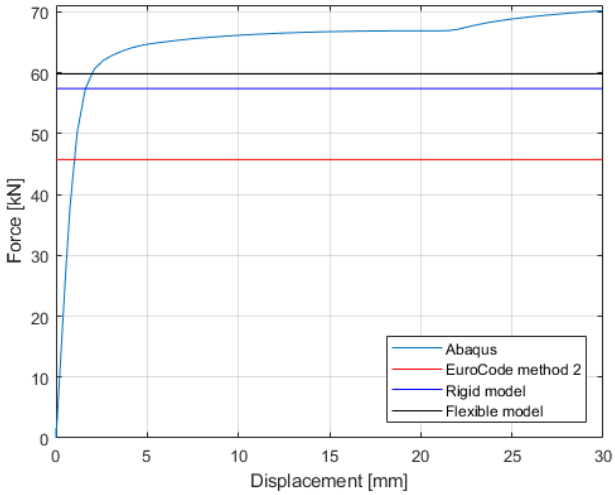

FIGURE C.34 – T20-06-20-05 model validation

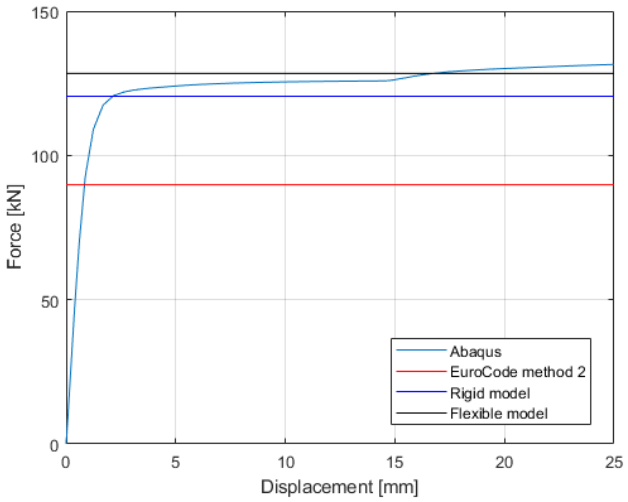

FIGURE C.35 – T22-07-30-06 model validation

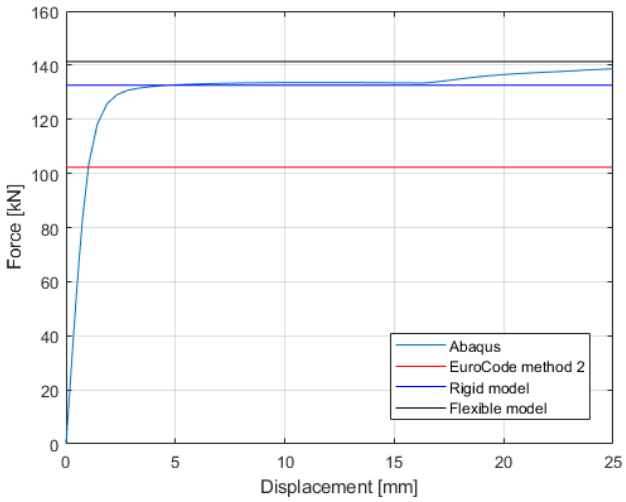

FIGURE C.36 – T22-08-30-05 model validation

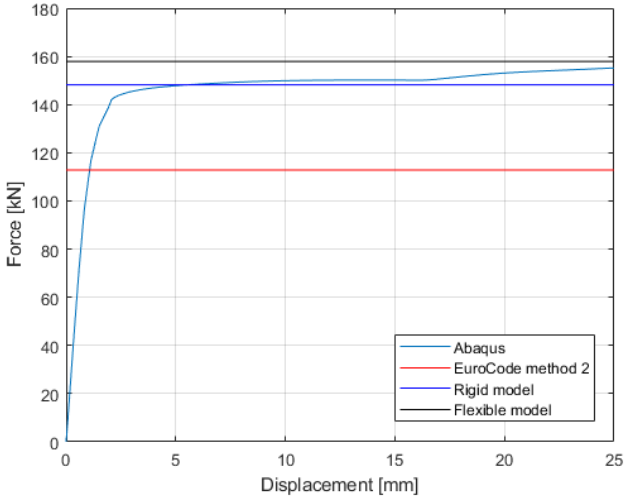

FIGURE C.37 – T24-08-30-05 model validation

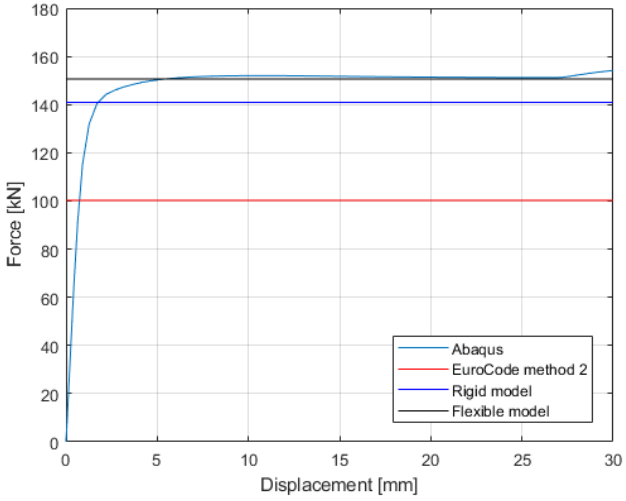

FIGURE C.38 – T27-06-30-06 model validation

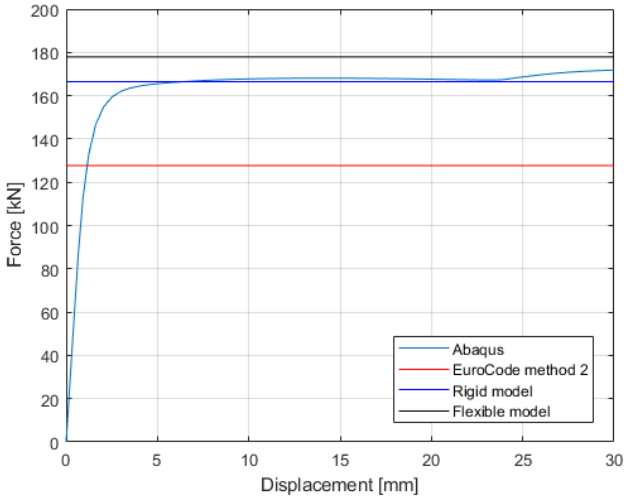

FIGURE C.39 – T27-08-30-05 model validation

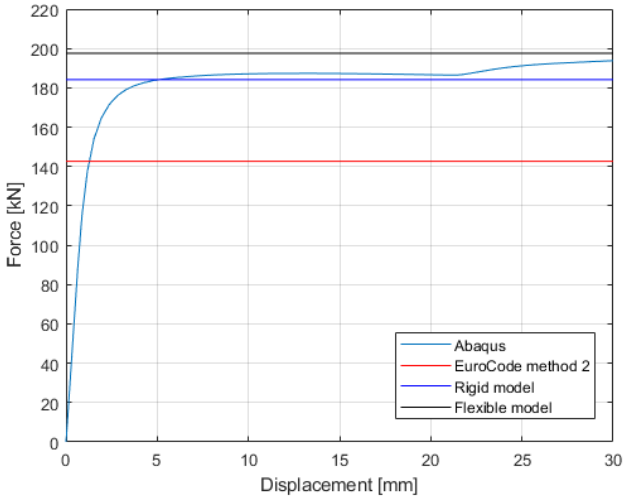

FIGURE C.40 – T30-08-30-05 model validation

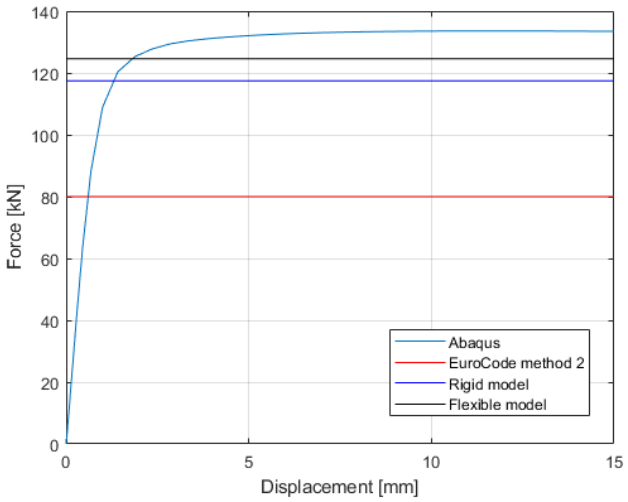

FIGURE C.41 – T27-14-50 model validation

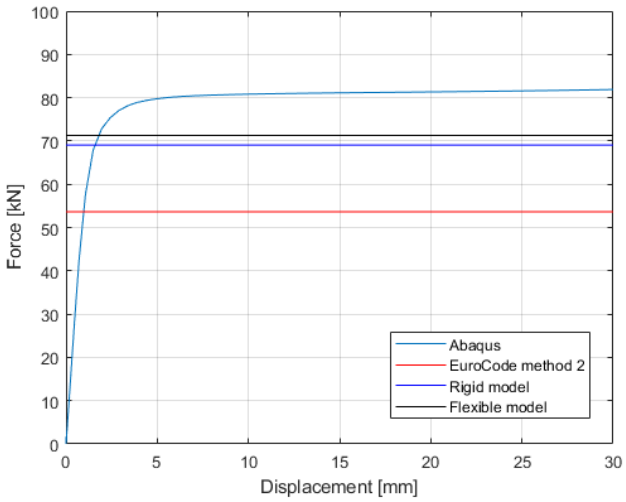

FIGURE C.42 – T27-14-72 model validation

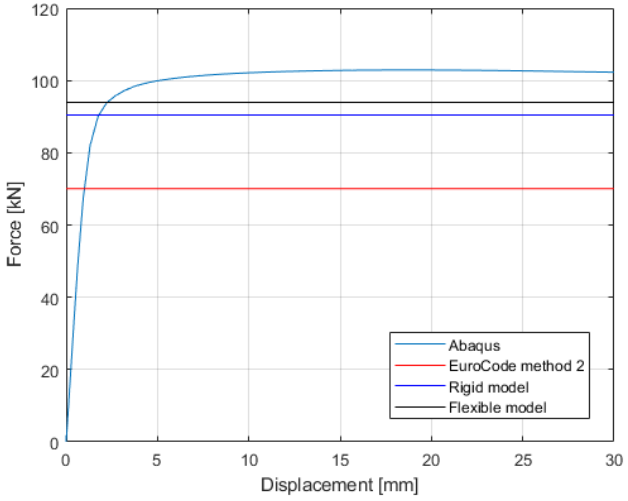

FIGURE C.43 – T27-16-72 model validation

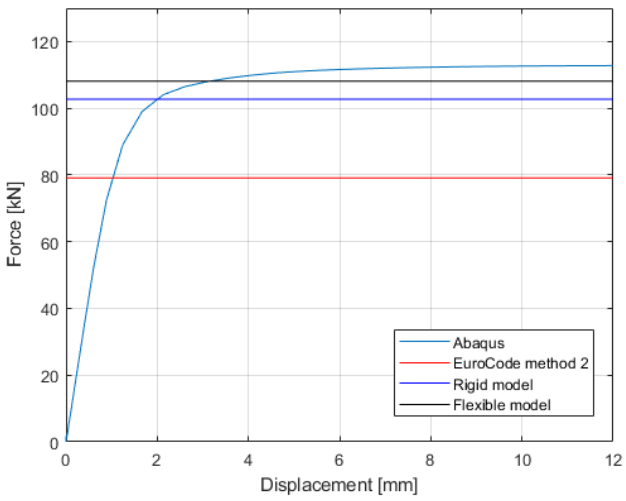

FIGURE C.44 – T27-17-72 model validation

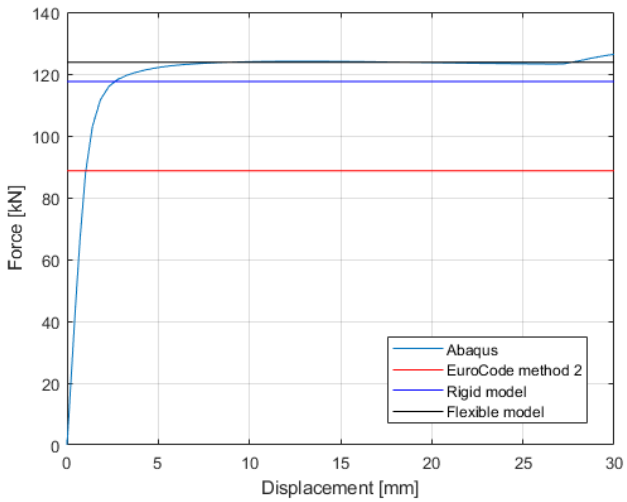

FIGURE C.45 – T27-18-72 model validation

Epruvete teste material
1 : 5

P19
Pb55x10...310
scara 1:5

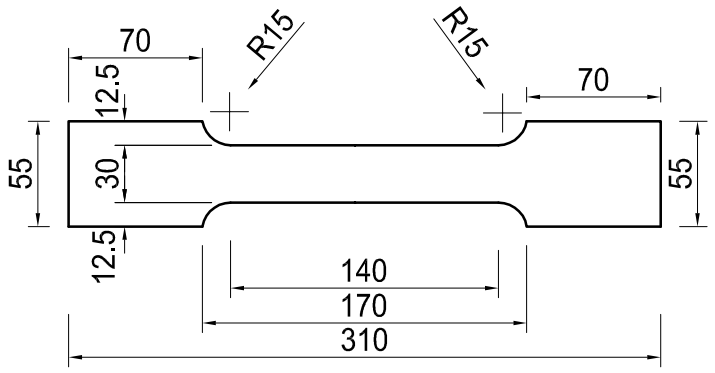

P22
Pb55x15...310
scara 1:5

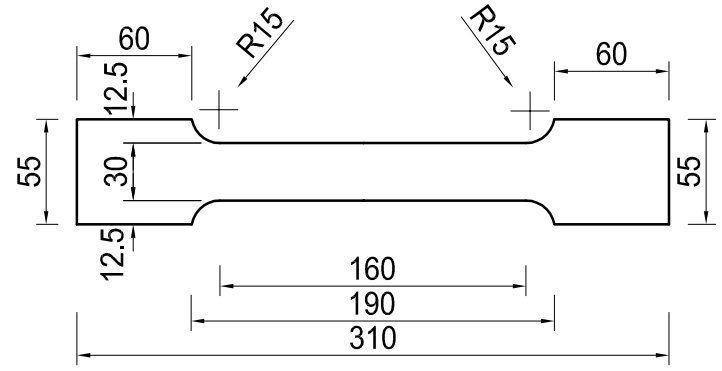

P20
Pb55x10...310
scara 1:5

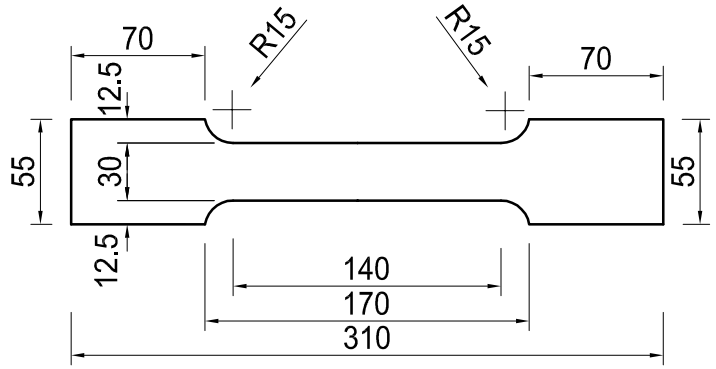

P23
Pb55x18...330
scara 1:5

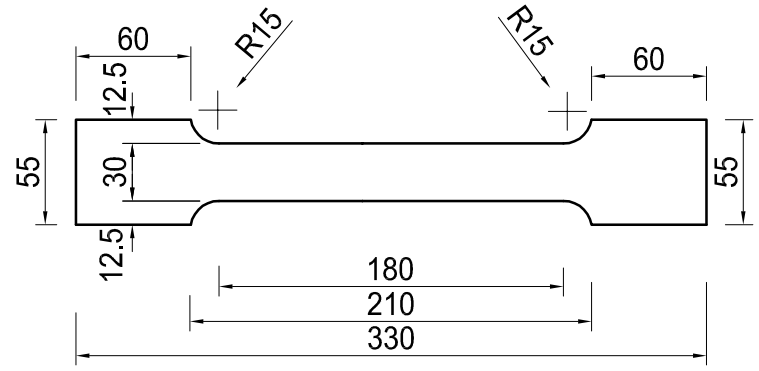

NOTA:

- Epruvetele detaliate in prezenta plansa se vor debita din materialul de baza folosit la confectionarea ansamblelor din plansele 01R-13R

P21
Pb55x12...310
scara 1:5

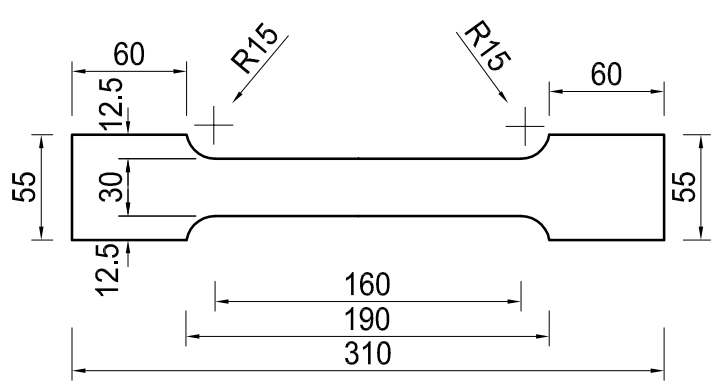

Universitatea Politehnica din Timisoara		EXTRAS DE MATERIALE									Planşa nr. 14-R	
		Denumirea proiectului	Incercari experimentale pe macrocomponente									
Ing. BOTH IOAN		Denumirea elementului	**Epruvete teste material**								3	buc
		Bucati asemenea		Dimensiunea [mm]		Lungimea [mm]	Masa in Kg				Cal. Mat.	OBS
Pozitia	Denumirea	in elem.	in toate elem.				pe m	pe buc.	pe elem	pe toate elem		
P19	Pb55x10	1	3	55	10	310	4.32	1.3	1.3	4.0	S355	
P20	Pb55x10	1	3	55	10	310	4.32	1.3	1.3	4.0	S235	
P21	Pb55x12	1	3	55	12	310	5.18	1.6	1.6	4.8	S235	
P22	Pb55x15	1	3	55	15	310	6.48	2.0	2.0	6.0	S235	
P23	Pb55x18	1	3	55	18	330	7.77	2.6	2.6	7.7	S235	
								Total Kg		26.6		
								Sudura 2.5%		0.7		
								Protectie 0.4%		0.1		
								Total Kg		**27**		

	NUME	SEMNĂTURA	CERINŢĂ	
UNIVERSITATEA "POLITEHNICA" DIN TIMISOARA Departamentul de Constructii Metalice si Mecanica Constructiilor				Beneficiar: **Universitatea Politehnica Timisoara Dep. CMMC** Amplasament: IOAN CUREA nr. 1 Timisoara
SPECIFICAŢIE	NUME:	SEMNĂTURA	SCARA:	Titlu proiect: **PC 55/2012 - INCERCARI EXPERIMENTALE MACROCOMPONENTE**
VERIFICAT	conf.dr.ing. Florea Dinu		1 : 5	
PROIECTAT	conf.dr.ing. Zaharia Raul		DATA:	Titlul planşei: **Epruvete teste material**
DESENAT	as.dr.ing. Both Ioan		07.2013	

Proiect nr. **__/2013**

Faza: ____

Planşa: **14-R**

297 x 420